(RADA)$_4$ Self-Assembling Peptide based Hydrogels: Design, Characterization and *In-Vitro* Biological Evaluation

by

Aditi Saini

A thesis submitted in partial fulfillment of the requirements for the degree of

Doctor of Philosophy

in

CHEMICAL ENGINEERING

Department of Chemical and Materials Engineering
University of Alberta

Abstract

Ionic self-assembling peptides have emerged as promising nano-biomaterials, with direct applications in the fields of bioengineering and applicative medicine. (RADA)$_4$ is a self-assembling 16 residue containing peptide, with alternating hydrophobic and hydrophilic residues. This characteristic amphiphilic nature of the peptide allows it to self-assemble into β-sheets, forming higher order three-dimensional (3D) structures. The resulting 3D hydrogels are non-immunogenic, highly hydrated (containing ≥ 99% water), and can respond to physiological stimuli. The (RADA)$_4$ hydrogels can serve as ECM (extra cellular matrix) scaffolds, assist in drug delivery, and can achieve rapid hemostasis.

This dissertation consists of two major parts: 1) fundamental study of the self-assembly of the model ionic complementary peptide (RADA)$_4$, and 2) *in-vitro* biocompatibility assessment of the (RADA)$_4$ peptides.

In the fundamental study, the secondary structure of (RADA)$_4$ was examined with Circular Dichroism (CD), and compared to that of its two variants: (RADA)$_4$K$_5$ and (RADA)$_4$S$_5$. The effect of peptide concentration and temperature on the secondary structure was also studied. It was found that all but (RADA)$_4$K$_5$ peptides formed successful β-sheets, consequently forming nanofibers, whereas (RADA)$_4$K$_5$ resulted in the formation of aggregates rich of primarily random coil sequences. Further, studies were conducted to determine the critical concentration of (RADA)$_4$K$_5$ for successful nanofiber formation. The 3D nanostructure of the peptide was affected by the amino acid sequence as well as by the temperature induced denaturation of the peptide. Quantitative structural analysis of all the samples were carried out using an online DICHROWEB

server, by comparing the secondary structure molar ellipticity of the peptides collected with that of seven reference proteins (data confirmed *via* X-ray crystallography).

Single-molecule Florescence Correlation Spectroscopy (FCS) was used to confirm the molecular interaction of the pristine $(RADA)_4$ nanofibers with 25% $(RADA)_4K_5$. The effect of hydration on these self-assembling peptides was investigated *via* Differential Scanning Calorimetry (DSC), over a range of temperatures. The Equilibrium Water Content (EWC) in $(RADA)_4$ was comparable to $(RADA)_4S_5$ and $(RADA)_4K_5$, even at varying compositions. The content of non-frozen bound water increased upon appending either Lysine or Serine residues to the $(RADA)_4$ peptide. Microscopy techniques such as Atomic Force Microscopy (AFM), and Transmission Electron Microscopy (TEM), were also employed to visually inspect the higher order structures formed by these peptides.

The second part of this dissertation focuses on the *in-vitro* biocompatibility of the $(RADA)_4$ based peptides. The PAC-1, CD62-P, and CD42 markers were used to study platelet activation (*via* Flow Cytometry) and a time based clotting analysis was conducted to evaluate the hemostatic ability of peptides. Complement C3a ELISA assay was conducted with $(RADA)_4$ based peptides to gain more insight into the biocompatibility. The pristine $(RADA)_4$ nanofibers caused a rapid clot formation, but yielded a low platelet activation and low C3a activation. Whereas, $(RADA)_4K_5$ peptide displayed a significantly higher complement activation, when compared to both $(RADA)_4S_5$, and the $(RADA)_4$ peptide, likely due to the free NH_3 groups and steric hindrance in packing. The overall trend of the platelet activation among the three variants of the peptides remained consistent: $(RADA)_4K_5$ activated the platelets to the highest, whereas $(RADA)_4S_5$, and $(RADA)_4$ showed comparable platelet activation. However, it should be noted

that both the platelet and complement activation by these peptides were lower than the already considered biocompatible biopolymers.

Lastly, morphology analysis of the platelets in contact with the hydrogels was conducted by calculating the Morphology Score (MS) using a Kunicki scoring system, and the platelets were visualized using Scanning Electron Microscopy (SEM). An overall Kunicki morphology score of above 385 was achieved for all the peptides, where a score of less than 200 represent poor retention of morphological characteristics associated with platelets that are active. Overall, the $(RADA)_4$ based peptides had a lower, or comparable platelet and complement activation, when compared with the already in-use biomaterials (such as poly(methyl methacrylate), and dextran), making them a desirable material to further investigate.

The work in this dissertation, not only provides the fundamental knowledge to design novel biomaterials for direct application in medicine, but also provides the stepping stone for further *in-vitro* and *in-vivo* biocompatibility analysis, required for any further medical application.

Preface

Contribution to Articles

The following pertains to my contribution to the articles in Chapter 4 and Chapter 5. I was responsible for the literature research, forming the research objective, planning experiments, protocol development, experimental setup and execution, data analysis, and writing of the manuscripts. Dr. Xia provided technical assistance in differential scanning calorimetry and circular dichroism. Mr. K. Koss provided the Transmission Electron Microscopy data for both the chapters and papers. Dr. D. V. Devine provided lab resources for platelet and complement assays, whereas Dr. K. Serrano assisted in platelet and complement activation data collection and analysis. I generated the first draft of the journal articles and worked with my supervisor (Dr. L. D. Unsworth) on subsequent drafts, with the analytical input from Dr. K. Serrano on Paper II (Chapter 5). I generated initial responses to the comments of the journal reviewers.

Chapter 4 of this thesis was published as: A. Saini, K. Koss, and L. D. Unsworth. "**Effect of Peptide Concentration on Water Structure, Morphology, and Thermal Stability of Self-Assembling (RADA)$_4$ Peptide Matrices**", *Journal of Biomaterials and Tissue Engineering*, 2014, 4 (11), 895-905.

Chapter 5 of this thesis was published as: A. Saini, K. Serrano, K. Koss, and L. D. Unsworth **"Evaluation of the Hemocompatibility and Rapid Hemostasis of (RADA)$_4$ Peptide-Based Hydrogels"**, *Acta Biomaterilia*, 2016, 31, 71-79

Dedication

To my paternal grandmother, *Chai ji,* for being the most amazing role model any little girl could

ever ask for.

There's Plenty of Room at the Bottom

"Feynman had described a process by which the ability to manipulate individual atoms and molecules might be developed, using one set of precise tools to build and operate another proportionally smaller set, so on down to the needed scale. In the course of this, he noted, scaling issues would arise from the changing magnitude of various physical phenomena: gravity would become less important, surface tension and Van der Waals would become more important."

Excerpt from Richard Feynman's inspiring lecture on the origin of nanotechnology, at the annual meeting of American Physical Society in Pasadena, California, on December 29th, 1959*

Acknowledgements

After all these years of hard work, dedication, commitment, and persistence, today is the day: writing this note of thanks, as the very last piece of my dissertation. It has been a period of intense learning for me; I have not only progressed in scientific arena, but also evolved at a personal level. Finishing my Ph.D. work successfully, and writing this dissertation has had a tremendous impact on me. I would like to acknowledge all the people who have supported and helped me throughout this life changing experience. As such, I would like to express my deepest gratitude towards them.

First and foremost, I would like to thank my supervisor Dr. Larry D. Unsworth, and my supervisory committee (consisting of Drs. Hasan Uludağ, and Hongbo Zeng) for providing me with constant guidance, support and motivation. I am grateful for the opportunity to be able to pursue my passion of research in applicative medicine, while using the tools provided by Chemical Engineering. I am truly thankful to be a part of the National Institute for Nanotechnology (NINT), National Research Council Canada, and being able to use their cutting edge technology for my scientific endeavours.

My gratitude is also extended towards Dr. Dana Devine for allowing me to work in her lab at the Centre of Blood Research at UBC. Hers and Dr. Katherine Serrano's guidance were monumental in the biocompatibility part of this project. I am also very grateful of the co-authors of my research papers as described in this dissertation. Their contribution was crucial for me to succeed in achieving this milestone.

Table of Contents

List of Figures

List of Tables

List of Abbreviations and Symbols

3D	Three-Dimensional
A	Alanine
Abs	Absorbance
ACD	Acid Citrate Dextrose
ADP	Adenosine Diphosphate
AFM	Atomic Force Microscopy
ANOVA	Analysis of Variance
CBS	Canadian Blood Services
CD	Circular Dichroism
D	Aspartic Acid
E	Glutamic Acid
DSC	Differential Scanning Caloriemetry
EDTA	Ethylenediaminetetraacetic Acid
ELISA	Enzyme-linked immunosorbent assay
FCS	Fluorescence Correlation Spectroscopy
FITC	Fluorescein Isothiocynate
FMOC	Fluorenylmethyloxycarbonyl
GPRP	Glycine-Proline-Arginine-Proline
ΔH	Melting Enthalpy of Sample (J/g)
$\Delta H°$	Melting Enthalpy of Bulk Water (J/g)
HA	Hyaluronic Acid
H(d)	Distorted Alpha Helix
H(r)	Regular Apha Helix
HPLC	High Performance Liquid Chromatography
HSA	Human Serum Albumin
HT(V)	High-tension Voltage
K	Lysine
MS	Mass Spectrometry
MRW	Mean Residue Molecular Weight (Da)
MW	Molecular Weight
n	Electron Lone Pair
OD	Optical Density
PB	Phosphate Buffer
PBS	Phosphate Buffered Saline
PE	Phycoerythrin
R	Arginine

S	Serine
SEM	Scanning Electron Microscopy
S(d)	Distorted Beta Sheet
S(r)	Regular Beta Sheet
S/N	Signal to Noise ratio
TEM	Transmission Electron Microscopy
Trp	Tryptophan
Tyr	Tyrosine
UV	Ultraviolet
W_d	Weight of Dry Sample (mg)
W_f	Free Water (%)
W_h	Weight of Hydrated Sample (mg)
W_{fb}	Frozen Bound Water (%)
W_{nf}	Non-Frozen Bound Water (%)
wt%	Weight Percentage
w/v (%)	Weight by Volume (Percentage)
α	Alpha
β	Beta
$[\Theta]$	Mean Residue Ellipticity (degree cm^2 dmol^{-1})
Θ	Raw Ellipticity (degree cm^2 dmol^{-1})
π^*	Anti-bonding Orbital
ϕ	Phi
ψ	Psi
ζ	Zeta Potential

Chapter 1

Scope of Dissertation

Ionic self-assembling peptides have an array of existing and potential nano-medical applications, ranging from drug delivery, to achieving rapid hemostasis. $(RADA)_4$ based peptide originates from the same class as the amphiphilic self-assembling peptide $(EAKA)_4$, which in turn was first characterized in a 34 amino acid long Zuotin yeast protein by Dr. Shuguang Zhang.

Despite the on-going applicative research involving $(RADA)_4$ peptides, not only there is a scientific gap in the fundamental understanding of self-assembly, but also there lacks a systematic *in-vitro* biological evaluation of these peptides. In order to design a more effective biomaterial and to analyze the human blood response to such material, a thorough understanding of both these areas is needed. The work summarized herein is designated to address these fundamental questions, elaborating the fundamentals of self-assembly of $(RADA)_4$ based peptides, but also evaluating their biocompatibility.

In Chapter 1, we present the Scope of Dissertation, and a synopsis of each chapter.

Chapter 2 provides a brief introduction of the ionic-self assembling peptides, including the research objective of the Ph.D. project.

Chapter 3 provides a detailed Literature Review of the ionic-self assembling peptides (focussing on the $(RADA)_4$ peptides), a brief history of the evolution of such peptides, (external and internal) forces responsible for their self-assembly, physiological factors affecting the self-assembly process. The chapter also focuses on the recent developments and proposed self-assembly mechanisms so far. Further, there is an in-depth analysis of various methods employed to study the two major parts of the dissertation (described in the Abstract section), and a comparison of the methods with other relevant methods was also reported. A brief subsection of the applications of the $(RADA)_4$ peptide is also reported. Finally, current scientific developments (involving *in-vivo* biocompatibility assays), as well as the brief review of the progress made with respect to self-assembling peptides in the last ten years was given.

In Chapter 4, we explore the Effect of Peptide Concentration on Water Structure, Morphology, and Thermal Stability of Self-Assembling $(RADA)_4$ Peptide Matrices. Specifically, we varied the concentration of $(RADA)_4$ peptide from 0.5% (w/v) to 3.0% (w/v), to study the effect of concentration on the secondary structure of the peptide *via* Circular Dichroism (CD). CD was also used to analyze the thermal stability of the peptide at the given concentrations by increasing the nanofiber temperature from 25°C to 80°C, and bringing it back to 25°C. Quantitative analysis of the secondary structure was also conducted using the Contin program of the DICHROWEB server. Further hydration state analysis of the peptides was conducted, followed by the visual inspection of the nanofiber formation via TEM.

Chapter 5 contains the Evaluation of the Hemocompatibility and Rapid Hemostasis of $(RADA)_4$ Peptide-Based Hydrogels, at the same concentrations of $(RADA)_4$ as reported in Chapter 4. Herein, the *in-vitro* biological evaluation of the $(RADA)_4$ peptide was conducted, by

2

studying the plasma clot analysis, platelet activation, as well as the complement C3a activation, upon incubation with the peptide. This chapter covers gaps in the literature by systematically conducting the basic biological assays needed to establish the biocompatibility of a nano biomaterial.

In Chapter 6, Effect of End Group on Nanofiber Self Assembly and Vicinal Water Structure, two variants of the $(RADA)_4$ peptide: $(RADA)_4K_5$, and $(RADA)_4S_5$, were used to study the effect of positively charged lysine residues and uncharged serine residues on the fundamental process of self-assembly. CD was studied to analyse the secondary structure analysis of the peptide, and it was found that all but $(RADA)_4K_5$ formed successful nanofiber formation. Further, the critical concentration for the $(RADA)_4K_5$ peptide self-assembly was experimentally determined. The single molecule fluorscence correlation was determined to confirm the interaction of the $(RADA)_4$ fibres with $(RADA)_4K_5$. Thermal stability of the $(RADA)_4$ peptide, along with its variants was also determined by increasing the peptide temperature from 25°C to 80°C, and recording the subsequent changes in the molar ellipticity. Lastly, the hydration state analysis of all these peptides was also conducted.

Chapter 7 evaluates the effect of physiochemical characteristics of self-assembling $(RADA)_4$ based peptide nanofibers on their *in-vitro* biological evaluation. A comparative study involving the platelet and complement activation of $(RADA)_4$ peptides and its variants $((RADA)_4K_5$, and $(RADA)_4S_5)$ was reported. Also western blot analyses of different proteins detected upon incubation with the peptides were presented. Finally, Kunicki morphology score of all the three peptides was reported to validate the viability of platelets in contact with the hydrogel systems.

Chapter 8 provides a general discussion on the overall conclusion of the studies and gives

future recommendations to pursue study involving the ionic self-assembling nanofibers.

Chapter 2

An Introduction of (RADA)₄ Based Ionic self-assembling Peptides

Ionic self-assembling peptides has recently been explored as promising biomaterials for an array of biotechnological and biomedical applications, due to their high water content, favourable structural features, and biocompatibility [1]. The self-assembling nature of these peptides allows them to spontaneously form supramolecular structures based on hydrogen, hydrophobic, electrostatic and van der Waals interactions. The naturally occurring peptides have additional benefits such as high biocompatibility, low cellular toxicity, and biodegradable benign by-products *in-vivo* [2].

(RADA)₄ peptide is a member of designed ionic self-assembling peptides. The primary sequence of the peptide is [COCH₃]-RADARADARADARADA-[CONH₂], where the alternating hydrophilic and hydrophobic residues gives rise to a β-sheet formation, resulting in the complementary ionic bonds on the hydrophilic surface. This peptide retains its characteristic β-sheets at extreme pH [3] and temperatures [3, 4]. The (RADA)₄ monomer is experimentally shown to be ~1.3 nm wide, ~ 5 nm long and ~0.8 nm thick in dimensions [3, 5, 6], thus supramolecular nanostructures can be rationally designed for specific applications (such as drug delivery). These monomers can spontaneously assemble nanofibers ranging from a few hundred

nanometers to a few microns in length, subsequently forming higher order interweaving nanofiber scaffolds: hydrogels, possessing a very high hydration (up to 99.5%). This peptide can be tuned to response to the physiological environment (pH, temperature, and electrolytic environment [7-9]), and can be either biomimetic or *de novo* designed. These $(RADA)_4$ peptide based ionic self-assembling peptides have been investigated for an array of applications such as: drug delivery carriers [10, 11], cardiovascular [12-15], neurosurgical [16-21], extracellular matrices soft tissue regeneration [22, 23], hemostatic agents [24, 25], as well as for bone and cartilage regeneration [26-35]. However, despite this on-going applicative research on the $(RADA)_4$ peptides, there is a limited understanding of their self-assembly process at a fundamental level. It is also well known that hydration affects the secondary structure of the self-assembling peptides [3], still there lacks a thorough investigation with the $(RADA)_4$ peptide and various kinds of water affecting the nanofiber formation. Moreover, some of the recent studies have suggested that nanofibers based on these self-assembling peptides are also generally non-immunogenic, lack an inflammatory response, and are non-thrombogenic [36, 37]. However, this proposal of biocompatibility has not been systematically proven.

Therefore, in this work, $(RADA)_4$ and its two variants: $(RADA)_4K_5$, and $(RADA)_4S_5$ were used to study the self-assembling characteristics of this amphiphillic peptide. Primarily, the concentration of the $(RADA)_4$ peptide itself was varied (from 0.5% (w/v) to 3.0% (w/v)), and this effect of change in concentration *via* nanofiber packing was observed in the alteration of secondary structure of the peptide. The secondary structural transition from random coils and α-helices to β-sheet was correlated with an increase in the non-frozen bound water, at higher peptide concentrations. The effect of temperature on nanofiber assemblies was also observed

quantitatively by thermal Circular Dichroism (CD), and qualitatively *via* Transmission Electron Microscopy (TEM). Followed by this information, the effect of varying the end groups of (RADA)$_4$ peptide was studied to understand the self-assembly process. (RADA)$_4$ appended with five serine residues showed successful β-sheet formation, whereas (RADA)$_4$ with five lysine residues did not. Subsequently, mixtures of the (RADA)$_4$ and (RADA)$_4$K$_5$ peptides were used to achieve nanofiber formation, and Fluorescence Correlation Spectroscopy (FCS) was used to ensure the interaction of (RADA)$_4$K$_5$ peptide with (RADA)$_4$ while forming nanofibers. The effect of temperature on the secondary structure of all these three peptides was also studied. Differential Scanning Calorimetry (DSC) was employed to study the differ kinds of water present in all the systems. *In-vitro* assessment of all these systems included, turbidimetric assay for plasma clotting time, flow cytometry, complement activation and platelet morphology.

References

[1] Peppas NA, Hilt JZ, Khademhosseini A, Langer R. Hydrogels in biology and medicine: From molecular principles to bionanotechnology. Adv Mater 2006;18:1345-60.

[2] Stephanopoulos N, Ortony JH, Stupp SI. Self-assembly for the synthesis of functional biomaterials. Acta Mater 2013;61:912-30.

[3] Ye Z, Zhang H, Luo H, Wang S, Zhou Q, Du X, et al. Temperature and pH effects on biophysical and morphological properties of self-assembling peptide RADA16-1. Journal of Peptide Science 2008;14:152-62.

[4] Saini A, Koss K, Unsworth LD. Effect of Peptide Concentration on Water Structure, Morphology, and Thermal Stability of Self-Assembling (RADA)$_4$ Peptide Matrices. Journal of Biomaterials and Tissue Engineering 2014;4:895-905.

[5] Zhang S, Holmes T, Lockshin C, Rich A. Spontaneous assembly of a self-complementary oligopeptide to form a stable macroscopic membrane. Proceedings of the National Academy of Sciences 1993;90:3334-8.

[6] Zhang SG, Lockshin C, Cook R, Rich A. Unusually stable beta-sheet formation in an ionic self-complementary oligopeptide. Biopolymers 1994;34:663-72.

[7] Asakura T, Sugino R, Okumura T, Nakazawa Y. The role of irregular unit, GAAS, on the secondary structure of Bombyx mori silk fibroin studied with C-13 CP/MAS NMR and wide-angle X-ray scattering. Protein Science 2002;11:1873-7.

[8] Wang YD, Ameer GA, Sheppard BJ, Langer R. A tough biodegradable elastomer. Nature Biotechnology 2002;20:602-6.

[9] Ruan L, Zhang H, Luo H, Liu J, Tang F, Shi Y-K, *et al*. Designed amphiphilic peptide forms stable nanoweb, slowly releases encapsulated hydrophobic drug, and accelerates animal hemostasis. Proceedings of the National Academy of Sciences of the United States of America 2009;106:5105-10.

[10] Liu J, Zhang L, Yang Z, Zhao X. Controlled release of paclitaxel from a self-assembling peptide hydrogel formed in situ and antitumor study *in vitro*. International Journal of Nanomedicine 2011;6:2143-53.

[11] Nishimura A, Hayakawa T, Yamamoto Y, Hamori M, Tabata K, Seto K, *et al*. Controlled release of insulin from self-assembling nanofiber hydrogel, PuraMatrix (TM): Application for the subcutaneous injection in rats. European Journal of Pharmaceutical Sciences 2012;45:1-7.

[12] Guo HD, Cui GH, Yang JJ, Wang C, Zhu J, Zhang LS, *et al*. Sustained delivery of VEGF from designer self-assembling peptides improves cardiac function after myocardial infarction. Biochem Biophys Res Commun 2012;424:105-11.

[13] Allen P, Melero-Martin J, Bischoff J. Type I collagen, fibrin and PuraMatrix matrices provide permissive environments for human endothelial and mesenchymal progenitor cells to form neovascular networks. J Tissue Eng Regen Med 2011;5:E74-E86.

[14] Tokunaga M, Liu ML, Nagai T, Iwanaga K, Matsuura K, Takahashi T, et al. Implantation of cardiac progenitor cells using self-assembling peptide improves cardiac function after myocardial infarction. J Mol Cell Cardiol 2010;49:972-83.

[15] Guo HD, Cui GH, Wang HJ, Tan YZ. Transplantation of marrow-derived cardiac stem cells carried in designer self-assembling peptide nanofibers improves cardiac function after myocardial infarction. Biochem Biophys Res Commun 2010;399:42-8.

[16] Yla-Outinen L, Joki T, Varjola M, Skottman H, Narkilahti S. Three-dimensional growth matrix for human embryonic stem cell-derived neuronal cells. J Tissue Eng Regen Med 2014;8:186-94.

[17] Leung GKK, Wang YC, Wu WT. Peptide nanofiber scaffold for brain tissue reconstruction. In: Duzgunes N, editor. Nanomedicine: Cancer, Diabetes, and Cardiovascular, Central Nervous System, Pulmonary and Inflammatory Diseases. San Diego: Elsevier Academic Press Inc; 2012. p. 177-90.

[18] Li XW, Katsanevakis E, Liu XY, Zhang N, Wen XJ. Engineering neural stem cell fates with hydrogel design for central nervous system regeneration. Prog Polym Sci 2012;37:1105-29.

[19] Liedmann A, Rolfs A, Frech MJ. Cultivation of Human Neural Progenitor Cells in a 3-dimensional Self-assembling Peptide Hydrogel. J Vis Exp 2012;7.

[20] Uemura M, Refaat MM, Shinoyama M, Hayashi H, Hashimoto N, Takahashi J. Matrigel Supports Survival and Neuronal Differentiation of Grafted Embryonic Stem Cell-Derived Neural Precursor Cells. J Neurosci Res 2010;88:542-51.

[21] Ellis-Behnke RG, Liang YX, You SW, Tay DKC, Zhang SG, So KF, et al. Nano neuro knitting: Peptide nanofiber scaffold for brain repair and axon regeneration with functional return of vision. Proceedings of the National Academy of Sciences of the United States of America 2006;103:5054-9.

[22] Chen K, Sahoo S, He P, Ng KS, Toh SL, Goh JCH. A Hybrid Silk/RADA-Based Fibrous Scaffold with Triple Hierarchy for Ligament Regeneration. Tissue Engineering Part A 2012;18:1399-409.

[23] Degano IR, Quintana L, Vilalta M, Horna D, Rubio N, Borros S, et al. The effect of self-assembling peptide nanofiber scaffolds on mouse embryonic fibroblast implantation and proliferation. Biomaterials 2009;30:1156-65.

[24] Ellis-Behnke R. At the nanoscale: nanohemostat, a new class of hemostatic agent. Wiley Interdisciplinary Reviews: Nanomedicine and Nanobiotechnology 2011;3:70-8.

[25] Wang T, Zhong XZ, Wang ST, Lv F, Zhao XJ. Molecular Mechanisms of RADA16-1 Peptide on Fast Stop Bleeding in Rat Models. Int J Mol Sci 2012;13:15279-90.

[26] Cigognini D, Satta A, Colleoni B, Silva D, Donega M, Antonini S, et al. Evaluation of Early and Late Effects into the Acute Spinal Cord Injury of an Injectable Functionalized Self-Assembling Scaffold. PLoS One 2011;6:15.

[27] Nakahara H, Misawa H, Yoshida A, Hayashi T, Tanaka M, Furumatsu T, et al. Bone Repair Using a Hybrid Scaffold of Self-Assembling Peptide PuraMatrix and Polyetheretherketone Cage in Rats. Cell Transplant 2010;19:791-7.

[28] Maher SA, Mauck RL, Rackwitz L, Tuan RS. A nanofibrous cell-seeded hydrogel promotes integration in a cartilage gap model. J Tissue Eng Regen Med 2010;4:25-9.

[29] Yoshimi R, Yamada Y, Ito K, Nakamura S, Abe A, Nagasaka T, et al. Self-Assembling Peptide Nanofiber Scaffolds, Platelet-Rich Plasma, and Mesenchymal Stem Cells for Injectable Bone Regeneration With Tissue Engineering. J Craniofac Surg 2009;20:1523-30.

[30] Guo J, Su H, Zeng Y, Liang YX, Wong WM, Ellis-Behnke RG, et al. Reknitting the injured spinal cord by self-assembling peptide nanofiber scaffold. Nanomed-Nanotechnol Biol Med 2007;3:311-21.

[31] Horii A, Wang XM, Gelain F, Zhang SG. Biological Designer Self-Assembling Peptide Nanofiber Scaffolds Significantly Enhance Osteoblast Proliferation, Differentiation and 3-D Migration. PLoS One 2007;2:9.

[32] Garreta E, Genove E, Borros S, Semino CE. Osteogenic differentiation of mouse embryonic stem cells and mouse embryonic fibroblasts in a three-dimensional self-assembling peptide scaffold. Tissue Eng 2006;12:2215-27.

[33] Yamaoka H, Asato H, Ogasawara T, Nishizawa S, Takahashi T, Nakatsuka T, *et al*. Cartilage tissue engineering chondrocytes embedded in using human auricular different hydrogel materials. Journal of Biomedical Materials Research Part A 2006;78A:1-11.

[34] Kisiday J, Jin M, Kurz B, Hung H, Semino C, Zhang S, *et al*. Self-assembling peptide hydrogel fosters chondrocyte extracellular matrix production and cell division: Implications for cartilage tissue repair. Proceedings of the National Academy of Sciences of the United States of America 2002;99:9996-10001.

[35] Misawa H, Kobayashi N, Soto-Gutierrez A, Chen Y, Yoshida A, Rivas-Carrillo JD, *et al*. PuraMatrix (TM) facilitates bone regeneration in bone defects of calvaria in mice. Cell Transplant 2006;15:903-10.

[36] Ellis-Behnke RG, Liang Y-X, David KC, Kau PWF, Schneider GE, Zhang S, *et al*. Nano hemostat solution: immediate hemostasis at the nanoscale. Nanomed-Nanotechnol Biol Med 2006;2:207-15.

[37] Zou Z, Zheng Q, Wu Y, Guo X, Yang S, Li J, *et al*. Biocompatibility and bioactivity of designer self-assembling nanofiber scaffold containing FGL motif for rat dorsal root ganglion neurons. J Biomed Mater Res Part A 2010;95A:1125-31.

Chapter 3

Literature Review

Ionic self-assembling Peptides: A Summary of Design Strategies, and Biocompatibility Evaluation

Abstract

(RADA)$_4$ peptide based ionic self-assembling peptides have been investigated for an array of applications such as: drug delivery carriers, extracellular matrices, nanofabrication models, hemostatic agents, as well as in three dimensional cell cultures and tissue engineering. This wide array of biomedical applications is primarily possible due to their underlying physicochemical characteristics, as well as biocompatibility. These peptides are also known to possess a high hydration (up to 99.5%), can be tuned to response to the physiological environment, can be either biomimetic or *de novo* designed. This review critically examines and reports the efforts made so far in understanding the self-assembling mechanism of these peptide based nanofibers, and the biocompatibility analysis conducted for the ultimate use in human body. Here, we also elaborate on various techniques employed to conduct secondary structure analysis, hydration studies, and

biocompatibility studies on the self-assembling peptides. As well as, we provide a review of other relevant techniques followed by a brief discussion of current opinions, on both the theoretical as well as experimental aspect of the techniques.

Keywords: Self-assembling peptide, Biomaterials, Hydrogels, Biocompatibility, Hydration, Secondary Structure

3.1 Introduction: Ionic Self-Assembling Peptides

"Human subtlety will never devise an invention more beautiful, more simple or more direct than does nature because in her inventions nothing is lacking, and nothing is superfluous."

~ Leonardo Da Vinci

(1452-1519)

Self-assembly is a ubiquitous phenomenon in nature, responsible in the formation of spontaneously associated well-defined structures both at micro- and macro- scales. Naturally occurring self-assembled structures can sometimes provide excellent inspiration to design and construct functional biomaterials [1]. Patterns and recognizable structures are common in nature. From how snowflakes are shaped to how bubbles assemble in a very recognizable form; objects seem to "put themselves together" in a very functional manner. This naturally occurring ubiquitous process is generally known as self-assembly. There lacks a consensus to specifically mark the beginning of this self-assembling process, as this phenomenon is possibly older than the life itself. Physicists would propose the spiral shape of the galaxy resulted from the self-assembly as much as a biologist would argue the molecular basis of the DNA itself being a product of self-

assembly. Hence, for the purpose of our article we are considering the definition of the self-assembly process as:

"Self-assembly is the spontaneous formation of organized structures [at all scales] through a stochastic process that involves pre-existing components, that is reversible, and can be controlled by proper design of the components, the environment, and the driving force"[2].

Also, as a general consensus, self-assembly can be further divided into a static and dynamic process.

"Static self-assembly is a subclass of the self-assembly processes that leads to structures in either local or global equilibrium, reducing its free energy whereas dynamic self-assembly leads to stable non-equilibrium structures"[2]. Additional characteristics of these two processes are given in Table 3.1.

Table 3.1: Primary Classes of Self-assembly Processes

Static Self-Assembly	Dynamic Self-Assembly
System does not dissipate energy	System does dissipate energy
Formation of the ordered structure may require energy, but results in a stable end product	The higher ordered structures are dynamic in nature
Plethora of research has been/is being conducted in this area	Research in this area is at its infancy
Primary examples include: Molecular crystals, globular proteins [3]	Primary examples include: patterns formed by the competition between reaction and diffusion in oscillating chemical reactions, and biological cellular systems [4, 5]

Further, self-assembly possesses three distinct features: order, interactions, and building blocks. Whereas, order pertains to the assembly of smaller subunits into a higher ordered structure, interactions involve covalent and non-covalent interactions (weak non-covalent

13

interactions being the primary force beside complementarity of the structure in molecular self-assembly), and building blocks can be any molecular/nano-level entity, which self-assembles into a larger structure. Also, the two primary approaches to producing structures in nanotechnology are: top-down and bottom-up. Top-down process pertains to concept of creating nanostructured systems by removing the excess portion of bulk material *via* physical, chemical, and mechanical means, whereas bottom up approach begins with the individual building blocks (at nanometre scale), which further assemble into higher order nanostructures with desirable characteristics (Figure 3.1).
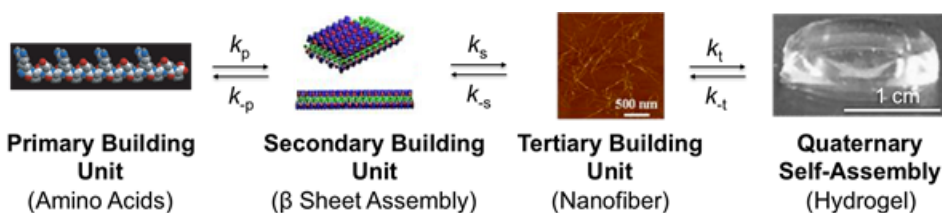
Figure 3.1: Proposed Scheme of General Self-Assembly Using (RADA)₄ Peptide.

The primary building unit ((RADA)$_4$ peptide consisting 16 amino acids), self-assembles into a more stable secondary building unit (β-sheet containing a polar (hydrophilic) and a non-polar (hydrophobic) surface). This first level of self-assembly involves the fine balance of several forces (here, ionic bonds, hydrogen bonds, and hydrophobic interactions). The nanofiber secondary unit further stabilizes itself in to a tertiary building unit, as nanofibers, upon the exposure to physiological salt concentration. These small nanofiber fragments then assemble into 3D scaffolds (hydrogel), characterizing quaternary self-assembly. The resulting hydrogels are formed from interwoven nanofiber matrices with very high water content.

(Adapted from Hauser. *et. al.* [6])

Self-assembling peptide amphiphiles have been actively used as peptide "lego" for the bottom-up creation of higher order stable and fine structures. This category of the peptide "lego" spontaneously assembles into well-formed nanofibers at the molecular level. The first member of peptide lego class was discovered from a segment of left-handed Z-DNA binding protein of yeast, Zuotin [7], which resulted in the development of a β-sheet forming class of self-assembling peptides.

The information gained through understanding the self-assembling characteristics of these peptides may assist to clinically control certain disease spreading by directing the self-assembly of their β-sheet containing undesirable amyloidal proteins found in various diseases, such as: Alzheimer's [8], diabetes mellitus (type II diabetes), prion diseases, familial amyloidosis, and light chain amyloidosis [9, 10]. Amyloid self-assembly in these diseases consists of a transition of the aggregated proteins from their normal fold into a predominantly β-sheet secondary structure, which is also presumed to be a generic structure for aggregated proteins in multiple diseases [8-12]. The basic amyloidogenic unit found in these proteins is thought to be the IAPP polypeptide [12, 13], consisting predominantly of aromatic residues. Current strategies targeted towards controlling the self-assembly of these β-sheet prominent peptides involve the physical/chemical blockage of assembling process by blocking π-stacking, using small molecules consisting of aromatic or electrostatic entities to stop the propagation of self-assembly, or involving β-sheet breakers to hinder the stacked assembly of the resulting peptides. However, despite the massive clinical significance of the amyloid formation process, no mechanism for their self-assembly (based on the underlying amino acids) have been identified so far.

This chapter provides a critical review of molecular self-assembly mechanisms of peptide forming β-sheet driven secondary structures, which later inter-molecularly self-assemble into supramolecular three-dimensional quaternary structures. In particular, we focus on the self-assembling mechanisms of (RADA)$_4$ based peptides. We explore contributing forces (such as hydrogen bonding, π-π stacking, Van der waals and electrostatic), and various factors (such as temperature, pH, amino acid length and type) affecting the self-assembly of these ionic amphiphilic peptides. Here we also provide comparative study of various techniques which can be used to analyze the secondary structure formation of peptides, conduct hydration state analysis, as well as we provide an overview of techniques employed the *in-vitro* evaluation of these self-assembling peptides. The ultimate goal of this chapter is to synthesize a list of self-assembling techniques for controlling and manipulating system characteristics at the molecular level, with the aim of constructing practical and functional engineered systems. We also provide an overview of techniques employed the *in-vitro* evaluation of self-assembling peptides.

3.1.1 Recent Works on Naturally and Synthetic Injectable Biomaterials

3.1.1.1 Naturally Derived Hydrogels

Naturally occurring polymers can be categorized as being composed of protein (collagen, gelatin, fibrin), polysaccharides (chitosan, hyaluronic acid, alginate, and agarose), DNA, or a combination of thereof. Collagen is one of the most abundant proteins of the connective tissue, and is secreted by fibroblasts and epithelial cells [14]. Collagen has a high tensile strength, as well as influences cell proliferation, adhesion, migration, differentiation, polarization, therefore participating in critical biological functions such as development, tissue maintenance,

16

regeneration, and repair. For commercial purposes collagen is usually extracted from amniotic membrane, where it is known to have desirable characteristics such as anti-inflammatory, anti-bacterial, anti-fibrosis, anti-scarring, low immunogenicity and reasonable mechanical features [15]. The most common application of collagen is providing extracellular matrix components as native scaffolds for cell support in tissue engineering. One of the biggest challenges with collagen is that it lacks comparable mechanical strength as the articular cartilage [16]. Elastin is another protein based injectable biomaterial studied as *in situ*-gelling hydrogels. The gelling mechanism of elastin-mimetic polymers is a result of the change in structure that occurs for the pentapeptide sequence (GVGVP)$_n$ above a critical temperature, which is known to undergo gelation above critical temperatures. One of the major limitations of elastin (and of the majority of naturally-derived biomaterials (Table 3.2)) is potential immunogenicity from trace protein contaminants and possible pathogen transmission [17]. Fibrin and fibrinogen play a significant role in blood clotting, the inflammatory response, cell-matrix interactions, wound healing and neoplasia, therefore making them attractive biomaterials [18]. Fibrin based hydrogels have been employed as tissue engineering scaffolds in adipose, cardiovascular, ocular, muscle, liver, skin, cartilage and bone tissues [18]. Fibrin hydrogels along with chondrocytes have shown promise for culturing cartilaginous matrix, both in *in-vitro* and *in-vivo*. Some of the major disadvantages of fibrin-based hydrogels are poor mechanical characteristics, and rapid enzyme-catalysed degradation. Gelatin retains the cell signalling sequence of its precursor collagen (RGD), which promotes cell adhesion, differentiation, and growth. Also, in comparison to collagen, gelatin displays lower antigenicity [19]. Gelatin-based scaffolds are used for osteochondral tissue engineering, as well as gelatin microparticles are used as carriers for delivery and local release of cells and growth factors [20].

17

Some of the most popular polysaccharides based naturally derived hydrogel systems are chitosan, hyaluronic acid, alginate and agarose. Recent work on these polysaccharide-based biomaterials have been reviewed by Oliveira and colleagues [21]. Chitosan is produced by the deacetylation of chitin. The deacetylation regulates its physicochemical properties (such as crystallization, and charge density), and is usually found to be ranging from 50-90% in the commercially available chitosan products [22]. Chitosan based hydrogels offer many advantages as naturally derived biomaterials, such as: biocompatibility, biodegradability, no pathologically induced inflammatory response, no induced infection/endotoxin, intrinsic antibacterial ability, and low immunological reactions [23]. Moreover, its amine groups provide further flexibility for chemical modifications for bioactivity and biofunctionalities (such as controlled degradation of chitosan by N-acetylation [24]). Also, chitosan and its degradation products can be repurposed in the synthesis and maintenance of components in articular cartilage (including chondroitin sulphate, hyaluronic acid, and type II collagen). However, one of the major limitations of chitosan is its insolubility in neutral solvents, and so far aqueous solutions of chitosan can only be obtained in acidic solutions with the protonation of $-NH_2$ group [25]. The improvement of the solubility of chitosan-based hydrogels through chemical modification still remains a current challenge. Hyaluronic acid (HA) is another polysaccharide-based biomaterial, which is naturally found in cartilage, synovial fluid, and the vitreous humor of the eye. HA immobilizes water in cartilage ECM structure and are largely responsible for the viscoelastic characteristics and lubrication of cartilage, which has applications in controlling osteoarthritis. Moreover, low and high molecular weight HA moieties may result in pro- and anti-inflammatory responses, respectively [26]. HA is known to play an important role in protein adhesion, cartilage regeneration [27] and providing attachment sites between chondrocytes and the ECM [27].

18

However, HA based hydrogels are limited in applications as they lack the adequate mechanical strength to survive the *in-vivo* applications. The challenge to significantly improve HA's mechanical properties, while retaining all the bio functions still remains. Alginate is another valuable naturally derived polysaccharide due to its biocompatibility, degradability, and low immunogenicity [28]. Current applications of alginate consist of scaffolds for neural tissue engineering, drug, protein/enzyme [29], and cell delivery, protein immobilization [30] and [31] bone and cartilage tissue engineering [32]. The gelation kinetics of alginate can be controlled by the concentration of divalent cations (such as calcium, barium and strontium) [28]. As the case with other polysaccharide based hydrogels one of the main limitations of alginate is its low mechanical strength compared to the native articular cartilage [33]. Despite the on-going efforts, limited improvement in mechanical strength of these hydrogels has been achieved, but at the cost of loosing biological functions (such as support of regeneration of cartilage tissue *in-vitro* culture with chondrocytes [34]).

Even though the naturally derived biomaterials are deemed biocompatible, biodegradable, and possess critical biological function, there are still a lot of concerns that remain. Most of the naturally derived hydrogels lack the required mechanical strength for their applications. Other factors such as issues of potential immunogenicity from trace protein contaminants and potential pathogen transmission remains. Further, technology still needs to be developed to overcome the batch-to-batch production variability of these biomaterials, which ultimately affect their gelation kinetics, and pore size/structure (imperative for cell encapsulation, and proliferation). Recent techniques exploring hybrid materials entailing functionalization: blending, crosslinking, and/or copolymerization are being used to combat these limitations. However, due these existing

disadvantages of the naturally derived biomaterials, synthetic biomaterials pose an attractive alternative.

Table 3.2: Characteristics of naturally derived hydrogels

	Naturally Derived Hydrogels	Origin	Gelation mechanism	Applications	Advantages	Limitations	Ref
Protein Based[a]	**Collagen (Type I)**	• Extracellular matrix protein	• Temperature and pH responsive gelation	• Tissue augmentation • Corneal shields • Hard and soft tissue implants • Drug delivery matrices • Release of therapeutic proteins • Tissue engineering scaffolds	• Favourable cell matrix interactions • Cell binding • Proteolytic degradation • GF binding • Biocompatible	• Pathogen transmission • Inability to tune final gel properties • Low tensile strength *in-vivo* for surgical applications	[35-37]
	Elastin	• Extracellular matrix protein	• Temperature responsive gelation	• Drug Delivery • Protein purification • Polymeric micelles • Biosensing	• Favourable cell matrix interactions • Mimics ECM • Support growth ad migration of cells during regeneration • Cell binding • Proteolytic degradation • GF binding • Can be produced as monodispersed polymer	• Pathogen transmission • Insoluble in water	[38, 39]
	Fibrin	• Globular protein present in the clotting cascade	• Gel formation occurs by changing the substrate concentration, addition of divalent cations (Ca^{2+}), pH and Temperature	• Tissue engineering scaffolds • Fibrin sealants • Functionalized fibrin (with transglutaminase crosslinking enzyme) • Fibrin adhesive • Cell migration • Wound healing	• Biocompatibile • Biodegradable • Underlying monomer is non-toxic • Can biologically interact with cells	• Virus transmission • Batch to batch variability • Rapid enzyme catalyzed degradation	[40, 41]
	Gelatin	• Derivative of collagen	• Ionic and chemical crosslinking	• Cell adhesion, migration, differentiation, and proliferation • Wound dressing • Hemostasis • Tissue engineering • Drug delivery • Sealant for vascular prostheses	• Favourable cell matrix interactions • High hydration • Biocompatible • Non-immunogenic • Low coagulation • Biodegradable	• Rapid enzyme catalyzed degradation • Low thermal and mechanical stability	[42, 43]

Polysaccharide Based[b]	**Chitosan**	• Formed by the n-deacetylation of chitin	• Gel formation occurs in response to the pH change from acidic to neutral • Ionic and or Chemical crosslinking	• Tissue engineering • Non-viral gene transfection agent • Drug delivery • GF delivery	• Inexpensive • Easy to use • Antibacterial properties • Structural similarity with glycosaminoglycan • Biocompatibility • Low toxicity • Degradability by human enzymes • Hydrophilic	• Biocompatibility has not been fully resolved • Extensive purifications required • Low cell matrix interaction • Low stability of ionic cross-linked gels	[44]
	HA	• Extracellular matrix constituent found in many human tissues	• Ionic crosslinking, Chemical crosslinking • Addition and condensation reactions	• Natural would healing process • Angiogenesis • Cellular signalling • Cellular and molecular delivery • Drug delivery • Wound repair • Morphogenesis • Matrix organization • Cartillage tissue engineering	• Biocompatible, Good cell matrix interaction • Non-immunogenic	• Does not form stimulus-responsive hydrogels • Weak mechanical properties • High degree of purification needed to eliminate immunogenicity • Unwanted inflammation of HA • Promotes tumour growth and metastasis	[45, 46]
	Alginate	• Derived from brown algae consisting of two repeating saccharide units (L-guluronic acid and D-mannuronic acid)	• Forms ionic crosslinks with the addition of divalent cations (Ca^{2+}, Mg^{2+}, Ba^{2+}, and S^{2+})	• Dental impression material, Supports tissue growth (such as cartilage) • Cell encapsulation • Cell transplantation • Wound dressing • Tissue engineering • Drug delivery	• Inexpensive, easy to use • Enhanced wound healing capabilities due to the stimulation of human monocytes	• Unable to specifically interact with host cells and tissues • Potentially immunogenic • Unsuccessful alginate hydrogels with cell-interactive motifs and covalently cross-linked structures • Low cell matrix interactions • Slow degradation rate • Uncontrolled degradation kinetics	[42, 47]

[a] GF, Growth factor

[b] HA, Hyaluronic acid/Hyaluronan

3.1.1.2 Synthetic Hydrogels

In contrast with naturally derived hydrogel materials, the use of synthetic hydrogels have more controllable properties such as degradation and mechanics, and are highly reproducible with less batch-to-batch variation. Synthetic polymers for the purpose of hydrogel formation can be classified into three categories: non-biodegradable, biodegradable, and bioactive polymers (Table 3.3).

Non-biodegradable (which can not be changed into natural harmless state for the environment) hydrogels are prepared from the copolymerization of various vinyl based monomers such as 2-hydroxyehtyl methacrylate (HEMA), 2-hydroxypropyl methacrylate (HPMA), acrylamide (AAm), acrylic acid (AAc), *N*-isopropylacrylamide (NIPAm), and methoxyl poly(ethylene glycol) (PEG) monoacrylate (mPEGMA or PEGMA), with the assistance of crosslinkers. Non-biodegradable hydrogels can also be produced by the self-assembly of Pluronic® polymers [48]. Pluronics® consist of a hydrophobic core and a hydrophilic PEG end blocks, self-assembling into micelles, which in turn result in hydrogel-like micelle networks [48]. One of the most important characteristics of non-biodegradable polymers is the mechanical stability, which can be controlled by the incorporation of crosslinking agents, co-monomers, and increasing the degree of crosslinking [49]. Another widely investigated non-biodegradable polymer is Polytheylene glycol (PEG) has many desirable characteristics as a biomaterial, such as solubility in water and in organic solvents, low immunotoxicity, low protein adhesion and non-immunogenicity [50, 51]. Moreover, the terminal hydroxyl groups of PEG can be further functionalized with various groups (carboxyl, thiol, and acrylate) and bioactive agents [52]. Polyvinyl alcohol (PVA) based synthetic hydrophilic hydrogels have been investigated in tissue-

engineering applications (such as cell adhesion [53] and functional precursors [54]). One of the other non-biodegradable polymers, P(NIPAAm) undergoes gelation in response to the change in temperature (precipitation and crosslinking of networks above the polymer's lower critical solution temperature (LCST) [55]). The gelation of the polymer leads in the formation of a highly dense structure as a result of loss of water content (which is imperative for the biocompatibility of these bio-polymers). The thermally controlled swelling/deswelling behaviour of these hydrogels allows them detach cell layers for engineering tissues of cornea and cell sheets [56, 57]. The LCST of this polymer can be tuned by the addition of hydrophilic monomers such as acrylic acid [55, 58].

Biodegradability is a vital characteristic for applications in tissue engineering. Polyesters are most commonly studied as biodegradable synthetic polymers for scaffold fabrications. Some of these polyesters are poly(lactic acid) (PLA), poly(glycolic acid) PGA, poly(ε-caprolactone) (PCL), and their derived copolymers. These copolymers can be crosslinked with the non-biodegradable polymers (mentioned above) for making them biodegradable.

The third category of synthetic polymers is known as bioactive polymers, which mediate cell-specific bioactivities such as cell adhesion, migration and cell mediated biodegradation. Usually bioactive entities are incorporated into synthetic hydrogels to mediate these cell specific functions [59]. These bioactive components can be incorporated in the hydrogel during or after the hydrogel assembly. Some of these hydrogels result with cell-adhesive [60, 61], enzyme-sensitive [62], growth-factor binding [63, 64] characteristics. Bioactive synthetic polymers offer many advantages over the natural hydrogels, such as batch-to-batch consistency, improved control for matrix architecture and chemical composition.

24

Table 3.3: Characteristics of synthetically derived hydrogels

	Synthetic Hydrogel	Gelation mechanism	Applications	Advantages	Limitations	Ref
Non-biodegradable[a]	PEG	• Photo-/co-polymerization • Free radical polymerisation • Condensation	• Bioconjugation • Drug delivery • Tissue engineering • Parenteral, topical, ophthalmic, oral and rectal preparations. • Polymeric matrices in controlled-release	• Chemically stable • Hydrophilic • Water soluble • Biocompatible • Non-immunogenic • Resistance to protein adsorption	• Naturally not biodegradable • Chemically more reactive than fat • Need to be delicately processed • More irritating to mucous membranes than fats • Posses minimal biological activity and low cell viability • Lack of cell specific	[52]
	PNIPAm	• Formation of H-bond between the water molecules and the amide groups. • Hydrophobic interactions between the isopropyl groups of PNIPAm side chain stabalize the structure	• To detach cell layers for engineering special tissues like cornea or cell sheets • pH sensitive drug delivery • Biosensors • Thin films • Tissue engineering scaffolds	• Biodegradable and biocompatible	• Not biodegradable, as the monomeric form is toxic • Poor mechanical properties • Not bioinert • Elastically poor • Slow shrinking/swelling of hydrogels • Hydrogel formulations *in vivo* leads to toxicity	[65]
	PVA	• Physical crosslinking *via* repeated freezing/thawing • Chemical crosslinking with gluteraldehyde or epichlorohydrin	• Tissue engineering applications • Contact lenses • Opthalmic biomaterials • Tendon repair • Drug delivery	• Biocompatible • Resist protein adsorption and cell adhesion • Controlled gelation • Supports cell viability • Can be modified with bioactive • Proteins • Easily degradable • Water soluble • Hydrophilic	• Prone to quick degradation *via* hydrolysis • Has low strength and thermal stability for certain applications • Limited biological performance • Limited mechanical strength	[53, 54]
	Poloxamer/ Pluronic ®	• Physiologically driven	• Drug delivery • Wound healing	• Thermoreversible • Favourable rheological characteristics • Optimal gel strength • Optimal adhesive characteristics • Facilitates drug stabilization	• Solution to gel transition occurs within a large temperature interval • Ophthalmic applications are limited due to agitation • Sublingual administration	[66]

					limitations due to unsuitable adhesion	
Biodegradable[b]	**PLA**	• Chemical and/or physical crosslinking	• Can be photopolymerized to form hydrolytically degradable hydrogels • Small tissue repair, sutures and tissue engineering scaffolds • Drug delivery	• Biodegradable • Easily functionalizable	• Very hydrophobic • Poor interaction with biological environments resulting in undesirable reactions *in vivo*	[67]
	PGA	• Chemical and/or physical crosslinking	• Can be photopolymerized to form hydrolytically degradable hydrogels	• Biodegradable • Biocompatible • Hydrophilic • Favourable mechanical characteristics • Favourable release kinetics	• Stability concerns for protein delivery	[68]
	PCL	• Chemical and/or physical crosslinking	• Can be photopolymerized to form hydrolytically degradable hydrogels • Electrospun material for fabricating tissue engineering scaffolds	• Biodegradable • Biocompatible	• Hydrophobic • Poor wettability • Lack of cell attachment • Uncontrolled biological interactions with the material • Slow degradation kinetics • Lack of bioactivity	[69, 70]
Bioactive[c]	**PEG Based** *Cell-adhesive* *Enzyme-sensitive* *GF-bearing Speciality* *Biofunctional*	• Photo-/co-polymerization • Free radical polymerisation • Condensation • Electrostatic interaction	• Cell specific adhesion • Proteolytic degradation • Signal molecule-binding • Mimics ECM • Guide cell functions and tissue formation	• Biodegradable • High porosity • Non-immunogenic • Easily produced at large scales • Enhanced biological activity • Controlled degradation rate	• Precise control of scaffold architecture and biofunctions • Cell-mediated delivery of GF without burst release	[50-52]

[a] PEG, Polyethylene glycol; PNIPAm, Poly(N-isopropylacrylamide); PVA, Polyvinyl alcohol

[b] PLA, Poly(lactic acid); PGA, Poly(glycolic acid); PCL, Poly(ε-caprolactone)

[c] GF, Growth factor; ECM, extracellular matrix

Individually, neither naturally derived nor synthetically produced polymers are capable of creating an ideal biomaterial with all the desirable characteristics. Naturally derived materials lack the desired mechanical characteristics, whereas the synthetic biomaterials are usually less hydrophilic, lack binding sites for cell adhesion and have undesirable biodegradability. Therefore, modern nanomedicine includes the formation of synthetic and natural hybrid biomaterials; thereby utilizing the best of both kinds of biomaterials; the synthetic component provides tuneable physical properties, while the natural component allows specific biological functions. These hybrid polymers can be easily synthesized on a mass scale, and tailored at a molecular level. These hybrid biopolymers are discussed in the following sections.

3.2 Ionic Self-Assembling Peptides in Aqueous Solutions

The ionic self-complementary peptides consist of hydrophobic and hydrophilic surfaces. The hydrophilic surface consists of alternating positive and negative charged amino acids, usually classified into several individual moduli (modulus I-IV), or a mixture thereof). These moduli are based on charge arrangements as given in the Table 3.4 below.

Currently synthetic self-assembling peptides such as (RADA)$_4$ and (EAKA)$_4$ are being explored as peptide hydrogels due to their excellent biocompatibility and biodegradability, adaptable structure (allowing specific interaction), and nanofibrous structure mimicking naturally occurring ECM [6, 71]. These biodegradable peptides consist of short oligomers containing alternative hydrophilic and hydrophobic amino acids, when further self-assemble into nanofibers containing a hydrophilic side (interacting with the solvent molecules), and a hydrophobic side

(forming a double sheet inside of the nanofiber). These resulting hydrogels serve many functions, such as drug delivery [72], cell encapsulation [73], cell migration [74], and tissue engineering [62]. In-depth applications of particularly (RADA)$_4$ based hydrogels are reported later in the chapter.

The charge orientation can be used in the reverse orientation; yielding an entirely different molecule. The (RADA)$_4$ peptide used in our study belongs to modulus I, as only the (RADA)$_4$ with this particular alternating charge orientation (Table 3.4) has been shown to achieve rapid and complete hemostasis [75, 76]. The (RADA)$_4$ peptide (module I) has hydrophilic and hydrophobic sides to form stable antiparallel β-sheet structures in aqueous solutions. Our study is a further attempt to not only understand this hemostatic capability of the (RADA)$_4$ peptide, but investigate the basic design and characterization of the assembled structures.

Table 3.4: Charge arrangements on the hydrophilic side of the ionic self-assembling peptides.

Modulus	Charge Arrangement
I	- + - + - + - +
II	- - + + - - + +
III	- - - - + + + +
IV	- - - - + + + +

Adapted from the information given by Zhang *et al* [77].

One of the first reported studies of ionic self-assembling peptides is from Zhang's group.

3.2.1 RGD Based Peptide Amphiphiles

It is thought that successful biomaterials entail essential characteristics of naturally occurring entities (biomimetic), is relatively cheap to synthesize, have robust structure, easily

reproducible, simple, and yet provide the ability to make desired changes to the higher ordered resulting structure. With the above stated characteristics in mind, and a specific task of mimicking the extracellular matrix (ECM), a class of RGD based self-assembling peptides has been studied. The tri-peptide RGD sequence was reported in 1984 [78] within the hydrophilic loop of the glycoprotein fibronectin as an independent cell attachment site. This tetrapeptide (RGDS) was also found in other proteins which may interact with cells, such as fibrinogen [79], a surface protein of *Escherichia Coli* [80], and a Sindbis virus coat protein [81]. Out of these proteins fibrinogen is of the most interest due to its interaction with fibronectin [82] and the platelet surface [83, 84]. Hence, the RGD based sequence of fibrin can be expected to participate in some stage of hemostasis by platelets.

Secondary structure analysis of the RGDS tetrapeptide revealed β-turn formation, resulting in a hydrophilic loop at the surface of the molecule, available for interaction with cell surfaces. It was concluded experimentally that the chemically analogous cysteine residue might replace the serine residue of the tetrapeptide sequence without substantial loss in cell attachment. However, the presence of arginine, aspartic acid, and glycine proved to be essential for cell activity [78].

3.3 Designing Strategies For Self-Assembly

The intrinsic characteristics of the naturally occurring 20 amino acids (such as electric charge, steric hindrance of the side chain, pk_a etc.) have been experimentally proven to dictate the type of secondary structure formation of the polypeptide such as α-helix or β-sheet [85]. Precise

understanding of how the amino acid characteristics govern the resulting secondary structure will facilitate design of self-assembling peptides. For instance, charged residues are found predominantly at both of the helical ends, but are absent in the β-sheets. Further, there is a preference of negatively charged residues (D, and E) to exist at the N-terminal helical end, and positively charged residues (H, K, and R) to occur at the C-terminal helical ends [86, 87]. Finkelstein and colleagues [88] concluded that there was no correlation due to interactions between adjacent pair residues in helical and non-helical regions of the non-globular proteins. Moreover, they concluded that the polypeptide secondary structure depends primarily on side-chain interactions with the backbone, rather than side chain-side chain interactions. Chou and Fasman [89], reported the protein conformation parameters for each of the 20 amino acids, by computing the X-ray crystallographic data of 15 proteins, containing 2473 residues. P_α, $P_{\alpha i}$, P_β, P_t and P_c are conformational parameters for α-helix, inner α-helix, β-sheets, β-turns and random coils, respectively. Table 3.5 provides a relative estimation of the particular secondary structure formation potential for each amino acid residue. The results showed that glutamic acid, alanine, leucine, and histidine are most prominent in helical regions; where leucine, alanine, glutamic acid, valine are found mostly in the inner helical cores. While methionine, valine, isoleucine, cysteine are present in the β-sheet formation, and proline, glycine, asparagine, and serine are most frequent coil residues in the proteins tested.

While predicting the amino acid secondary structure it should be considered that helix formation is primarily dependent on the nearest neighbour (as it consists of one hydrogen bond to the fourth nearest neighboring residue), and is a rapid cooperative phenomenon, whereas β-sheet formation has slower kinetics as distant amino acids are brought to close proximity [90]. Inner

helical residues consist of two hydrogen bonds, whereas random coils have no known hydrogen bonds. Moreover, it has been shown (with poly (Y) in water) [91] that coil to β-sheet transition is slower than coil to helix transition.

Table 3.5: Intrinsic characteristics of the naturally occurring L-amino acids.

Theoretically calculated pK_a values of the amino acids are given. Frequencies of α-helical (P_α), inner α-helical ($P_{\alpha i}$), β-sheet (P_β), β-turn (P_t), and coil regions (P_c), with their respective average conformational parameters are given.

Amino Acid	One Letter Code	pK_a (NH$_3^+$)	pK_a (COOH)	pK_a (R-group)	P_α	$P_{\alpha i}$	P_β	P_t	P_c
Arginine*	R	9.00	2.03	12.10	0.79	0.67	0.90	1.00	1.20
Histidine	H	9.09	1.70	6.04	1.24	0.87	0.71	0.69	0.92
Lysine**	K	9.16	2.15	10.67	1.07	1.13	0.74	1.01	1.05
Aspartic Acid*	D	9.66	1.95	3.71	0.98	0.53	0.80	1.26	1.09
Glutamic Acid	E	9.58	2.16	4.15	1.53	1.45	0.26	0.44	0.87
Serine**	S	9.05	2.13	-	0.79	0.70	0.72	1.56	1.27
Threonine	T	8.96	2.20	-	0.82	0.75	1.20	1.00	1.05
Asparagine	N	8.76	2.16	-	0.73	0.53	0.65	1.68	1.33
Glutamine	Q	9.00	2.18	-	1.17	0.98	1.23	0.56	0.79
Cysteine	C	10.28	1.91	8.14	0.77	0.33	1.30	1.17	1.07
Glycine	G	9.58	2.34	-	0.53	0.53	0.81	1.68	1.42
Proline	P	10.47	1.95	-	0.59	0.00	0.62	1.54	1.45
Alanine*	A	9.71	2.33	-	1.45	1.59	0.97	0.57	0.66
Valine	V	9.52	2.27	-	1.14	1.42	1.65	0.30	0.66
Isoleucine	I	9.60	2.26	-	1.00	1.22	1.60	0.58	0.78
Leucine	L	9.58	2.32	-	1.34	1.91	1.22	0.53	0.66
Methionine	M	9.08	2.16	-	1.2	1.25	1.67	0.67	0.61
Phenylalanine	F	9.09	2.18	-	1.12	1.14	1.28	0.71	0.81
Tyrosine	Y	9.04	2.24	10.10	0.61	0.58	1.29	1.25	1.19
Tryptophan	W	9.34	2.38	-	1.14	1.33	1.19	1.11	0.82

The protein conformation parameters are obtained by dividing the frequency of residues in α-helical, inner α-helical, β-sheet, β-turns and coil regions by the average frequency of residues in these respective regions.

*Amino acids involved in the (RADA)$_4$, and **amino acids in the variants of (RADA)$_4$ peptide studied herewith. The P_α, $P_{\alpha i}$, P_β, and P_c parameters were adapted from Chou and Fasman [89], and P_t was adapted from a follow-up study conducted by Chou and Fasman [92]

In a polypeptide consisting both a-helix and β-sheet, α-helix formation is expected to occur before the β-sheet formation, as the experimentally helix initiation has been proven to proceed faster than the β-sheet formation [93]. However, the β-sheet formation will take precedence, over the α-helices, when the P_β is higher than the P_α value [89].

Upon comparing the experimental Zimm-Bragg initiation parameters describing the thermodynamic properties of the coil-helix transitions (from poly (α-amino acids) [94], it can be concluded that the helix nucleation begins at the centres of the helix (where the P_α values are highest), and propagates in both directions, until terminated by strong helix breakers (where P_α values are lowest), at both ends. Also, the central nucleating residue of the helix centre must have both amino and carbonyl groups hydrogen bonded, whereas at the helical ends only one hydrogen bond formation is necessary. Similarly, amino acids with the highest P_β values initiate β-strand/turn formation, and residues with the lowest P_β values are expected to terminate the propagation. Glycine, proline, tyrosine and asparagine are considered strong helix breakers, whereas leucine is a strong helix former (Table 3.6). The studies by Chou and Fasman [89, 92] provide a good extrapolative model for secondary structure prediction, and can be summarized as the following set of general predictive rules:

I)   Helical Structure Formation

- Four subsequent helical residues (H_α or h_α or $2I_\alpha$) mark the helix nucleation site (provided there are $\leq 1/3$ helix breakers (B_α or b_α), and $\geq \frac{1}{2}$ helix formers, in the polypeptide chain). Please refer to the Table 3.6 for further description of these values.

- The helix propagation stops in _both_ the directions in the presence of tetrapeptides with $<P_\alpha>$ less than 1.00, or if there is a β-region initiation.

- Proline does not exist at the C-terminal end or in the inner helix.

- Amino acids proline, aspartic acid, and glutamic acid are found at the N-terminus of the helix; whereas histidine, lysine and arginine are found at the C-terminus.

- Overall, a polypeptide chain of six or more amino acids with $<P_\alpha>$ more than 1.03, and $<P_\alpha>$ greater than $<P_\beta>$, and satisfying the above stated conditions is expected to result in a successful helix formation.

II) Beta Region Formation

- Three subsequent β residues (H_β or h_β) indicate the nucleation of a β-sheet (provided there are $\leq 1/3$ β-sheet breakers (B_β or b_β), and $\geq \frac{1}{2}$ β-sheet formers, in the polypeptide)

- The β-sheet can be expected to terminate in _both_ the directions in the presence of tetrapeptides with $<P_\beta>$ less than 1.00, or if there is a α-helix initiation.

- N-terminus of the β-sheet rarely contains charged residues, and their presence is also very uncommon at the C-terminus, as well at the inner β-region. Tryptophan occupies the N-terminus of the β-sheet.

- Overall, a polypeptide consisting of five or more residues with $<P_\beta> \geq <P_\alpha>$, and abiding by the conditions stated above result in a β-sheet.

Although these studies [89, 92] provide a basic model to predict amino acid secondary structure, it should be noted that the study was limited to peptides from 50-300 amino acid chain length [92], and also does not test the effect of temperature or pH on change in these

conformations. The study also attempted to deduce the helix and beta sheet initiation amino acids, however due to a high variability of conditions (such transitioning into another structure), it remained inconclusive. Computational methods [95] can also be used to predict the secondary structure in peptides, however the computed values (derived from the X-ray crystallography) [89, 92], have proven to be more accurate. Moreover, Chou and Fasman [92] stated that their statistically driven predictive modelling is more accurate than the results from CD spectra, however there fail to provide any scientific evidence. Also, there needs to be additional investigation done to understand the impact of environmental factors (such as solvents, pH, salt, and temperature) on the $<P_\alpha>$ and $<P_\beta>$ values, as it has been proven that the organic solvents can propagate a conformational change from β-sheet to α-helices [96], and from α-helices back to β-sheets [97].

Table 3.6: Amino acids in their hierarchical order in their helical and beta-region assignments.

Amino Acid	P_α	Helical Assignment	Amino Acid	P_β	β-Sheet Assignment
Glu	1.53	H_α	Met	1.67	H_β
Ala	1.45	H_α	Val	1.65	H_β
Leu	1.34	H_α	Ile	1.60	H_β
His	1.24	h_α	Cys	1.30	h_β
Met	1.20	h_α	Tyr	1.29	h_β
Gln	1.17	h_α	Phe	1.28	h_β
Val	1.14	h_α	Gln	1.23	h_β
Trp	1.14	h_α	Leu	1.22	h_β
Phe	1.12	h_α	Thr	1.20	h_β
Lys	1.07	I_α	Trp	1.19	h_β
Ile	1.00	I_α	Ala	0.97	I_β
Asp	0.98	I_α	Arg	0.90	i_β
Thr	0.82	I_α	Gly	0.81	i_β
Arg	0.79	I_α	Asp	0.80	i_β
Ser	0.79	I_α	Lys	0.74	b_β
Cys	0.77	I_α	Ser	0.72	b_β
Asn	0.73	b_α	His	0.71	b_β
Tyr	0.61	b_α	Asn	0.65	b_β
Pro	0.59	B_α	Pro	0.62	b_β
Gly	0.53	B_α	Glu	0.26	B_β

H_α, and H_β are strong α helical and β region formers; h_α, and h_β are α helical and β region formers; I_α, and I_β are weak α helical and β region formers; i_α, and i_β are indifferent to α helical and β region formation, b_α, and b_β are α helix and β region breakers; whereas, B_α, and B_β are strong α helical and β region breakers, respectively.

The P_α and P_β values are adapted from Chou and Fasman [89], whereas the helical and beta region assessment is adapted from their later study[92].

It has been proposed that helixes are longer than the β-sheets, as when the first turn of the helix is formed the rest of the structure propagates easily and rapidly in a zipper-like mechanism. Whereas, β-sheet has a more stable conformation (poly (α-amino acids), and form thermodynamically stable structures, such as silk fibroins. Moreover, if an ionic peptide consists

of 50% of charged residues, with alternating hydrophobic moieties, the peptide results in distinct polar and non-polar surfaces, ultimately forming a β-sheet prominent structure [98-100]. Further, it has been suggested that increasing the length of the ionic-complementary peptide (and keeping the composition consistent) further stabilizes the macroscopic structure [98, 99]. If the peptide is only composed of one type of charged amino acids (negative or positive), combined with the alternating hydrophobic amino acids (such as V, F or Y), it does not self-assemble into a macroscopic peptide matrix. Instead, these peptides result in disordered precipitates in the presence of salts or pH changes [101-103]. However, when the aromatic phenylalanine residues are inserted in the (RADA)$_4$ peptide, successful β-sheet formation was observed [104]. It was found the not only the insertion of phenylalanine residues but also the position of these added residues does not affect the hydrogen bonding supramolecular antiparallel β-sheet formation. However, it was found that RADAFI (with modulus I, Table 3.4) readily forms the tape-like and spirally twisted interconnecting network structures, whereas the self-assembly of RADAFII (with modulus II, Table 3.4) nanostructures was significantly slower, and lead to shorter nanofiber formation. It was established that the branching of fibrils defined the spontaneous growth of the RADAFI systems, and the self-assembly of these nanofibers included both elongation, and thickening of fibers almost simultaneously, ultimately twisting to form the interconnected elastic 3D structures. It was also concluded that the central phenylalanine residue substantially increased the stability of the twisted β-sheet fragments, thereby accelerating the network formation. The strength of both the phenylalanine consisting RADA systems was higher than the pristine RADA peptide, indicating that introducing a phenylalanine residue creates stronger network by the virtue of the additional π-π interactions. The supramolecular helical structures of both variants consisting of phenylalanine residue was explained as a result of a combination of an increase in

the overall hydrophobicity, π-π stacking due to the center phenylalanine residues, as well as the hydrogen bonds [104].

3.4   Contributing Forces in Self-Assembly

Self-assembly is spontaneous association of molecules, achieved in thermodynamically favourable conditions. This thermodynamic equilibrium is attained with the balancing of attractive and repulsive forces in the molecular system. Some of the major forces responsible for molecular self-assembly are given in Table 3.7. However, it should be noted that these forces vary from system to system. Since, none of the strong chemical bonds are involved in self-assembly, the predominant driving forces consist of hydrophobic attraction and electrostatic repulsion forces [105].

Table 3.7: Driving forces of molecular self-assembly

Attractive Force	Repulsive Force
Van der waals	Electric Double-Layer
Solvation	Solvation
Depletion	Hydration
Bridging	Steric
Hydrophobic	
π-π Stacking	
Hydrogen Bond	
Coordination Bond	

Adapted from Lee [105] (2008)

For the formation of an organized and hierarchical three-dimensional structure a third class of force is involved; this force is known as directional/functional force. As the name implies, this force helps in providing a direction of self-assembly to form well-defined higher

order structures. In the absence of this directional/functional force a one step self-assembly process usually results in the formation of random and non-hierarchical aggregates. Lee [105] proposes this hierarchical step-wise pattern consists of a primary building unit (e.g. amino acids), for the initial step of self-assembly. This primary unit is controlled by the balance between the intermolecular and colloidal forces. The resulting structure/aggregate formed (e.g. β-sheets) are the primary self-aggregates, and can act as building units (secondary building units) of the subsequent (secondary) self-assembly process (e.g. nanofibers). The resulting secondary self-aggregate can be the building unit of the next self-assembly process. Provided the primary forces in this process are molecular/colloidal forces, further assembly of the structures (e.g. 3D hydrogel) is possible as tertiary and quaternary self-assemblies (Figure 3.1). It is thought that the attractive forces are primarily responsible for the initial self-assembly, whereas the repulsive opposition forces drive the subsequent force balance [105].

It is found that proteins with hydrophobic and hydrophilic surfaces usually have their charged residues exposed to the outer surface offering favourable interactions with water, whereas the hydrophobic residues are hidden facing away from water. It is also noticed that structural complementarity and local interactions primarily drive the formation of secondary structures such as α-helix, and β-sheet, prior to forming any tertiary/quaternary self-assemblies [1].

It has been hypothesized, especially for the ionic-complementary (RADA)$_4$ peptide self-assembly that the assembly of these peptides to three dimensional matrices occur in the following steps, however direct experimental observations still remain pending:

1) The primary step for this type of self-assembly is the intermolecular hydrogen bonding between peptide backbones, 2) formation of the intermolecular ionic bonds from the side chains of one face of β-sheet, with positively and negatively charged residues, 3) formation of hydrophobic interactions between the alanine groups and methyl groups on the other face of the β-sheet 4) formation of the overlap interactions between the individual peptides, and 5) coordination by salt ions between the intermolecular ionic groups [106].

3.4.1 Hydrogen Bonding

Hydrogen bonding is a strong and directional intermolecular interaction, with the increase in the dielectric constant of water as it transforms into ice (unlike typical polar molecules). Hydrogen bond strength in comparison with other bonds is illustrated in Figure 3.2. Hydrogen bond is formed when highly electronegative atoms i.e. fluorine, oxygen, and nitrogen are covalently bonded with hydrogen, forming a polar molecule.
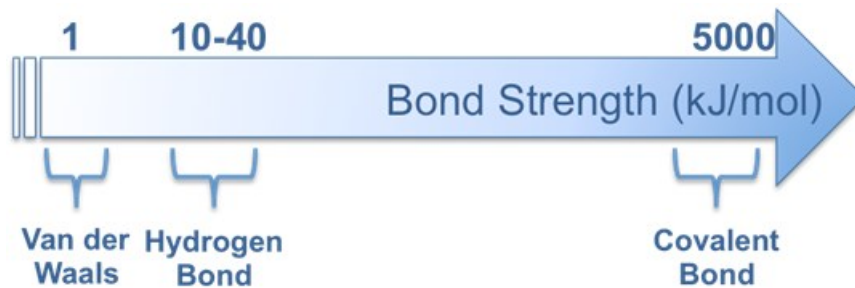
Figure 3.2: Illustration of relative strength of various kinds of bonds.

The bond strength is an approximation, and water-water hydrogen bond falls in the range of ~12-20kJ/mol.

The intramolecular O-H distance is comparable to that of a covalent bond (0.10 nm), but the intermolecular O-H distance (0.176 nm) is much less than the summation of two van der

Waals radii but still larger than the covalent distance. Hence the intramolecular hydrogen bond is thought to be covalent in nature [107]. The directionality (due to the interaction site) sets hydrogen bonding apart from other bonds, and results in different types of hydrogen-bonded structures, such as: linear chains, rings, dimers, layered sheets, and three dimensional structures. For self-assembling molecules (such as DNA (deoxyribose nucleic acid), RNA (ribonucleic acid) and peptides (such as $(RADA)_4$ intramolecular hydrogen bonding provides structural integrity [105]. Hence, hydrogen bonding plays an instrumental tool in the amphiphilic packing of the self-assembling peptide to higher order structures, such as hydrogels.

It was initially thought that the hydrophobic interaction between the aliphatic carbon tails of the amphiphilic peptides were the primary driving force for their self-assembly [108]. However, further investigations revealed the β-sheet formation between the peptide regions of a molecule is a crucial factor in self-assembly instead [109, 110]. Hence, particular attention has been devoted to the importance of the hydrogen bonding to the stability of the nanofibers, as well as the effect on the nanostructural morphology. It has been shown experimentally [111] that the hydrogen bond formed by the (four) amino acids immediate to the hydrophobic core of the amphiphilic peptide is the most important for the self-assembly and final nanostructure as compared to those at the periphery. These amino acids in the interior of the resulting nanofiber stabilize the hydrogel structure by the formation of β-sheets, as their conformational freedom is more restricted in the densely packed core regions. It was also noted that the hydrogen bonding directly correlated to an increase in storage modulus, and β-sheet formation, pertaining to a stronger gel formation (assessed by oscillatory rheology, and macroscopically). Whereas, methylated residues (thereby preventing hydrogen bonding) resulted in a random coil formation

(observed *via* CD), even after lowering the pH or by adding Ca^{2+} ions, suggesting the reduction in strength, average length, quantity of nanofibers, and/or quality of cross links between the between the fibers upon methylation of the core residues. Additionally, it was found that the critical number of hydrogen bonds for the stabilization of amphiphillic nanostructure is four, as upon blocking these potential hydrogen bonds, the energy of the remaining ones is insufficient to stabilize the supramolecular aggregates in a hydrogel formation. However it should be noted that the study only involved one type of amphiphiles (with the hydrophobic alkyl tail, with an amphiphilic RGD based head group appended with a glycine linker), and more studies on other amphiphillic peptides are necessary to gain conclusive evidence. Nevertheless, the study [111] provided valuable information to manipulating hydrogen bonding for the formation of desired higher ordered structures, with a preferred geometric preference.

There have been various other hydrogel designs proposed in the literature, which utilize the inter- and intra-molecular ability of the underlying amino acids to form hydrogen bonds. Rusli and co-workers [112] report the formation of cellular whisker/poly(vinyl acetate) nanocomposites *via* the intramolecular hydrogen bonding. Ghoussoub and colleagues [113] report the formation of reversible pH-responsive hydrogels formed with potassium stabilized association of bis-guanine telechelic (PEG) polymers. Inter- and intramolecular hydrogen bonding has also been proven to embark a shape memory effect (stretching and drying of water-swollen nanocomposites) on self-assembling cellulose based nanowhiskers (CNWs) [114]. A plethora of information is provided by the reviews conducted by Habibi and colleagues [115] on structural analysis of hydrogen bonding involved self-assembling peptides.

3.4.2 π-π Stacking

The π-stacking interactions pertain to the attractive covalent interactions among the π bond containing aromatic constituents. The steric constrains resulting in the formation of these ordered stacking structures have a prominent role in the self-assembly processes resulting in the formation of 3D supramolecular structures [116-119].

The π-interactions play an important role in the self-assembly of the DNA, and RNA molecules. There is plethora of research [119-124] reporting the incorporation of aromatic components in conjunction with peptides for self-assembly, which takes advantage of the π-π interactions among other forces to stabilize the resulting 3D structure. One such system consists of N-fluorenylmethoxycarbonyl diphenylalanine (Fmoc-FF), which forms fibrous hydrogels under physiological conditions [125]. The following conditions for successful self-assembly of the Fmoc-FF, and thereby for other aromatic peptides were proposed after conducting an array of spectroscopic techniques: primarily, the peptide moiety of the molecule should consist of an anti-parallel β-sheet arrangement. Secondly, the aromatic (fluorenyl) rings should be arranged for π-stacking *via* an anti-parallel arrangement with another, within the structure [125]. This arrangement facilitates the surface exposure of bioactive ligands such as epitopes and enzyme cleavable linkers, increasing the biological availability of these peptides, for 3D cell cultures [120] and enzyme-responsive hydrogels [126].

The proposed structure of Fmoc-FF can only be satisfied with the formation of a cylindrical structure formed *via* interlocking the lateral π- π interactions of four twisted anti—parallel β-sheets. Subsequently, these cylinders are expected to line up side-by-side to form a flat

ribbon [125]. It should be noted that this proposed 3D structure has limited general validity, as other peptide consisting of different aromatic amino acids should be tested.

Beta-sheet prominent amyloid fibrils also rely on the interactions between aromatic units, for molecular recognition and self-assembly [116-119]. It has been experimentally proven that stacking interactions provide energetic contributions, as well as order and provide directionality in the self-assembly of amyloid structures. It has been proposed that the most likely way of π-stacking in amyloid fibrils involves a parallel-displaced π-stacking, resulting in the aromatic rings in an off-cantered parallel orientation, and the overall structural organization is driven by the restricted geometries of the stacking interactions [119].

The ionic self-assembling peptide (RADA)$_4$ has been modified with the addition of phenylalanine residues at different positions (RADAFI and RADAFII) to study the effect of aromatic residues on the peptide's self-assembly. It was concluded that the presence of a centre π-π stacking between the two β-sheet forming strands play a vital role in promoting the twisted nanofiber morphology, resulting in a stronger nanofiber network. Moreover, effective entrapment of the molecules containing the phenyl group though π-π interaction was witnessed in both the (RADA)$_4$ peptides containing the phenylalanine residues [104]. Even though the study [104] provides valuable information on π-stacking in the self-assembly of aromatic RADAF peptides, they fail to put the structural, and rheological parameters in perspective by comparing it with the pristine (RADA)$_4$ peptide.

3.4.3 **Hydration and Hydrophobic Forces**

Hydration force is defined as a repulsive force occurring between different electrostatically charged molecules, especially when the molecules are in close proximity of each other in aqueous media. The term was coined for the first time in 1970s [127] to describe the forces responsible for the swelling of electrically neutral phospholipid bilayers in distilled water. The hydration force is repulsive when interacting with the hydrophilic surfaces, and attractive when surfaces are hydrophobic in nature. Furthermore, the primary hydration force pertains to the enthalpic adsorption energy of successive water layers to an interface, resulting in the reduction of its entropy, whereas the secondary hydration force is associated with weaker interactions, often with larger decay lengths [128]. In the case where the hydrated solute is a counterion, the decay of secondary hydration force is naturally the Debye or the Gouy-Champan length (Figure 3.3) linked to the relaxation length of surface solvation. Hydration is perceived as a force between bodies much larger than the water molecules that hold them together [128]. This seemingly benign force can produce osmotic stress with a pressure of ~ 1000 atm, usually with an exponential decay lengths of 2-4Å [129]. Especially, in considering intermolecular forces in water, solvation is an imperative force required for the stability of the resulting structures. It has been experimentally shown that solvation of non-charged polar groups sustain lower energies, whereas charged or neutral polar surfaces have their hydration forces varying exponentially, with a decay length close to the molecular size of the solvent [128]. Molecular dynamics simulations of β-sheet forming peptides have proven that hydrophobic contacts precede the growth of backbone hydrogen bonds [130].

While it is well accepted that the water (hydrophobic effect) plays a significant role in peptide self-assembly in water, the precise underlying mechanism of hydration forces facilitating this assembly, remain controversial. When two strongly hydrophobic surfaces (as in the case of (RADA)$_4$ nanofibers), are brought together to a critical distance, it has been postulated that a "dewetting" transition occurs between the two surfaces, and the resulting vacuum drives the subsequent self-assembly or hydrophobic collapse. This phenomenon has been theoretically proposed [131], and the critical role of "dewetting" in the hydrophobic effect has been studied using analytical theories and simulations of simple solutes [132-135], and protein systems [136, 137]. It has been proven *via* simulations that when two strongly hydrophobic nanoscale plates are brought together to a separation sterically feasible to accommodate more than one layer of water between them, the water is expelled [138]. Moreover, fully atomistic simulations have shown that water not only drives the assembly, but also rather facilitates proper packing of the hydrophobic surfaces in the final stages of assembly (as shown in Figure 3.1) [139-141].

The simulations on the antiparallel β-sheet forming AB 16-22 peptide (Ac-K^{16}-L^{17}-V^{18}-F^{19}-F^{20}-A^{21}-E^{22}-NH$_2$) [142] (where the superscripts pertain to the number of repeats of the before mentioned amino acid), showed that the charged side chains (K^{16} and E^{22}) orient themselves towards the solvent, whereas the hydrophobic residues form the interior of the protofilament. The simulations result in the favourable energetic interactions between the hydrophobic side chains, leading to the self-assembly of these nanofibers *via* the expulsion of water [143].

Work done in our lab [144] in investigating the role of water molecules in the self-assembly of (RADA)$_4$ and (RADA)$_4$S$_5$, has concluded that the assembly of the pristine (RADA)$_4$ nanofibers resulted in the desolvation of interfacial surfaces; whereas an increase in the number

of net water molecules were witnessed upon (RADA)$_4$S$_5$ assembly. It was suggested that since the hydrophobic interactions are one of the driving forces in the self-assembly of (RADA)$_4$ peptide, removal of water molecules ("dewetting") is expected. However, since hydrogen bonding played a significant role in the self-assembly of (RADA)$_4$S$_5$ peptide, addition of water molecules was foreseen. Further it was suggested that due to the involvement of the hydrogen bonds in the self-assembly of the (RADA)$_4$S$_5$ peptide, a part of the free bulk water bound to this peptide chain may have been carried into the self-assembling interface. The results showed that hydrophobic interactions (pertaining to the alanine residues), were the primary driving forces for the (RADA)$_4$ peptide, and that (RADA)$_4$S$_5$ entropically self-assembly resulted in the formation of a more hydrated interface [144].

3.4.4 Van Der Waals Force

The study of intermolecular forces was quantified when the Dutch physicist J.D. van der Waals amended the ideal gas equation to account for the finite size of the molecules (the term b), and the attractive intermolecular forces (the term a/V^2), now known as the van der Waals forces (Equation 3.1).

$$\left(P + {a}/{V^2}\right)(V - b) = RT \qquad \textbf{Equation 3.1}$$

Where P is the pressure, V is the total volume of the container, R is the universal gas constant and T is the absolute temperature.

The Van der Waals forces derive from dipole or induced-dipole interactions at the atomic and molecular level. Even though the van der Waals interactions are seemingly weak when compared to other interactions in the self-assembly of nanofibers, but presumably the large

number of closely arranged van der Waals forces in the packing of secondary structure of peptides play a significant role in stabilizing the higher order resulting structures.

3.4.5 **Electrostatic Force**

If the only force acting between similar entities in a medium is van der Waals, then all the particles in the system can be expected to coagulate, and eventually precipitate. However, due to the dielectric constant of the medium, the particles are charged, and lead to electrostatic repulsion. The electrostatic interactions are one of the most prominent forces found in the self-assembly processes. Herein, only the electrostatic forces applicable to the self-assembling systems in solution are discussed. According to Israelachvili [107], a surface can be charged in two ways:

i)   Due to the dissociation or ionization of the surface groups (in case of amino acids the prominent groups are -COOH or –NH$_2$). The theoretical pI for the (RADA)$_4$ peptide is ~6.25, whereas the experimental value was determined to be 7.20 [145]. It is expected that the pH $\leq$ 7.20, the peptide would be positively charged due to the protonation of arginine and aspartic acid residues, whereas the overall charge on the peptide would be negative at pH $\geq$ 7.20. Different ionic states of the (RADA)$_4$ peptide are given in the table (with respect to the experimental pH of 7.20).

Table 3.8: Ionic species present in the peptide (RADA)₄ solution at 25°C.

pH	Major Ions
1.0	H^+
1.8	H^+
4.0	H^+
7.2	H^+/OH^-
9.6	OH^-
12.6	OH^-
13.0	OH^-

Adapted from Ye *et al* [145](2008). The isoelectric point of the peptide is at pH 7.20. The values are experimentally determined by Ye *et al* [145].

ii)   The surface charging can also occur *via* adsorption of ions from solution onto an uncharged surface.

After the surface is charged, an equal but oppositely charged counter ions bind to the surface, forming a "first" layer known as Stern or Helmholtz layer. The Stern layer consists of the "fixed" counter-ions, whereas the "un-fixed" counter-ions result in a shear plane. The subsequent second layer of ions (attracted to the counter-ions, of the Stern layer, and shear plane) is known as Gouy-Chapman layer. This layer consists of a more diffused ion concentration and extends to the point where the bulk ion distribution resumes. Due to the presence of the two distinct parallel layers, this overall structure is known as electric double layer (Figure 3.3).
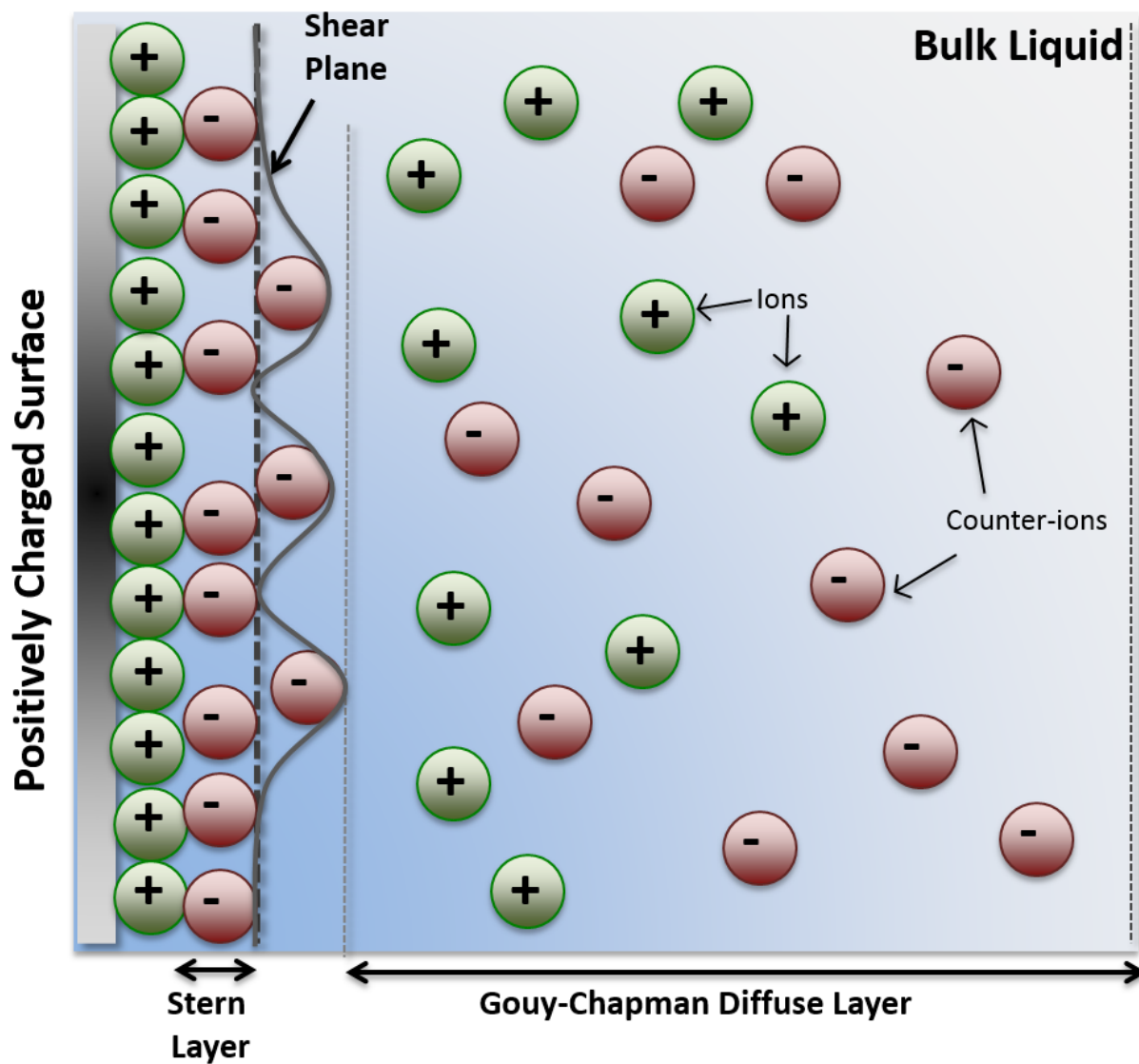
Figure 3.3: Schematic of Electric Double Layer (EDL)

An illustration of EDL on a positively charged surface in aqueous medium. The Stern layer consists "fixed" counter-ions, followed by a shear plane containing "un-fixed" counter-ions. Distribution of counter-ions and ions in the Gouy-Chapman layer is also shown.

When the self-assembling peptides (such as $(EAKA)_4$ and $(RADA)_4$) are in water, the electrostatic repulsions between the like charges on opposing peptides result in a significant energy barrier for self-assembly. However, this energy barrier can be lowered down with the

49

addition of ions, which promote peptide gelation by forming an electric double layer that screens the repulsive charges and permits β-sheet assembly [146, 147].

The electric potential decreases linearly from the surface potential (ψ_0) to the stern potential (ψ_s), and then decays exponentially to zero in the diffuse layer (ψ_d) (Figure 3.4). This relationship can be expressed mathematically as given in Equation 3.2 [107]:

$$\psi = \psi_d \, exp[-Kx]$$ **Equation 3.2**

Whereas x is the distance from the surface, and K is the Debye-Hückel parameter (K^{-1}, represents the "thickness" of the double layer), which can be defined as, given in Equation 3.3.

$$K = \sqrt{[2N_A ce^2 z^2/\varepsilon kT]}$$ **Equation 3.3**

Where N_A is the Avogadro's constant, c is the electrolyte concentration of ion valence z, e is the electric charge, ε is the medium permittivity, k is the Boltzman constant and T is the temperature of the medium [107].

It is evident from Equation 3.2, that the electric potential is dependent on the ionic composition of the medium. If the value of k increases, the potential decreases (resulting in a compressed double layer).

There is no experimental technique to directly measure the thickness of double layers, and the change in potential [148]. However, the electrokinetic potential (known as zeta potential, ζ), can be (indirectly) experimentally determined, and is usually considered similar to the Stern potential, ψ_d, even though zeta potential is the electric potential in the electric double layer, at the shear plane (Figure 3.4).
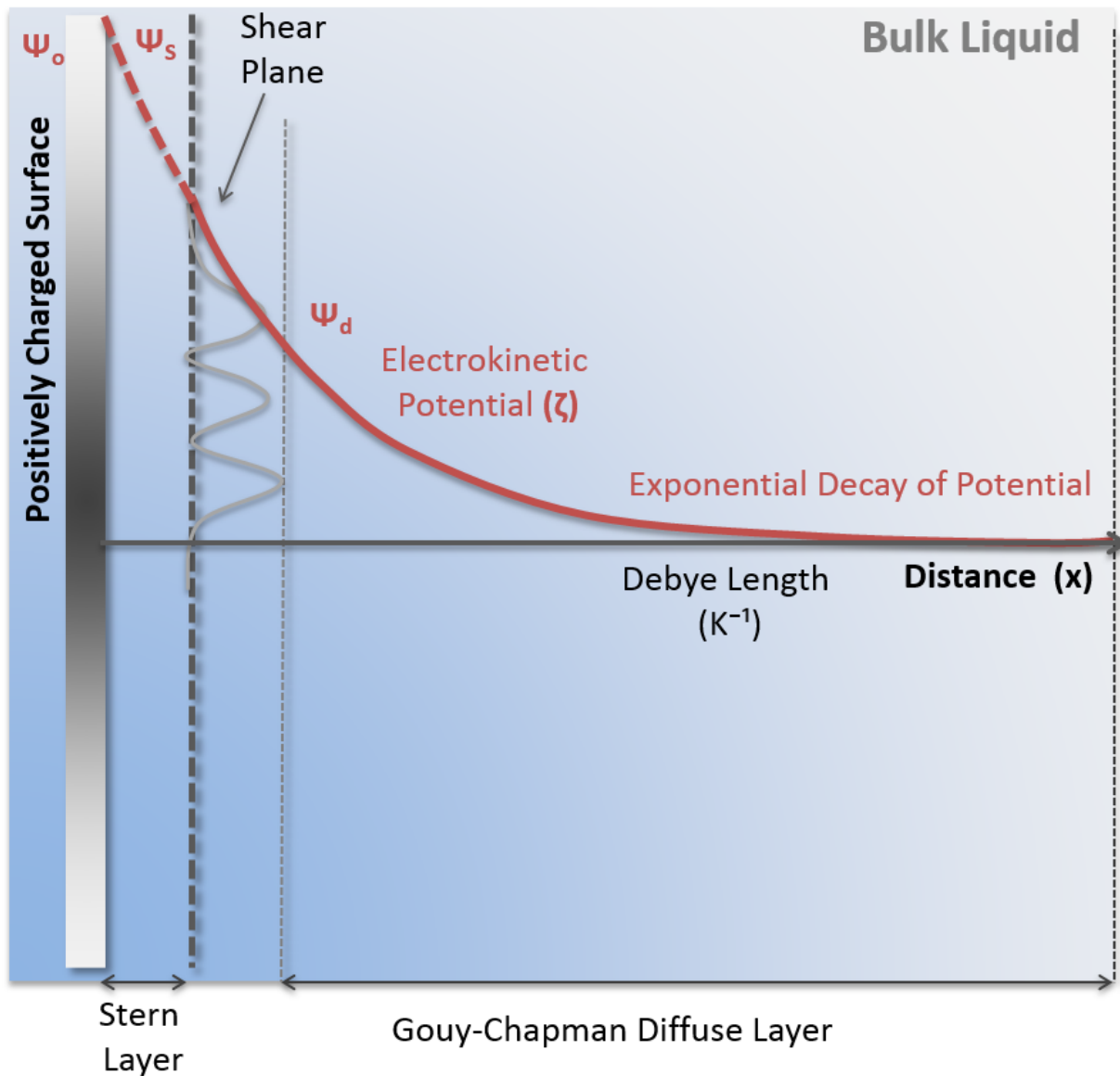
Figure 3.4: Schematic of potential density profile on Electric Double Layer (EDL).

The linear decrease of the electric potential is denoted in dashed red (▬ ▬ ▬), whereas the exponential decay is shown by solid red line (▬▬).

The total forces acting on the colloid based systems are always the sum of electric double-layer force and the van der Waals force. This school of thought has been evolved over a period of time, and now known as the Derjaguin-Landau-Verwey-Overbeek (DLVO) theory, where the

total interaction potential between two planer colloidal surfaces can be expressed as in Equation 3.7.

$$U\ (x) = 64k_BTn_\infty\gamma^2\ exp(-kx) - (A/12\pi)\ /\ x^2 \qquad \textbf{Equation 3.4}$$

Where k_B is the Boltzman's constant, T is the temperature (K), n is the ion concentration in bulk, K^{-1} is the Debye length, A is the Hamaker constant, x is the distance between two surface [107].

Specifically, with respect to the peptide self-assembly, the DLVO theory provides a semi-quantitative interpretation for the order of magnitudes for gelation time, employing a simple model for the interactions responsible for peptide self-assembly. The self-assembling kinetics of the β-sheet predominant (FKFE)$_2$ peptides have been reported using the DLVO model. It was found that at pH> pI (6.14), U_{DLVO}^{max} was less than k_BT, implying that the potential barrier is not significant and that the block monomers can form a stable network. It was also concluded that when the molecule consists of an overall neutral charge, the charges are screened, resulting in a rapid self-assembly of the nanofibers. However, when the nanofiber has a net charge (of positive or negative), the self-assembly is primarily driven by hydrophobic effect, but hindered by electrostatic repulsion, leading to an overall increase in the self-assembling time itself [149].

3.4.6 Steric Hindrance

Steric or overlap forces are long-range force induced by the adsorbed or grafted biomolecules onto the surfaces. Some factors, which may influence the steric forces, are: peptide-peptide interaction, peptide-solvent interaction, and the physical/chemical conditions of the system, including the solvent, temperature, and nature of charge. The peptide-induced forces can

be repulsive or attractive, depending on the affinity of the solvent with the peptide [105]. For instance if the solvent has a high affinity with the peptide, the solvent molecules are constrained when the peptide chains contact each other; this reduces the dielectric constant of the medium, resulting in the large repulsive force than predicted by the conventional Gouy-Chapman theory (Figure 3.3)[105].

3.5   Factors Affecting Self-Assembly of (RADA)$_4$ Peptide Based Hydrogels

The self-assembly of these amphiphilic peptides is sensitive to many physiological factors such as pH, temperature, and electrolyte concentration. The fundamental significance of using temperature change (varying thermal energy) is to analyse the strength of an interaction. Usually the increase in the thermal energy leads to a decrease in intermolecular cohesive energy, resulting in the disorganization of individual entities. The effect of temperature on (RADA)$_4$ peptide has been studied experimentally is presented in the following chapters, and hence the relevant literature has been provided in those chapters. This section would critically discuss the literature focussed on the response of self-assembling hydrogels to these other factors.

3.5.1   pH

pH is one of the distinguishing characteristics of a diseased state (when compared to the normally functional tissue), and can even sometime vary with the progression of a disease. Also, pH variation exists among different sites of the body (Table 3.9). Therefore, hydrogels responding to specific pH are of particular interest as they can be finely tuned by the environmental pH but also provide targeted and desired response to a precise location. Moreover,

hydrogels responding to the change in pH can be degraded within body over time, making them ideal candidates for implanted materials or circulating drug delivery vehicles.

Table 3.9: Dynamic pH range for specific human tissue sites.

Tissue Site	pH Range
Blood	7.34-7.45
Stomach	1.0-3.0
Small intestine	4.8-8.2
Colon	7.0-7.5
Extracellular tumour	7.2-6.5
Early endosome	6.0-6.5
Late endosome	4.5-5.0
Vagina	3.8-4.5
Inflamed wound tissue	5.4-7.4

Adapted from Schmaljohann, *et al.* [150]

Hydrogels usually respond to the change in the pH by swelling or de-swelling, pertaining to the presence of the ionisable pendant groups in the peptide's backbone [151]. Upon exposure to an aqueous solution with optimum pH (and other physiological conditions), these pendant groups ionize and result in the build-up of a fixed charge along the peptide. The surface charge of the individual amino acids can be selectively changed by changing the pH (above or below their pK_a (acid dissociation constant) values), which in turn regulates the intra- and inter-fiber interactions of the peptide. The pH variation result in either the absorption of expulsion of water from the peptide network, resulting in the swelling or de-swelling of the resulting hydrogels, respectively [151].

Anionic hydrogel networks have the pendant groups that are ionized in solutions at a pH greater than their pKa, hence, the anionic hydrogel swells at pH > pKa due to the large osmotic

pressure generated by the presence of the ions. Conversely, the cationic pendant groups are ionized at pH less than their pKa, leading to their swelling at those pH values.

The swelling behaviour of the ionic hydrogels is dictated by the characteristics of the peptide, the properties of the swelling medium, and the peptide-solvent interactions. The composition of the swelling medium determines the pH and ionic strength of the solution, which is controlled by the primary counter ions in solution [151]. According to the hydrogel network acts as semi-permeable membrane to those counter ions, influencing the osmotic balance between the hydrogel and external swelling solution resulting in water imbibition. The ionic exchange causing this osmotic balance is impacted by the ionic interactions present in a charged gel (ionisable groups and the degree of ionization) [152-154]. The mathematical relationship between the counter ion concentration and ionic osmotic swelling pressure is given in Equation 3.5 [154].

$$\pi_{ion} = RT \sum (C_i - C_i^*)$$ **Equation 3.5**

Where C_i and C_i^* are the counter ion concentrations inside and outside of the gel, respectively, R is the universal gas constant, and T is the absolute temperature.

It should be noted that the swelling and de-swelling behaviour of the hydrogels could be controlled by other factors along with pH, such as affinity with water molecules, elasticity underlying peptides, and the crosslinking of the hydrogel [154]. It has been proposed that overall swelling capacity of an ionic hydrogel system such as (RADA)4 is also influenced by the ionic strength of the surrounding swelling medium, as well as the ions within the hydrogel [153-155].

Self-assembling peptide amphiphiles (consisting of a peptide head and an alkyl tail) are inspired from the naturally abundant silk fibroin structure. It was found that the self-assembly of

particularly C12-GAGAGAGY peptide amphiphile is highly dependent on the medium's pH; the peptide was found in a cylindrical nanofibers with planar β-sheet at pH 9, whereas it forms twisted nanofibers with twisted β-sheet at pH 4 [156]. Varying the pH not only alters the secondary structure formation but also the resulting tertiary and or quaternary structure (Figure 3.5). In another study [157] the self-assembling peptide amphiphiles (consisting of a hydrophobic alkyl tail, a β-sheet-forming peptide sequence, and a charged amino acid sequence) have been designed to transform from spherical micelles to nanofibers under pH reduction, stimulating the acidic environment in the presence of malignant tissue.
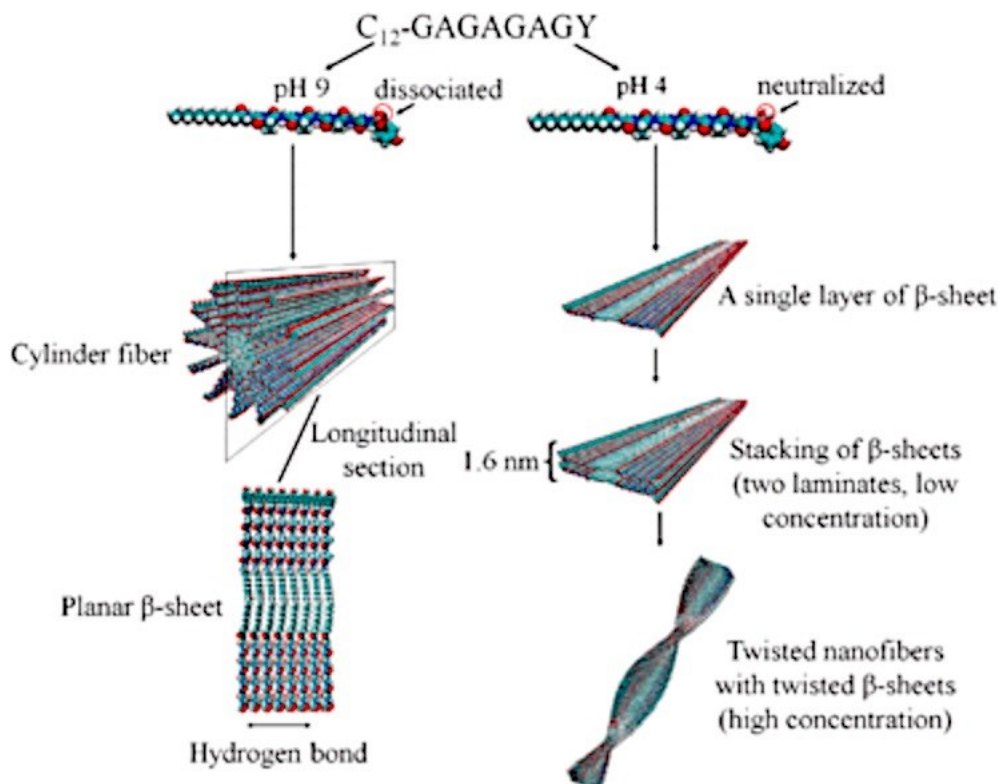
Figure 3.5: Effect of pH on the self-assembling peptide amphiphile C12-GAGAGAGY

Adapted from Zhang, *et al.* [156]

Studies conducted by Zhang *et al.* [7, 77, 98, 99] have been focussed on the self-assembling of ionic complementary peptides. Particularly one of these studies [145] specifically investigated the effect of pH on the self-assembly of (RADA)$_4$ peptides. The pI (isoelectric point) of the (RADA)$_4$ peptide was experimentally determined by titration to be 7.20. The quantitative and qualitative secondary structure analysis of the (RADA)$_4$ peptide showed that at pH<pI (of (RADA)$_4$ peptide), the peptide retained its characteristic β-sheet structure, and self-assembled into long nanofibers. At the pH<pI the peptide is primarily positively charged due to the protonation of arginine and aspartic acid residues. However a decrease in the β-sheet content

by 10% was observed at pH 1.0 (Figure 3.6). On the other hand, upon exposing the peptide to a higher pH (of ~13) drastically disassembled the β-sheet structure and instead formed small globular aggregates. It was postulated [145] the lower pH (with the increase in the unordered component, and β-turn) would facilitate the nanofiber elongation by increasing the nucleation process. Both the electrostatic and hydrophobic interactions are thought to play a role in the self-assembling of these (RADA)₄ peptides. Hence, at physiological pH of 7.4 (close to the pI of (RADA)₄ peptide) elongated nanofibers can be expected. However, the morphological analysis showed close to no nanofiber formation and it was proposed that perhaps due to the increased β-strand, β-turn and unordered structure of this zwitterionic peptide, the nanofiber growth of the peptides in a singular direction was impeded, resulting in the formation of aggregates. On the other hand, increase in the pH of the solution lead to the deprotonation of the asparagine and aspartic acid residues, thereby increasing the unordered structural content and resulting in smaller globular aggregates. Moreover, the increase in the pH disrupted the overall charge distribution along the peptides, resulting in the observed aggregates rather than well-organized β-sheet formation. It can be deduced from this study that the β-sheet structure was particularly impaired at extreme pH values.
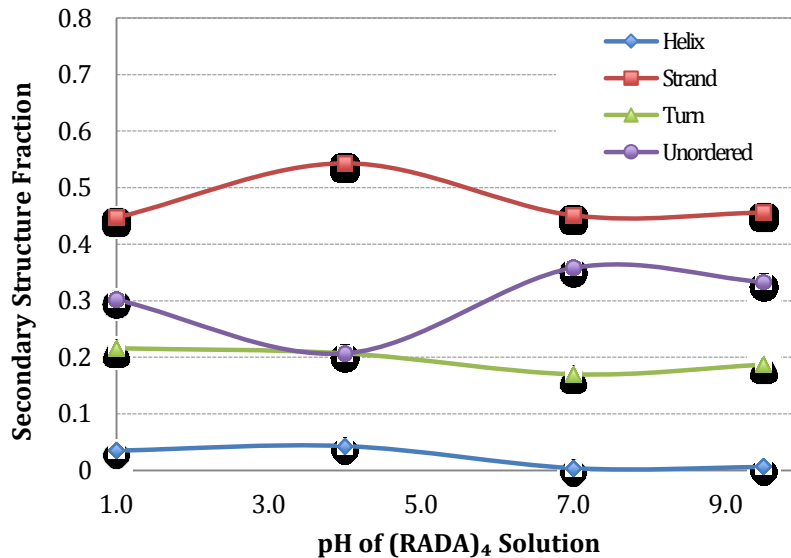
Figure 3.6: Estimated secondary structure composition of (RADA)$_4$ peptide as a function of pH

The peptide secondary structure fraction was calculated from the data presented by Ye *et al* [145]. The total Helix and Strand fractions were calculated by adding both the helix (H(r) and H (d)) and strand (S(r) and S(d)) components, respectively. Where r and d represent the regular and distorted components, respectively.

Based on the study reported by Ye *et al*.[145], and Chen *et al*.[158] (RADA)$_4$ based peptide amphiphiles form hydrophobic region hexadecanoic, followed by a β-sheet forming region of four consecutive alanine residues, and a charged region of four consecutive lysine residues on the N-terminus of the (RADA)$_4$ peptide. It was proposed that at higher pH, the screening of the repulsive forces on the charged residues adjacent to the β-sheet region would result in parallel β-sheet formation, thereby elongating the micelles into cylindrical nanofibers.

3.5.2 Amino Acid Type

The basic structure and introduction of using amino acids as building blocks is given in section 3.6; this section contains unique characteristics of certain amino acids, influencing their self-assembly. Out of the naturally occurring 20 amino acids only Glycine is achiral. Another amino acid, Proline (P) is different from the group because of its conformational rigidity pertaining to the cyclic pyrrolidine side group. Proline is commonly found as the first residue of α-helix, edge of β-sheets, or β-turns, subsequently aiding in the intramolecular folding of peptide self-assembly [159, 160]. Due to the presence of imidazole ring histidine (H) amino acid poses challenges in the self-assembly as well, however it is still able to participate in the π-stacking [161]. Hydrophilic amino acid cysteine (C) with its thiol side chain stabilizes hydrophobic interactions in micelles (when compared with the side chain of the achiral non-polar amino acid glycine, and polar amino acid serine (S)) [162]. Moreover, the thiol side chain of cysteine usually takes part in the disulphide cross-linking and chemical modifications [163].

3.5.3 Amino Acid Length

Even though the modification of N-terminus of the primary building blocks is deemed necessary for self-assembly to occur, a few studies have established hydrogelation consisting unmodified N-terminus oligopeptides as short as two peptide (dipeptide) length. Dipeptide containing hydrophobic amino acids Isoleucine (I) and Phenylalanine (F) has been reported to form fibrillar network resulting in successful hydrogels at concentrations >1.5 wt (%), at pH 5.8 [164]. Another dipeptide consisting of α,β-dehydrophenylalanine residue (ΔPhe) containing

dipeptide H-Phe-ΔPhe-OH is also known to form stable hydrogel structures at 0.2 wt (%) at pH 7.0 [165].

It can also be assumed that the longer the hydrophobic "tail" of these peptide amphiphiles, the harder the solubility of the peptide would be, consequently increasing the possibility of aggregation.

3.5.4 Presence of Monovalent and Divalent Ions

Salt plays a significant role in the self-assembly process of peptides, into stable structures. Poly(Val-Lys) is found to change its secondary structure from random coil to a stable β-sheet in the presence of NaCl [166]. Poly(Phe-Lys) [167], and poly (Tyr-Lys) [168], and other ionic-complementary peptides have been reported to form high-molecular weight complexes in the presence of salts. Salt induced (PBS) peptide aggregation has also been found in the β-amyloid protein found in Alzheimer's brain plaques [169].

3.6 Recent Developments in And Proposed Mechanisms For Peptide Based Biomaterials

Molecular self-assembly is a ubiquitous phenomenon found in nature and is defined as the spontaneous organization of components into ordered structures and patterns of varying scales. Primarily, self-assembly is driven by intrinsic characteristics of the molecule themselves, and typically does not require the formation of chemical bonds. This process allows fine-tuning of the resulted supramolecular structures *via* controlling the underlying molecular chemistry,

assembling environments (pH, solvents, linkers and temperatures), and assembly kinetics. Usually these resulted 3D supramolecular hydrogels are designed to be degraded within a controlled timescale and environment.

Peptides are biologically occurring oligomers made from the amino acid monomers linked *via* peptide (amide bonds). Amino acids consist of an amine ($-NH_2$) and carboxylic acid (-COOH) functional groups, along with residue specific side-chains. To date 500 amino acids are known, 240 of which are found in nature [170]. However, only 23 L-amino acids are of significance in human biochemistry as they are basic blocks for protein building, and only 20 of these amino acids are directly encoded by codons in human body. Going further nine of these amino acids are known as essential as they can not be synthesized by human body and should be consumed. The amino acids can be grouped in various ways, the most common being according to the chemical composition (pK_a values and charge at physiological pH of 7.4) of the side chain R-groups. A dipeptide is formed between two amino acids after the expulsion of water molecules, and the peptide chain can be extended in a similar manner.

The basic 20-proteinogenic naturally occurring L-amino acids are of immense biological significance they not only control the ultimate structure of all the protein (and enzymes) in body, but also synthesize neurotransmitters and control metabolism, among other functions. Currently, amino acids are being extensively studied in applicative medicine and tissue engineering primarily due to their ability to form biocompatible biodegradable by-products.

Hydrogels are three-dimensional cross-linked networks of hydrophilic peptides. Peptide based hydrogels are extensively being sought for an array of biomedical applications as they possess the following highly desirable characteristics mimicking biological environment.

Table 3.10: Number of publications per year studying self-assembling hydrogels.

Publication Date	2006	2007	2008	2009	2010	2011	2012	2013	2014	2015	2016
Number of Publications	46	68	109	129	157	208	202	212	274	288	98

ISI knowledge was used as the bibliographic database.

3.7 Review of Secondary Structure Analysis Methods to Study Self-Assembly of Peptides

3.7.1 Secondary Structure: Circular Dichroism

Circular Dichroism is a powerful technique widely employed to study the secondary structure of self-assembled peptides, and proteins. The method is based on chirality of the peptides where the circularly polarized light absorbed right (RCPL) and left (LCPL) dictates differences in absorbance (ΔA), and molar extinction coefficient ($\Delta\varepsilon$) as per Equation 3.6 (where λ is the wavelength).

$$\Delta A\,(\lambda) = A(\lambda)_{LCPL} - A(\lambda)_{RCPL} \qquad \textbf{Equation 3.6}$$

The Equation 3.6 can further be incorporated into the Beer-Lambert law, considering the molar absorptivity (ε), resulting in Equation 3.7, where c is the molar concentration (g/mL) and l is the optical path length (cm).

$$\Delta A = (\varepsilon_L - \varepsilon_L)cl \qquad\qquad \text{Equation 3.7}$$

Most commonly the CD data is reported in molar ellipticity, $[\Theta]$ (deg.cm^2/dmol), which is calculated using the relationship between the peptide concentration and raw ellipticity (Θ), as given in Equation 3.8.

$$[\Theta] = \frac{\Theta \, X \, MRW}{c \, X \, l \, X10} \qquad\qquad \text{Equation 3.8}$$

Where MRW is the mean residue molecular weight (Da). Furthermore, molar ellipticity can readily be translated to molar circular dichroism by the relationship given in Equation 3.9.

$$\Delta\varepsilon = \frac{[\Theta]}{3298.2} \qquad\qquad \text{Equation 3.9}$$

Data is collected between the far UV wavelengths of 180-260 nm, where the peptide chromophore $n\pi^*$ (210 nm) and $\pi\pi^*$ (190 nm) transitions (due to electron delocalization) occur (Figure 3.7 **(A)**), and usually have the extinction coefficient of $\sim 10^5$, where n is lone pair of electron, and π^* denotes the anti-bonding orbital. The amide chormophores are also sensitive to backbone dihedral angles, thereby predicting the peptide secondary structure. The CD absorption is modulated by the interactions between the $\pi \rightarrow \pi^*$ coupling between the peptide groups, mixing of $n \rightarrow \pi^*$, and $\pi \rightarrow \pi^*$ within a peptide group, and mixing of $n \rightarrow \pi^*$ and $\pi \rightarrow \pi^*$ between the peptide groups.
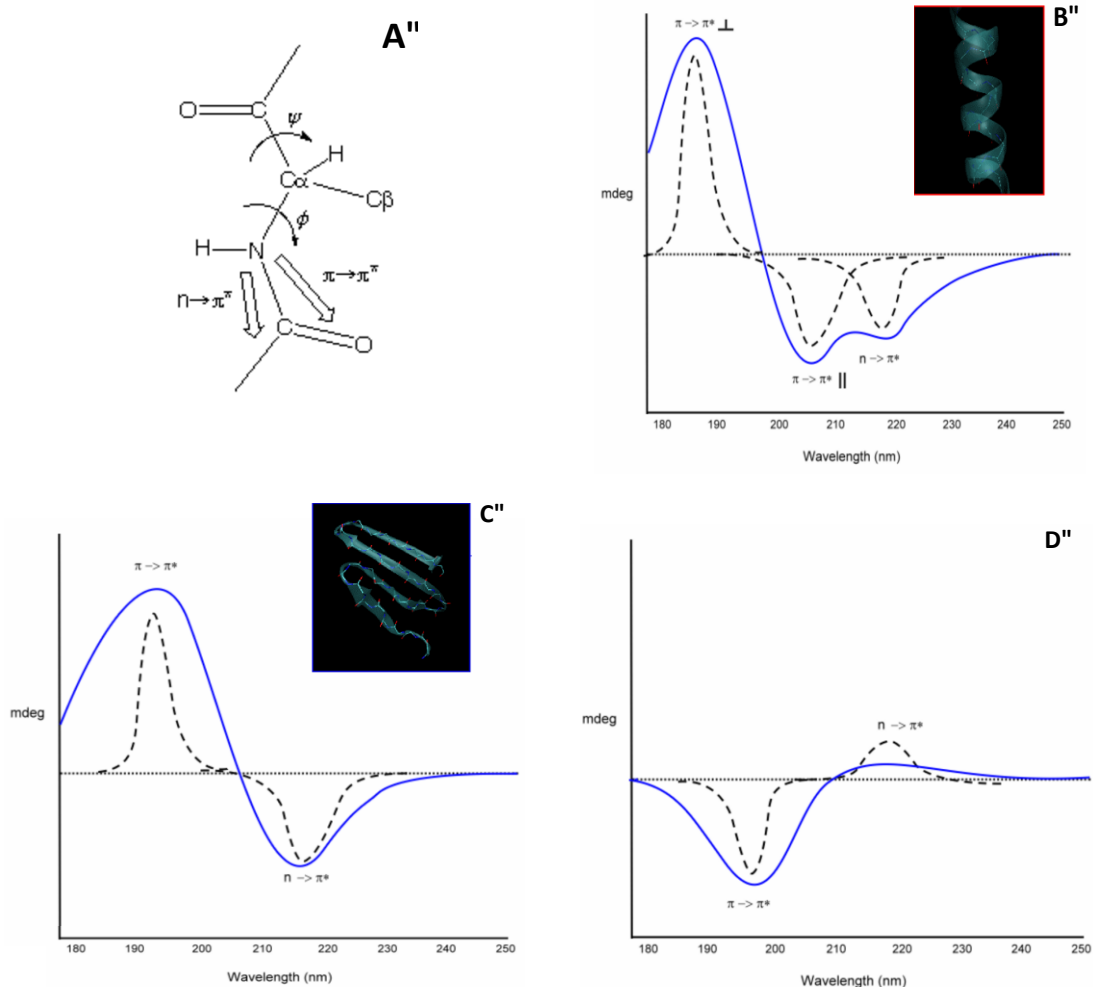
Figure 3.7: Far-UV CD adsorption spectra to determine the variation in the long-range order in the amide chromophore

(A) Schematic indicating amide bond electron energy absorption, where n→p* is centered on 220 nm and p→p* is around 190 nm. The peptide bond dictates the intensity and energy of these transitions. Adsorption spectra of Poly-L-Lysine along with the energy transitions: (B) α-helix, exiton coupling of the $\pi \rightarrow \pi^*$ transitions result in the crest at ~192 nm, and a trough at 209 nm (the trough at 22nm is indicative of the red shift of n→ π^*), (C) β-sheet, crest at 218 nm (due to π→π* shift), and trough at 196 nm (n→ π^* shift) and (D) Random coil, with the crest at 212 nm (π→ π^*) and trough at n→π*). (Adapted from Carter. et. al. [171, 172])
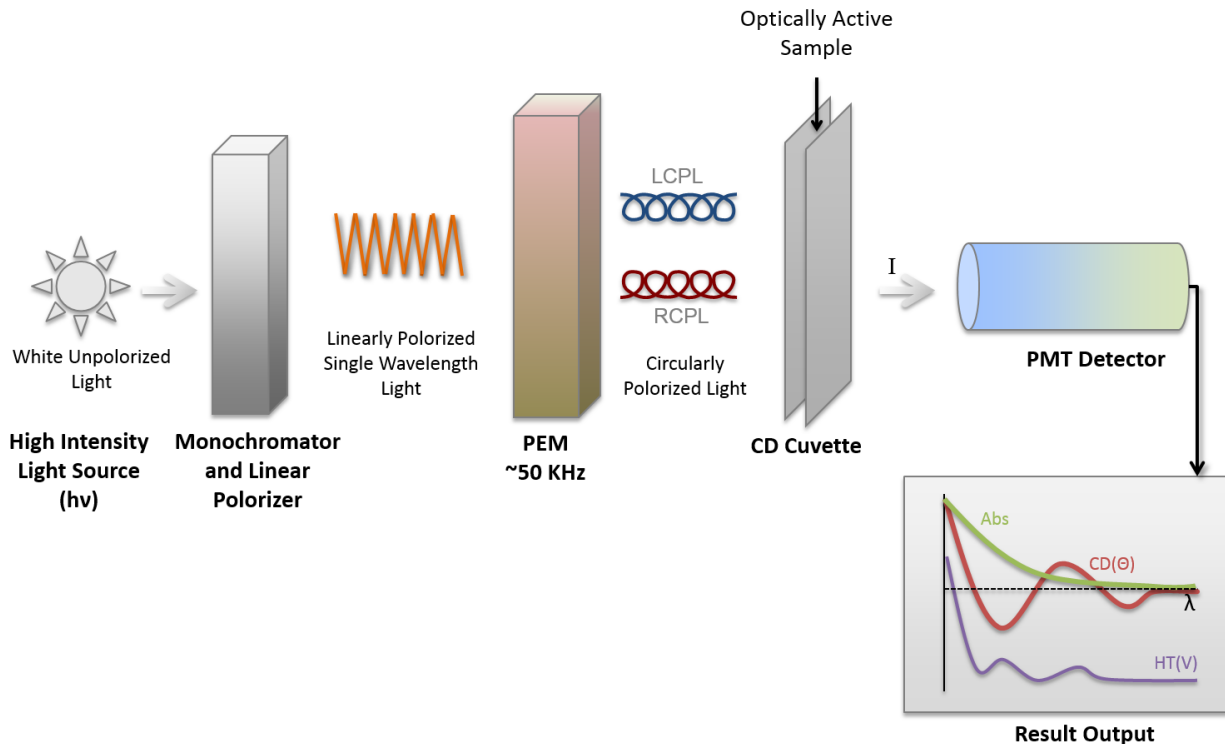
Figure 3.8: General schematic of the basic principle of CD spectrometer instrument.

Light is linearly polarized and passed through a monochromator. The resulting single wavelength light then passes through the Photo Elastic Modulator (PEM), which transforms the linear light to circular polarized light, indicated as RCPL (Right Circularly Polarized Light), and LCPL (Left Circularly Polarized Light). The orientation of the incident circular polarized light changes upon interaction with a chiral sample. The resulting spectra is then collected by the Photo Multiplier Tube (PMT), and transmitted as the Absorbance (Abs), Molar Ellipticity (CD (Θ)), and High Tension Voltage (HT(V)). The collected spectra can then be used to calculate secondary structure composition of the sample.

CD is considered a gold standard in particularly determining a single type of secondary structure such as α-helix, parallel or antiparallel β-pleaded sheets, regularly repeating β turns, or unordered/random structures [173, 174]. The α-helix is the most common form of secondary structures, and was first modelled in 1951 [175]. The most commonly occurring α-helix contains

3.6 residues per turn. Two other types of helices are 3_{10} helices (with a tighter coil consisting of 3.0 residues per turn), and π helices containing (with a looser coil containing 4.1 residues per turn) [176]. β-sheet is the second most abundant form of secondary structure found in nature. β-sheets are formed by β-strands, consisting of either parallel or anti-parallel strands of amino acids, with fully extended peptide backbones, and hydrogen bonds between adjacent β-strands [177]. The third most common secondary structure is the turn, created when the hydrogen bonds are formed within the primary sequence of the polypeptide chain. For this to occur, C_α atoms of the amino acids involved in the bonding must be within 7 Å of each other, and with neither of the amino acids participating with another secondary structure. β-turns are characterized as ϒ-, α- and π-turns, which represent the separation of C_α atoms by two, four, and five residues respectively [178, 179]. The final category of secondary structure is of random/unordered structure, consisting of unstructured segments of the polypeptide chain liking other kinds of secondary structural moieties with one another [173].

The characteristic CD spectrum of α-helix consists of negative ellipticities (trough) at 208 and 220 nm, and a positive ellipticity (crest) at 190 nm [180]. The CD spectrum for a structure composed of primarily β-pleaded sheets shows a trough at 220-230 nm (Figure 3.9), with a crest around 200-210 nm and a strong trough at 180-190 nm. However, theoretical analysis of β-sheet has shown that various kinds of β-sheets as well as β-turn have similar spectra [181]. The random coil show a distinct trough around 198 nm and a crest around 220 nm [182].
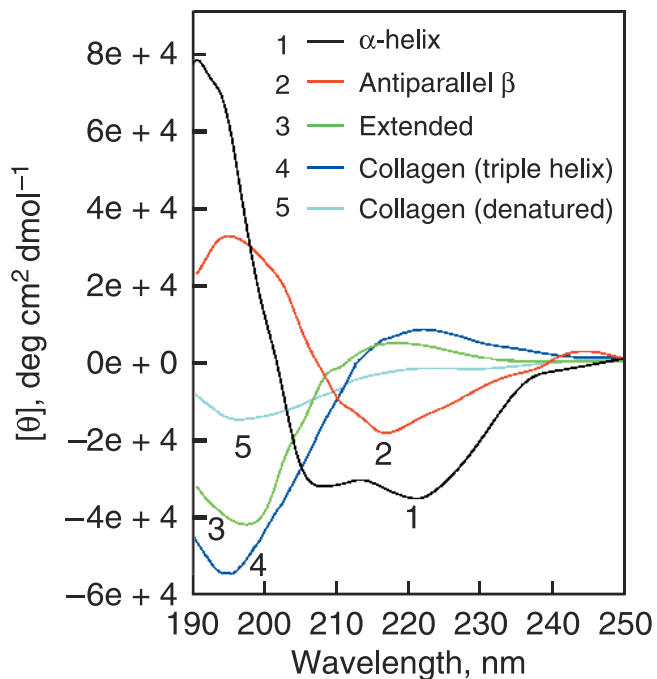
Figure 3.9 Characteristic Circular Dichroism (CD) spectra of peptide secondary structure.

CD spectra collected represented poly-L-lysine structure with predominantly α-helix confirmation (at pH 10.8, (1-black)), antiparallel β-sheet (at pH 11.1, (2-red)), extended conformation (at pH 5.7, (3-green), and placental collagen in its triple helix (4, blue) and denatured (5, cyan) conformations.

(Adapted from Greenfield, [182])

3.7.1.1 Comparison With Other Methods

There are several other spectroscopic techniques (beside CD) used to directly quantify the secondary structure in peptides, such as Raman, FTIR, and NMR to mention few. It is beyond the scope of this chapter to go through in detail of those techniques, however a quick comparison of those methods with CD is provided herewith.

Although molecular simulation is a budding field with respect to peptide structure estimation, however it has been suggested that computer simulations should be considered as a complement to, or an extension of experimental work. The Monte Carlo (MC) computation are one of the most popular simulations to generate peptide conformation, and the energy of these conformations consist of the Boltzmann distribution, and the structures can be computed upon considering the energy minimization. Furthermore, simulations should be conducted with the consideration of the peptide's functional characteristics, such as structure stability with respect to the changes in pH, temperature, and physiological conditions [183].

3.7.2 Hydration State Analysis: Differential Scanning Calorimetry

Most of the amphiphillic nanofiber networks have a high affinity for water, yet due to the presence of highly cross-linked network they do not dissolve in water and retain their 3D structure. Water can penetrate in between the peptide chain of the network, resulting in the swelling and formation of the hydrogel structure. Moreover, water is thought to be an essential factor in the biological response induced by the exposure to artificial surfaces. Water molecules are thought to serve as an adhesion medium, subsequently affecting cell morphology and other cellular functions. Hence, the structure of adsorbed water molecules on a blood-contacting surface significantly affects their blood compatibility[184-187]. Differential scanning calorimetry (DSC) is a powerful technique to study the role of self-organized water molecules at biointerfaces. Primarily there are two categories of water present in swollen hydrogels, which influence the protein adsorption and platelet activation properties of the hydrogels [188]. These two types are: loosely adsorbed frozen water, and tightly bound non-frozen water (Figure 3.10).
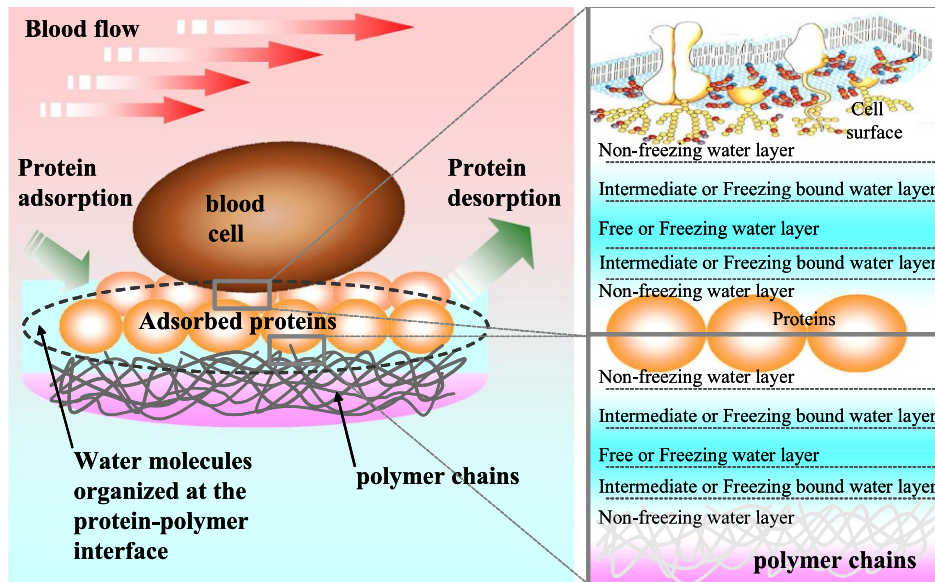
Figure 3.10: Illustration of biomaterial interaction with blood, and the involvement of various categories of water.

Adapted from Tanaka *et al* (2010) [189].

As shown in the Figure 3.11, water can be categorized as bulk water and the hydrated water (which interacts with the hydrogel system). Hydrated water can further be categorized into non-frozen water (which is non-crystallizable (Even at -100°C), due to strong interaction with the underlying peptide), and frozen (loosely bound water) which is crystallisable. Frozen water consists of free water (which is crystallisable at 0°C, and is marginally affected by the peptide or non-frozen water), and frozen bound water (which can crystallize in heating process below 0°C, and is affected by peptide and or non-frozen water) [189, 190]. Although some researchers report only one type of frozen water[190-193], and some report more than one type of frozen water[188, 194], essentially the most significant categories to consider in the hydration analysis of any system are (given in red in Figure 3.11) 1) free water, and 2) bound water (which is equal to non-frozen water + frozen bound water in Figure 3.11). However, the current hydrogel systems such

70

as poly (glycerol methacrylate) [190, 193] and (RADA)$_4$ [191] hydrogels consist of only one kind of frozen bound water.
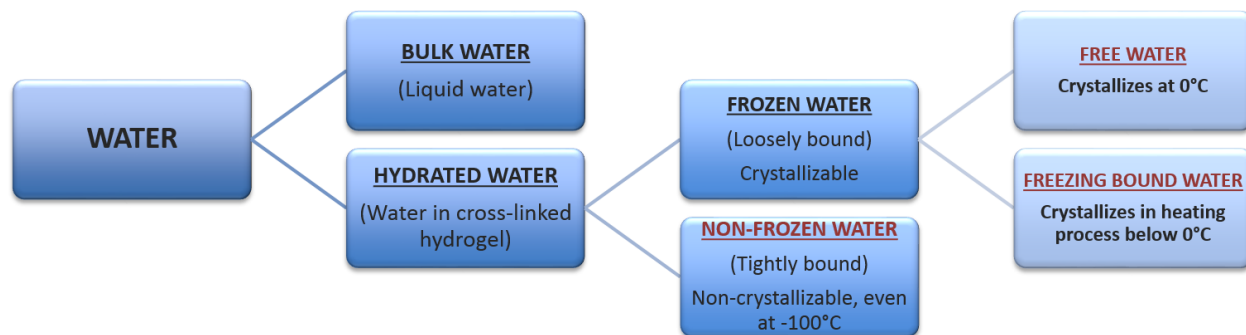
Figure 3.11: Classification of various kinds of water present in biopolymers.

The hydrated water can be categorized into three types: non-frozen water, frozen water and free water, on the basis of equilibrium water content (EWC), and the enthalpy changes due to the phase transition observed by DSC.

Reformatted and adapted from Tanaka *et al* (2010) [189]

The frozen water is loosely absorbed to the hydrogel structure, whereas non-frozen water is tightly bound and shows no freezing and melting transition during DSC heat variations [190]. Typical thermograms of various categories of water are given in Figure 3.12.
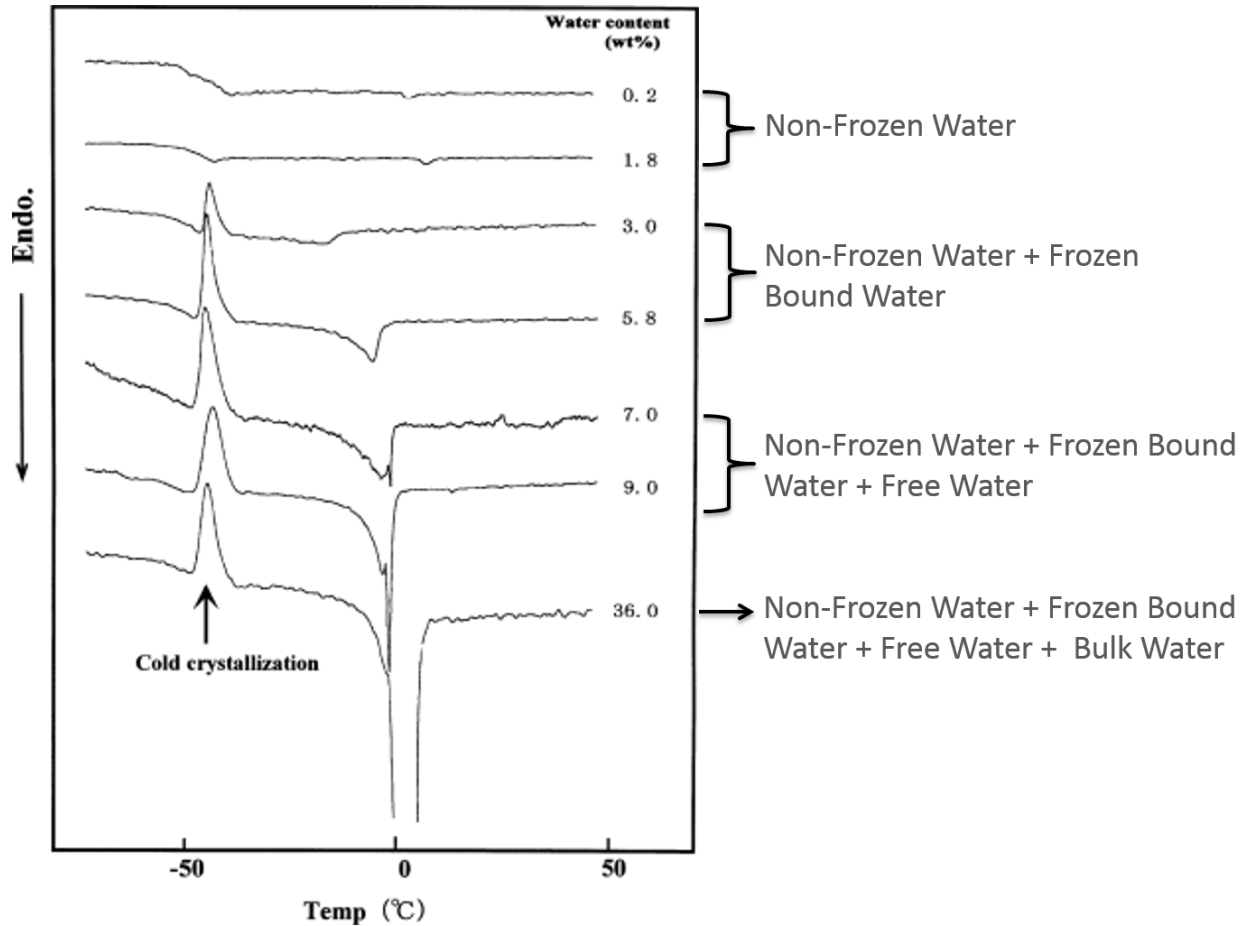
Figure 3.12: Typical DSC thermograms of dry and hydrated hydrogels with varying amounts of water

Heating curves of poly (2-methoxyethyl acrylate) PMEA hydrogels.

Reformatted and adapted from Tanaka *et al* (2000) [195]

The relationship between equilibrium water content (EWC) with the three kinds of water non-frozen bound water (W_{nf}), frozen bound water (W_{fb}), and free water (W_f)) can be described by the Equation 3.10 below:

$$EWC\ (wt\%) = W_{nf}(wt\%) + W_{fb}\ (wt\%) + W_f\ (wt\%) \qquad \textbf{Equation 3.10}$$

$$EWC = \frac{W_h - W_d}{W_h} \times 100 \qquad \textbf{Equation 3.11}$$

The non-frozen bound water content is indirectly measured in DSC assays, and can be obtained from the difference between the EWC (Equation 3.11) of the hydrogels and the calculated frozen water (Equation 3.12). Frozen and non-frozen water contents can be determined by using the area under the resulting thermograms, along with the EWC. The frozen water content can be determined using Equation 3.12, where melting enthalpy of the bulk water is usually taken to be 334 J/g.

$$W_f = \frac{\Delta H}{\Delta H^\circ} \ X \ 100 \qquad\qquad \textbf{Equation 3.12}$$

Here W_f is the weight of frozen water present in the sample (%), ΔH is the melting enthalpy of the sample (J/g), and ΔH° is the melting enthalpy of the bulk water (J/g) [190, 191].

It is postulated that as the EWC increases, the dissociation of the physical interactions (such as hydrogen bonds) can increase, leading to the decrease in the frozen water molecules [196]. Free water has good mobility, as there are no interactions with the peptide chains, but non-frozen bound water is involved in hydrogen bonding with the hydrogels. This phenomenon was consistent in the case of (RADA)$_4$ peptides, where a decrease in the concentration of the peptide not only increased the total EWC , but also a decrease in the non-frozen water content was observed [191]. Information about the various water contents in the assembled (RADA)$_4$ hydrogels is not only significant in understanding their equilibrium and dynamic swelling behavior, but in estimating solute transport and other diffusive characteristics of these hydrogel systems.

3.7.2.1 Comparison With Other Relevant Methods

Differential thermal analysis (DTA) is an alternative technique to DSC, where the difference in temperature between a substance and reference material is measured as a function of temperature, while the sample and reference are subjected to controlled temperature program. Transformations pertaining to the change in specific heat or the enthalpy transitions can be detected by DTA.

Thermogravimetric analysis measures the mass of a sample as the temperature increases. However, this method is primarily useful for determining sample purity and water, rather than various kinds of water in the sample. Therefore TG is typically used together with either DSC or DTA. Other less commonly used techniques are evolved gas thermoanalysis (EGA), thermomicroscopy (TOA) or Thermosonimetry (TS).

However, due to the immense development of the DSC (from a half-quantitative DTA method), the underlying theory of heat flux in the DSC is highly evolved, and well understood. Hence, DSC is used as a fast and reliable method to study thermal characteristics of a material [197].

3.8 Applications of Self-Assembling Peptides

3.8.1 Extra Cellular Matrix (ECM) Analog

The design strategy of an ECM matrix involves conjugating the naturally occurring cell attachment and neurite outgrowth motif RGD [198], which is found in the integrins of ECM

proteins (such as laminin, fibroectin, and collagen), to the engineered peptides [198, 199]. It has been concluded that changing the glycine residue with the alanine residue (RGD → RAD), does not affect the cell attachment activity, however while substituting valine for glycine (RGD → RVD) the cell attachment is significantly affected [200]. Even though both of the substituted amino acids belong to the hydrophobic subclass, it is likely that the isopropyl side chain of valine is responsible for this observed reduction in cell attachment. It was found that diverse cell types, including fibroblasts and keratinocytes attached to both (EAKA)$_4$ and (RADA)$_4$ peptides, and retained their natural round morphologies [99]. (RADA)$_4$ peptides have also been shown to support extensive neurite growth [106]. It is proposed that these ECM analogs can be used to encapsulate stem cells, allowing them to differentiate into desired cell types with specific growth factors, and then transported into the needed tissues [106]; however, future experiments still need to be performed to confirm the reliability of this application.

3.8.2 Angiogenesis

Self-assembling peptides have proven to remodel existing blood vessels into new vasculature. The heparin-binding peptide amphiphiles are designed with Cardin-Weintrab heparin-binding domain to specifically bind heparin sulphate-like glycosaminoglycans. The polysaccharide is known to screen charges on the amphiphile molecules and trigger the peptide self-assembly to nanofibers, thereby exposing the polysaccharide to the nanofiber surface. This assembly process allows the capture of various proteins known to have heparin-binding domains such as fibroblast growth factor 2 (FGF-2), bone morphogenetic protein 2 (BMP-2), and vascular endothelial growth factor (VEGF) (these proteins are known to participate in angiogenesis signalling and blood vessel formation) [201].

The $(RADA)_4$ nanofibers are also known to create a scaffold-like tissue bridging structure providing a framework for axonal regeneration after CNS injury [202].

3.8.3 Hemostatic Agents

The $(RADA)_4$ nanofibers have proven to be the novel "nanohemostatic" agents, arresting bleeding in less than 15 seconds, when applied to a wound, without employing any of the traditional hemostatic therapies, such as cauterization, vasoconstriction, coagulation, pressure application or the use of cross-linked adhesives [75]. Many protein (such as, collagen and fibrin) based biomaterials have been studied extensively in the past for the purpose of achieving hemostasis, but they all resulted in limited success due to the lack of severe hemorrhage control [203, 204]. However, $(RADA)_4$ based hydrogels have been reported to not only have achieved complete, but rapid hemostasis under severe hemorrhagic conditions [75].

3.8.4 Other Applications

There are other numerous applications of these self-assembling peptide, some of them are briefly described in the Table 3.11 below.

Table 3.11: Current applications of self-assembling peptides

Applications	Basic Principle	Peptide Examples	References
Antimicrobial agents	• Cationic and hydrophobicity plays an important role in the effectiveness of microbial killing. • Permeation and disruption of bacterial membranes	A_9K, Lipopeptide, C_{16} analogues, membrane translocation sequence TAT	[205-207]
Cell culture scaffold for tissue engineering	• Fmoc-RGD exposed mimicking extracellular matrix (ECM) promotes cell differentiation	C_{16}-$V_3A_3E_3$, C_{16}-$V_3A_3E_3$RGDS	[208, 209]
Drug (doxorubicin) and gene delivery (p53 and luciferase reporter gene)	• The amphiphilic characteristics of the self-assembling peptides facilitate the internalisation of the drugs/genes encapsulated. • Cationic peptide amphiphiles are used as drug and gene delivery carriers. • Increased cationic charge density on the outside of the micellar shell facilitated better DNA binding and protection from enzymatic degradation capability.	H_5R_{10}, $H_{10}R_{10}$, $A_{12}H_5K_{10}$, $(AF)_6H_5K_{15}$	[210, 211]
Nanofabrication and biomineralisation (hydroxyapatite)	• Templates for nanowires, and nanocircuits, as well as hydroxyapatite nucleation from the cysteine rich residues	C_{16}– $C_4G_3S(p)RGD$–OH	[108, 212-214]

3.9 *In-Vito* Biocompatibility of the Self-Assembling Peptides

The *in-vitro* biocompatibility is necessary prior to proceeding to any *in-vivo* application of any biomaterial, however there is a lack of thorough review studies provided on particularly assessing the biocompatibility of self-assembling peptides. Therefore, this section will summarize the tools and techniques available for analysing the biocompatibility of the self-assembling peptides showing promise as potential biomaterials. This section also provides the current merits and current limitations of these methods by critically analysing the current literature.

Pursuing the ultimate goal of developing biocompatible material most of the research so far has been focussed to develop inert material, which does not react with platelets and coagulation factors. However due to the lack of well organized systematic studies, complexity of biological pathways, human to human test result variations, there lacks an agreement on various issues pertaining to *in-vitro* biocompatibility of materials. For example, there is still no consensus if a biocompatible biomaterial should be hydrophilic or hydrophobic.

3.9.1 **Platelet Activation**

Human platelets are anuclear blood elements derived from megakaryocytes, and are the second most common moiety in the blood (circulating between 150 to 450 X 10^9/L). Platelets are discoid in shape, with the dimensions of 2 to 4 X 0.5 μm, a mean volume of 7 to 11 X 10^{-15} L, and individual platelet concentration ranging from 150 to 400 X 10^6 platelets/ml [215]. Platelets play a very significant role in an array of pathophysiological functions (Table 3.12), therefore their presence/activity can be assessed *via* numerous assays, however, the majority of the tests focus on their ability to achieve hemostasis. Some of the primary functions of platelet are given in Table 3.12.

Table 3.12: The Primary Functions of Platelet Activation

Hemostasis and Thrombosis	Maintenance/Regulation of Vascular Tone	Inflammation	Host Defense	Tumour Biology
[216, 217]	[218]	[219, 220]	[221, 222]	[223]
Adhesion	Uptake or Serotonin in Inactivated State	Atheroslerosis	Phagocytosis	Tumour Growth
Activation	Release of Serotonin	Allergic Asthma	Internalization of Viruses and Bacteria	Tumour Eradication
Spreading	Release of Thromboxane	Renal Diseases	Eradicating Bacteria	Tumour Metastasis
Secretion	Release of Prostaglandins in Activated State	Chemotaxis	Superoxide Production	
Procoagulant Activity		Platelet-Leukocyte Interactions	Releasing Platelet Microbicidal Proteins	
Aggregation				
Clot Retraction				
Tissue Repair				

Platelets are critical to analyze overall biocompatibility of a material due to their capability of adhering, aggregating (Figure 3.13), and subsequently releasing their granule contents, altering their surface characteristics to support blood coagulation.
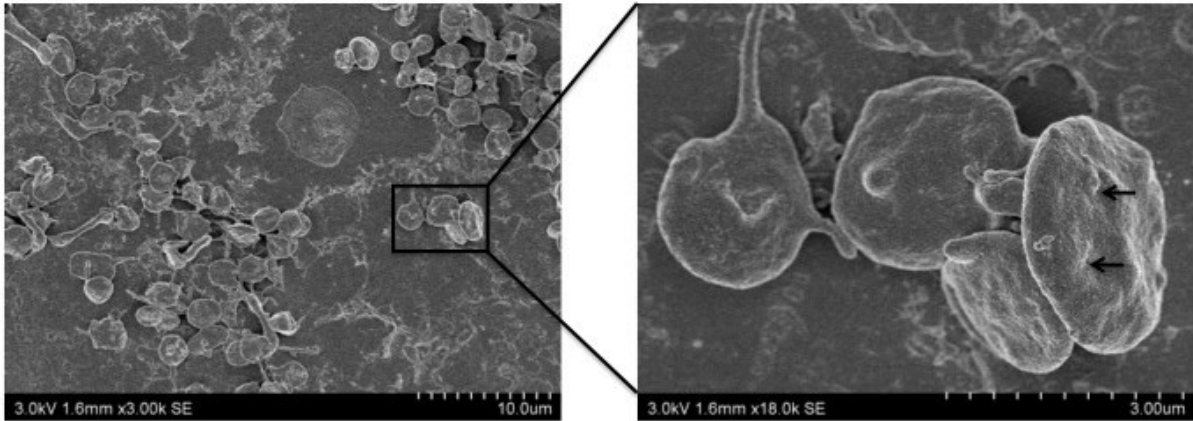
Figure 3.13: Platelet Aggregation Viewed *Via* Scanning Electron Microscopy

(A) Clusters of aggregated platelets in contact with a biomaterial. (B) Inset: discoid platelet, with visible surface indentations (←) represent the communication channels of the open canalicular (OCS) systems and the cell walls.

Images were captured Via Scanning Electron Microscopy (Chromium sputter coating~20 nm).

Assessing platelet activation (Figure 3.14) upon contact of a biomaterial is a valuable measure of the biocompatibility of that material. Platelets are activated upon the contact of a thrombogenic surface *via* the interaction of an extracellular stimulus involving coupling of the specific receptors on the platelet plasma membrane [224], which results in the release of serotonin and histamine, a fall in the platelet adenosine triphosphate (ATP) into the ambient fluid [225].
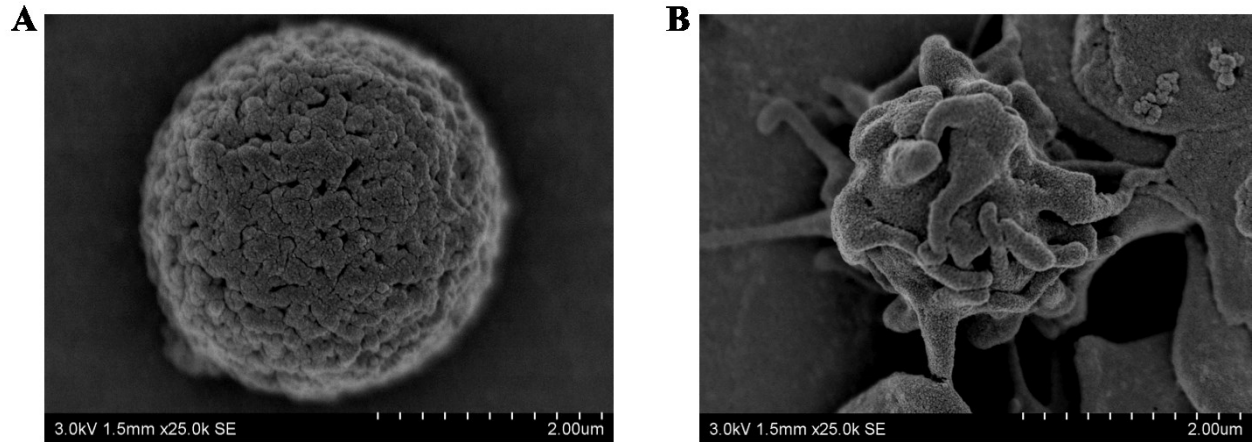
Figure 3.14: Platelet Activation Viewed *Via* Scanning Electron Microscopy

(A) Discoid shape of resting (inactivated) platelets The presence of irregular convoluted gyri and sulci structures. (B) Activated dendritic platelet in contact after the exposure to external stimuli (presence of a biomaterial). The surface convolutions extend into folds on the pseudopods in all directions.

Images were captured *Via* Scanning Electron Microscopy (Chromium sputter coating~20 nm).

The initial platelet responses then result in an array of physiological events included (but not limited to) change in platelet morphology, degranulation and loss of mitochondria, platelet aggregation (Table 3.13).

Table 3.13: Physiologic Responses of Platelet Activation

Response	Result
Platelet Release Reaction	Physiologically active compounds in platelet granules are secreted, such as platelet factor 4, thrombospondin, β-thromboglobulin, Adenosine Diphosphate (ADP) and Serotonin [226, 227]
Release of *P*-Selectin	Mediate adhesion of activated platelet to neutrophils, monocytes and a subset of lymphocytes [228, 229]
Initiation of Platelet Eicosanoid Pathway	Release of arachidonic acid from platelet phospholipids and the synthesis and release of prostaglandinds and thromboxane B_2 [230]
Platelet Shape Change with Pseudopodia	Promotes platelet-platelet contact and adhesion, Promotes association of tenase and prothrombinase complexes on its phospholipids [231]
Exocytotic Budding into Platelet Microparticles (PMPs)	Rich in factor Va, platelet factor 3, and phospholipid-like procoagulant activity [232, 233]

There are over 20 platelet receptors for adhesion and activation; among which GPIIb/IIIa has the highest density (40-80,000 receptors on resting platelets, with another 20-40,000 are present inside the platelets, in a granule membranes and canalicular systems) [234]. Therefore, it is one of the most readily used detectors of platelet adhesion and subsequent activation. The GPIIb/IIIa is present in its inactive form in the resting platelets, however changes its conformation in activated platelets exposing the high-affinity binding site for soluble fibrinogen protein [234]. Beside GPIIb/IIIa receptor, *P*-selectin is considered the other most prominent marker for platelet adhesion to access the biocompatibility of a material. *P*-selectin (translocated to the surface during α-granule release [235]) is thought to facilitate the association between platelets and leukocytes, ultimately leading to thrombin generation [236]. Most of the studies however assess the presence of more than one receptor to provide any conclusive views on

biocompatibility [237, 238]. As well as, we have assessed the biocompatibility of the self-assembling (RADA)$_4$ peptide using both *P*-Selectin, as well as GPIIa/IIIb receptors [239].

3.9.1.1 Current Views on Assessing Biocompatibility *via* Platelet Activity

There is plethora of literature on evaluating biocompatibility of any biomaterial *via* the presence of platelets (through quantifying platelet adhesion and activation receptors), however there lacks a consensus if the lack of platelets (subsequently creating a non-thrombogenic surface) in a system makes it truly biocompatible. One critical factor, which is commonly overlooked, is platelet consumption, defined as the removal from the circulation resulting in platelet turnover (rather than aggregating as a part of thrombus formation). Although it is scientifically accepted to extrapolate platelet survival as platelet function, it should be noted that this widely accepted generalization of biocompatibility is based on certain assumptions. Therefore, usually more than one assay should be carried out to properly biologically evaluating any material. For example, a clotting time analysis, along with the platelet activation assay will provide a better understanding of biocompatibility as the former is considered a fair measure of platelet turnover [240]. Also, it has been found that merely platelet adhesion is not an indicator of platelet activation, as shown in *ex-vivo* by the generation of PMPs by PVA (Polyvinyl Alcohol) hydrogels, in the absence of platelet adhesion [241].

3.9.1.2 Platelet Activation By Flow-Cytometry

Flow cytometry is a powerful platelet analyzing technique, which detects platelets both *in-vitro* and *in-vivo via* antigens, surface bound proteins, platelet activation, measurement of reticulated platelets, intracellular calcium and PMP measurements *in-vivo* and *in-vitro*. Activated

platelets also generate several fragments, and debris, resulting in a solution with particles of varying sizes. To overcome this issue particular clusters of cells are isolated or "gated", allowing the successful analysis of platelets in the mixed population. Single populations of platelets are substantiated and selected on the basis of platelet forward scatter *vs.* side scatter characteristics.

Forward scattered light (FSC) is proportional to cell-surface area/size, and provides means to detect particles greater than a selected size (independent of their fluorescence). Side scatter light (SSC) is proportional to cell granularity or internal complexity of the molecule [242] (Figure 3.15).
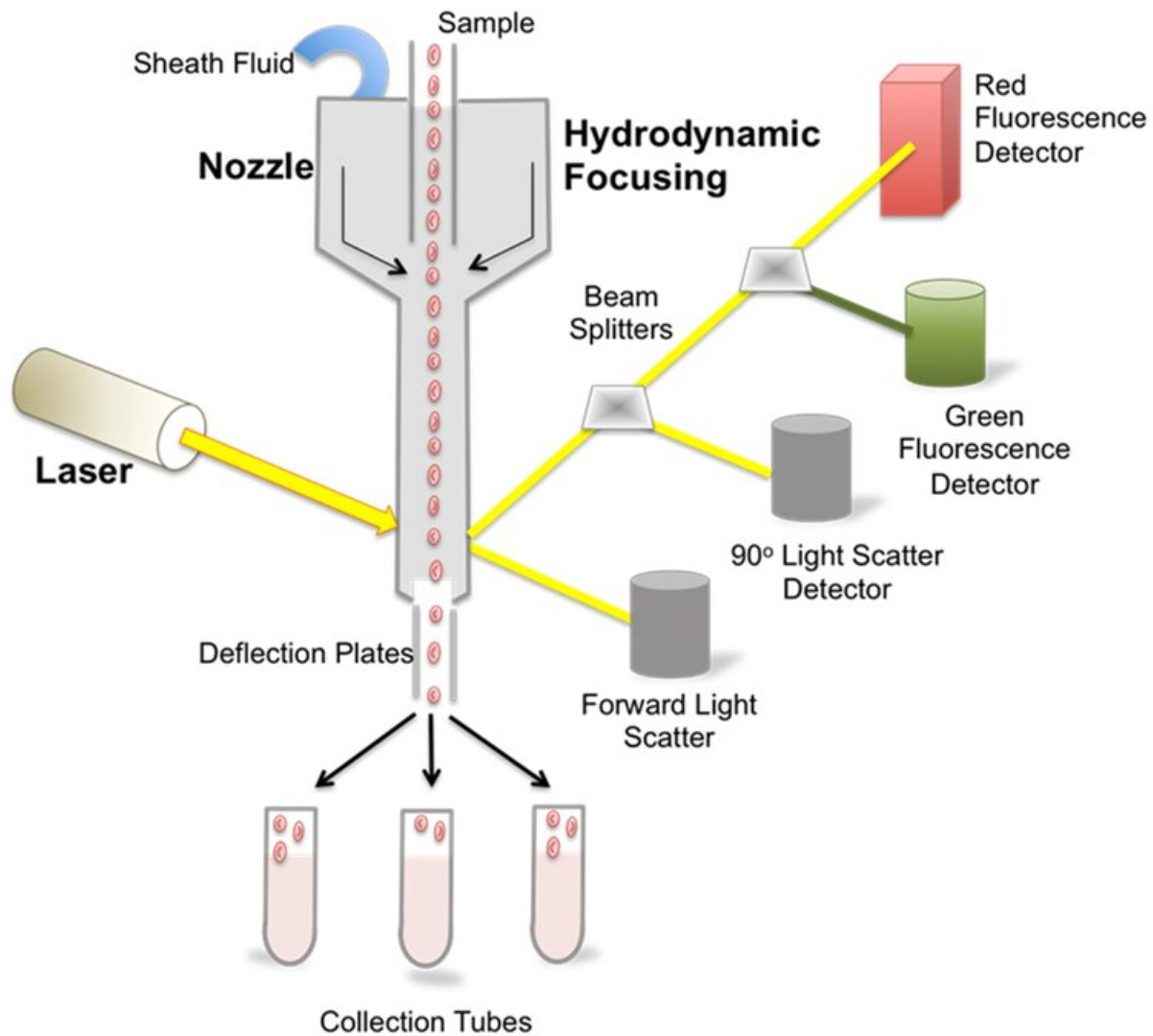
Figure 3.15: Schematic of a typical flow-cytometry setup.

Flow cytometer operates by hydrodynamically suspending cells in a single file, which is interrogated by more than one laser. Where the green fluorescence detector measures the cell surface markers, the 90° light scatter classifies the cells according to granularity, and the forward light scatter classifies the cells according to cell size.

As the general consensus for *in-vitro* biocompatibility evaluation of platelets [238], usually five thousand platelet events are collected, where events positive for CD42 are monitored

to confirm the identity of platelets [243]. Further the fluorescence measurement gates are adjusted to include the upper five per cent of signals obtained with isotype control antibodies. Only the signals collected within the gates for the test samples were counted as positive events for the antibody markers.
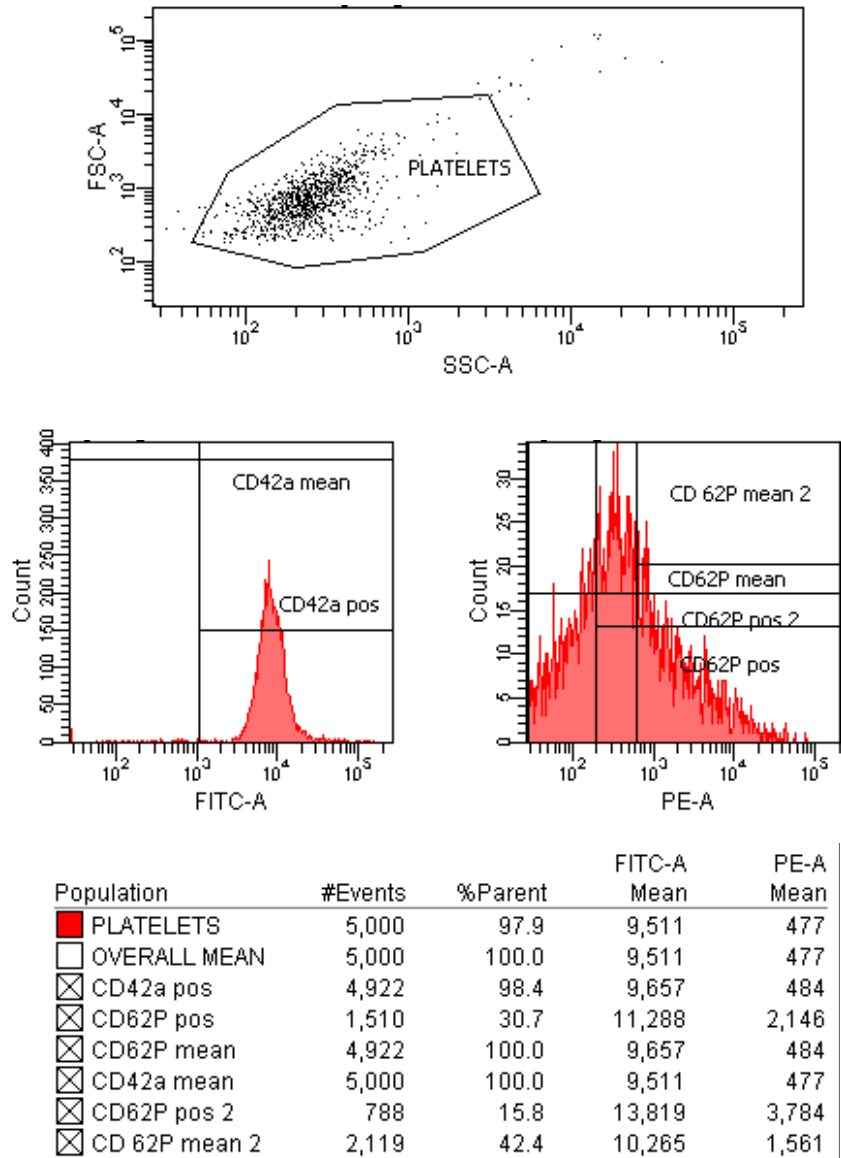
Figure 3.16: *In-vitro* platelet activation induced by thrombin measured *via* CD62 in flow cytometry.

Platelet rich plasma was reacted concurrently with fluorescein-labeled antibody to CD41 and CD62P (platelet surface *P*-selectin).

Data for events within the selected gate (marked platelets (Figure 3.16)) is displayed in the subsequent plots, (usually provided as the percentage of subpopulations (subsets) present Figure 3.16.

Population	#Events	%Parent	FITC-A Mean	PE-A Mean
PLATELETS	5,000	97.6	442	7,547
OVERALL MEAN	5,000	100.0	442	7,547
CD42b pos	4,856	97.1	454	7,770
PAC-1 pos	61	1.3	5,442	6,734
PAC-1 mean	4,856	100.0	454	7,770
CD42b mean	5,000	100.0	442	7,547
PAC-1 pos 2	1,071	21.4	1,510	7,332
PAC-1 mean 2	5,000	100.0	442	7,547
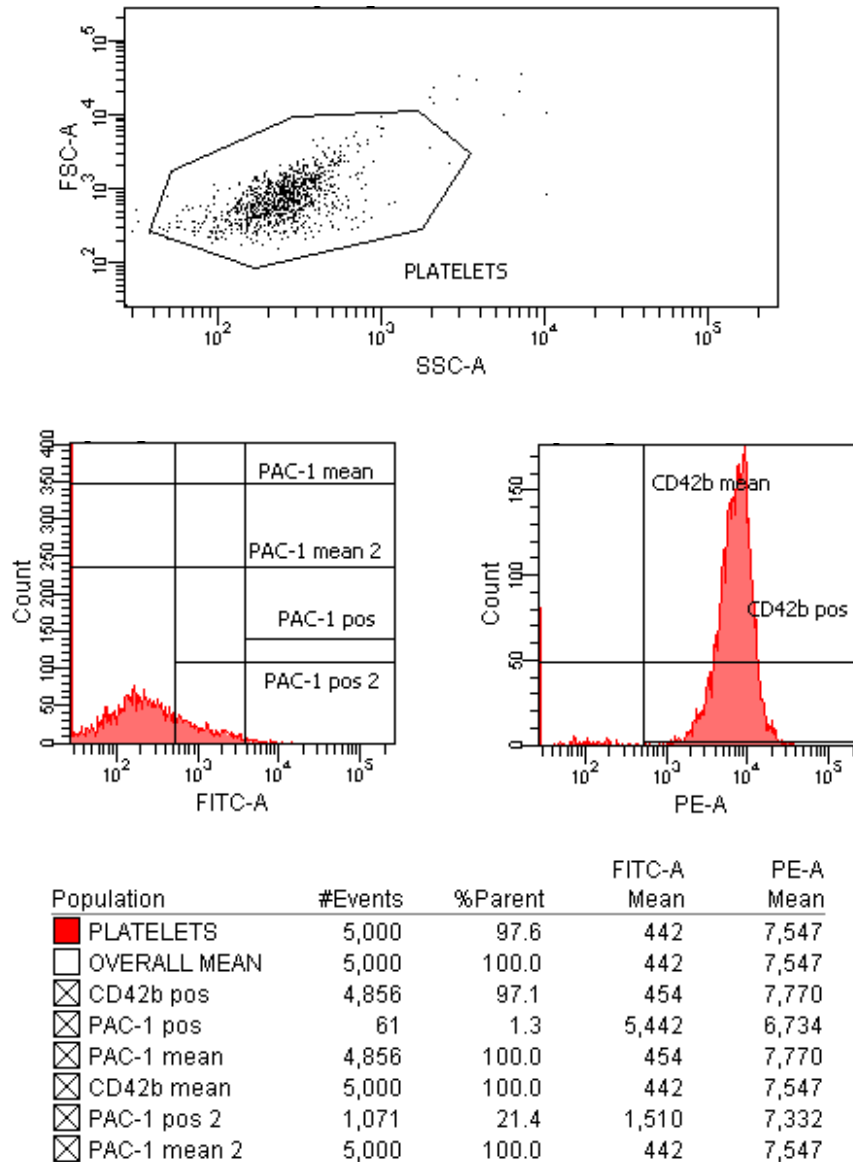
Figure 3.17: *In-vitro* platelet activation induced by thrombin measured *via* PAC-1 in flow cytometry.

Platelet rich plasma was reacted concurrently with fluorescein-labeled antibody to CD41 and PAC1 (activated GPIIb/IIIa).

Flow-cytometry can also be employed to measure platelet turnover by labelling platelets *in-vivo* with NHS-biotin (*N*-hydroxysuccinimido-biotin) and monitoring their disappearance by flow-cytometry. Flow cytometry is considered a gold standard for platelet assessment; it requires

88

a low sample volume for assays and it is conducted on whole blood. The only challenges

mentioned by scientists with respect to this method are: the requirement of expensive equipment;

flow cytometer, and an experienced technician [244].

3.9.1.3 Comparison With Other Platelet Detection Methods

Beside flow cytometry, there are a plethora of other techniques, which could be employed

for platelet analysis. These tests primarily based on detecting platelet aggregation; shear stress

platelet contribution to clot strength, and urinary thromboxane metabolites. One comprehensive

review of these pertinent techniques is provided by Pakala *et al* [244]. Beside flow cytometry

some other techniques to assess platelet presence/activation are: light transmission platelet

aggregometry, whole blood aggregometry, lumiaggregometery, thrombelastography. While these

techniques offer many advantages such as in-vivo testing, rapid assays, and are receptor specific;

they are prone to artifact presentation or are an indirect measure of platelet activation/presence.

Whereas flow cytometry not only offers a rapid assay with a low volume of sample, but includes

whole blood for testing and is considered a gold standard [244].

However, one of the major concerns for using flow cytometry is that it does not mimic

physiological primary hemostasis that inside of a vessel wall. Physiological fluid dynamics has

not only shown the effect of shear conditions on platelet transport to the vessel walls, but also in

dictating specific ligand expression for platelet adhesion [245]. Therefore, high importance has

been placed on the platelet adhesion and thrombus formation studies conducted under flow

conditions [246]. Once such method employs the bench-top cone and plate apparatus named

platelet function analyzer (PFA), which is sensitive to many variables influencing platelet

function such as: platelet number abnormalities, hematocrit, drug and dietary effect, platelet receptor defect, von Willebrand factor defect, release and granular defects [247]. The theoretical principal for cone and plate method involves the laminar flow with uniform shear stress over the plate surface covered by a rotating cone, where the shear force as each point on the plate surface is directly related to the angular velocity and inversely related to the distance of the cone from the plate [248]. Currently, a commercial version of the plate and cone method has been used for testing platelet adhesion and aggregation on a collagen or extracellular matric (ECM)-coated plates [249, 250], where the adhesion of the platelets to the plate is dependant upon plasma von Willebrand factor, fibrinogen binding, platelet GP Ib and GP IIb/IIIa and platelet activation events. Another informative comparative review on platelet function testes has been provided by Paniccia *et al* [251].

3.9.1.4 Approaches To Improve Biocompatibility by Controlling Overall Platelet Economy

In an attempt to increase biocompatibility of polyvinyl alcohol (PVA) based hydrogels heparin was immobilized to a glutaraldehyde cross-linked PVA *via* its amino acid terminus [252], as heparin therapy is known to result in thrombocytopenia [253]. However, the *in-vitro* platelet reactivity in heparin-PVA remained similar to the one without immobilized heparin (pristine PVA), in a variety of experimental assays [252]. Heparin treatment to achieve better biocompatibility still remains questionable, as heparin surfaces are known to both increase [254, 255], and decrease [256] platelet adhesion.

In an attempt to reduce platelet turnover PVA hydrogels have also been surface modified with polyethylene glycol (PEG) [257], and C18 alkyl groups[258]; however, neither of the

90

techniques resulted in the reduction of platelets in the blood. Nevertheless, hydrophobic surfaces (by fully [258] or partially [259] alkylating surfaces) have not only shown to eradicate thrombocytopenia, but also reduced platelet turnover. However, *in-vitro* pre-treatment of heparinized agarose gel columns with plasma or purified antithrombin III was shown to significantly reduce platelet retention, suggesting the formation of heparin/antithrombin III during the process.

3.9.1.5 Factors Affecting Platelet Activation

One of the critical factors affecting platelet activation is flow/sheer rate, which not only affects the transport coefficients (from bulk to the surface and vice versa), but also the activation of key factors including leukocytes (and possibly platelets), and also dilutes the concentration of the activated components [260]. An array of flow chambers with diverse geometries has been used to measure platelet adhesion under controlled flow conditions (a comprehensive review of such devices is conducted by Slack *et al.* [261]). One of the major considerations in designing flow chambers is to mimic the flow rate provided in general vasculature; one such design consists of the cone-and-plate system entailing laminar flow conditions [262]. Even with recirculation and controlling the residence/contact time (to 15 mins), no significance difference in the degree of platelet activation was found with the shear rates between $170\text{-}1000\text{s}^{-1}$, however upon increasing the contact time to 40 mins (and keeping the shear rate constant at 500 s^{-1}), a significant increase in the platelet microparticles was found [262].

91

Platelet adhesion to fibrinogen (*via* GPIIb/IIIa) is found to be efficient below 600-900 s^{-1}, and von Willebrand factor (vWF) over 6000 s^{-1}[263]. Whereas, platelet aggregation is dependent on shear rate at over 7200 s^{-1} [264].

Furthermore, a direct linear relationship between the water content of hydrogel and rate of platelet consumption in baboon AV shut model has been established [265].

3.9.2 **Platelet Morphology**

Platelets upon exposure to external stimuli (such as, foreign particles and surfaces) alter their shape from the resting normal discoid form to more rounded structures possessing blebs and multiple pseudopodia [266].
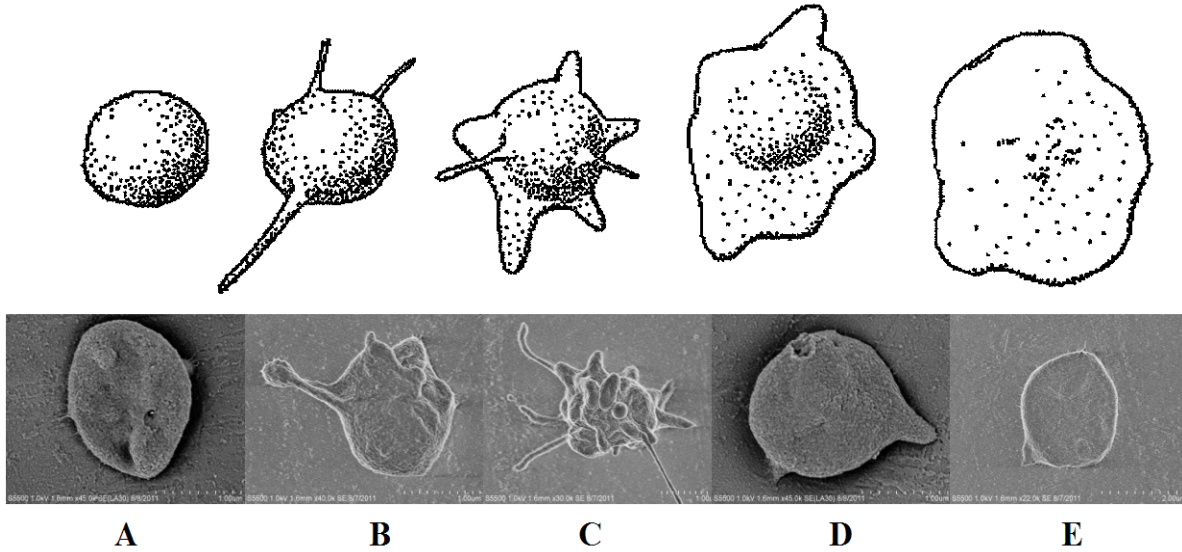
Figure 3.18: Stages of Platelet Activation

The stages of spreading are defined as stated as following: Top; Diagrammatic depiction of platelet spreading. Adapted from Goodman *et. al.* [266]. Bottom: Images were captured *Via* Scanning Electron Microscopy (Chromium sputter coating~20 nm), and are categorized as: (A) Round, R or discoid: with the absence of any pseudopodes; (B) Dendritic, D or early pseudopodial; one or more pseudopodia with no evident flattening; (C) Spread Dendritic, SD or intermediate pseudopodial: one or more pseudopodia flattened, hyaloplasm not spread between psedopodia; (D) Spreading, S: hyaloplasm spread between pseudopodia; and (E) Fully Spread, FS: hyloplasm extensively spread, no distinct pseudopodia.

This change in platelet shape can be monitored *via* oil immersion microscopy (Figure 3.18) and computed using a modified Kunicki scoring system [231], as described in Equation 3.13.

$$MS = [(D \times 4) + (S \times 2) + (B \times 1)] \qquad \textbf{Equation 3.13}$$

Where, MS is the morphology score, D is the number of discoid shaped platelets, S is the number of spiny sphere shaped platelets and B is the number of balloon shaped platelets. A

Kunicki score of less than 200 implies poor retention of morphological characteristics associated with platelets that are activated [231].

3.9.2.1 Comparison With Other Platelet Morphology Assesment Techniques

Kunicki method of morphology scoring is a well-accepted technique to assess platelet morphology, however it can be very time consuming and the scoring may not be reproducible between observers. Hence, an alternative technique involving "shimmering or swirling" effect, which disappears, when platelets lose their discoid shape, can be employed [267]. This method is considered more reproducible than the Kunicki morphology scoring, but has significantly less sensitivity than the earlier. Another method known as the extent of shape change (ESC) correlates more with the morphology scoring [268]. ESC employs an aggregometer to define the ADP induced shape changes in platelets. However, not only ESC is very labour intensive, but not accurate (as it indirectly measures the platelet shape change, by using mean platelet volume). An excellent review of platelet quality tests based on platelet morphology is provided by Maurer-Spurej and Chipperfield [269], from Canadian Blood Services, Vancouver, BC.

3.9.3 Turbidimetric assay for plasma clotting time

Upon the exposure to blood, biomaterials are known to initiate a complex series of events including: protein adsorption, platelet and leukocyte activation and adhesion, complement activation and coagulation [270]. This series of reactions eventually dictates the host response to these materials. The coagulation pathway involves a series of proteolytic reactions (including the intrinsic and extrinsic pathways) resulting in the formation of a fibrin clot. Evaluation of anticoagulant activity based on plasma coagulation has been recognized as a standard test to

estimate blood compatibility of a biomaterial [271]. The extent of coagulation is studied using the time for clot formation upon recalcification of platelet-poor plasma incubated with the biomaterials under investigation.

This turbidimetric assay is conducted to monitor the changes in optical density when platelet-poor human plasma and biomaterials (hydrogels) are incubated in the presence of calcium chloride, where increasing turbidity is indicative of the formation of fibrin clots.

3.9.3.1 Comparison with other plasma clotting assays

One of the simplest methods to measure plasma clot is combining the procoagulant component with plasma and observing the time until a thin strands of fibrin is visible [272]. However, this method is not only prone to observer-to-observer discretion, but is also hard to reproduce with different environmental factors (such as temperature, and humidity). Therefore, instrumental methods are favoured to improve the accuracy and reproducibility of the clotting time. One of the mechanical techniques to measure plasma-clotting time employs fibrometer; which has been widely used for standard clotting studies such as prothrombin time and the activated partial thromboplastin time [273]. Another technique to measure plasma clotting is thromboelastograph, which measures a number of dynamic parameters such as clot strength, in addition to the time until clot formation [274]. However, thromboelastograph is an expensive technique. Other optical methods focussing on detecting specific enzyme functions of the clotting pathway use either a chromogenic or fluorogenic substrate. However, these assays only provide insight into a particular part of the clotting pathway and do not translate well in clotting *in-vivo*. More complex methods [275] can be employed to measure thrombin generation for computing

the downstream effect of procoagulants; however, they are highly expensive techniques and require specialized equipment.

3.9.4 Complement Activation

Along with platelet activation, complement activation plays a key role in the body's defense mechanism. Complement pathway is a non-cellular and non-specific defense system, for immune surveillance and hemostasis [276]. The complement system is also a mediator for tissue growth and regeneration [277].

Complement activation products (such as C3b) are directly known to enhance intravascular coagulation by fibrin deposition [278]. Complement activation is also known to be responsible for procoagulant activities, such as platelet activation, tissue factor expression [279], and modification of the activity of mast cells [280] and basophils [281]. Therefore, the material's interaction with complement is considered a very important aspect of its hemocompatibility [282]. It is believed that three distinct pathways can initiate the complement system: the classical pathway (CP), the alternative pathway (AP), and the Lectin pathway (LP). It is well accepted that complement induced in the presence of biomaterials usually proceeds *via* the AP pathway, whereas the contact with negatively charged surfaces or the use of certain drugs (such as protamine sulfate), may result in the activation of complement through the CP [283]. All three pathways ultimately converge to generate the same central effector molecule C3b, *via* the activity of C3-convertases and the C3-activating enzyme complexes, subsequently forming a C5 convertase splitting C5. [284, 285] (Figure 3.19). C5a is a potent anaphylatoxin, and C5b promotes the assembly of C6-C9 components, resulting in the formation of C5B-9 complement

complex (not shown in Figure 3.19). All the pathways ultimately culminate at the membrane attack complex (MAC), responsible for the cell damage and lysis. A more exhaustive list of the proteins involved in the core complement cascade is provided by Ricklin and colleagues [276].
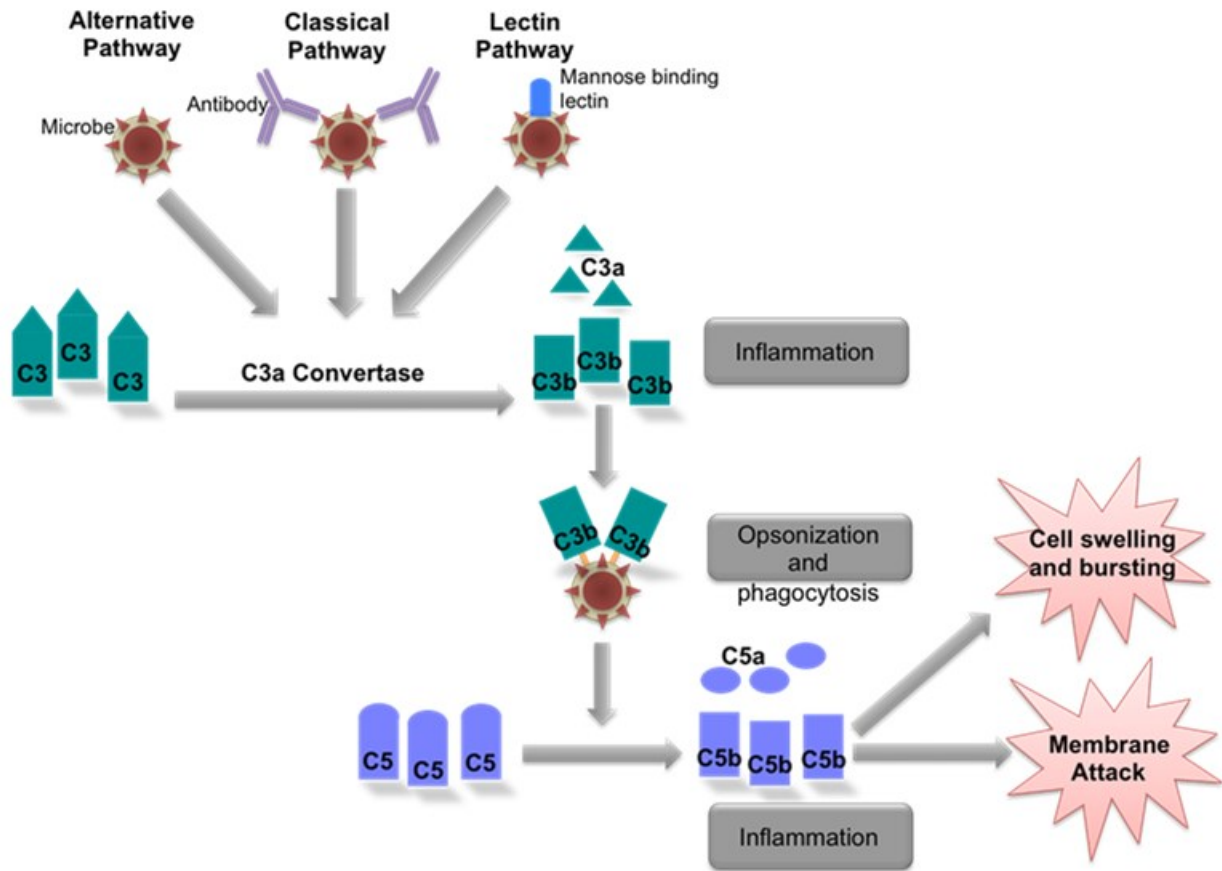
Figure 3.19: An overview of complement activation pathway

Complement activation proceeds in a sequential manner, resulting in a cascade of reactions. The activation cascade can be activated by alternative, classical or lectin pathway. The alternative pathway antigens such as endotoxin, polysaccharides or cell wall components react with the C3b. The classical pathway is activated by the antigen-antibody complex. Lectin pathway is activated though mannose-binding lectin protein. All the three pathways ultimately result in the cleaving of C3 into C3a and C3b by C3a convertase. Where C3a is involved in stimulating inflammation, and C3b reacts with other complement components to form C3a convertase, as well as assist in opsonization and phagocytosis. The subsequent cleavage of C5 to C5a and C5b also enhances inflammation, and form a membrane attack complex (consisting of several complement factors), resulting in cell lysis.

Complement activation can be marked by an array of anaphylatoxins released [286]. The anaphylatoxin C3a itself is very short lived and is cleaved rapidly to the more stable C3a-desArg, which is quantified conducting an enzyme immunoassay [287]. As an anaphylatoxin, C3a has a broad proinflammatory impact on cells such as cytokine expression and chemotaxis [288, 289], as well as it plays a crucial role in both the coagulation and complement cascades [290]. Activation of C5 on the other hand has proven to be responsible for the induction of polymorphonuclear leukocytes (PMN) [291], P-selectin expression on the platelets (Section 3.9.1) [292], and surface expression of P-selectin on endothelial cells [293]. Upon controlling the generation of C5a and C5B-9, leukocyte and platelet activation was blocked [294].

3.9.4.1 Complement Activation with Various Functional Groups

It is also observed that complement activation varies with different functional groups. For example, Sperling and colleagues [295] found that –OH groups attributed to high complement activation, and it has been suggested [296] that the hydroxyl group activates complement *via* the alternative pathway. The proposed and well accepted activation mechanism [297] of the complement system on surfaces bearing –OH groups is as following: Upon C3 hydrolysis to C3a in plasma (Figure 3.19), the thioester group in the C3b molecule is exposed to its surface, consequently reacting with the nucleophilic hydroxyl group on the surface. This process further amplifies the complement activation and triggers the complement loop activation *via* the alternative pathway. However, the studies in our lab showed (RADA)$_4$ peptide consisting of (-OH containing) serine groups elicited less C3a when compared to both: pristine (RADA)$_4$ and (RADA)$_4$K$_5$. It can be postulated that despite the presence of –OH groups, the different underlying polymer structures in both of the studies played a role in activating complement to

different levels. In agreement with our theory, Labarre and colleagues [298] also found that not only the density of the –OH surface groups plays an important part in complement activation, but the underlying polymer also plays an important part. Further studies have explored the effect of amino ($-NH_2$), methyl ($-CH_3$), and carboxyl (-COOH), in addition to the hydroxyl (-OH) group have on the activating complement. It was found that among these groups –OH group elicited the most complement, whereas all the other functional groups had low complement activation *via* either the classical or the alternative pathways.

It was postulated that the $-NH_3$ group, would elicit similar level of complement activation as the –OH group, as both share nucleophilic characteristics. Low molecular weight amines in blood were found to react with thioester group of C3 [299], and C3b [300]. Studies in our lab also showed significantly high complement activation with $(RADA)_4$ consisting of $-NH_3$ group bearing lysine residues. However, Arima and colleagues [296] found that amount of C3a released into serum after exposure to amine group bearing self-assembling monolayer was much lower than the one with –OH group. Toda and colleagues [301] also found no complement activation with amine groups. The authors [301] proposed that under physiological pH the positively charged amino group attracts various negatively charged serum proteins (such as albumin), forming a layer of proteins adsorbed to the surface through electrostatic interactions. The protein layer interrupts access of C3b to the surface amino groups, and hence, failing in the formation of C3 convertase. It has been concluded that the behavior of complement system in the presence of the amino groups is still poorly understood; and hence, more systematic study with one consistent underlying polymer needs to be conducted to investigate the complement response further. A brief overview of these results is provided in the Table 3.14 below.

Table 3.14: Complement activation on self assembling, surfaces bearing various functional groups

Alkanethiol surface	Complement Activation	Measured Component	Ref
–OH: C_{11}–OH 100%,	Strong activation	C5a	[295]
–CH$_3$: C_{15}–CH$_3$ 100%,	Minimal activation	C5a	[295]
–COOH: C_{10}–COOH 100%,	Moderate activation	C5a	[295]
–OH 49%: C_{11}–OH (49%)+C_{10}–COOH (51%),	High activation	C5a	[295]
–OH 89%: C_{11}–OH (89%)+C_{10}–COOH (11%),	Strong activation	C5a	[295]
–CH$_3$ 53%: C_{15}–CH$_3$ 53%+C_{15}–COOH (47%).	Minimal activation	C5a	[295]
–C11NH$_2$/C11CH$_3$	Minimal activation	C3b	[301]
–C11NH$_2$/C10COOH	Strong activation	C3b	[301]

3.9.4.2 Complement Activation with Different Biomaterials

When a biomaterial comes in contact with blood, complement activation is one of the reactions of inflammatory response, as a part of body's defense mechanism. Surface-induced complement activation has been known to activate cell-adhesion, platelet aggregation, and platelet activation, resulting in thrombosis [302]. Hence, complement activation is considered an index to measure of the biocompatibility of a material. An ideal biomaterial is expected to have low C3a activation upon in contact with human blood. Hence, complement activation induced by various biomaterials has been studied, with an ultimate goal of designing biocompatible surfaces of synthetic materials. A brief overview of complement activation on some reference biomaterials is given in the Table 3.15 below.

Upon monitoring complement activation (on surface and fluid phases) in biomaterials it was found that the requirements for the formation and stability of the C3 convertase on the artificial surfaces differed from those found on biological membranes [303, 304]. Contrary to our discussion in section 3.9.4.1 with respect to various functional groups eliciting complement; C3 convertase formation was not dependent on the presence of –OH or –NH_2 functional groups on the biomaterials [303, 305], and the binding of factors B and H to some biomaterial surfaces was found to be independent of complement activation and unaffected by the presence or absence of C3 [303]. It can also be concluded that the hydrophobicity of a biomaterial dictates the orientation and/or conformation of the adsorbed C3 [306]. For instance, when adsorbed to the hydrophobic surface, C3 primarily exposes the binding site specific to factor H only, whereas factor B binds to the C3 adsorbed on a hydrophilic surface.

Cellulosic membranes were widely used for hemodialysis; however, their ability to strongly activate complement lead to the subsequent development of new dialysis membranes with improved biocompatibility. It was thought that the –OH group on the polysaccharide surface of cellulose cotton fibers promoted the deposition of C3b on the surface, resulting in very high levels of C3a and C5a in the blood samples. One of the techniques to mask the C3 activating tendency of the –OH groups was to acetylation of the groups which substantially reduced the blood C3a levels (due to the low binding of C3b and increased binding of C3b inactivating factor H) [307, 308]. The two other commercially available hemodialysis membranes: polymethylmethacrylate (PMMA) and polysulfone (PS), also considered biocompatible due to their low complement activation [307]. It was found that biomaterials such as poly(N-vinylpyrrolidone) (PVP) [238]and (RADA)$_4$ [239] had minimal complement activation.

In an attempt to make biocompatible biomaterials, efforts have been made to reduce protein adsorption and cell adhesion. One of these strategies involves introducing hydrophilic groups on surfaces. However, even though Cuprophan membrane consists of hydrophilic surface, it is an effective complement activator (Table 3.15). Further studies are conducted with modifying the surfaces with hydrophilic surfaces with polyethylene oxide (PEO), and assessing the resulting complement activation potential. PEO is an uncharged, hydrophilic and non-immunogenic biopolymer that can be physically adsorbed or covalently attached to the surfaces, to achieve biocompatibility [309]. For example, after adsorbing hydrophilic layer of PEO onto the Stealth® liposomes and nanospheres surfaces resulted in the increase in their half-lives presumably due to increased biocompatibility [310]. Another approach to reduce complement activation on synthetic materials is to promote adsorption of factor D onto the surfaces [311], whereas factor D is an enzyme imperative to the activation of AP, and is inactive when bound to certain surfaces.

Table 3.15: Level of complement activation (strong, moderate, and low) with various commonly studied biomaterials.

Strong	Moderate	Low
Polyvinyl chloride (PVC) [312]	Cuprophan [307, 312]	Linear polyglycidol (LPG) [307]
Hydroxymethyl methacrylate (HEMA) [313]	Cellulose acetate [308]	Trisacryl® [298]
Oligo(ethylene glyco) (OEG) [314]	Hemophan [307]	Polysulfone
Sephandex® [298]	Polycarbonate [307]	Reused cuprophan [307]
Polyacrylonitrile (PAN)	C_{10}–COOH [295]	Polyacrylonitrile sodium methallylsulfonate [308]
C_{11}–OH [295]	Hetastarch [238]	Poly (acrylonitrile co-allyl sulphonate) (AN69S) [312]
Polyvinyl chloride plasticised with di-2-ethyl-hexyl-phthalate (PVC/DEHP) [312]	Hyperbranched Polyglycidol (HPG) [238]	C_{15}–CH$_3$ [295]
		(RADA)$_4$ [239]
		Poly(N- vinylpyrrolidone) (PVP) [238]
		PEG 350 [238]
		Dextran [238]

Sephandex® is a crosslinked dextran, whereas, Trisacryl® is an -OH bearing hydrogel microsphere prepared by polymerisation of N-acryloyl-2-amino-2-(hydroxymethyl)-1,3-propanediol in the presence of a crosslinking agent.

3.9.4.3 Comparison with other Complement Activation Techniques

Berger and colleagues [287] have provided in-depth validation of the ELISA (enzyme lined immunosorbent assay) for complement activation, where they assayed three complement proteins: iC3b, Factor Bb, and C3a. The study concluded that iC3b measurements underestimated complement activation, whereas the presence of factor Bb was a reliable indicator of complement

activation, and C3a was a highly relevant measure of complement activation. It was postulated that the some of the C3b (prior to converting into iC3b) remained bound to the surface and is not assessed *via* plasma analysis; thereby making iC3b a poor assessor of complement analysis. Whereas, even though factor Bb assay is a good measure for complement activation, it is an indirect measure of C3a activation. The ELISA C3a activation kits have evolved as a gold standard to evaluate complement activation by a biomaterial. However, there remains a debate if to use plasma (yielding lower background levels) [315, 316], or serum (better mimicking the non-anticoagulant situation, since heparin has inhibitory effect on both the classical and alternative pathways) [317] to examine the C3a activation. C3a assays in our lab were conducted with platelet poor-plasma. Also, there is no significant difference found in complement activation of several biomaterials, in the presence of citrate and $MgCl_2$ [283]. A brief comparison of some of the basic techniques to study complement activation is given in the Table 3.16 below.

Table 3.16: Standard techniques to study complement activation

		Type of Assay	Advantages	Limitations	Ref
Functional Assay	**Total complement activity of the classical, lectin, and alternative pathways**	Hemolytic assay Involves the deposition of serum activated products with pathway specific factors	▪ Simplified, ▪ Reproducible ▪ Suitability for automated systems	▪ Prone to false positives	[318, 319]
	Activity of individual components	Titration of individual complement proteins	▪ Specific ▪ Easy to perform	▪ Sensitive to environmental conditions (temperature)	[318]
	Enzyme immunoassay (EIA)	Functional C1 inhibitor activity	▪ Provide screening deficiencies of the classical, lectin and the alternative pathways. Does not depend on availability of sensitized erythrocytes	▪ None	[287, 320]
Immunochemical Assays for Individual Components	**Surface Plasmon Resonance (SPR)**	Detects adsorbed immunoglobulins (C1q, C4, C3b, C3c)	▪ Probes proteins at interfaces	▪ Setting of optical units is relatively simple	[296]
	Ellipsometry	Detects adsorbed immunoglobulins (C1q, C4, C3b, C3c)	▪ Probes proteins at interfaces	▪ Complicated procedure	[321]
	Quartz Crystal Microbalance (QCM)	Detects adsorbed immunoglobulins (C1q, C4, C3b, C3c)	▪ Provides information on the adsorbed mass, as well as on viscoelastic properties of proteins	▪ None	[322]
Assays for complement-binding Auto-antibodies	**The enzyme-linked immunosorbent assay (ELISA)**	Detects complement fragments: C3a, iC3b, C5a, and SC5b-9	▪ Gold standard for complement activation ▪ Copious amount of literature to compare with.	▪ Data should be compared with a large panel of healthy controls ▪ Hampered by high background signals due to spontaneous alternative pathway activation	[287]

The complement activation assays described in this chapter are focused on *in-vitro* assessment; therefore, we would provide a brief overview of the *in-vivo* techniques currently available to evaluate the complement activation of materials. Unlike *in-vitro* analysis, EDTA plasma should be used, and serum should not be used for *in-vivo* analysis of the complement

activation (to prevent *ex-vivo* activation). Principally, same assays can be used to study the *in-vivo* complement activation, as *in-vitro*, however some modifications to the tests should be made (for example, to adjust for the protein concentration of body fluids). Usually, the activation of terminal complement complex (TCC), is used as a marker for complement activation, since it pertains to the end of the final terminal pathway [323]. Surface plasmon resonance (SPR) is another complement analysis technique, which allows monitoring of individual biomolecular interactions between complement components [296]. In contrast to the ELISA techniques, SPR detects dynamic processes of protein deposition on the material surface, thereby; both of these techniques provide complementary information to examine complement activation. Other techniques to study complement activation are immune histochemistry, and animal *in-vivo* studies.

3.10 Concluding Remarks

Design and applications of the self-assembly of peptide amphiphiles have been extensively studied for both research and applications. This review highlights some of the key representative studies of the various kinds of self-assembling peptides, which are currently being studied or used as biomaterials. The prime focus of this review is to understand the self-assembly mechanism of the ionic self-assembling oligopeptides. Over the period of time, we have come to understand the underlying forces dictating self-assembly. The primary focus of early scientific endeavours involved studying the intermolecular and interatomic short-range forces (driving molecular packing). This lead to further investigation in the long-range forces (such as van der Waals, electric double-layer forces, and steric hindrances), which determine if the two entities are

able to get close enough in the first place, before the short-range forces may further stabilize the self-assembled structure. It is found that the interfacial assembly of the peptides is a fine balance of many forces, such as electrostatic interactions, hydrophobic interactions, ionic strength, and hydrogen bonding. Since, the peptide structure vary with respect to the amino acid composition and length, these driving forces vary from peptide to peptide.

The fundamental characteristics of these peptides can be studied *via* several methods, such as CD, FCS and DSC; these methods along with other commonly used methods are also reviewed in this chapter. Finally, a brief overview of the self-assembling peptide's applications is provided. The knowledge gained through the on-going research in this area will provide guidance for future design of these peptide-based biomaterials.

References

[1] Zhao X, Pan F, Xu H, Yaseen M, Shan H, Hauser CAE, *et al*. Molecular self-assembly and applications of designer peptide amphiphiles. Chemical Society Reviews 2010;39:3480-98.

[2] Pelesko JA. Self assembly. [electronic resource] : the science of things that put themselves together: Boca Raton : Taylor & Francis, 2007.; 2007.

[3] Whitesides GM, Grzybowski B. Self-assembly at all scales. Science 2002;295:2418-21.

[4] Jakubith S, Rotermund HH, Engel W, Vonoertzen A, Ertl G. Spatiotemporal concentration patterns in a surface-reaction - propagating and standing waves, totating spirals and turbulence. Phys Rev Lett 1990;65:3013-6.

[5] Hess B. Periodic patterns in biology. Naturwissenschaften 2000;87:199-211.

[6] Hauser CAE, Zhang S. Designer self-assembling peptide nanofiber biological materials. Chemical Society Reviews 2010;39:2780-90.

[7] Zhang SG, Lockshin C, Herbert A, Winter E, Rich A. Zuotin, a putative Z-binding-protein in saccaromycescervisiae. Embo Journal 1992;11:3787-96.

[8] Harper JD, Lansbury PT. Models of amyloid seeding in Alzheimier's disease and scrapie: Mechanistic truths and physiological consequences of the time-dependent solubility of amyloid proteins. Annual Review of Biochemistry 1997;66:385-407.

[9] Dobson CM. Protein misfolding, evolution and disease. Trends in Biochemical Sciences 1999;24:329-32.

[10] Sipe JD, Cohen AS. Review: History of the amyloid fibril. Journal of Structural Biology 2000;130:88-98.

[11] Sunde M, Blake CCF. From the globular to the fibrous state: protein structure and structural conversion in amyloid formation. Quarterly Reviews of Biophysics 1998;31:1.

[12] Azriel R, Gazit E. Analysis of the structural and functional elements of the minimal active fragment of islet amyloid polypeptide (IAPP) - An experimental support for the key role of the phenylalanine residue in amyloid formation. J Biol Chem 2001;276:34156-61.

[13] Tenidis K, Waldner M, Bernhagen J, Fischle W, Bergmann M, Weber M, *et al*. Identification of a penta- and hexapeptide of islet amyloid polypeptide (IAPP) with amyloidogenic and cytotoxic properties. Journal of Molecular Biology 2000;295:1055-71.

[14] Lodish H. Cloning Expeditions: Risky but Rewarding. Mol Cell Biol 2013;33:4620-7.

[15] Cen L, Liu W, Cui L, Zhang WJ, Cao YL. Collagen tissue engineering: Development of novel biomaterials and applications. Pediatr Res 2008;63:492-6.

[16] Yamaoka H, Asato H, Ogasawara T, Nishizawa S, Takahashi T, Nakatsuka T, *et al*. Cartilage tissue engineering chondrocytes embedded in using human auricular different hydrogel materials. Journal of Biomedical Materials Research Part A 2006;78A:1-11.

[17] Rodríguez-Cabello JC, Arias FJ, Rodrigo MA, Girotti A. Elastin-like polypeptides in drug delivery. Advanced Drug Delivery Reviews 2016;97:85-100.

[18] Ahmed TAE, Dare EV, Hincke M. Fibrin: A versatile scaffold for tissue engineering applications. Tissue Eng Part B-Rev 2008;14:199-215.

[19] Zhao W, Jin X, Cong Y, Liu Y, Fu J. Degradable natural polymer hydrogels for articular cartilage tissue engineering. Journal of Chemical Technology and Biotechnology 2013;88:327-39.

[20] Holland TA, Tabata Y, Mikos AG. Dual growth factor delivery from degradable oligo(poly(ethylene glycol) fumarate) hydrogel scaffolds for cartilage tissue engineering. Journal of Controlled Release 2005;101:111-25.

[21] Oliveira JT, Reis RL. Polysaccharide-based materials for cartilage tissue engineering applications. J Tissue Eng Regen Med 2011;5:421-36.

[22] Suh JKF, Matthew HWT. Application of chitosan-based polysaccharide biomaterials in cartilage tissue engineering: a review. Biomaterials 2000;21:2589-98.

[23] Kumar M, Muzzarelli RAA, Muzzarelli C, Sashiwa H, Domb AJ. Chitosan chemistry and pharmaceutical perspectives. Chem Rev 2004;104:6017-84.

[24] Freier T, Koh HS, Kazazian K, Shoichet MS. Controlling cell adhesion and degradation of chitosan films by N-acetylation. Biomaterials 2005;26:5872-8.

[25] Rinaudo M, Pavlov G, Desbrieres J. Influence of acetic acid concentration on the solubilization of chitosan. Polymer 1999;40:7029-32.

[26] Campo GM, Avenoso A, Nastasi G, Micali A, Prestipino V, Vaccaro M, *et al*. Hyaluronan reduces inflammation in experimental arthritis by modulating TLR-2 and TLR-4 cartilage expression. Biochim Biophys Acta-Mol Basis Dis 2011;1812:1170-81.

[27] Solchaga LA, Yoo JU, Lundberg M, Dennis JE, Huibregtse BA, Goldberg VM, *et al*. Hyaluronan-based polymers in the treatment of osteochondral defects. J Orthop Res 2000;18:773-80.

[28] Cohen DL, Malone E, Lipson H, Bonassar LJ. Direct freeform fabrication of seeded hydrogels in arbitrary geometries. Tissue Eng 2006;12:1325-35.

[29] Ribeiro CC, Barrias CC, Barbosa MA. Calcium phosphate-alginate microspheres as enzyme delivery matrices. Biomaterials 2004;25:4363-73.

[30] Martinsen A, Storro I, Skjakbraek G. Alginate as immobilization material.3. Diffisuonal properties. Biotechnol Bioeng 1992;39:186-94.

[31] Alsberg E, Anderson KW, Albeiruti A, Franceschi RT, Mooney DJ. Cell-interactive alginate hydrogels for bone tissue engineering. J Dent Res 2001;80:2025-9.

[32] Alsberg E, Anderson KW, Albeiruti A, Rowley JA, Mooney DJ. Engineering growing tissues. Proceedings of the National Academy of Sciences of the United States of America 2002;99:12025-30.

[33] Setton LA, Elliott DM, Mow VC. Altered mechanics of cartilage with osteoarthritis: human osteoarthritis and an experimental model of joint degeneration. Osteoarthritis Cartilage 1999;7:2-14.

[34] Lee KY, Mooney DJ. Alginate: Properties and biomedical applications. Progress in Polymer Science 2012;37:106-26.

[35] Chevallay B, Herbage D. Collagen-based biomaterials as 3D scaffold for cell cultures: applications for tissue engineering and gene therapy. Medical and Biological Engineering and Computing;38:211-8.

[36] Weinberg CB, Bell E. A blood-vessel model constructed from collagen and cultured vascular cells. Science 1986;231:397-400.

[37] Wallace DG, Rosenblatt J. Collagen gel systems for sustained delivery and tissue engineering. Advanced Drug Delivery Reviews 2003;55:1631-49.

[38] Annabi N, Mithieux SM, Weiss AS, Dehghani F. The fabrication of elastin-based hydrogels using high pressure CO(2). Biomaterials 2009;30:1-7.

[39] Simnick AJ, Lim DW, Chow D, Chilkoti A. Biomedical and biotechnological applications of elastin-like polypeptides. Polym Rev 2007;47:121-54.

[40] Karfeld-Sulzer LS, Siegenthaler B, Ghayor C, Weber FE. Fibrin Hydrogel Based Bone Substitute Tethered with BMP-2 and BMP-2/7 Heterodimers. Materials 2015;8:977-91.

[41] Schense JC, Hubbell JA. Cross-linking exogenous bifunctional peptides into fibrin gels with factor XIIIa. Bioconjugate Chemistry 1999;10:75-81.

[42] Balakrishnan B, Mohanty M, Umashankar PR, Jayakrishnan A. Evaluation of an in situ forming hydrogel wound dressing based on oxidized alginate and gelatin. Biomaterials 2005;26:6335-42.

[43] Kuijpers AJ, Engbers GHM, Krijgsveld J, Zaat SAJ, Dankert J, Feijen J. Cross-linking and characterisation of gelatin matrices for biomedical applications. Journal of Biomaterials Science-Polymer Edition 2000;11:225-43.

[44] Bhattarai N, Gunn J, Zhang MQ. Chitosan-based hydrogels for controlled, localized drug delivery. Advanced Drug Delivery Reviews 2010;62:83-99.

[45] Burdick JA, Prestwich GD. Hyaluronic Acid Hydrogels for Biomedical Applications. Advanced Materials 2011;23:H41-H56.

[46] Allison DD, Grande-Allen KJ. Review. Hyaluronan: A powerful tissue engineering tool. Tissue Eng 2006;12:2131-40.

[47] Bouhadir KH, Lee KY, Alsberg E, Damm KL, Anderson KW, Mooney DJ. Degradation of partially oxidized alginate and its potential application for tissue engineering. Biotechnol Prog 2001;17:945-50.

[48] Park KH. Improved long-term culture of hepatocytes in a hydrogel containing Arg-Gly-Asp (RGD). Biotechnol Lett 2002;24:1131-5.

[49] Lin CC, Metters AT. Hydrogels in controlled release formulations: Network design and mathematical modeling. Advanced Drug Delivery Reviews 2006;58:1379-408.

[50] Buxton AN, Zhu J, Marchant R, West JL, Yoo JU, Johnstone B. Design and characterization of poly(ethylene glycol) photopolymerizable semi-interpenetrating networks for chondrogenesis of human mesenchymal stem cells. Tissue Eng 2007;13:2549-60.

[51] Yang F, Williams CG, Wang DA, Lee H, Manson PN, Elisseeff J. The effect of incorporating RGD adhesive peptide in polyethylene glycol diacrylate hydrogel on osteogenesis of bone marrow stromal cells. Biomaterials 2005;26:5991-8.

[52] Zhu JM. Bioactive modification of poly(ethylene glycol) hydrogels for tissue engineering. Biomaterials 2010;31:4639-56.

[53] Schmedlen KH, Masters KS, West JL. Photocrosslinkable polyvinyl alcohol hydrogels that can be modified with cell adhesion peptides for use in tissue engineering. Biomaterials 2002;23:4325-32.

[54] Ossipov DA, Brannvall K, Forsberg-Nilsson K, Hilborn J. Formation of the first injectable poly(vinyl alcohol) hydrogel by mixing of functional PVA precursors. J Appl Polym Sci 2007;106:60-70.

[55] Stile RA, Burghardt WR, Healy KE. Synthesis and characterization of injectable poly(N-isopropylacrylamide)-based hydrogels that support tissue formation in vitro. Macromolecules 1999;32:7370-9.

[56] Takezawa T, Mori Y, Yoshizato K. Cell culture on a thermoresponsive polymer surface. Bio-Technology 1990;8:854-6.

[57] Higuchi A, Aoki N, Yamamoto T, Miyazaki T, Fukushima H, Tak TM, *et al*. Temperature-induced cell detachment on immobilized pluronic surface. Journal of Biomedical Materials Research Part A 2006;79A:380-92.

[58] Stile RA, Healy KE. Poly(N-isopropylacrylamide)-based semi-interpenetrating polymer networks for tissue engineering applications. 1. Effects of linear poly(acrylic acid) chains on phase behavior. Biomacromolecules 2002;3:591-600.

[59] Freudenberg U, Hermann A, Welzel PB, Stirl K, Schwarz SC, Grimmer M, *et al*. A star-PEG-heparin hydrogel platform to aid cell replacement therapies for neurodegenerative diseases. Biomaterials 2009;30:5049-60.

[60] Hern DL, Hubbell JA. Incorporation of adhesion peptides into nonadhesive hydrogels useful for tissue resurfacing. J Biomed Mater Res 1998;39:266-76.

[61] Shin H, Jo S, Mikos AG. Biomimetic materials for tissue engineering. Biomaterials 2003;24:4353-64.

[62] Kopesky PW, Vanderploeg EJ, Sandy JS, Kurz B, Grodzinsky AJ. Self-assembling peptide hydrogels modulate in vitro chondrogenesis of bovine bone marrow stromal cells. Tissue engineering Part A 2010;16:465-77.

[63] Silva AK, Richard C, Bessodes M, Scherman D, Merten OW. Growth factor delivery approaches in hydrogels. Biomacromolecules 2009;10:9-18.

[64] Zisch AH, Lutolf MP, Hubbell JA. Biopolymeric delivery matrices for angiogenic growth factors. Cardiovascular pathology : the official journal of the Society for Cardiovascular Pathology 2003;12:295-310.

[65] Patenaude M, Hoare T. Injectable, Degradable Thermoresponsive Poly(N-isopropylacrylamide) Hydrogels. ACS Macro Letters 2012;1:409-13.

[66] Dumortier G, Grossiord JL, Agnely F, Chaumeil JC. A review of poloxamer 407 pharmaceutical and pharmacological characteristics. Pharm Res 2006;23:2709-28.

[67] Saffer EM, Tew GN, Bhatia SR. Poly(lactic acid)-poly(ethylene oxide) Block Copolymers: New Directions in Self-Assembly and Biomedical Applications. Curr Med Chem 2011;18:5676-86.

[68] Park KE, Kang HK, Lee SJ, Min BM, Park WH. Biomimetic nanofibrous scaffolds: Preparation and characterization of PGA/chitin blend nanofibers. Biomacromolecules 2006;7:635-43.

[69] Cipitria A, Skelton A, Dargaville TR, Dalton PD, Hutmacher DW. Design, fabrication and characterization of PCL electrospun scaffolds-a review. Journal of Materials Chemistry 2011;21:9419-53.

[70] Aghdam RM, Najarian S, Shakhesi S, Khanlari S, Shaabani K, Sharifi S. Investigating the effect of PGA on physical and mechanical properties of electrospun PCL/PGA blend nanofibers. J Appl Polym Sci 2012;124:123-31.

[71] Stupp SI. Self-assembly and biomaterials. Nano Lett 2010;10:4783-6.

[72] Anirudhan TS, Divya PL, Nima J. Synthesis and characterization of novel drug delivery system using modified chitosan based hydrogel grafted with cyclodextrin. Chem Eng J 2016;284:1259-69.

[73] Jayawarna V, Richardson SM, Hirst AR, Hodson NW, Saiani A, Gough JE, *et al*. Introducing chemical functionality in Fmoc-peptide gels for cell culture. Acta Biomater 2009;5:934-43.

[74] Galler KM, Aulisa L, Regan KR, D'Souza RN, Hartgerink JD. Self-assembling Multidomain Peptide Hydrogels: Designed Susceptibility to Enzymatic Cleavage Allows Enhanced Cell Migration and Spreading. Journal of the American Chemical Society 2010;132:3217-23.

[75] Ellis-Behnke RG, Liang Y-X, Tay DKC, Kau PWF, Schneider GE, Zhang S, *et al*. Nano hemostat solution: immediate hemostasis at the nanoscale. Nanomedicine : nanotechnology, biology, and medicine 2006;2:207-15.

[76] Wang T, Zhong XZ, Wang ST, Lv F, Zhao XJ. Molecular Mechanisms of RADA16-1 Peptide on Fast Stop Bleeding in Rat Models. Int J Mol Sci 2012;13:15279-90.

[77] Zhang S. Fabrication of novel biomaterials through molecular self-assembly. Nat Biotech 2003;21:1171-8.

[78] Pierschbacher MD, Ruoslahti E. Cell attachment activity of a fibronectin can be duplicated by small synthetic fragments of the molecule. Nature 1984;309:30-3.

[79] Watt KWK, Cottrell BA, Strong DD, Doolittle RF. Amino acid sequence studies on the alpha-chain of human-fibrinogen - overlappign sequences providing the complete sequence. Biochemistry 1979;18:5410-6.

[80] Clement JM, Hofnung M. Gene sequence of the lambda receptor, an outer-membrane protein of Excherichia-coli K12. Cell 1981;27:507-14.

[81] Rice CM, Strauss JH. Nucleotide-sequence of the 26S messenger-RNA of Sindbis virus and deduced sequence of the encoded virus structural proteins. Proceedings of the National Academy of Sciences of the United States of America-Biological Sciences 1981;78:2062-6.

[82] Ruoslahti E, Vaheri A. Interaction of soluble fibroblast surface antigen with firbinogen and fibrin - Identitiy with cold insoluble globulin of human plasma. Journal of Experimental Medicine 1975;141:497-501.

[83] Plow EF, Ginsberg MH. Specific and saturable binding of plasma fibronectin to thrombin-stimulated human platelets. J Biol Chem 1981;256:9477-82.

[84] Plow EF, Marguerie G. Inhibition of fibrinogen binding to human platelets by the tetrapeptide glycyl-L-prolyl-Larginyl-L Proline. Proceedings of the National Academy of Sciences of the United States of America 1982;79:3711-5.

[85] Anfinsen CB, Haber E, Sela M, White FH. Kinetic of formation of native ribonuclease during oxidation of reduced polypeptide chain. Proceedings of the National Academy of Sciences of the United States of America 1961;47:1309.

[86] Cook DA. Relation between amino acid sequence and protein conformation. Journal of Molecular Biology 1967;29:167.

[87] Ptitsyn OB. Stastical analysis of distribution of amino acid residues among helical and non-helical regions in glubular proteins. Journal of Molecular Biology 1969;42:501.

[88] Finkelst.Av, Ptitsyn OB. Statistical analysis of correlation among amino acid residues in helical, beta-structural and non-regulatar regions of globular proteins. Journal of Molecular Biology 1971;62:613.

[89] Chou PY, Fasman GD. Conformational parameters for amino-acid in helical, beta- sheet, and random coil regions calculated from proteins. Biochemistry 1974;13:211-22.

[90] Engel J, Schwarz G. Cooperative conformational transitions of linear biopolymers. Angewandte Chemie-International Edition 1970;9:389.

[91] Conio G, Patrone E, Salaris F. Conformational transitions of poly(L-Tyrosine) in mixed ethanol solvents. Macromolecules 1971;4:283.

[92] Chou PY, Fasman GD. Prediction of protein conformation. Biochemistry 1974;13:222-45.

[93] Snell CR, Fasman GD. Kinetics and thermodynamics of alpha helix-/-beta transconfromation of poly(L-lysine) and L-leucine copilymers - Compensation phenomenon. Biochemistry 1973;12:1017-25.

[94] Zimm BH, Bragg JK. Theory of the phase transition between helix and random coil in polypeptide chains. Journal of Chemical Physics 1959;31:526-35.

[95] Nagano K. logical analysis of mechanism of protein folding.1. Prediction of helices, loops, an beta-structures from primary structure. Journal of Molecular Biology 1973;75:401-20.

[96] Dubey VK, Shah A, Jagannadham MV, Kayastha AM. Effect of organic solvents on the molten globule state of procerain: beta-sheet to alpha-helix switchover in presence of trifluoroethanol. Protein and peptide letters 2006;13:545-7.

[97] Liu G, Prabhakar A, Aucoin D, Simon M, Sparks S, Robbins KJ, *et al*. Mechanistic Studies of Peptide Self-Assembly: Transient alpha-Helices to Stable beta-Sheets. Journal of the American Chemical Society 2010;132:18223-32.

[98] Zhang S, Holmes T, Lockshin C, Rich A. Spontaneous assembly of a self-complementary oligopeptide to form a stable macroscopic membrane. Proceedings of the National Academy of Sciences 1993;90:3334-8.

[99] Zhang S, Holmes TC, DiPersio CM, Hynes RO, Su X, Rich A. Self-complementary oligopeptide matrices support mammalian cell attachment. Biomaterials 1995;16:1385-93.

[100] Xiong H, Buckwalter BL, Shieh HM, Hecht MH. Periodicity of polar and nonpolar amino acids is the major determinant of secondary structure in self-assembling oligomeric peptides. Proceedings of the National Academy of Sciences 1995;92:6349-53.

[101] Brack A, Orgel LE. [beta] structures of alternating polypeptides and their possible prebiotic significance. Nature 1975;256:383-7.

[102] Bippon WB, Chen HH, Walton AG. Spectroscopic characterization of poly(Glu-Ala). Journal of Molecular Biology 1973;75:369-75.

[103] Trudelle Y. Conformational study of the sequential (Tyr-Glu)n copolymer in aqueous solution. Polymer 1975;16:9-15.

[104] Zhao Y, Tanaka M, Kinoshita T, Higuchi M, Tan T. Nanofibrous scaffold from self-assembly of beta-sheet peptides containing phenylalanine for controlled release. Journal of Controlled Release 2010;142:354-60.

[105] Lee YS. Self-assembly and nanotechnology : a force balance approach: Hoboken, N.J. : John Wiley & Sons, c2008.; 2008.

[106] Holmes TC, de Lacalle S, Su X, Liu GS, Rich A, Zhang SG. Extensive neurite outgrowth and active synapse formation on self-assembling peptide scaffolds. Proceedings of the National Academy of Sciences of the United States of America 2000;97:6728-33.

[107] Israelachvili JN. Intermolecular and surface forces: Burlington, MA : Academic Press, 2011.
Third edition.; 2011.

[108] Hartgerink JD, Beniash E, Stupp SI. Self-Assembly and Mineralization of Peptide-Amphiphile Nanofibers. Science 2001;294:1684-8.

[109] Behanna HA, Donners J, Gordon AC, Stupp SI. Coassembly of amphiphiles with opposite peptide polarities into nanofibers. Journal of the American Chemical Society 2005;127:1193-200.

[110] Beniash E, Hartgerink JD, Storrie H, Stendahl JC, Stupp SI. Self-assembling peptide amphiphile nanofiber matrices for cell entrapment. Acta Biomaterialia 2005;1:387-97.

[111] Paramonov SE, Jun HW, Hartgerink JD. Self-assembly of peptide-amphiphile nanofibers: The roles of hydrogen bonding and amphiphilic packing. Journal of the American Chemical Society 2006;128:7291-8.

[112] Rusli R, Shanmuganathan K, Rowan SJ, Weder C, Eichhorn SJ. Stress-Transfer in Anisotropic and Environmentally Adaptive Cellulose Whisker Nanocomposites. Biomacromolecules 2010;11:762-8.

[113] Ghoussoub A, Lehn J-M. Dynamic sol-gel interconversion by reversible cation binding and release in G-quartet-based supramolecular polymers. Chemical Communications 2005:5763-5.

[114] Mendez J, Annamalai PK, Eichhorn SJ, Rusli R, Rowan SJ, Foster EJ, et al. Bioinspired Mechanically Adaptive Polymer Nanocomposites with Water-Activated Shape-Memory Effect. Macromolecules 2011;44:6827-35.

[115] Habibi Y, Lucia LA, Rojas OJ. Cellulose Nanocrystals: Chemistry, Self-Assembly, and Applications. Chem Rev 2010;110:3479-500.

[116] Gillard RE, Raymo FM, Stoddart JF. Controlling self-assembly. Chemistry-a European Journal 1997;3:1933-40.

[117] Claessens CG, Stoddart JF. pi-pi interactions in self-assembly. Journal of Physical Organic Chemistry 1997;10:254-72.

[118] Shetty AS, Zhang JS, Moore JS. Aromatic pi-stacking in solution as revealed through the aggregation of phenylacetylene macrocycles. Journal of the American Chemical Society 1996;118:1019-27.

[119] McGaughey GB, Gagne M, Rappe AK. pi-stacking interactions - Alive and well in proteins. J Biol Chem 1998;273:15458-63.

[120] Jayawarna V, Ali M, Jowitt TA, Miller AE, Saiani A, Gough JE, et al. Nanostructured hydrogels for three-dimensional cell culture through self-assembly of fluorenylmethoxycarbonyl-dipeptides. Advanced Materials 2006;18:611-+.

[121] Yang ZM, Xu KM, Wang L, Gu HW, Wei H, Zhang MJ, et al. Self-assembly of small molecules affords multifunctional supramolecular hydrogels for topically treating simulated uranium wounds. Chemical Communications 2005:4414-6.

[122] Yang ZM, Gu HW, Zhang Y, Wang L, Xu B. Small molecule hydrogels based on a class of antiinflammatory agents. Chemical Communications 2004:208-9.

[123] Reches M, Gazit E. Formation of closed-cage nanostructures by self-assembly of aromatic dipeptides. Nano Letters 2004;4:581-5.

[124] Schnepp ZAC, Gonzalez-McQuire R, Mann S. Hybrid biocomposites based on calcium phosphate mineralization of self-assembled supramolecular hydrogels. Advanced Materials 2006;18:1869-+.

[125] Smith AM, Williams RJ, Tang C, Coppo P, Collins RF, Turner ML, et al. Fmoc-Diphenylalanine self assembles to a hydrogel via a novel architecture based on pi-pi interlocked beta-sheets. Advanced Materials 2008;20:37-+.

[126] Toledano S, Williams RJ, Jayawarna V, Ulijn RV. Enzyme-triggered self-assembly of peptide hydrogels via reversed hydrolysis. Journal of the American Chemical Society 2006;128:1070-1.

[127] Jordine ESA. Specific interactions which need nonequilibrium particle/particle models. Journal of Colloid and Interface Science 1973;45:435-9.

[128] Parsegian VA, Zemb T. Hydration forces: Observations, explanations, expectations, questions. Current Opinion in Colloid & Interface Science 2011;16:618-24.

[129] Horn RG, Israelachvili JN, Marra J, Parsegian VA, Rand RP. Comparison of the forces measured between phosphatidylcholine bilayers. Biophysical Journal 1988;54:1185-6.

[130] Hwang W, Zhang SG, Kamm RD, Karplus M. Kinetic control of dimer structure formation in amyloid fibrillogenesis. Proceedings of the National Academy of Sciences of the United States of America 2004;101:12916-21.

[131] Berard DR, Attard P, Patey GN. Cavitation of a lennard-jones fluid between hard walls, and the possible relevance to the attraction measured between hydrophobic durfaces. Journal of Chemical Physics 1993;98:7236-44.

[132] Zangi R, Hagen M, Berne BJ. Effect of ions on the hydrophobic interaction between two plates. Journal of the American Chemical Society 2007;129:4678-86.

[133] Hummer G, Garde S. Cavity expulsion and weak dewetting of hydrophobic solutes in water. Phys Rev Lett 1998;80:4193-6.

[134] Ashbaugh HS, Paulaitis ME. Effect of solute size and solute-water attractive interactions on hydration water structure around hydrophobic solutes. Journal of the American Chemical Society 2001;123:10721-8.

[135] Huang X, Margulis CJ, Berne BJ. Dewetting-induced collapse of hydrophobic particles (vol 100, pg 11953, 2003). Proceedings of the National Academy of Sciences of the United States of America 2006;103:19605-.

[136] Hua L, Huang X, Liu P, Zhou R, Berne BJ. Nanoscale dewetting transition in protein complex folding. J Phys Chem B 2007;111:9069-77.

[137] Liu P, Huang XH, Zhou RH, Berne BJ. Observation of a dewetting transition in the collapse of the melittin tetramer. Nature 2005;437:159-62.

[138] Wallqvist A, Berne BJ. Computer simulation of hydrophobic hydration forces on stacked plates at short range. J Phys Chem 1995;99:2893-9.

[139] Cheung MS, Garcia AE, Onuchic JN. Protein folding mediated by solvation: Water expulsion and formation of the hydrophobic core occur after the structural collapse. Proceedings of the National Academy of Sciences of the United States of America 2002;99:685-90.

[140] Guo WH, Lampoudi S, Shea JE. Posttransition state desolvation of the hydrophobic core of the src-SH3 protein domain. Biophysical Journal 2003;85:61-9.

[141] Shea JE, Onuchic JN, Brooks CL. Probing the folding free energy landscape of the src-SH3 protein domain. Proceedings of the National Academy of Sciences of the United States of America 2002;99:16064-8.

[142] Balbach JJ, Ishii Y, Antzutkin ON, Leapman RD, Rizzo NW, Dyda F, *et al*. Amyloid fibril formation by A beta(16-22), a seven-residue fragment of the Alzheimer's beta-amyloid peptide, and structural characterization by solid state NMR. Biochemistry 2000;39:13748-59.

[143] Soto P, Griffin MA, Shea J-E. New insights into the mechanism of Alzheimer amyloid-beta fibrillogenesis inhibition by N-methylated peptides. Biophysical Journal 2007;93:3015-25.

[144] Kabiri M, Bushnak I, McDermot MT, Unsworth LD. Toward a Mechanistic Understanding of Ionic Self-Complementary Peptide Self-Assembly: Role of Water Molecules and Ions. Biomacromolecules 2013;14:3943-50.

[145] Ye Z, Zhang H, Luo H, Wang S, Zhou Q, Du X, *et al*. Temperature and pH effects on biophysical and morphological properties of self-assembling peptide RADA16-1. Journal of Peptide Science 2008;14:152-62.

[146] Caplan MR, Moore PN, Zhang SG, Kamm RD, Lauffenburger DA. Self-assembly of a beta-sheet protein governed by relief of electrostatic repulsion relative to van der Waals attraction. Biomacromolecules 2000;1:627-31.

[147] Caplan MR, Schwartzfarb EM, Zhang SG, Kamm RD, Lauffenburger DA. Control of self-assembling oligopeptide matrix formation through systematic variation of amino acid sequence. Biomaterials 2002;23:219-27.

[148] Guggenheim EA. The conceptions of electrical potential difference between two phases and the individual activities of ions. J Phys Chem 1929;33:842-9.

[149] Savin T, Doyle PS. Electrostatically tuned rate of peptide self-assembly resolved by multiple particle tracking. Soft Matter 2007;3:1194-202.

[150] Schmaljohann D. Thermo- and pH-responsive polymers in drug delivery. Advanced Drug Delivery Reviews 2006;58:1655-70.

[151] Gupta P, Vermani K, Garg S. Hydrogels: from controlled release to pH-responsive drug delivery. Drug Discovery Today 2002;7:569-79.

[152] Khare AR, Peppas NA, Massimo G, Colombo P. Measurement of the swelling force in ionic polymeric networsk.1. Effect of pH and ionic content. Journal of Controlled Release 1992;22:239-44.

[153] Peppas NA, Hilt JZ, Khademhosseini A, Langer R. Hydrogels in biology and medicine: From molecular principles to bionanotechnology. Advanced Materials 2006;18:1345-60.

[154] Khare AR, Peppas NA. Swelling and deswelling of anionic copolymer gels. Biomaterials 1995;16:559-67.

[155] Brannonpeppas L, Peppas NA. Equilibrium swelling behaviour of dilute ionic hydrogels in electrolytic solutions. Journal of Controlled Release 1991;16:319-30.

[156] Zhang J, Hao R, Huang L, Yao J, Chen X, Shao Z. Self-assembly of a peptide amphiphile based on hydrolysed Bombyx mori silk fibroin. Chemical Communications 2011;47:10296-8.

[157] Ghosh A, Haverick M, Stump K, Yang XY, Tweedle MF, Goldberger JE. Fine-Tuning the pH Trigger of Self-Assembly. Journal of the American Chemical Society 2012;134:3647-50.

[158] Chen YR, Gan HX, Tong YW. pH-Controlled Hierarchical Self-Assembly of Peptide Amphiphile. Macromolecules 2015;48:2647-53.

[159] Mart RJ, Osborne RD, Stevens MM, Ulijn RV. Peptide-based stimuli-responsive biomaterials. Soft Matter 2006;2:822-35.

[160] Schneider JP, Pochan DJ, Ozbas B, Rajagopal K, Pakstis L, Kretsinger J. Responsive Hydrogels from the Intramolecular Folding and Self-Assembly of a Designed Peptide. Journal of the American Chemical Society 2002;124:15030-7.

[161] Wang LJ, Sun N, Terzyan S, Zhang XJ, Benson DR. Histidine/tryptophan pi-stacking interaction stabilizes the heme-independent folding core of microsomal apocytochrome b(5) relative to that of mitochondrial apocytochrome b(5). Biochemistry 2006;45:13750-9.

[162] Heitmann P. A model for sulfhydryl groups in proteins. Hydrophobic interactions of the cysteine side chain in micelles. Eur J Biochem 1968;3:346.

[163] Hartgerink JD, Beniash E, Stupp SI. Peptide-amphiphile nanofibers: A versatile scaffold for the preparation of self-assembling materials. Proceedings of the National Academy of Sciences of the United States of America 2002;99:5133-8.

[164] Sanchez de Groot N, Parella T, Aviles FX, Vendrell J, Ventura S. Ile-Phe dipeptide self-assembly: Clues to amyloid formation. Biophysical Journal 2007;92:1732-41.

[165] Panda JJ, Mishra A, Basu A, Chauhan VS. Stimuli responsive self-assembled hydrogel of a low molecular weight free dipeptide with potential for tunable drug delivery. Biomacromolecules 2008;9:2244-50.

[166] Brack A, Orgel LE. Beta structures of alternating polypeptides and their possible prebiotic significance. Nature 1975;256:383-7.

[167] Seipke G, Arfmann HA, Wagner KG. Synthesis and properties of alternating poly*lys-phe) and comparison with random copolymer poly (lys51, phe 49). Biopolymers 1974;13:1621-33.

[168] Peggion E, Terbojev.M, Borin G, Cosani A. CConformational studies on polypeptides - effect of sodium perchlorate on conformation of poly-L-Lysine and of random copolymers of L-lysine and L-phenylalanine in aqeous solution. Biopolymers 1972;11:633.

[169] Hilbich C, Kisterswoike B, Reed J, Masters CL, Beyreuther K. Aggregation and secondary structure of synthetic amyloid beta-A4 peptides of alzheimers- disease. Journal of Molecular Biology 1991;218:149-63.

[170] Wagner I, Musso H. New naturally occuring amino acids. Angewandte Chemie-International Edition in English 1983;22:816-28.

[171] Carter D, Farid RS. Circular Dichroism (CD) Spectroscopy. Theory of Protein CD2003.

[172] Richardson JS. The anatomy and taxonomy of protein structure. Advances in protein chemistry 1981;34:167-339.

[173] Greenfie.N, Fasman GD. Computed circular dichroism spectra for evaluation of protein conformation. Biochemistry 1969;8:4108.

[174] Pribic R, Vanstokkum IHM, Chapman D, Haris PI, Bloemendal M. Protein secondary structure from Fourier transform infrared and or circular dichroism spectra. Analytical Biochemistry 1993;214:366-78.

[175] Pauling L, Corey RB, Branson HR. The structure of proteins - 2 Hydrogen bonded helical configurations of the polypeptide chain. Proceedings of the National Academy of Sciences of the United States of America 1951;37:205-11.

[176] Schulz G, Schirmer RH. Patterns of Folding and Association of Polypeptide Chains. Principles of Protein Structure: Springer New York; 1979. p. 66-107.

[177] Pauling L, Corey RB. Configurations of polypeptide hcains with favoured orientations around single bonds. 2 new pleated sheets. Proceedings of the National Academy of Sciences of the United States of America 1951;37:729-40.

[178] Rose GD, Gierasch LM, Smith JA. Turns in peptides and proteins. Advances in Protein Chemistry 1985;37:1-109.

[179] Venkatac.Cm. Stereochemical criteria for polypeptides and proteins.V. Conformation of a system of 3 linked peptide units. Biopolymers 1968;6:1425.

[180] Johnson WC, Tinoco I. Circular dichroism of polypeptide solutinos in vacuum ultravoilet. Journal of the American Chemical Society 1972;94:4389.

[181] Wicken JS, Woody RW. Conformational changes in liver alcohol dehydrogenase upon nucleotide binding - detection by circular dichroism of dye complexes. Archives of Biochemistry and Biophysics 1974;162:12-6.

[182] Greenfield NJ. Using circular dichroism spectra to estimate protein secondary structure. Nature Protocols 2006;1:2876-90.

[183] Fraga S, Parker JMR. Modeling of peptide and protein structures. Amino Acids 1994;7:175-202.

[184] Andrade JD, Lee HB, Jhon MS, Kim SW, Hibbs JB. Water as biomaterial. Transactions American Society for Artificial Internal Organs 1973;19:1-7.

[185] Wang RLC, Kreuzer HJ, Grunze M. Molecular conformation and solvation of oligo(ethylene glycol)-terminated self-assembled monolayers and their resistance to protein adsorption. J Phys Chem B 1997;101:9767-73.

[186] Kataoka K, Ito H, Amano H, Nagasaki Y, Kato M, Tsuruta T, *et al*. Minimized platelet interaction with poly(2-hydroxyethyl methacrylate-block-4-bis(trimethylsilyl)methylstyrene) hydrogel showing anomalously high free water content. Journal of Biomaterials Science-Polymer Edition 1998;9:111-29.

[187] Ide M, Mori T, Ichikawa K, Kitano H, Tanaka M, Mochizuki A, *et al*. Structure of water sorbed into poly (MEA-co-HEMA) films as examined by ATR-IR spectroscopy. Langmuir 2003;19:429-35.

[188] Tanaka M, Mochizuki A, Ishii N, Motomura T, Hatakeyama T. Study of blood compatibility with poly(2-methoxyethyl acrylate). Relationship between water structure and platelet compatibility in poly(2-methoxyethylacrylate-co-2-hydroxyethylmethacrylate). Biomacromolecules 2002;3:36-41.

[189] Tanaka M, Mochizuki A. Clarification of the Blood Compatibility Mechanism by Controlling the Water Structure at the Blood-Poly(meth)acrylate Interface. Journal of Biomaterials Science-Polymer Edition 2010;21:1849-63.

[190] Mequanint K, Patel A, Bezuidenhout D. Synthesis, swelling behavior, and biocompatibility of novel physically cross-linked polyurethane-block-poly(glycerol methacrylate) hydrogels. Biomacromolecules 2006;7:883-91.

[191] Saini A, Koss K, Unsworth LD. Effect of Peptide Concentration on Water Structure, Morphology, and Thermal Stability of Self-Assembling (RADA)(4) Peptide Matrices. Journal of Biomaterials and Tissue Engineering 2014;4:895-905.

[192] Mueller-Plathe F. Different states of water in hydrogels? Macromolecules 1998;31:6721-3.

[193] Mequanint K, Sheardown H. 2-methacryloyloxyethyl N-butylcarbamate: a new co-monomer for synthesis of polyurethane hydrogels with improved mechanical properties for biomedical applications. Journal of Biomaterials Science-Polymer Edition 2005;16:1303-18.

[194] Zhang JM, Teng HX, Zhou XS, Shen DY. Frozen bound water melting induced cooperative hydration of poly(vinyl methyl ether) in aqueous solution. Polymer Bulletin 2002;48:277-82.

[195] Tanaka M, Motomura T, Ishii N, Shimura K, Onishi M, Mochizuki A, *et al*. Cold crystallization of water in hydrated poly(2-methoxyethyl acrylate) (PMEA). Polymer International 2000;49:1709-13.

[196] Kim SJ, Park SJ, Kim SI. Properties of smart hydrogels composed of polyacrylic acid/poly(vinyl sulfonic acid) responsive to external stimuli. Smart Mater Struct 2004;13:317-22.

[197] Höhne G, Hemminger W, Flammersheim HJ. Differential scanning calorimetry: Berlin ; New York : Springer, c2003.

2nd rev. and enl. ed.; 2003.

[198] Yamada KM. Adhesive recognition sequences. J Biol Chem 1991;266:12809-12.

[199] Hynes RO, Lander AD. Contact and adhesive specificities in the associations, migrations, and targeting of cells and axons. Cell 1992;68:303-22.

[200] Prieto AL, Edelman GM, Crossin KL. Multiple integrins mediate cell attachment to cytotactin/tenascin. Proceedings of the National Academy of Sciences 1993;90:10154-8.

[201] Cui HG, Webber MJ, Stupp SI. Self-Assembly of Peptide Amphiphiles: From Molecules to Nanostructures to Biomaterials. Biopolymers 2010;94:1-18.

[202] Ellis-Behnke R. At the nanoscale: nanohemostat, a new class of hemostatic agent. Wiley Interdisciplinary Reviews: Nanomedicine and Nanobiotechnology 2011;3:70-8.

[203] Zwischenberger JB, Brunston RL, Swann JR, Conti VR. Comparison of two topical collagen-based hemostatic sponges during cardiothoracic procedures. Journal of Investigative Surgery 1999;12:101-6.

[204] Sabel M, Stummer W. The use of local agents: Surgicel and Surgifoam. European Spine Journal 2004;13:S97-S101.

[205] Mitra RN, Shome A, Paul P, Das PK. Antimicrobial activity, biocompatibility and hydrogelation ability of dipeptide-based amphiphiles. Organic & Biomolecular Chemistry 2009;7:94-102.

[206] Chen C, Pan F, Zhang S, Hu J, Cao M, Wang J, et al. Antibacterial Activities of Short Designer Peptides: a Link between Propensity for Nanostructuring and Capacity for Membrane Destabilization. Biomacromolecules 2010;11:402-11.

[207] Liu L, Xu K, Wang H, Jeremy Tan PK, Fan W, Venkatraman SS, et al. Self-assembled cationic peptide nanoparticles as an efficient antimicrobial agent. Nat Nano 2009;4:457-63.

[208] Webber MJ, Tongers J, Renault M-A, Roncalli JG, Losordo DW, Stupp SI. Development of bioactive peptide amphiphiles for therapeutic cell delivery. Acta Biomaterialia 2010;6:3-11.

[209] Mata A, Hsu L, Capito R, Aparicio C, Henrikson K, Stupp SI. Micropatterning of bioactive self-assembling gels. Soft Matter 2009;5:1228-36.

[210] Wiradharma N, Tong YW, Yang Y-Y. Self-assembled oligopeptide nanostructures for co-delivery of drug and gene with synergistic therapeutic effect. Biomaterials 2009;30:3100-9.

[211] Wiradharma N, Khan M, Tong YW, Wang S, Yang YY. Self-assembled cationic peptide nanoparticles capable of inducing efficient gene expression in vitro. Advanced Functional Materials 2008;18:943-51.

[212] Dickerson MB, Sandhage KH, Naik RR. Protein- and Peptide-Directed Syntheses of Inorganic Materials. Chem Rev 2008;108:4935-78.

[213] Jiang H, Guler MO, Stupp SI. The internal structure of self-assembled peptide amphiphiles nanofibers. Soft Matter 2007;3:454-62.

[214] Sargeant TD, Guler MO, Oppenheimer SM, Mata A, Satcher RL, Dunand DC, et al. Hybrid bone implants: Self-assembly of peptide amphiphile nanofibers within porous titanium. Biomaterials 2008;29:161-71.

[215] Sefton MV, Gemmell CH, Gorbet MB. What really is blood compatibility? Journal of Biomaterials Science-Polymer Edition 2000;11:1165-82.

[216] Kjaerheim A, Hovig T. Hemostatic blood platelet plugs in rabbits. Journal of Ultrastructure Research 1962;6:138.

[217] Jorgensen L, Borchgrevink CF. Platelet plug in normal persons.2. Histological appearance of plug in secondary bleeding time test. Acta Pathologica Et Microbiologica Scandinavica 1963;57:427.

[218] Mustard JF, Rowsell HC, Murphy EA. Animal and laboratory techniques for evaluating blood coagulation1964.

[219] Klinger MHF, Jelkmann W. Role of blood platelets in infection and inflammation. Journal of Interferon and Cytokine Research 2002;22:913-22.

[220] Stokes KY, Granger DN. Platelets: a critical link between inflammation and microvascular dysfunction. Journal of Physiology-London 2012;590:1023-34.

[221] Movat HZ, Weiser WJ, Glynn MF, Mustard JF. Platelet phagocytosis and aggregation. Journal of Cell Biology 1965;27:531.

[222] Danon D, Jerushalmy Z, Devries A. Incorporation of influenza birus in human blood in-vitro -electron microscopical observation. Virology 1959;9:719-22.

[223] Franco AT, Corken A, Ware J. Platelets at the interface of thrombosis, inflammation, and cancer. Blood 2015;126:582-8.

[224] Blockmans D, Deckmyn H, Vermylen J. Platelet activation. Blood Reviews 1995;9:143-56.

[225] Movat HZ, Mustard JF, Taichman NS, Uriuhara T. Platelet aggregation and release of ADP serotonin and histamine associated with phagocytosis of antigen-antibody complexes. Proceedings of the Society for Experimental Biology and Medicine 1965;120:232.

[226] Gasic GJ. Role of plasma, platelets, and endothelial-cells in tubor metasis. Cancer and Metastasis Reviews 1984;3:99-116.

[227] Rendu F, Brohard-Bohn B. The platelet release reaction: granules' constituents, secretion and functions. Platelets 2001;12:261-73.

[228] Rinder HM, Tracey JL, Rinder CS, Leitenberg D, Smith BR. Neutrophil but not monocyte activation inhibits P-selectin-mediated platelet adhesion. Thrombosis and haemostasis 1994;72:750-6.

[229] Rinder HM, Bonan JL, Rinder CS, Ault KA, Smith BR. Dynamics of leukocyte-platelet adhesion in whole-blood. Blood 1991;78:1730-7.

[230] Santos MT, Valles J, Marcus AJ, Safier LB, Broekman MJ, Islam N, et al. Enhancement of platlet reactivity and modulation of eicosanoid production by intact erythrocytes - a new approach to platelet activation and recruitment. Journal of Clinical Investigation 1991;87:571-80.

[231] Kunicki TJ, Tuccelli M, Becker GA, Aster RH. Study of variables affecting quality of platelets stored at room-temperature. Transfusion 1975;15:414-21.

[232] Sims PJ, Wiedmer T. Induction of cellular procoagulant activity by the membrane attack complex of complement. Seminars in Cell Biology 1995;6:275-82.

[233] Jy WC, Mao WW, Horstman LL, Tao JG, Ahn YS. Platelet microparticles bind, activate and aggregate neutrophils in vitro. Blood Cells Molecules and Diseases 1995;21:217-31.

[234] Calvete JJ. Clues for understanding the structure and function of a prototypic human integrin - the platelet glycoprotein IIB/IIIA complex. Thrombosis and haemostasis 1994;72:1-15.

[235] McEver RP, Martin MN. A monoclonal- antibody to a membrane glycoprotein binds only to the activated platelts. J Biol Chem 1984;259:9799-804.

[236] Mickelson JK, Lakkis NM, Villarreal-Levy G, Hughes BJ, Smith CW. Leukocyte activation with platelet adhesion after coronary angioplasty: a mechanism for recurrent disease? Journal of the American College of Cardiology 1996;28:345-53.

[237] Kainthan RK, Gnanamani M, Ganguli M, Ghosh T, Brooks DE, Maiti S, et al. Blood compatibility of novel water soluble hyperbranched polyglycerol-based multivalent cationic polymers and their interaction with DNA. Biomaterials 2006;27:5377-90.

[238] Kainthan RK, Hester SR, Levin E, Devine DV, Elliott BD. In vitro biological evaluation of high molecular weight hyperbranched polyglycerols. Biomaterials 2007;28:4581-90.

[239] Saini A, Serrano K, Koss K, Unsworth LD. Evaluation of the hemocompatibility and rapid hemostasis of (RADA)$_4$ peptide-based hydrogels. Acta Biomaterialia 2016;31:71-9.

[240] Mustard JF, Rowsell HC, Murphy EA. platelet economy (platelet survival and turnover). British Journal of Haematology 1966;12:1.

[241] Gemmell CH, Yeo EL, Sefton MV. Flow cytometric analysis of material-induced platelet activation in a canine model: Elevated microparticle levels and reduced platelet life span. J Biomed Mater Res 1997;37:176-81.

[242] Lazarus AH, Wright JF, Blanchette V, Freedman J. Analysis of platelets by flow cytometry. Transfusion Science 1995;16:353-61.

[243] Saini A, Serrano K, Koss K, Unsworth LD. Evaluation of the hemocompatibility and rapid hemostasis of (RADA)4 peptide-based hydrogels. Acta Biomater 2016;31:71-9.

[244] Pakala R, Waksman R. Currently available methods for platelet function analysis: advantages and disadvantages. Cardiovascular revascularization medicine : including molecular interventions 2011;12:312-22.

[245] Goldsmith HL, Turitto VT. Rheological aspects of thrombosis and hemostasis - basic principals and applications -ICTH-report - Subcommittee on rheology of the international committee on thrombosis and hemostasis. Thrombosis and haemostasis 1986;55:415-35.

[246] Sakariassen KS, Hanson SR, Cadroy Y. Methods and models to evaluate shear-dependent and surface reactivity-dependent antithrombotic efficacy. Thromb Res 2001;104:149-74.

[247] Favaloro EJ. Utility of the PFA-100 (R) for assessing bleeding disorders and monitoring therapy: a review of analytical variables, benefits and limitations. Haemophilia 2001;7:170-9.

[248] Einav S, Dewey CF, Hartenbaum H. Cone-and-plate apparatus - a compact system for studying well charactersized turbulant flow fields. Exp Fluids 1994;16:196-202.

[249] Varon D, Dardik R, Shenkman B, KotevEmeth S, Farzame N, Tamarin I, *et al*. A new method for quantitative analysis of whole blood platelet interaction with extracellular matrix under flow conditions. Thromb Res 1997;85:283-94.

[250] Shenkman B, Savion N, Dardik R, Tamarin I, Varon D. Testing of platelet deposition on polystyrene surface under flow conditions by the cone and plate(let) analyzer: Role of platelet activation, fibrinogen and von Willebrand factor. Thromb Res 2000;99:353-61.

[251] Paniccia R, Priora R, Alessandrello Liotta A, Abbate R. Platelet function tests: a comparative review. Vascular Health and Risk Management 2015;11:133-48.

[252] Cholakis CH, Sefton MV. In-vitro platelet interatctions with a heparin-polyvinyl alcohol hydrogel. J Biomed Mater Res 1989;23:399-415.

[253] King DJ, Kelton JG. Heparin-associated thrombocytopenia. Annals of Internal Medicine 1984;100:535-40.

[254] Salzman EW, Merrill EW, Binder A, Wolf CF, Ashford TP, Austen WG. Protein-platelet interaction on heparinized surfaces. J Biomed Mater Res 1969;3:69-81.

[255] Leininger RI. Polymers as surgical implants. CRC critical reviews in bioengineering 1972;1:333-81.

[256] Olsson P, Lagergren H, Larsson R, Radegran K. Prevention of platelet adhesion and aggregation by a glutardialdehyde-stabilized heparin surface. Thrombosis and haemostasis 1977;37:274-82.

[257] Llanos GR, Sefton MV. Immobilization of poly(ethylene glycol) onto a poly(vinyl alcohol) 2. Evaluation of thrombogenicity.. J Biomed Mater Res 1993;27:1383-91.

[258] Strzinar I, Sefton MV. Preparation and thrombogenicity of alkylated and polyvinyl alcohol coated tubing. J Biomed Mater Res 1992;26:577-92.

[259] Duncan AC, Sefton MV, Brash JL. Effect of C-4-, C-8- and C-18-alkylation of poly(vinyl alcohol) hydrogels on the adsorption of albumin and fibrinogen from buffer and plasma: limited correlation with platelet interactions. Biomaterials 1997;18:1585-92.

[260] Basmadjian D. The effect of flow and mass transport in thrombogenesis. Annals of Biomedical Engineering 1990;18:685-709.

[261] Slack SM, Turitto VT. Flow chambers and their standardization for the use in studies of thrombosis - on behalf of the subcommittee on rheology. Thrombosis and haemostasis 1994;72:777-81.

[262] Skarja GA, KinloughRathbone RL, Perry DW, Rubens FD, Brash JL. Cone-and-plate device for the investigation of platelet biomaterial interactions. J Biomed Mater Res 1997;34:427-38.

[263] Savage B, Saldivar E, Ruggeri ZM. Initiation of platelet adhesion by arrest onto fibrinogen or translocation on von Willebrand factor. Cell 1996;84:289-97.

[264] Goto S, Handa S, Takahashi E, Abe S, Handa M, Ikeda Y. Synergistic effect of epinephrine and shearing on platelet activation. Thromb Res 1996;84:351-9.

[265] Hanson SR, Harker LA, Ratner BD, Hoffman AS. In vivo evaluation of artificial surfaces with a non human primate model of arterial thrombosis. Journal of Laboratory and Clinical Medicine 1980;95:289-304.

[266] Goodman SL. Sheep, pig, and human platelet-material interactions with model cardiovascular biomaterials. Journal of Biomedical Materials Research 1999;45:240-50.

[267] Bertolini F, Murphy S. A multicenter evaluatino of reproducibility of swirling in platelet concentrates. Transfusion 1994;34:796-801.

[268] Holme S, Moroff G, Murphy S. A multi-laboratory evaluation of in vitro platelet assays: the tests for extent of shape change and response to hypotonic shock. Transfusion 1998;38:31-40.

[269] Maurer-Spurej E, Chipperfield K. Past and Future Approaches to Assess the Quality of Platelets for Transfusion. Transfusion Medicine Reviews 2007;21:295-306.

[270] Basmadjian D, Sefton MV, Baldwin SA. Coagulation on biomaterials in flowing blood: some theoretical considerations. Biomaterials 1997;18:1511-22.

[271] Vogler EA, Siedlecki CA. Contact activation of blood-plasma coagulation. Biomaterials 2009;30:1857-69.

[272] He S, Antovic A, Blomback M. A simple and rapid laboratory method for determination of haemostasis potential in plasma II. Modifications for use in routine laboratories and research work. Thromb Res 2001;103:355-61.

[273] Hemker HC, Giesen P, AlDieri R, Regnault V, de Smed E, Wagenvoord R, et al. The Calibrated Automated Thrombogram (CAT): A universal routine test for hyper- and hypocoagulability. Pathophysiol Haemost Thromb 2002;32:249-53.

[274] Isbister GK. Procoagulant Snake Toxins: Laboratory Studies, Diagnosis, and Understanding Snakebite Coagulopathy. Seminars in Thrombosis and Hemostasis 2009;35:93-103.

[275] Filippovich I, Sorokina N, Pierre LS, Flight S, de Jersey J, Perry N, et al. Cloning and functional expression of venom prothrombin activator protease from Pseudonaja textilis with whole blood procoagulant activity. British Journal of Haematology 2005;131:237-46.

[276] Ricklin D, Hajishengallis G, Yang K, Lambris JD. Complement: a key system for immune surveillance and homeostasis. Nature Immunology 2010;11:785-97.

[277] Markiewski MM, DeAngelis RA, Strey CW, Foukas PG, Gerard C, Gerard N, *et al*. The Regulation of Liver Cell Survival by Complement. Journal of Immunology 2009;182:5412-8.

[278] Nangaku M, Couser WG. Mechanisms of immune-deposit formation and the mediation of immune renal injury. Clinical and experimental nephrology 2005;9:183-91.

[279] Esmon CT. The impact of the inflammatory response on coagulation. Thrombosis Research 2004;114:321-7.

[280] Wojta J, Huber K, Valent P. New aspects in thrombotic research: Complement induced switch in mast cells from a profibrinolytic to a prothrombotic phenotype. Pathophysiology of Haemostasis and Thrombosis 2003;33:438-41.

[281] Wojta J, Kaun C, Zorn G, Ghannadan M, Hauswirth AW, Sperr WR, *et al*. C5a stimulates production of plasminogen activator inhibitor-1 in human mast cells and basophils. Blood 2002;100:517-23.

[282] Gorbet MB, Sefton MV. Biomaterial-associated thrombosis: roles of coagulation factors, complement, platelets and leukocytes. Biomaterials 2004;25:5681-703.

[283] Janatova J. Activation and control of complement, inflammation, and infection associated with the use of biomedical polymers. Asaio J 2000;46:S53-S62.

[284] Walport MJ. Advances in immunology: Complement (First of two parts). N Engl J Med 2001;344:1058-66.

[285] Walport MJ. Advances in immunology: Complement (Second of two parts). N Engl J Med 2001;344:1140-4.

[286] Chenoweth DE. Complement Activation Produced by Biomaterials. Artificial Organs 1988;12:508-10.

[287] Berger M, Broxup B, Sefton MV. Using ELISA to evaluate complement activation by reference biomaterials. J Mater Sci-Mater Med 1994;5:622-7.

[288] Sayah S, Ischenko AM, Zhakhov A, Bonnard AS, Fontaine M. Expression of cytokines by human astrocytomas following stimulation by C3a and C5a anaphylatoxins: Specific increase in interleukin-6 mRNA expression. Journal of Neurochemistry 1999;72:2426-36.

[289] Takabayashi T, Vannier E, Clark BD, Margolis NH, Dinarello CA, Burke JF, *et al*. A new biologic role for C3a and C3a desArg - Regulation of TNF-alpha and IL-1 beta synthesis. Journal of Immunology 1996;156:3455-60.

[290] Amara U, Rittirsch D, Flierl M, Bruckner U, Klos A, Gebhard F, *et al*. Interaction Between the Coagulation and Complement System. In: Lambris JD, editor. Current Topics in Complement Ii2008. p. 71-9.

[291] Chenoweth DE, Hugli TE. Demonstration of specific C5A receptor on intact human polymorphonuclear leukocytes. Proceedings of the National Academy of Sciences of the United States of America 1978;75:3943-7.

[292] Wiedmer T, Sims PJ. Participation of protein-kinases in complement C5B-9-induced shedding of platelet plasma-membrane vesicles. Blood 1991;78:2880-6.

[293] Foreman KE, Vaporciyan AA, Bonish BK, Jones ML, Johnson KJ, Glovsky MM, *et al*. C5A-Induced expression of P-selectin in endothelial cells. Journal of Clinical Investigation 1994;94:1147-55.

[294] Rinder CS, Smith MJ, Rinder HM, Cortright DN, Brodbeck RM, Krause JE, *et al*. Leukocyte effects of C5a-receptor blockade during simulated extracorporeal circulation. Ann Thorac Surg 2007;83:146-52.

[295] Sperling C, Schweiss RB, Streller U, Werner C. In vitro hemocompatibility of self-assembled monolayers displaying various functional groups. Biomaterials 2005;26:6547-57.

[296] Arima Y, Toda M, Iwata H. Surface plasmon resonance in monitoring of complement activation on biomaterials. Advanced Drug Delivery Reviews 2011;63:988-99.

[297] Nilsson B, Ekdahl KN, Mollnes TE, Lambris JD. The role of complement in biomaterial-induced inflammation. Mol Immunol 2007;44:82-94.

[298] Labarre D, Laurent A, Lautier A, Bouhni S, Kerbellec L, Lewest JM, et al. Complement activation by substituted polyacrylamide hydrogels for embolisation and implantation. Biomaterials 2002;23:2319-27.

[299] Pangburn MK, Mullereberhard HJ. Relation of a putative thioester bond in C-3 to activation of the alternative pathway and the binding of the C3B to biological targets of complement. Journal of Experimental Medicine 1980;152:1102-14.

[300] Sim RB, Sim E. Autolytic fragmentation of complement components C-3 and C-4 and its relationship to covalent binding activity. Annals of the New York Academy of Sciences 1983;421:259-76.

[301] Toda M, Iwata H. Effects of Hydrophobicity and Electrostatic Charge on Complement Activation by Amino Groups. ACS Appl Mater Interfaces 2010;2:1107-13.

[302] Hayashi K, Fukumura H, Yamamoto N. In vivo thrombus formation induced by complement activation on polymer surfaces. J Biomed Mater Res 1990;24:1385-95.

[303] Cheung AK, Parker CJ, Wilcox LA, Janatova J. Activation of complement by hemodialysis membranes - polyacrylonitrile binds more C3a than cuprophan. Kidney Int 1990;37:1055-9.

[304] Cheung AK, Parker CJ, Janatova J, Brynda E. Modulation of complement aactivation on hemodialysis memebranes by immobilized heparin. Journal of the American Society of Nephrology 1992;2:1328-37.

[305] Janatova J, Cheung AK, Parker CJ. Bio-medical polymers differ in their capacity to activate complement. Complement and Inflammation 1991;8:61-9.

[306] Lin YS, Hlady V, Janatova J. Adsorptino of complement proteins on surfaces with hydrophobicity gradient. Biomaterials 1992;13:497-504.

[307] Hakim RM, Fearon DT, Lazarus JM. Biocompatibility of dialysis membranes - effects of chornic complement activaiton. I Kidney Int 1984;26:194-200.

[308] Moll S, Demoerloose P, Reber G, Schifferli J, Leski M. Comparison of 2 hemodialysis memebranes, polyacrilonitrile and cellulose-acetate, on complement and coagulation systems. Int J Artif Organs 1990;13:273-9.

[309] Gref R, Domb A, Quellec P, Blunk T, Muller RH, Verbavatz JM, et al. The controlled intravenous delivery of drugs using PEG-coated sterically stabilized nanospheres. Advanced Drug Delivery Reviews 2012;64:316-26.

[310] Verrecchia T, Spenlehauer G, Bazile DV, Murrybrelier A, Archimbaud Y, Veillard M. Non-steatlth poly(lactic acid albumin) and stealth polly(lactiv acid-polyethylene glycol) nanoparticles as injectable drug carriers. Journal of Controlled Release 1995;36:49-61.

[311] Pascual M, TolkoffRubin N, Schifferli JA. Is adsorption an important characteristic of dialysis membranes? Kidney Int 1996;49:309-13.

[312] Lamba NMK, Courtney JM, Gaylor JDS, Lowe GDO. In vitro investigation of the blood response to medical grade PVC and the effect of heparin on the blood response. Biomaterials 2000;21:89-96.

[313] Payne MS, Horbett TA. Complement activation by hydroxyethymethacrylate-ethylmethacrylate copolymers. J Biomed Mater Res 1987;21:843-59.

[314] Benesch J, Svedhem S, Svensson SCT, Valiokas R, Liedberg B, Tengvall P. Protein adsorption to oligo(ethylene glycol) self-assembled monolayers: Experiments with fibrinogen, heparinized plasma, and serum. Journal of Biomaterials Science-Polymer Edition 2001;12:581-97.

[315] Gawryl MS, Simon MT, Eatman JL, Lint TF. An enzyme linked immunoabsorbent assay for the quantification of the terminal complement complex from cell-membranes or in activated human sera. J Immunol Methods 1986;95:217-25.

[316] Ziats NP, Pankowsky DA, Tierney BP, Ratnoff OD, Anderson JM. Adsorption of hageman-factor (Factor XII) and other human plasma proteins to biomedical polymers. Journal of Laboratory and Clinical Medicine 1990;116:687-96.

[317] Mollnes TE, Garred P, Bergseth G. Efffect of time, temperature, and anticoagulats on in-vitro complement activation - consequences for collection and preservation of samples to be examined for complement activation. Clinical and Experimental Immunology 1988;73:484-8.

[318] Rapp HJ, Borsos T. Molecular basis of complement activation. 1970.

[319] Mayer MM. Complement. Historical perspectives and some current issues. Complement (Basel, Switzerland) 1984;1:2-26.

[320] Ziccardi RJ, Cooper NR. Development of an immunochemical test to assess C1 inactivator function in human-serum and its use for the diagnosis of hereditary angioedema. Clinical Immunology and Immunopathology 1980;15:465-71.

[321] Wettero J, Askendal A, Bengtsson T, Tengvall P. On the binding of complement to solid artificial surfaces in vitro. Biomaterials 2002;23:981-91.

[322] Andersson J, Ekdahl KN, Lambris JD, Nilsson B. Binding of C3 fragments on top of adsorbed plasma proteins during complement activation on a model biomaterial surface. Biomaterials 2005;26:1477-85.

[323] Mollnes TE, Vandvik B, Lea T, Vartdal F. Intrathecal complement activvation in nurogical diseases evaluated by analysis of terminal complement complex. J Neurol Sci 1987;78:17-28.

Chapter 4

Effect of Peptide Concentration on Water

Structure, Morphology, and Thermal Stability of Self-Assembling

(RADA)$_4$ Peptide Matrices

Coauthors who contributed to this research are: Kyle Koss, and Larry D. Unsworth
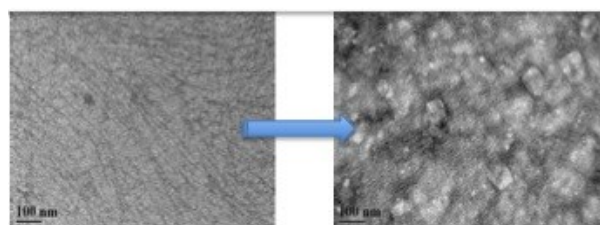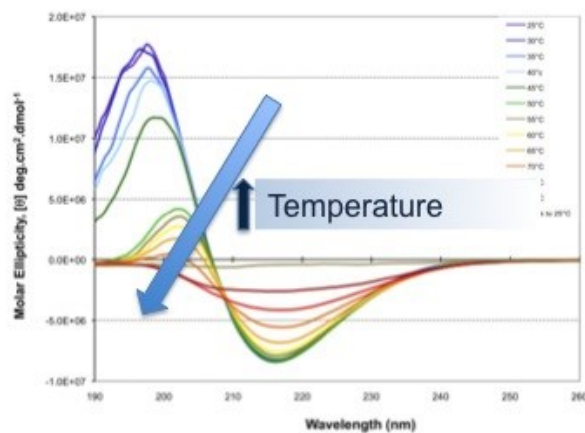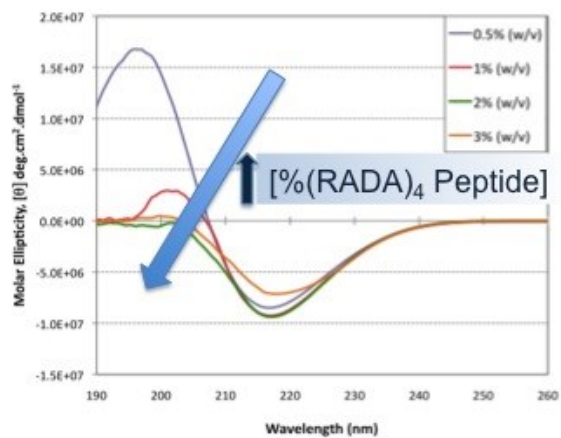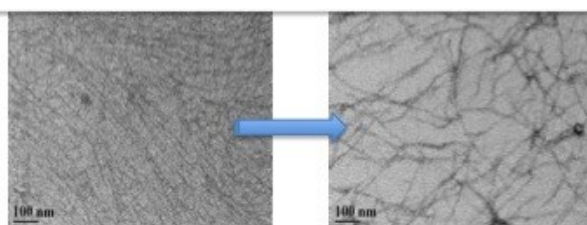
Graphical Abstract 1

Abstract

In order to elucidate design principles for peptide-based materials, we investigate $(RADA)_4$ oligopeptides that self-assemble to form β–sheet rich nanofibers that further develop into a viscoelastic 3D matrix in aqueous solution. Despite the fact that these materials can form hydrogels that are up to 99.5%(w/v) water, there is a limited understanding of water structure within these matrices. $(RADA)_4$ nanofibers were formed in solutions at various temperatures (25 to 80ºC, and cooled to 25ºC) and peptide concentrations (0.5-3.0% (w/v)), and characterized using Circular Dichroism (CD), Transmission Electron Microscopy (TEM) and Differential Scanning Calorimetry (DSC). CD and TEM results showed some contradictions, where CD data suggested no nanofiber had formed but TEM images clearly showed nanofibers present. These results call into question previously published results where CD has been used solely for proving nanofiber formation. It was found that secondary structure of assembled peptides was affected by peptide concentration. Of significant interest was the structure of the water within the self-assembled structures, where it was observed using DSC that the bound water structure was dramatically affected by peptide concentration. The unexpected results showed that at 3.0%(w/v) of peptide the amount of non-frozen water approached 80%, perhaps reflecting the synergy between closely packed nanofiber surfaces in interacting with water. However, it could be that the bound water content may also play a role in the structural transition from α-helices to β-sheets that may occur as nanofibers developed. Further understanding how to control this water structure could lead to novel ways of drug delivery through tuning the molecular mobility of water within the 3-D matrix itself.

4.1 Introduction

Self-assembly is a ubiquitous phenomenon found in nature and is defined as the spontaneous organization of components into ordered structures and patterns of varying scales [1]. Specifically, peptide self-assembly has been of immense interest, as peptides offer an array of advantages over the other biomaterials, such as: molecular interaction specificity, potential biodegradable products, intrinsic bioactivity, etc. Also, peptide based nanomaterials are easier to synthesize and can be reproduced with specific structural characteristics. So far hydrogel materials made from amphiphilic self-assembling peptides are considered to be amenable for many tissue-engineering applications such as: scaffolds for drug delivery [2], biomolecular sensors [3], fillers for the treatment of osteoarthritis [4], vesicles for sustained release of hydrophilic compounds [5], and models for integrin-independent cell adhesion and growth [6]. Recent studies have also shown cell attachment, differentiation, neurite outgrowth and the formation of functional synapses by cultured neuronal cells on peptide matrix scaffolds [7, 8]. However, despite the presence of the desirable characteristics the practical applications of these peptides have been hindered due to the limited understanding of their self-assembling process at a fundamental level.

There are various factors thought to influence peptide self-assembly including: (i) amino acid composition, (ii) pH, (iii) ionic strength, (iv) solvent composition, (v) peptide concentration, (vi) temperature, and (vii) vicinal water content. Some of these factors have been previously investigated; influence of amino acid sequence and pH on self-assembly have been reported on (RADA)$_4$ [9] and other similar ionic-complementary peptide such (EAKA)$_4$ and its variants [10]. The effect of ionic strength on the self-assembly of these amphiphilic peptides have been studied

130

extensively [10, 11], as well as the effect of solvent composition on amyloid β-peptide fragments[12]. Ye and colleagues [9] concluded that at low pH values (~1.0) (RADA)$_4$ is able to hold the nanofiber structure, however, the β-sheet content is reduced; on the other hand at a pH value of 13.0 the peptide drastically losses its signature β-sheet structure and assembles into different small-sized globular aggregates. The study also concluded that when the (RADA)$_4$ peptide was heat-denatured from 25 to 80ºC it possessed the typical β-sheet structure, but self-assembled into smaller sized globular aggregates at higher temperature. Since, the practical application of (RADA)$_4$ peptide in tissue engineering entails using certain peptide concentrations for specific organ applications [13], at physiological body temperature, it is vital to analyze how the change in peptide concentration affects nanofiber assembly, and other morphological characteristics. Temperature effects were studied as a means of understanding the stability of the structures formed as a function of peptide concentration. Additionally, the underlying swelling behavior of the hydrogels may be affected by the physical cross-linking of nanofibers, which may be directly affected by the change in the peptide concentration. As the peptide concentration increases it is likely the amount of nanofiber content increases as well as the associated surface area for water to interact with. Hence, in this study we have focused on the effect of peptide concentration, temperature and internal hydration on the self-assembly of peptides.

Self-assembling peptides, *viz*., (RADA)$_4$ has been shown to form nanofibers in physiologically relevant solutions, and the resulting nanostructures are applicable to minimally invasive therapies (i.e. injectable), able to respond to external stimuli under physiological conditions, facilitate 3-D cellular activities, while maintaining an internal hydration of up to 99.5 % (w/v) water [9, 14, 15]. The latter feature suggests that these self-assembling nanofiber

131

systems are able to dramatically affect the surrounding aqueous solution and perhaps dictate the water structuring within the hydrogel environment itself. Moreover, recent studies have [16] suggested that nanofibers based on these self-assembling peptides are also generally non-immunogenic, lack an inflammatory response, and are non-thrombogenic [13]; suggestions that have not been systematically proven as of yet. Furthermore, despite the current studies exploring various characteristics and applications of $(RADA)_4$ peptide, there is a limited understanding of self-assembly of $(RADA)_4$ at a fundamental level. Therefore, the goal of this study is to understand the self-assembling mechanism of ampiphilic $(RADA)_4$ nanofibers by systematically varying the peptide concentration as well as the solution temperature.

The characteristic amphiphilic nature of $(RADA)_4$ (R, arginine; A, alanine; D, aspartic acid; acetylated and amidated N- and C-termini, respectively) is thought to be responsible for the peptide's structural stabilization as higher three dimensional structures. The alternating hydrophobic and hydrophilic components, including positive and negative charged residues, is responsible for stable nanofiber formation (Figure 4.1). The hydrogen bonding between neighboring peptide backbones, and ionic bonding among intra- and inter-peptide and the water content are believed to play a critical role in stabilizing a possible cross-β- structural motif [9]. In fact the abundance of partially charged amino acids may facilitate water interactions with the formed nanofibers directly. Here, the presence of this signature β-structural motif for $(RADA)_4$ is confirmed *via* Circular Dichroism (CD) and full nanofiber structures were observed using transmission electron microscopy (TEM). Furthermore, the effect of increasing peptide concentration and solution temperature on the underlying secondary structure of $(RADA)_4$ was analyzed using Contin (model for deciphering secondary structures from circular dichroism (CD)

data). Hydration state analysis was conducted using Differential Scanning Calorimetry (DSC) to determine the effect of peptide amount on vicinal water structuring.

Figure 4.1: Chemical structure of (RADA)4

4.2 Materials and methods

4.2.1 Peptide Synthesis

Self-assembling peptide, (RADA)4, ([COCH3]-RADARADARADARADA-[CONH2]) was commercially synthesized and purified by SynBioSci (Livermore, CA) using FMOC (Fluorenylmethyloxycarbonyl) amino acid derivatives. Acetyl and amide groups protected the N- and C-termini, respectively. High Performance Liquid Chromatography (HPLC) and Mass Spectrometry (MS) were used to determine a peptide purity of ~98%, and molecular weight (MW) of 1713.2, respectively. The determined MW was similar to the expected MW of 1713.8. These peptides were used without further purification.

4.2.2 Hydrogel Preparation

Peptide solution was prepared by dissolving (RADA)4 peptide powder in syringe filtered (0.2 μm) MilliQ water. Hydrogels were prepared by sonicating the aqueous peptide stock

solution (2510 Branson sonicator, Crystal Electronics, Newmarket, ON) for 15 min at 25°C, diluting this solution with syringe filtered, 10x PBS (pH 7.4) such that the final working peptide concentrations were 0.5, 1.0, 2.0 or 3.0% (w/v) and so that a final 1x PBS (150 mM) solution was obtained. These solutions were then allowed to self-assemble at 37°C for the desired time required for characterization (as detailed below). In the case of CD experiments phosphate buffer was used instead of PBS as PBS leads to too low signal to noise ratio in the wavelength region of interest. However, similar protocols were used for PB as for PBS.

4.2.3 Circular Dichroism

CD spectra were collected (Jasco J-810 spectropolarimeter) over the wavelength range of 180-300 nm. CD protocol was followed as described elsewhere [17], except for the changes mentioned below: Criterion for low wavelength cutoff was kept at HT(V) value of 500 or lower. The spectra were collected on samples prepared by diluting stock peptide solution in water to a working concentration of 0.5% (w/v) of (RADA)$_4$, and analyzed at room temperature. The structural contents of the peptides in solution were determined using a demountable quartz cuvette (Folio Instruments, Kitchener, ON). The quartz cuvette had a path length of 0.10 mm. Spectropolarimeter's scan mode was set to continuous and data pitch of 0.5 nm. Briefly, each final spectrum was the average of ten scans. The molar ellipticity was calculated using the relationship for peptide concentration and raw ellipticity.

$$[\Theta] = \frac{\Theta \times MRW}{c \times l \times 10}$$

Equation 4.1

Where [Θ] is the molar ellipticity (deg·cm^2/dmol), Θ is the raw ellipticity (m.deg), c is the sample concentration (g/mL), l is the optical path length (cm), and MRW is the mean residue molecular weight (Da). The three simultaneous data acquisition signals were: HT(V), Absorbance and CD (Θ). Background was subtracted from the sample signal, and the resulting CD signal converted to Molar Ellipticity as described elsewhere [18]; the mean residue molecular weight (Da) was obtained by dividing of sample molecular mass in Da with the number of amino acid residues present. The Molar Ellipticity was plotted against Wavelength (nm) for further data analysis.

To evaluate the CD spectra obtained in this study, they were compared with that of poly-L-lysine containing varying composition of three standard conformations of secondary structures: α, β and random coil [19]. To determine the quantitative aspects of the conformation changes in (RADA)$_4$, the approximate α-helix, β-turns and β-sheet content was determined using deconvolution program Contin, which computes the secondary structure of a protein from its far-UV CD spectra, as provided by Dr. W.C. Johnson (Corvallis, OR) and accessed on the DICHROWEB server (located at http://www.cryst.bbk.ac.uk/cdweb). Measured CD spectra are first broken into several basic spectra, and these basis spectra are compared to a reference library of CD spectra (containing 7 reference data sets (Ibasis7 λ = 240-190 nm)) composed of standard proteins with well-known structures *via* X-Ray crystallography. The relative fractions of secondary structure (such as α-helix and β-sheet) are given as output from Contin. A graphical output of the experimental and reconstructed data is also provided. NRMSD (normalized mean root square deviation) values less than 0.5 indicating that the Contin program and the reference selected are suitable for CD analysis for (RADA)$_4$ peptide. The secondary structures are composed of

135

six categories: H(r) is regular α-helix; H(d) is distorted α-helix; S(r) is regular β-strand; S(d) is distorted β-sheets; β-sheet Turn; Unordered. The average length pertains to the number of residues of α-helical and β-segments. The average length of α-helical segments in the reference proteins is 9.24 residues, and that of a β-strand segments is 5.02 residues.

4.2.4 **Differential Scanning Calorimetry (DSC)**

DSC (TA DSC/TGA Q 2000 Thermal Analyzer, TA Instruments, Grimsby, ON) was conducted on hydrogels in 150 mM PBS working concentrations of 0.5, 1.0, 2.0 and 3.0% (w/v) of (RADA)$_4$. Hermatic pans were purchased from TA Instruments (Grimsby, ON). Samples were cooled to -40°C at the rate of 5°C/min and then heated to 50°C, at the same rate, under a nitrogen atmosphere. In order to determine the total water of the system, the before DSC weights and the mass of dried peptide were used.

Non-frozen water contents were obtained from the difference between the equilibrium water content of the hydrogels and the calculated frozen water (Equation 4.2) [20]:

$$EWC = \frac{Wh - Wd}{Wh} \times 100$$ **Equation 4.2**

where EWC is the equilibrium water content (%), Wh is the weight of hydrated water sample (mg), and Wd is the weight of dry water sample (mg). The three kinds of water present in any polymer can be represented by Equation 4.3 [20]:

$$EWC\ (wt\%) = Wnf\ (wt\%) + Wfb\ (wt\%) + Wf\ (wt\%)$$ **Equation 4.3**

Where Wnf is the non-frozen water content (mg), W_{fb} is the frozen, bound water content (mg), and W_f is the free water content (mg).

Frozen and non-frozen water contents were determined by using the area under the resulting thermograms along with equilibrium water content. The frozen water content was calculated using Equation 4.4, where melting enthalpy of the bulk water was taken to be 334 J/g [20]:

$$W_{frozen} = \frac{\Delta H}{\Delta H^0} \, X \, 100 \qquad\qquad \textbf{Equation 4.4}$$

where W_{frozen} is the weight of frozen water present in the sample (%), ΔH is the melting enthalpy of the sample (J/g), and ΔH^o Melting enthalpy of the bulk water (J/g).

4.2.5 Transmission Electron Microscopy

Samples were loaded onto perforated formvar carbon coated copper grids (Ted Pella, Inc.). A 4% uranyl acetate stain was applied to the peptide samples. All TEM was performed on an FEI Morgagni.

4.3 Results and Discussion

4.3.1 Nanofiber Assembly

Peptide self-assembly is of direct significance to the field of biotechnology, nanotechnology, and therapeutic medicine. Self-assembling capability of (RADA)$_4$ in aqueous solution was investigated using CD [21]. Since the peptide contains four alkaline arginine

residues (pI = 10.76), four acidic aspartic acid residues (pI = 2.77), and eight alanine residues (pI = 6.00) (Figure 4.1), its theoretical pI is 7.20: a result that has been experimentally confirmed [9]. Hence, the peptide is expected to be neutral at the physiological pH of 7.4, carrying partial positive and negative charges that may facilitate water interactions with the nanofibers [22].

Scanning Electron Microscope (SEM) studies have revealed that the network of interwoven fibers for pure (RADA)$_4$ systems have a diameter of 10-20 nm and the resulting hydrogels have a pore size of 5-200 nm [23-27]. These studies have also established using CD that the formation of a strong secondary β-sheet structure for these systems is considered imperative for self-assembly into nanofibers and this β-sheet signal is now considered the proof for the presence of nanofibers [6, 25]. Figure 4.2 summarizes the observed molar ellipticity profile of 0.5% (w/v) of (RADA)$_4$ as a function of wavelength. The CD spectrum observed for 100% (RADA)$_4$ shows a typical ellipticity profile for a β-sheet structure [19] and is similar to those already reported for the (RADA)$_4$ peptide [24]; having a peak at ~195-206 nm and a minimum molar ellipticity at ~210-220 nm that indicates the presence of a backbone twist and β-sheet, respectively.
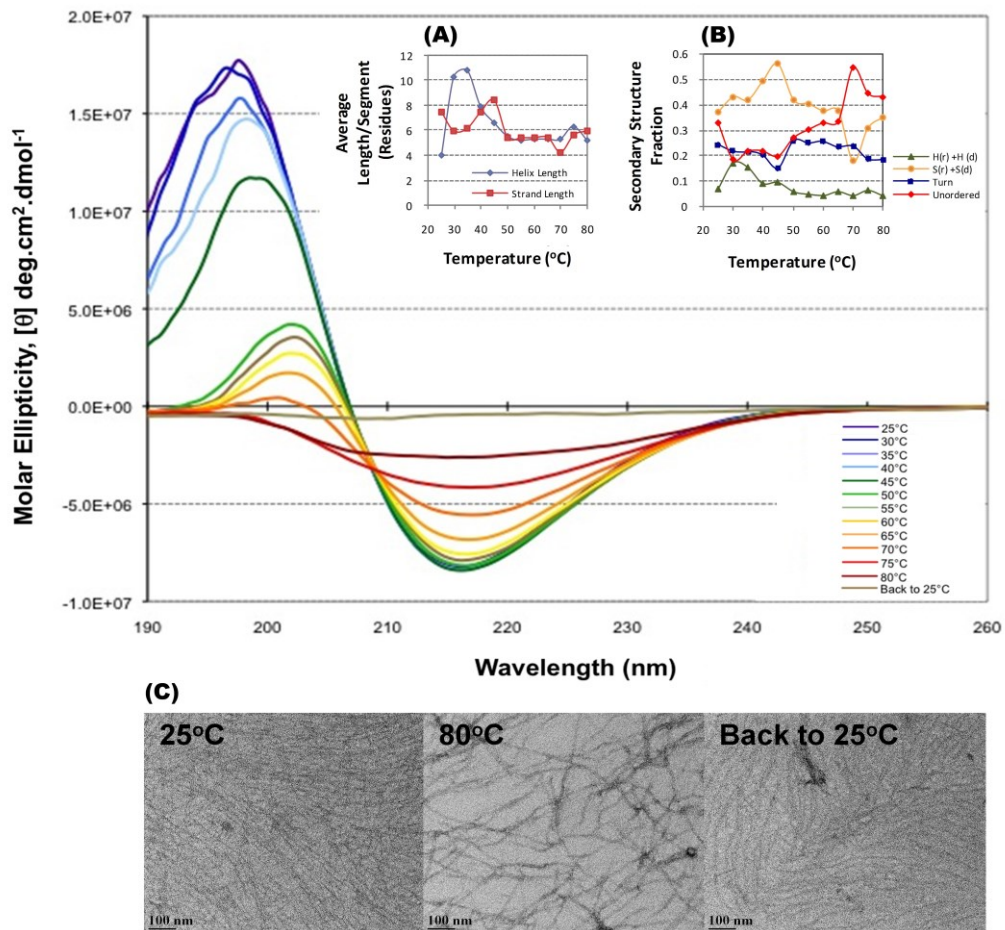
Figure 4.2 The effect of temperature on morphology and self-assembly of 0.5% (w/v) (RADA)₄.

CD results yielded a typical β-sheet twist (max at 195-200 nm) and β-sheet (min 215-216 nm), with a decrease in both as temperature approached 80°C and no observable increase upon returning to 25°C (in diH₂O). Inset: (A) Estimated average length per segment of (RADA)₄ as a function of temperature; (B) Estimated secondary structure composition of (RADA)₄ as a function of temperature; (C) TEM images of samples at 25°C, 80°C, and after cooling back to 25°C, scale bar 100 nm. Despite a lack of β-sheet twist and reduced β-sheet at 80°C and after returning to 25°C, TEM data show the presence of nanofibers at these conditions. CD related data represent the average of ten scans, with HT(V) values < 500, and TEM images are representative of multiple images over the sample (not shown).

Figure 4.2 to Figure 4.5 summarize the effect of temperature and peptide concentration (0.5 to 3.0% (w/v)) on nanofiber properties, as analyzed using both CD and TEM. The position and the relative magnitude of the mean-residue ellipticity was monitored to examine the secondary structures and their relative contents in the (RADA)$_4$ peptide at various concentrations. The Contin method, with a reference protein set, was applied to calculate the secondary structure contents of the systems understudy using the raw mean ellipticity. It was expected that with an increase in peptide concentration, the propensity of nanofiber crosslinking would be affected, resulting in altered intermolecular association and, thus, overall stability of the resulting structure [9]. CD measurements (Figure 4.2-Figure 4.5) showed that (RADA)$_4$ was able to retain its characteristic β-sheet structure (trough at ~210-218 nm) at all concentrations at 25°C, but the peak at 195-206 nm pertaining to the backbone twist in the fibers is present at 0.5% and 1.0% (w/v) (RADA)$_4$ but absent at higher concentrations of 2.0% and 3.0% (w/v) (RADA)$_4$. The backbone twist (peak at 195-206 nm) pertains to the alternating fluctuations in the dihedral angles to prevent the individual β-sheet from splitting apart, hence contributing to the β-sheet stability. Since the relative stability of the anti-parallel β-sheet depends largely on inter and intra-chain interactions involving the side chains and hence on the efficiency of packing of strands in the β-sheet [28], it can be well assumed that at higher peptide concentrations (2.0-3.0% (w/v)) impedes the efficient fiber packing, reflected in the low amount of backbone twists present at those concentrations. The peptide also exhibited an overall decrease in the β-sheet strands as seen in Figure 4.2-Figure 4.5 (B) where the S(r) + S (d) decreased from 36.8% (0.5% (w/v)) to 30.8% (3.0 % (w/v)), at 25°C; this could be due to the steric hindrance imposed by a high peptide concentration, impeding the long order structure required for β-twist formation and consequently

affecting the structure of the nanofibers. In addition to this, at higher concentrations TEM images (Figure 4.2-Figure 4.5 (C)) seem to indicate bundling of nanofibers into fibrils that may also inhibit the formation of the β-twist. A repective decrease in length of helix segments from 7.4 to 5.3 residues per segment for 0.5 and 3.0% (w/v) (RADA)$_4$ (Figure 4.2-Figure 4.5 (A) at 25°C was also observed. Simultaneously, while increasing the peptide concentration from 0.5 to 3.0% (w/v) overall total amount of α-helices present in the system also decreased from 6.6 to 4.4 % (Figure 4.2-Figure 4.5 (B), H(r) + H(d)) at 25°C. However, interestingly a slight increase to 43.7% in overall β-sheet content was observed for 1.0% (w/v) at 25°C, which is suggestive of high enough concentration for (RADA)$_4$ for β-sheet prominent intermolecular packing Interestingly the only overall increase was observed in the unordered structures upon increasing the peptide concentration from 0.5 to 3.0% (w/v), from 32.6% to 48.5% (Figure 4.2-Figure 4.5 (B), Unordered) at 25°C. The data also suggests that (RADA)$_4$ self-assembly is driven towards a more ordered three dimensional structure as enabled by a closer β-sheet packing, and loose α-helix packing from 0.5% (w/v) to 1.0% (w/v), but the concentration higher than 1.0% (w/v) impedes further β-sheet formation. It is well known that (RADA)$_4$ nanofibers exhibit a strong β-sheet peak upon assembly and, it is supposed that as the β-sheet content of a nanofiber system increases, so too does its structural stability. Additionally, the direct correlation of higher β-sheet content and lower unordered structure being the prerequisites of successful (RADA)$_4$ nanofiber formation has been proven previously [9].
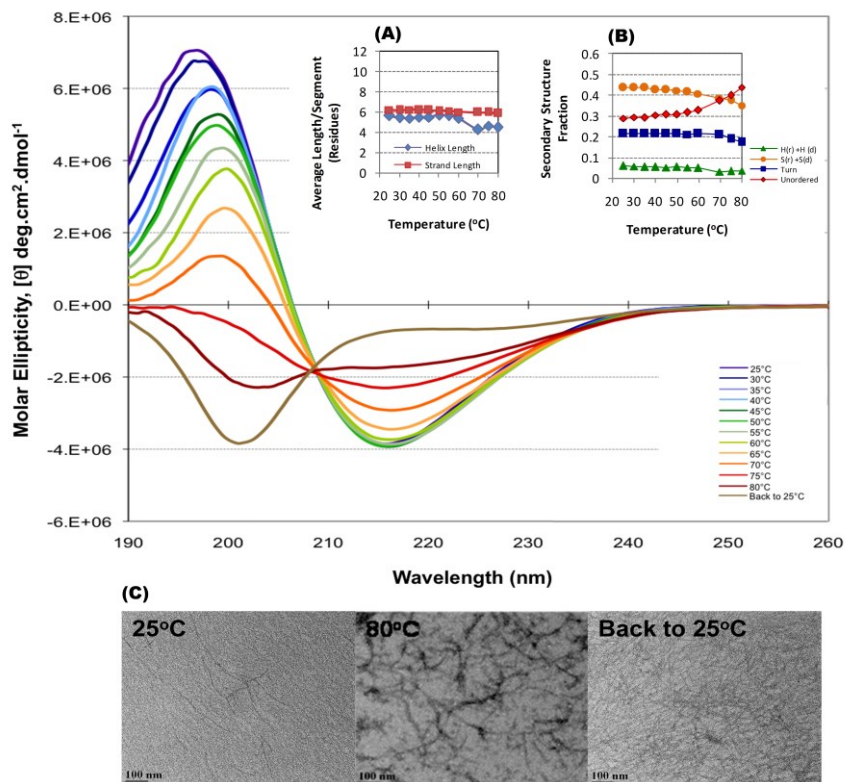
Figure 4.3 The effect of temperature on morphology and self-assembly of 1.0% (w/v) (RADA)₄.

CD results yielded a typical β-sheet twist (max at 195-200 nm) and β-sheet (min 215-216 nm), with a decrease in both and inversion at 75°C without any observable increase upon returning to 25°C (in diH₂O). Inset: (A) Estimated average length per segment of (RADA)₄ as a function of temperature; (B) Estimated secondary structure composition of (RADA)₄ as a function of temperature; (C) TEM images of samples at 25°C, 80°C, and after cooling back to 25°C, scale bar 100 nm. Despite a lack of β-sheet twist and decreased β-sheet at 80°C and after returning to 25°C, TEM data show the presence of disrupted nanofibers at 80°C and reformed nanofiber matrix at 25°C formed from shorter nanofibers. CD related data represent the average of ten scans, with HT(V) values < 500, and TEM images are representative of multiple images over the sample (not shown).

142
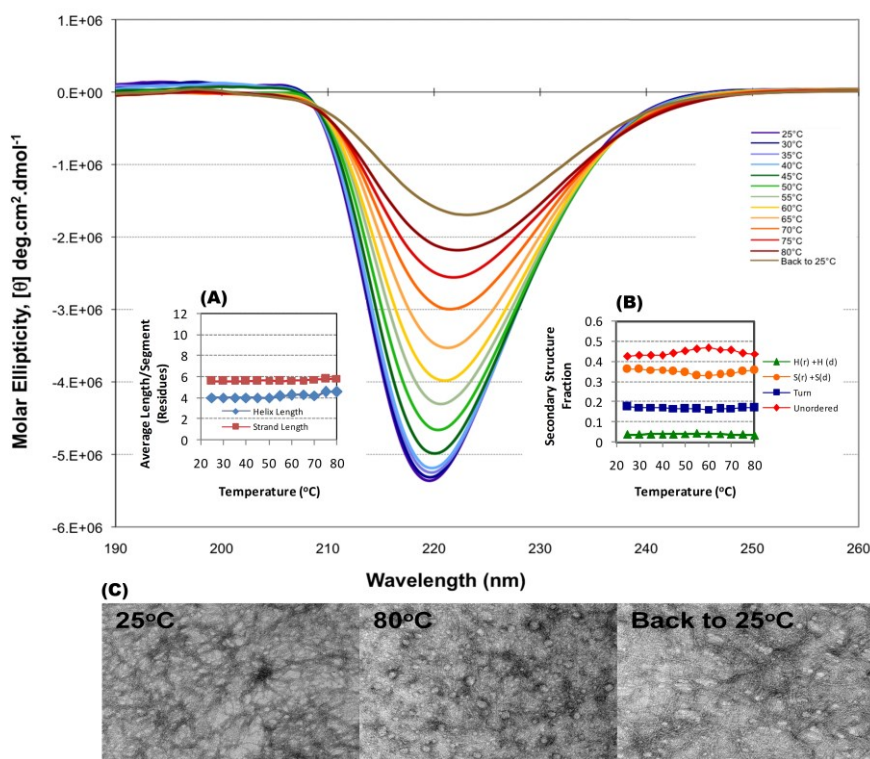
Figure 4.4 The effect of temperature on morphology and self-assembly of 2.0% (w/v) (RADA)4.

CD results yielded no typical β-sheet twist (max at 195-200 nm) and a mix of β-sheet (min 215-216 nm) and unordered structure (min 220 nm), with a decrease as 80°C was approached and a similar response after returning to 25°C (in diH$_2$O). Inset: (A) Estimated average length per segment of (RADA)4 as a function of temperature; (B) Estimated secondary structure composition of (RADA)4 as a function of temperature; (C) TEM images of samples at 25°C, 80°C, and after cooling back to 25°C, scale bar 100 nm. Despite a lack of β-sheet twist at all temperatures in CD data, the TEM data show fiber and fibril formation. β-sheet decreases in CD data at 80°C and after returning to 25°C, TEM data show mixtures of aggregates and nanofibers at 80°C and upon returning to 25°C. CD related data represent the average of ten scans, with HT(V) values < 500, and TEM images are representative of multiple images over the sample (not shown).
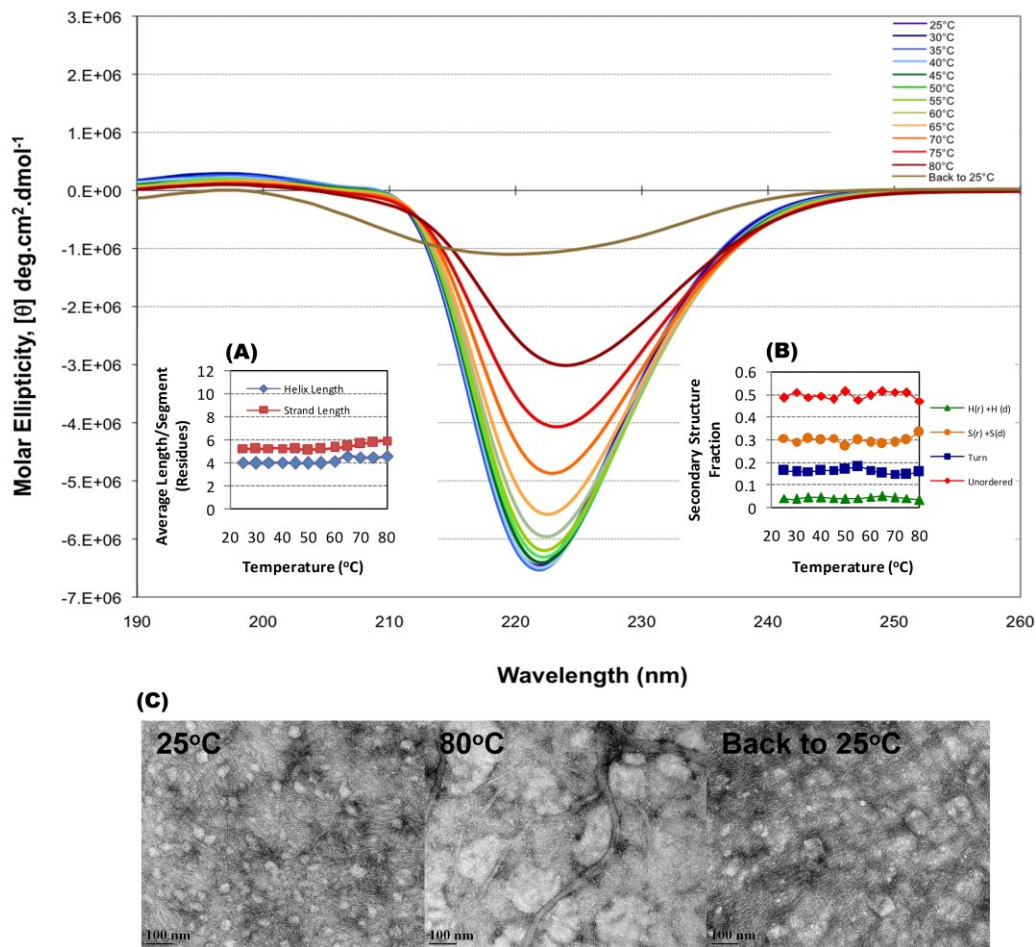
Figure 4.5 The effect of temperature on morphology and self-assembly of 3.0% (w/v) (RADA)₄.

CD results were similar as 2.0%(w/v) system. Inset: (A) Estimated average length per segment of (RADA)₄ as a function of temperature; (B) Estimated secondary structure composition of (RADA)₄ as a function of temperature; (C) TEM images of samples at 25°C, 80°C, and after cooling back to 25°C, scale bar 100 nm. Despite a lack of β-sheet twist at all temperatures in CD data, the TEM data show fiber and fibril formation. β-sheet decreases in CD data at 80°C and after returning to 25°C, TEM data show a mixture of aggregates and nanofibers at 80°C and upon returning to 25°C. CD related data represent the average of ten scans, with HT(V) values < 500, and TEM images are representative of multiple images over the sample (not shown).

Nanofiber structures are observed from the TEM results for all peptide concentrations (Figure 4.2-Figure 4.5 (C)). Nanofibers appear elongated and more refined as the $(RADA)_4$ concentration increases from 0.5 - 1.0 (w/v) (Figure 4.2 and Figure 4.3 (C)); however, appear in fibrils upon reaching 2.0%(w/v) or higher peptide amounts, increasing in thickness and complexity with further increase in peptide concentration (Figure 4.4 and Figure 4.5 (C)). It is not possible to obtain secondary structural information from these images. However, the fewer clear structures observed in CD at higher concentrations might also be due to dense and complex networks obfuscating their finer details.

4.3.2 Hydration State Analysis

Determining the structure of the water within the 3-D morphology of the assembled $(RADA)_4$ hydrogels is not only significant in understanding their equilibrium and dynamic swelling behavior, but in estimating solute transport and other diffusive characteristics of these hydrogel systems. Even at a high concentration of 3.0% (w/v), $(RADA)_4$ peptide solutions are essentially 97% water, yet able to hold a defined shape. Hence, not only is it thought that water interaction is crucial for nanofiber formation itself [15], it is also believed that water-nanofiber interactions may affect secondary phenomena like peptide packing. By definition, water that easily freezes (i.e. frozen water) is loosely adsorbed to the nanofiber and exhibits the same transition temperature as bulk water [29], whereas on-frozen water (i.e. bound water) is strongly associated with the nanofiber and exhibits no freezing/melting transition. DSC was performed to estimate the content of different types of water present in $(RADA)_4$ based hydrogels as a function of peptide concentration. Both frozen and non-frozen water are known to be present in swollen hydrogels, relative fractions of which are determined from the area enclosed by a DSC endotherm

peaks. As anticipated, as the peptide concentration increased the Equilibrium Water Content (EWC) in the system decreased (Table 4.1). Likewise, as the content of $(RADA)_4$ peptide increased from 0.5 to 3.0 % (w/v) the amount of frozen water decreased from ~90 to ~21%. Conversely, the non-frozen bound water content increased from ~9 to 77%. It is thought that this dramatic increase in non-frozen water content may be directly due to the level of surface area present in the nanofiber sample; the more peptide, the more nanofiber surface area that the water can interact with. Furthermore, it should also be noted that while increasing the $(RADA)_4$ concentration from 0.5 to 3.0% (w/v) , there is a substantial increase of 15.9% in the unordered structures (Figure 4.2-Figure 4.5 (B)) present in the system, which are known to strongly interact with the bound water [30]. Interestingly enough, even though there is a negligible increase in the unordered structure content from 1.0 to 2.0% (w/v), there is more than double increase in the non-frozen bound water content (16 to 65%). As this change doesn't seem to be due to the unordered structure of the peptides, it is possible that the hydrogel pore sizes are small enough that multiple layers of water extending from the surface of the nanofiber are confined to such an extent that they become rigid and perform as non-frozen water. This also demonstrates that both frozen and non-frozen water contents of $(RADA)_4$ hydrogel can be readily altered by regulating the concentration of the peptide, where water molecules residing on or penetrating into these nanofibers may be formed by hydrogen bonding for hydrophilic materials, and more strongly *via* ionic solvation (i.e. like zwitterionic materials) [22]. In the case of $(RADA)_4$ based nanofibers, it is likely that exposure of the charged residues (arginine and aspartic acid) to water facilitated the increase in their non-frozen waters due to a stronger interaction between the charged moieties and the vicinal water molecules. Hence, it can be concluded that at 3.0% (w/v) $(RADA)_4$ has

146

relatively lower bound water content than expected for its concentration of peptide, but that this system also had a lower β-sheet formation; a correlation discussed next.

The CD data (Figure 4.2-Figure 4.5 (B)) indicates that the observed secondary structure of (RADA)$_4$ transitions from an α-helix to β-sheet (including β-sheet turn) dominated conformation as peptide concentration increases from 0.5 to 2.0 %(w/v). The associated hydration studies (Table 4.1) show that this movement from α-helix to β-sheet structures in (RADA)$_4$ are accompanied with dramatic changes in non-frozen water content: ~8.5 to 65% for 0.5 to 2.0 %(w/v) (RADA)$_4$, respectively. The transformation of α-helix and random coils to β-sheet structure, for a wide range of proteins and peptides has been widely investigated [31-33]. Where it has been found that non-frozen bound water enhances the mobility of biopolymers by expanding its conformational space through decreasing its inter- and intra-molecular friction and, in this case, perhaps decreasing the effective energy barrier that exists for conformational changes from α-helices to β-sheets to occur [30]. It may be that for this system, non-frozen bound water may act in a similar fashion and increase the peptide extensibility, flexibility and workability [34]. Silk has been studied for the specific purpose of understanding biopolymer-water interactions [35], as the water soluble silk-I form is known to rapidly transform into a water insoluble silk-II fibroin form [34]. A similarity of the wide-angle X-ray diffraction (WAXD) patterns of (RADA)$_4$ pertaining to the presence of β-sheet structures to those in Silk II (containing antiparallel β-sheet structures) has already been established [36]. However, it should be noted that the β-sheet forming domains in silk proteins have primarily hydrophobic rather than hydrophilic side chains. It has been found that exposure of silk fibroin materials to organic solvents, mechanical stress, high salt concentration, and thermal treatments result in the

formation of insoluble β-sheet structure [37-40], hence dictating the importance of water in the stabilization of secondary structure. Furthermore, Hu and colleagues [30] concluded in their study investigating silk-water relationships during β-sheet formation that non-frozen bound water acts as a plasticizer, resulting in a non-frozen bound water-silk structure, prior to the transition of α-helices and random coils to β-sheets. Perhaps a similar mechanism is being observed here for $(RADA)_4$, whereby the increase in concentration from 0.5 to 3.0% (w/v) results in an increase in relative β-sheet structure stabilization that is ultimately facilitated *via* the increase in non-frozen water content of 8.5 to 77 % (Table 4.1). The lower percentage of non-frozen bound water present at 8.5% and 16 % for 0.5 and 1.0 % (w/v) $(RADA)_4$, respectively, provided limited mobility to the nanofibers, and hence stabilizing them into α-helix structures (Table 4.1). The results provided herewith are consistent with a previous study investigating the effect of hydration on solid state $(RADA)_4$, where the increase in bound water content lead to the rapid conversion to β-strands and organization into β-sheets, hence confirming the role of non-frozen water as plasticizers in self-assembly of $(RADA)_4$ nanofibers [36]. Therefore, not only is the effect of water confinement and nanofiber surface area of importance in water structuring, but also it may be that water structuring also influences the transitions in peptide secondary structures.

Table 4.1 Water phases chemical structure of self-assembling peptide (RADA)4 hydrogels as a function of peptide concentration.

Frozen and non-frozen water content representing loosely interacting and strongly interacting bound water within the peptide matrix. Data represent average $\pm$ 1 SD, n>5.

(RADA)4 Content (%, w/v)	Equilibrium Water Content (%)	Frozen water (%)	Non-frozen water (%)
3	96 ± 1	21 ± 6	77 ± 4
2	98 ± 1	33 ± 2	65 ± 2
1	99 ± 2	83 ± 2	16 ± 1
0.5	98.7 ± 0.4	90.2 ± 0.8	8.5 ± 0.8

4.3.3 Effect of Peptide Concentration on Nanofiber Thermal Stability

Variable temperature experiments were performed on different concentrations of ((RADA)4 (0.5-3.0% (w/v)) in order to gain further insight into the role of heating on nanofiber structure. Thermal transitions corresponding to the secondary structure transitions of (RADA)4 could also provide more information regarding the role of bound water on the varying concentrations of the peptide. Heat is thought to denature the peptide secondary structure of (RADA)4 by destroying its non-covalent interactions [9]. Moreover, the increase in temperature is known to provide thermal energy to the system and when there is enough the peptide-peptide interactions can be disrupted [9]. Upon heating the peptide-water system to higher temperature, the energetic barrier-trapping solid like water molecules was hypothesized to be broken, resulting in the transformation of some non-frozen bound water to free water molecules. The relocation of water molecules across the peptide molecular layers may go hand in hand with overall structural transformation [30]. Hence, water molecules are thought to play a very important role in the peptide-water systems, especially upon heating. Temperature was increased from 25 to 80°C, and

spectra was accumulated every 5°C to monitor changes in the secondary structure of the peptides. Furthermore the temperature was decreased from 80 to 25°C in the same manner to analyze if the effect temperature had on nanofibers was reversible.

Increasing the peptide concentration from 0.5 to 1.0% (w/v) yielded an increase in β-sheet and unordered structure, with a decrease in α-helix. Whereas, $(RADA)_4$ at 3.0 % (w/v) displayed a relatively lower β-sheet content and a higher α-helix and unordered structures (Figure 4.2-Figure 4.4 (B)). When increasing temperature, it was expected that a decrease in β-sheet content would occur due to the weakening of electrostatic and hydrophobic interactions. With the increase in temperature from 25 to 80°C, a decrease in the α-helix and β-sheet content was observed in $(RADA)_4$ at 0.5, 1.0 and 2.0 % (w/v) with an increase in the unordered structures (Figure 4.2-Figure 4.4 (B)). Consistent with a previous study [36] on solid state $(RADA)_4$ for all the weight by volume concentrations of $(RADA)_4$ the major increase in β-sheet content occurs between 30-60°C. Dehydration of these systems usually leads to loss of long and intermediate-range diffusion [29, 41, 42], necessary for β-sheet formation. Furthermore, there was a less uniform order present in the nanofiber arrangement (nanofibers are spaced apart) when heating 0.5% and 1.0% (w/v), as shown in the TEM images. However, an increase in the β-sheet content along with a decrease in the unordered structure was observed with 3.0%(w/v), when increasing the temperature from 25 to 80°C (Figure 5 (B)), suggesting the loosening of the nanofiber mesh with the increase in the temperature, allowing for the necessary intra-molecular interactions required for the successful β -sheet formation. This is reflected in the TEM images, as there are distinct bundle-like fibers visible after heating to 80°C, which may suggest structures with increased β -sheet formation, and fewer α-helices. Even though the effect of temperature study

150

by Ye and colleagues [9] involved (RADA)$_4$ at one concentration, the pattern observed in their investigation (decrease in the β-sheet content, with an increase in unordered structure, with the increasing temperature from 20-80°C), is similar to the subsystems tested herewith. Also, an exact opposite pattern of secondary structure transition (i.e. an increase in the α-helix and unordered structures with a decrease in the β-sheet content) was observed with 3.0% (w/v), upon decreasing the temperature from 80-25°C. Moreover, it was observed that the heat denaturation of 3.0% (w/v) (RADA)$_4$, was reversible to some extent, without any shifts in the trough positions for the absorbed wavelength (215 nm), and with the insignificant change in trough depth. This is further supported by TEM as the images for 25°C are indistinguishable. However, all the other (RADA)$_4$ systems (0.5-2.0% (w/v)) displayed a few nanometers of shift (to the higher wavelength) in their peak and trough values upon cooling, suggesting a slight variability in their β structure geometry upon cooling (barrels, sheets, β-helices, etc). In addition, a decrease in the negative and positive molar ellipticity for (RADA)$_4$ systems (0.5-2.0% (w/v)) suggest either an intra-molecular peptide bonding or peptide aggregation upon cooling from the higher temperature to room temperature. Another interesting observation was the lack of the backbone twist (characterized by the peak at 195 nm) at the 2.0% (w/v) and higher of the (RADA)$_4$ nanofibers, indicating a dense packing of β-sheets upon the increase in concentration. The morphological properties of peptide (RADA)$_4$ also varied with respect to change in nanofiber concentrations; (RADA)$_4$ at 0.5 and 1.0 % (w/v) displayed individual nanofibers very similar in density, while 2.0 and 3.0 % (w/v) (RADA)$_4$ displayed thick bundles with pores. Furthermore, as evident by the TEM images (Figure 4.2-Figure 4.5 (C)), relatively small variability in the nanofiber shapes was observed upon cooling. Considering the time given for cooling in the experiment was merely

three minutes per accumulation (and minimum 30 minutes are required for hydrogel formation), it can be concluded that the temperature induced changes in the (RADA)$_4$ systems (0.5-3.0% (w/v)), are reversible to some extent, provided more time given for nanofiber stabilization and formation.

4.4 Conclusions

In this study, various techniques were employed to investigate the underlying self-assembly mechanisms of (RADA)$_4$ peptide. Analysis of CD measurements showed that (RADA)$_4$ was able to retain its characteristic β-sheet structure (indicated by the trough at 210-218 nm and a peak at 195-206 nm) at all concentrations tested herewith. Contin analysis revealed that while increasing the peptide concentration from 0.5 to 3.0% (w/v) a decrease in the β-sheet content, average strand length segment, and α-helices, and an increase in the total amount of unordered structures present in the system was observed. The results suggest that (RADA)$_4$ self-assembly towards a more ordered three dimensional structure is enabled by structural transition from α-helices to β-sheet dominated conformations, and by the closer packing of β-sheet structures. Additionaly, hydration studies reveal that there are significant changes in water structure as a function of peptide concentrations. This change in water structure may be due to nanofiber surface area, coupled with confined water in pores. Also, structural transition of these peptides is facilitated by the presence of intermolecular bound water that ultimately decreases the effective barrier height for conformational change from α-helices to β-sheets. The results presented herein provide insight in understanding the molecular basis of self-assembly.

Acknowledgements

AUTHOR INFORMATION

Corresponding Author

Larry D. Unsworth, Ph.D., P.Eng.

Phone: 780-492-6020

Fax: 780-492-2881

E-mail: larry.unsworth@ualberta.ca

Author Contributions

The manuscript was written through contributions of all authors: AS planned, conducted, evaluated all experiments except TEM, wrote the article, and responded to reviewer comments; KK conducted and evaluated all TEM experiments; LDU planned and evaluated the experimental work and assisted in article preparation. All authors have given approval to the final version of the manuscript.

References

[1] Whitesides GM, Grzybowski B. Self-assembly at all scales. Science 2002;295:2418-21.

[2] Johnson TD, Christman KL. Injectable hydrogel therapies and their delivery strategies for treating myocardial infarction. Expert Opinion on Drug Delivery 2013;10:59-72.

[3] Buenger D, Topuz F, Groll J. Hydrogels in sensing applications. Progress in Polymer Science 2012;37:1678-719.

[4] Janssen I, Koene M, Lischer C. Intraarticular applikation of polyacrylamide hydrogel as a treatment of osteoarthritis in the distal interphalangeal joint: case series with 12 horses. Pferdeheilkunde 2012;28:650-6.

[5] Uchida Y, Fukuda K, Murakami Y. The hydrogel containing a novel vesicle-like soft crosslinker, a "trilayered" polymeric micelle, shows characteristic rheological properties. Journal of Polymer Science Part B-Polymer Physics 2013;51:124-31.

[6] Zhang SG, Holmes TC, Dipersio CM, Hynes RO, Su X, Rich A. Self-complementary oligopeptide matrices support mammalian-cell attachment. Biomaterials 1995;16:1385-93.

[7] Holmes TC, de Lacalle S, Su X, Liu GS, Rich A, Zhang SG. Extensive neurite outgrowth and active synapse formation on self-assembling peptide scaffolds. Proceedings of the National Academy of Sciences of the United States of America 2000;97:6728-33.

[8] Schachner M. Neurobiology - Nervous engineering. Nature 2000;405:747-8.

[9] Ye ZY, Zhang HY, Luo HL, Wang SK, Zhou QH, Du XP, *et al*. Temperature and pH effects on biophysical and morphological properties of self-assembling peptide RADA16-1. Journal of Peptide Science 2008;14:152-62.

[10] Hong Y, Lau LS, Legge RL, Chen P. Critical self-assembly concentration of an ionic-complementary peptide EAK16-1. The Journal of Adhesion 2004;80:913-31.

[11] Hong YS, Legge RL, Zhang S, Chen P. Effect of amino acid sequence and pH on nanofiber formation of self-assembling peptides EAK16-II and EAK16-IV. Biomacromolecules 2003;4:1433-42.

[12] Castelletto V, Hamley IW, Harris PJF, Olsson U, Spencer N. Influence of the Solvent on the Self-Assembly of a Modified Amyloid Beta Peptide Fragment. I. Morphological Investigation. Journal of Physical Chemistry B 2009;113:9978-87.

[13] Ellis-Behnke RG, Liang Y-X, Tay DKC, Kau PWF, Schneider GE, Zhang S, *et al*. Nano hemostat solution: immediate hemostasis at the nanoscale. Nanomedicine : nanotechnology, biology, and medicine 2006;2:207-15.

[14] Segers VFM, Lee RT. Local delivery of proteins and the use of self-assembling peptides. Drug Discovery Today 2007;12:561-8.

[15] Zhang SG, Lockshin C, Cook R, Rich A. Unusally stable beta-sheet formation in an ionic self-complementary oligopeptide. Biopolymers 1994;34:663-72.

[16] Zou ZW, Zheng QX, Wu YC, Guo XD, Yang SH, Li JF, *et al*. Biocompatibility and bioactivity of designer self-assembling nanofiber scaffold containing FGL motif for rat dorsal root ganglion neurons. Journal of Biomedical Materials Research Part A 2010;95A:1125-31.

[17] Greenfield NJ. Using circular dichroism spectra to estimate protein secondary structure. Nature Protocols 2006;1:2876-90.

[18] Snatzke G. Circular Dichroism: Principles and Applications. New York: VCH Publishers; 1994. p. 59-84.

[19] Greenfield N, Fasman GD. Computed circular dichroism spectra for the evaluation of protein conformation. Biochemistry 1969;8:4108-16.

[20] Mequanint. K S, H. 2-Methacryloyloxyethyl N-butylcarbamate: A new comonomer for hydrogel syntheses with improved hydrophilicity and mechanical properties for ophthalmic applications. Journal of Biomaterials Science, Polymer Edition 2005;16:1303-18.

[21] Beychok S. Poly-alpha-amino acids: Protein Models for Conformational Studies. New York: Marcel Dekker; 1968.

[22] Chen SF, Li LY, Zhao C, Zheng J. Surface hydration: Principles and applications toward low-fouling/nonfouling biomaterials. Polymer 2010;51:5283-93.

[23] Zhang S, Holmes T, DiPersio M, Hynes RO, Su X, A. R. Self-complementary oligopeptide matrices support mammalian cell attachment. Biomaterials 1995;16:1385-93.

[24] Yokoi H, Kinoshita T, Zhang S. Dynamic reassembly of peptide RADA16 nanofiber scaffold. Proceedings of the National Academy of Sciences 2005;102:8414-9.

[25] Zhang S, Holmes T, Lockshin C, A. R. Spontaneous assembly of a self-complementary oligopeptide to form a stable macroscopic membrane. Proceedings of the National Academcy of Sciences USA 1993;90:3334-8.

[26] Gelain F, Bottai D, Vescovi A, Zhang S. Designer Self-Assembling Peptide Nanofiber Scaffolds for Adult Mouse Neural Stem Cell 3-Dimensional Cultures. Public Library of Science 2006:1-11.

[27] Holmes T, De Lacalle S, Su X, Liu G, Rich A. Extensive neurite outgrowth and active synapse formation on self-assembling peptide scaffolds. Proceedings of the National Academcy of Sciences USA 2000;97:6728-33.

[28] Chou KC, Nemethy G, Scheraga HA. Effect of amino acid composition on the twist and the relative stability of parallel and anti-parallel beta sheets. Biochemistry 1983;22:6213-21.

[29] Kim YS, Dong LM, Hickner MA, Glass TE, Webb V, McGrath JE. State of water in disulfonated poly(arylene ether sulfone) copolymers and a perfluorosulfonic acid copolymer (nafion) and its effect on physical and electrochemical properties. Macromolecules 2003;36:6281-5.

[30] Hu X, Kaplan D, Cebe P. Dynamic protein-water relationships during beta-sheet formation. Macromolecules 2008;41:3939-48.

[31] Shen CL, Murphy RM. Solvent effects on self-assembly of beta-amyloid peptide. Biophys J 1995;69:640-51.

[32] Wood SJ, Maleeff B, Hart T, Wetzel R. Physical, morphological and functional differences between pH 5.8 and 7.4 aggregates of the Alzheimer's amyloid peptide AP. J Mol Biol 1996;256:870-7.

[33] Barrow CJ, Yasuda A, Kenny PTM, Zagorski MG. Solution conformations and aggregational properties of synthetic amyloid beta-peptides of the alzhiemeres disease- analysis of circular dichroism spectra. J Mol Biol 1992;225:1075-93.

[34] Hu X, Kaplan D, Cebe P. Determining beta-sheet crystallinity in fibrous proteins by thermal analysis and infrared spectroscopy. Macromolecules 2006;39:6161-70.

[35] Altman GH, Diaz F, Jakuba C, Calabro T, Horan RL, Chen JS, et al. Silk-based biomaterials. Biomaterials 2003;24:401-16.

[36] Cormier AR, Ruiz-Orta C, Alamo RG, Paravastu AK. Solid State Self-Assembly Mechanism of RADA16-I Designer Peptide. Biomacromolecules 2012;13:1794-804.

[37] Hu X, Kaplan D, Cebe P. Effect of water on the thermal properties of silk fibroin. Thermochim Acta 2007;461:137-44.

[38] Chen X, Shao ZZ, Marinkovic NS, Miller LM, Zhou P, Chance MR. Conformation transition kinetics of regenerated Bombyx mori silk fibroin membrane monitored by time-resolved FTIR spectroscopy. Biophys Chem 2001;89:25-34.

[39] Motta A, Fambri L, Migliaresi C. Regenerated silk fibroin films: Thermal and dynamic mechanical analysis. Macromol Chem Phys 2002;203:1658-65.

[40] Jin HJ, Kaplan DL. Mechanism of silk processing in insects and spiders. Nature 2003;424:1057-61.

[41] Doster W, Settles M. Protein-water displacement distributions. BBA-Proteins Proteomics 2005;1749:173-86.

[42] Hodge RM, Bastow TJ, Edward GH, Simon GP, Hill AJ. Free volume and the mechanism of plasticization in water-swollen poly(vinyl alcohol). Macromolecules 1996;29:8137-43.

Chapter 5

Evaluation of the Hemocompatibility and Rapid Hemostasis of

(RADA)$_4$ Peptide-Based Hydrogels

Coauthors who contributed to this research are: Katherine Serrano, Kyle Koss, and Larry D.

Unsworth

(RADA)$_4$ Hydrogel

Injured blood vessel

Low C3a Activation

Low Platelet Activation

(RADA)$_4$ induced rapid hemostasis
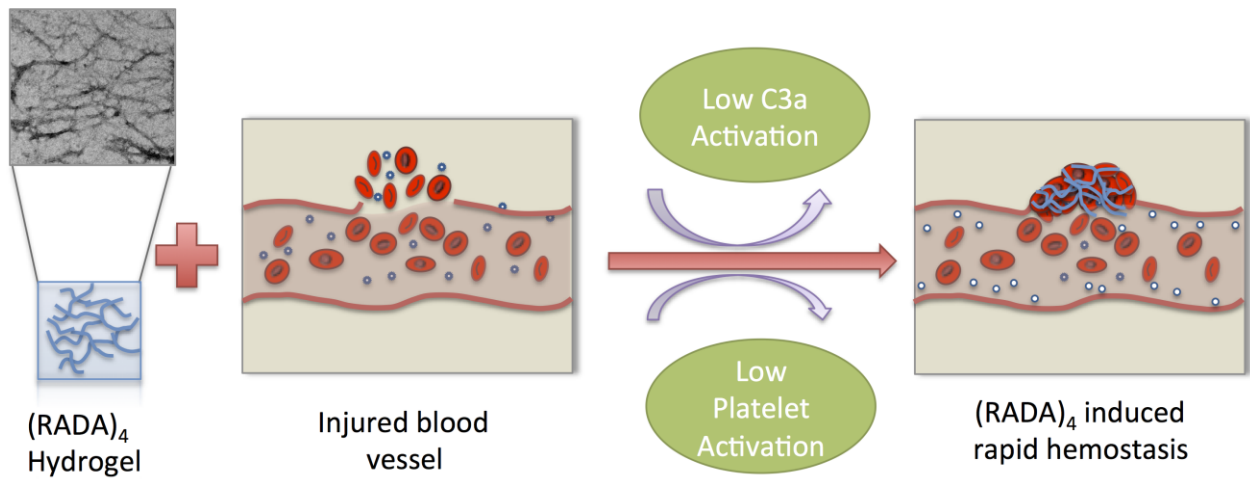
Graphical Abstract 2

Abstract

(RADA)$_4$ peptides are promising biomaterials due to their high degree of hydration (<99.5% (w/v)), programmability at the molecular level, and their subsequent potential to respond to external stimuli. Interestingly, these peptides have also demonstrated the ability to cause rapid (~15 seconds) hemostasis when applied directly to wounds. General hemocompatibility of (RADA)$_4$ nanofibers was investigated systematically using clot formation kinetics, C3a generation, and platelet activation (morphology and CD62P) studies. (RADA)$_4$ nanofibers caused a rapid clot formation, but yielded a low platelet activation and low C3a activation. The study suggests that the rapid hemostasis observed when these materials are employed results principally from humoral coagulation, despite these materials having a net neutral charge and high hydration at physiological conditions. The observed rapid hemostasis may be induced due to the available nanofiber surface area within the hydrogel construct. In conclusion, our experiments strongly support further development of (RADA)$_4$ peptide based biomaterials.

5.1 Introduction

Self-assembling peptides have various tissue-engineering applications such as drug delivery [1], membrane protein stabilization [2], 3D peptide nanofiber scaffolds, etc. [3, 4]. Particularly, $(RADA)_4$ peptide based hydrogels have traits that make them amenable for soft-tissue applications, in physiologically relevant solutions [5, 6]. These traits include, net neutral charge, applicable to minimally invasive therapies (i.e. injectable), able to respond to external stimuli under physiological conditions, facilitate 3-D cellular activities, while maintaining an internal hydration of up to 99.5% (w/v) water [7-9]. Also, $(RADA)_4$ based hydrogels have been observed to achieve complete hemostasis in ~15 seconds, without employing any of the traditional hemostatic therapies, such as cauterization, vasoconstriction, coagulation, pressure application or the use of cross-linked adhesives [10]. Many protein (such as, collagen and fibrin) based biomaterials have been studied extensively in the past for the purpose of achieving hemostasis, but they all resulted in limited success due to the lack of severe hemorrhage control [11, 12]. However, $(RADA)_4$ based hydrogels have been reported to not only have achieved complete, but rapid hemostasis under severe hemorrhagic conditions [10]. Despite the seemingly revolutionary hemostatic capabilities of $(RADA)_4$ hydrogels, the correlations between underlying material properties with the general hemocompatibility of these materials have not been thoroughly investigated [10, 13]. Elucidation of the mechanisms that underlie this somewhat surprising hemostatic ability may hold a key that will facilitate a revolutionary approach to the design of blood-contacting biomaterials.

The primary physiological response to any biomaterial involves the accumulation of a layer of host proteins derived from plasma or interstitial fluids and that this protein-surface

interaction may dictate subsequent host responses [14, 15]. Previous work has shown that material properties can have a profound effect on how biomaterials interact with protein rich solutions like blood. In fact, fundamental studies have shown that, for surfaces, the key for limiting protein-surface interactions seems to depend upon having hydrophilic, electrically neutral, and hydrogen-bond acceptor moieties [16]; also present on the $(RADA)_4$ systems employed in this study. Hence here, we assess the hemocompatibility of the $(RADA)_4$ peptide by investigating biomaterial induced immunological and inflammatory responses including the activation of coagulation and complement systems.

A few studies have demonstrated the first applications of $(RADA)_4$ in nanotechnology to achieve complete and rapid hemostasis [10, 13]. One of these studies investigated $(RADA)_4$ as an extracellular matrix to facilitate neuronal regeneration, but instead discovered immediate hemostasis when applied directly to open wounds [10]. Interestingly, the mechanism was not tissue specific, as complete hemostasis was observed in various organs and tissues: brain, spinal cord, high pressure femoral artery wounds, highly vascularized liver wounds and skin punches [10]. In an attempt to understand the underlying mechanism responsible for this rapid onset of hemostasis various concentrations of the $(RADA)_4$ peptide were studied (1.0, 2.0, 3.0 and 4.0% (w/v)), and the transmission electron microscopy (TEM) of the tissues were also conducted, however, the resulting observations were somewhat inconclusive [10]. Further work [13] focused on this topic also concluded that the longer the $(RADA)_4$ nanofibers, the higher was the storage modulus (G`), resulting in more control of bleeding. However, even though these studies had similar theories about the rapid hemostasis *via* $(RADA)_4$ nanofibers, they lack the experimental evidence relating molecular assembly of these fibers with their hemostatic capabilities, as well as

any biocompatibility analysis. Therefore, in this work we report the *in-vitro* evaluation of $(RADA)_4$ based hydrogels hemocompatibility involving: complement activation, platelet morphology and activation, as well as clot formation kinetics.

Complement is a key component of humoral immunity, and its activation leads to the enzymatic cleavage of C3 into C3a and C3b; where C3a mediates an array of inflammatory responses such as smooth muscle contraction, histamine release from mast cells, vasodilation, increased vascular permeability, and chemotaxis [17]. Whereas platelets serve in hemostasis to preserve the integrity of the vascular wall through the formation of a platelet plug [18]. Material-induced platelet activation is associated with undesirable thrombotic complications of the devices, and is rapid and occurs *via* platelet attachment, membrane alteration, spreading, the release of granule contents and aggregation [19-21]. Herein, platelet activation was determined *via* monitoring the expression of CD62P protein on the activated platelets (for CD42 positive platelets) [22, 23]. A detailed morphological analysis of platelets upon incubation with $(RADA)_4$ nanofibers was also conducted and analyzed using a morphology score. Clotting kinetics for these hydrogels were evaluated using a turbidimetric assay using recalcified, platelet-poor human plasma. The lack of platelets in this assay allows for the analysis of the clot formation purely as a function of protein-surface interactions: surface activation leading to clot formation. Hence, the rapid hemostatic ability of the $(RADA)_4$ peptide nanofibers was evaluated not only as a function of platelet activation but also *via* cell free clot kinetics. This work provides an in-depth hemocompatibility analysis of hydrogels composed of $(RADA)_4$ nanofibers for the first time.

5.2 Materials and methods

Briefly, whole blood was collected from three healthy unmedicated donors, who provided informed consent in accordance with the current CBS and National Ethics Board standards. Blood collected in this manner was used for all subsequent plasma related assays, as described below.

5.2.1 Peptide synthesis

Self-assembling peptide, $(RADA)_4$ ([Ac]-RADARADARADARADA-[NH$_2$]) was commercially synthesized and purified by SynBioSci (Livermore, CA) using FMOC amino acid derivatives. High performance liquid chromatography and mass spectrometry were used to determine peptide purity and molecular weight (MW). Peptide purity was ~98%, with a calculated MW of 1713.2 that was very similar to the expected MW of 1713.8. These peptides were used without further purification.

5.2.2 Hydrogel preparation

Peptide solution was prepared by dissolving $(RADA)_4$ peptide powder in syringe-filtered (0.2 μm) MilliQ water. Hydrogels were prepared by sonicating the aqueous peptide stock solution (2510 Branson sonicator, Crystal Electronics, Newmarket, ON) for 15 min at 25°C. Aqueous peptide solutions were diluted with syringe filtered, 10x phosphate buffer saline (Sigma-Aldrich P7059, pH 7.4) such that the final working peptide concentrations were 0.5, 1.0, 2.0 or 3.0 % (w/v) and so that a final 1x PBS (150 mM) solution was obtained. Solution pH was adjusted to 7.4 through drop wise addition of concentrated NaOH and/or HCl. Peptides were

allowed to self-assemble at 37°C for 30 min, and stored overnight at 4°C. Prior to use, peptide solutions were sonicated for 30 min at 37°C, pipetted as needed, and rested for at least 30 min to allow time for complete self-assembly [24].

5.2.3 Transmission Electron Microscopy

Samples were loaded onto perforated formvar carbon coated copper grids (Ted Pella, Inc.). A 4% uranyl acetate stain was applied to the peptide samples. All TEM was performed on an FEI Morgagni electron microscope.

5.2.4 Plasma Clot Analysis

The plasma clot assay was conducted as previously described [25]. Various concentrations of the $(RADA)_4$ hydrogels (0.5% (w/v) to 3.0% (w/v)) were thoroughly mixed and incubated with an equal volume of platelet-poor human plasma for 30 minutes at 37°C in a 96 well microtiter plate. An equal volume of 0.025 M $CaCl_2$ was injected into the wells and the optical density at 405 nm was measured with a BioTek ELx808 plate reader, at 1-minute intervals over a period of 60 minutes. All experiments were repeated four times.

5.2.5 Complement C3a Activation

Complement C3a studies were performed using platelet-poor human plasma with a commercially available kit (Quidel, San Diego, CA) as per the manufacturer's protocol. Briefly, plasma (5 μl) was incubated at 37°C with an equal volume of hydrogel for 30 min and then ethylenediaminetetraacetic acid (EDTA at pH 7.4) was added to a final concentration of 18.5 μM for quenching the reaction. The final reaction volumes of 500 μl were handled using the provided

C3a Plus MicrovueTM Quidel ® plates. 1X PBS (pH 7.4) was used as control for the experiments. Due to the number of samples and set up times, etc., these final experimental solutions (i.e. plasma, (RADA)$_4$ hydrogels and EDTA) were stored at -80°C overnight and thawed at 37°C prior determining C3a levels (as per the manufacturer's protocol). The assay was analyzed using a 4-parameter curve fit. The experiment was conducted in duplicates and the values are given as the average of two measurements.

5.2.6 **Platelet Activation**

Platelet activation studies were carried out as described elsewhere [26]. Blood was drawn using a 10 cc syringe into an acid citrate dextrose (ACD) tube (11.5 mM citric acid monohydrate, 88.5 mM trisodium citrate dihydrate, 111 mM dextrose, pH 6.0, anticoagulant at a ratio of 1:9), purchased from Beckton Dickinson (Franklin Lakes, NJ). Platelets were analyzed within two hours. Platelet-rich plasma (PRP) was isolated by centrifuging whole blood at room temperature for 15 min, at 146 x g (Beckman Coulter, Mississauga, ON). PRP (20 µl) was incubated at 37°C with an equal volume of hydrogel for 30 min. The experimental control being platelets exposed to a 1X PBS (pH 7.4) solution. The experiment was conducted in duplicates and the values are given as the average of two measurements.

Platelet activation state was investigated using a Beckman Coulter fluorescence flow cytometer EPICS XL-MCL model (Miami, FL). Five microliters of a platelet agonist such as, thrombin or adenosine diphosphate (ADP) were added to activate platelets as a positive control with 5 µl of phycoerythrin (PE) conjugated anti-CD62P antibodies (Immunotech Coulter, Mississauga, ON). The positive controls also had 3 µl of fibrin polymerization inhibitor peptide,

GPRP. Three microliters of anti-CD42-PE or anti-CD42-FITC antibodies were used as pan platelet markers. Mouse IgG and IgM isotypes conjugated to the same chromophore (PE or FITC) were used as the non-specific binding controls. Lastly, 1X PBS (pH 7.4) was added to the samples to achieve a final volume of 50 μl. 30 min incubation in the dark at room temperature was then carried out. Subsequently, the samples were diluted with one mL of 1X PBS (pH 7.4) for flow cytometric analysis. Platelets were diluted with the phosphate buffer until the concentration of 200 X 10^6/ml.

Single populations of platelets were substantiated and the gate for the underlying area was selected on the basis of platelet forward scatter (FSC) versus side scatter characteristics (SSC). Five thousand platelet events were collected. Events positive for CD42a or CD42b were monitored to confirm the identity of the platelets. The fluorescence measurement gates were adjusted to include the upper 5% of signals obtained with the isotype control antibodies. The signals collected within the gates for the test samples were counted as positive events for the antibody marker. Data is reported as the percentage of positive events.

5.2.7 Platelet Morphology

Platelet morphology was performed by isolating PRP as described previously [26]. PRP (15 μl) was incubated at 37ºC with an equal volume of hydrogel for 30 min. To fix the samples, 30 μl of 4% paraformaldehyde was added and samples stored at room temperature and analyzed by phase contrast microscopy (Nikon, Mississauga, ON) using a 1000X oil immersion lens. The sample size for analysis was 100 platelets and values were reported as the average of three sets totaling 300 platelets. The platelets were categorized by shape as, discoid, spiny sphere, and

balloons [27]. The morphology score was calculated by the modified Kunicki scoring system [27], described below in Equation 5.1:

$$MS = [(D \times 4) + (S \times 2) + (B \times 1)]$$ **Equation 5.1**

Where, MS is the morphology score, D is the number of discoid shaped platelets, S is the number of spiny sphere shaped platelets and B is the number of balloon shaped platelets.

5.2.8 Statistical analysis

Statistical analyses were performed using VassarStats: Website for Statistical Computation (http://vassarstats.net/). Results are presented as a mean $\pm$ SD. Multiple comparisons between groups were performed by one-way ANOVA followed with Tukey's HSD *post hoc* analysis. Differences were reported as statistically significant at $p<0.05$.

5.3 Results and Discussion

5.3.1 Nanofiber assembly

Previous work in our lab has confirmed the successful nanofiber formation in (RADA)$_4$ based hydrogels at various concentrations [24]. A typical strong secondary β-sheet (minimum mole residue ellipticity (deg.cm^2/decimole) at 216-218 nm) and backbone twist (maximum mole ellipticity at ~ 195 nm) are considered the prime standard for nanofiber formation for the (RADA)$_4$ peptide [28, 29]. We demonstrated that (RADA)$_4$ was not only able to retain its characteristic β-sheet structure, but also exhibited an increase in the relative β -sheet content with increasing concentration from 0.5% to 3.0% (w/v) pertaining to the increase in crosslinking of the

peptide at these concentrations [24]. In addition to CD, TEM was also used to examine the effect of (RADA)$_4$ concentration (0.5, 1.0, 2.0 and 3.0% (w/v)) upon the nanofiber/hydrogel morphology (Figure 5.1). The morphological properties of the (RADA)$_4$ nanofibers changed significantly upon altering its concentration, ranging from long extensively interwoven three dimensional nanofibers at 0.5% (w/v) to more interwoven densely packed and cross linked aggregated bundle shape structures at 2.0 and 3.0 % (w/v). The fewer clear structures observed in TEM at higher concentrations might be due to dense and complex networks obfuscating their finer details. The fiber diameters were found to be more than 10 nm, which is consistent with previous studies [8, 30]. Even though the (RADA)$_4$ peptide is neutrally charged at pH ~7.4 [8], the presence of electrostatic charges on the argenine and aspartatic acid residues seem to play a significant role in the cross linking of the nanofibers, as well as interaction with the non-frozen bound water molecules [24].
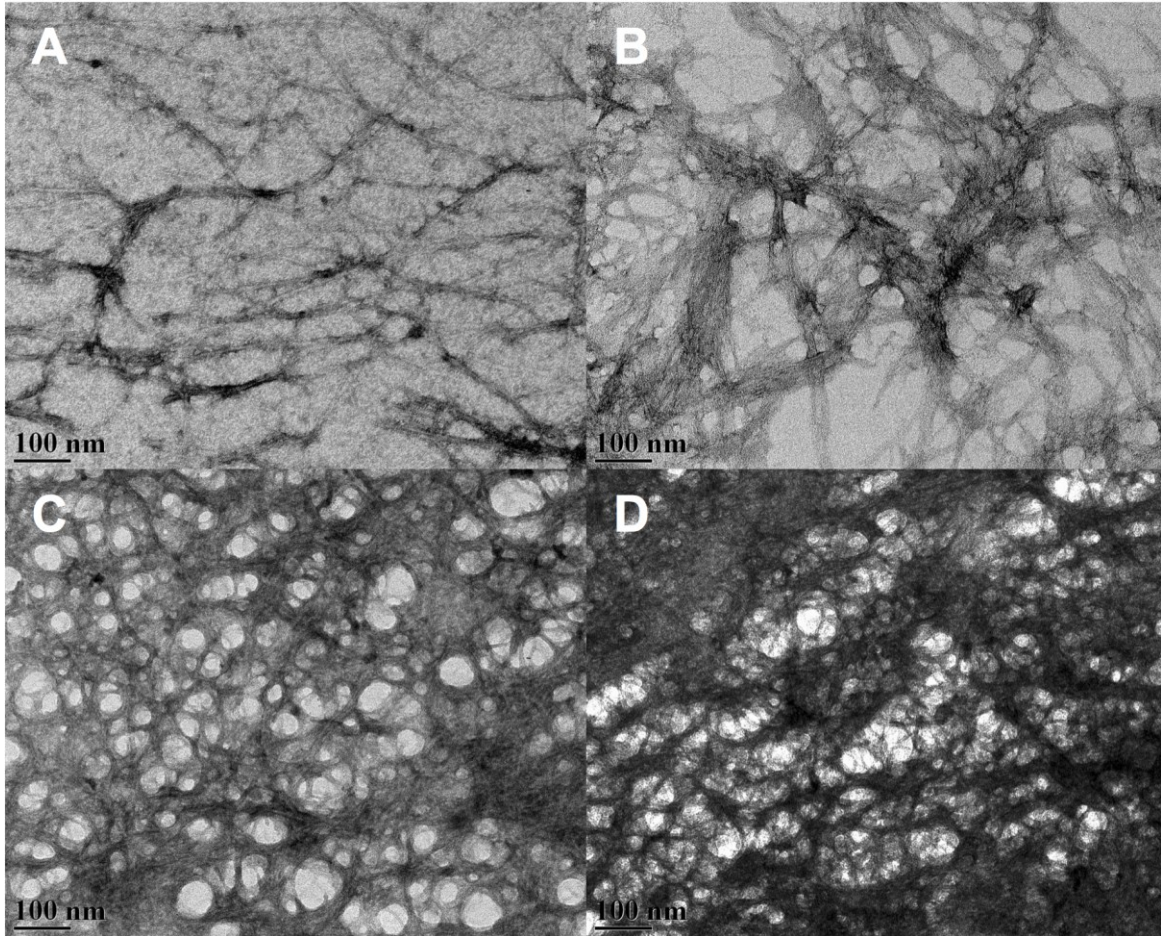
Figure 5.1 Typical TEM images for the (RADA)₄ nanofiber hydrogel at different concentrations .

Peptide morphology was examined dispersed in PBS buffer at 25°C (A) 0.5% (w/v), (B) 1.0% (w/v), (C) 2.0% (w/v), and (D) 3.0% (w/v). The morphology changed with an increase in peptide amount, ranging from interwoven nanofibers (A) to more densely packed (B), and aggregated structures (C and D).

5.3.2 *In-vitro* hemocompatibility assessment

In this study, hydrogels were formed using four (0.5, 1.0, 2.0 and 3.0% (w/v)) (RADA)$_4$ concentrations for conducting the hemocompatibility evaluation. Interestingly, even though the applications of (RADA)$_4$ based hydrogels are well documented, there lacks a thorough investigation into the clotting kinetics, platelet and complement activation, which is vital to understanding the design of blood contacting devices in general. Furthermore, these hemocompatibility assays should allow further insight into understanding the rapid hemostasis mechanism reported for the hydrogels.

5.3.3 Turbidimetric assay for plasma clotting time

Blood-material associated interactions are known to initiate a complex series of events including: protein adsorption, platelet and leukocyte activation and adhesion, complement activation and coagulation [31]. This series of reactions eventually dictates the host response to these materials. The coagulation pathway involves a series of proteolytic reactions (including the intrinsic and extrinsic pathways) resulting in the formation of a fibrin clot. Evaluation of anticoagulant activity based on plasma coagulation has been recognized as a standard test to estimate blood compatibility of a biomaterial [32]. The extent of coagulation was studied using the time for clot formation upon recalcification of platelet-poor plasma incubated with (RADA)$_4$ hydrogels.

This turbidimetric assay was conducted to monitor the changes in optical density when platelet-poor human plasma and hydrogels were incubated in the presence of calcium chloride, where increasing turbidity is indicative of the formation of fibrin clots. Figure 2 shows the

absorbance profile (at 405 nm) for a range of hydrogel concentrations. Following the addition of CaCl$_2$ to the plasma rich hydrogel systems, it was expected that an initial lag phase would be observed, followed by a rise and plateau in optical density that coincides with clot development. This trend was observed for the phosphate buffer saline control, where after a lag phase of ~18 min occurred prior to the onset of clot formation and a plateau was reached within ~43 min. However, all the hydrogel systems tested using PPP showed an exceptionally brief lag period for the initiation of the clot formation, reaching a plateau within ~2 minutes upon adding CaCl$_2$ (Figure 2). We propose the increase in nanofiber density promotes the interaction of the charged amino acids, along with the adsorption of water molecule; thereby facilitating the plasma protein interaction with the individual fibers present in the hydrogel. Overall, this interaction results in the increase in turbidity due to the formation of a plug involving plasma proteins and nanofiber interactions (Figure 2). It is also evident from Figure 2 that, with the exception of 2.0% (w/v) (RADA)$_4$ nanofiber solution, the turbidity displayed dose dependency that may be due to an increase in surface area of the nanofibers that forms with increasing peptide concentration; coinciding with TEM images of materials deposited with constant volumes of the various hydrogel solutions (Figure 1). The interaction between the (RADA)$_4$ nanofiber and plasma proteins is potentially controlled by the resulting internal hydrogel's surface area as well as the surface characteristics. This increased surface area is expected to increase the interaction between plasma proteins, potentially resulting in a short clotting lag period. Furthermore, an increase in the turbidity was not only dose-dependent with various hydrogel systems, but also statistically significant ($p < 0.05$ one way ANOVA) when compared to the PBS control.
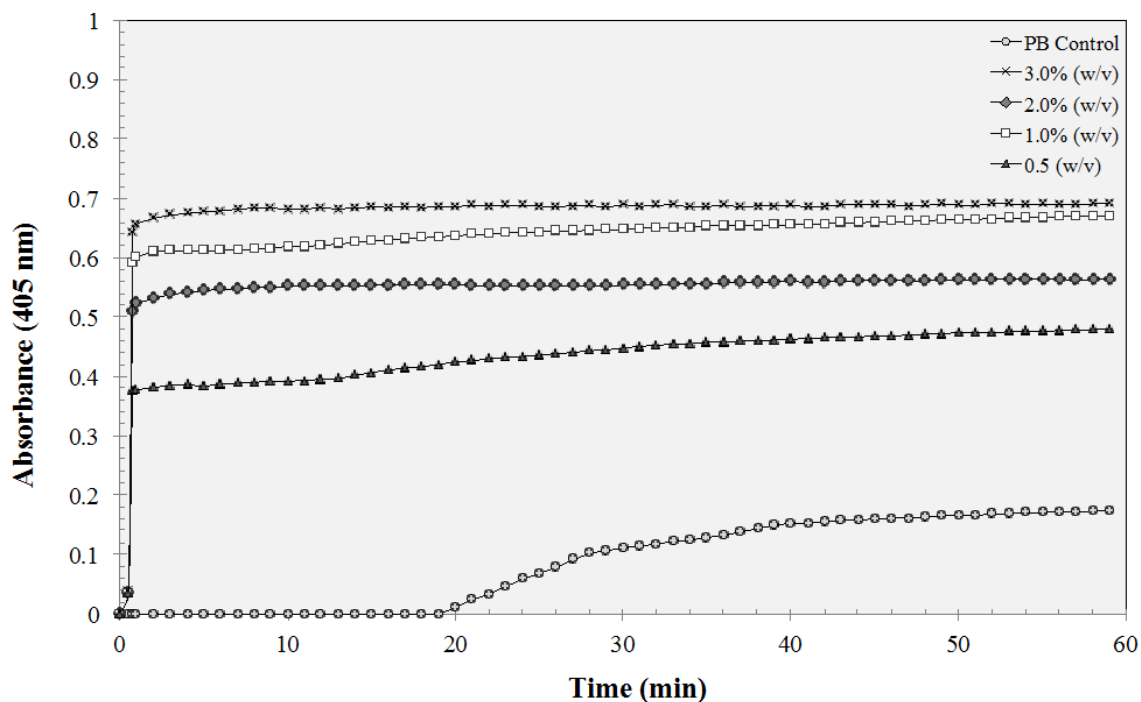
Figure 5.2 Clot formation kinetics in platelet poor plasma upon incubation with (RADA)₄ hydrogels

The clot formation includes (RADA)₄ peptide from 0.5-3.0% (w/v), and PB control. Data shown represents average, where 1 SD < 0.005, n=4, p<0.05 (one way ANOVA).

Several mechanisms have been proposed for the rapid hemostatic behavior of (RADA)₄ nanofiber solutions [10, 13]. It was concluded that the rapid hemostatic behavior upon incubation with (RADA)₄ was not due to clot formation because no blood clot was observed with the naked eye [13] and blood flow stopped within ~15-20 seconds [10], whereas blood clots are thought to take up to 1-2 minutes to form after injury [33]. Upon studying clot formation kinetics using platelet-poor human plasma (Figure 2), results reveal a rapid clot formation event as compared to controls (despite the lack of platelets or shear, in the *in-vitro* systems). These data may indicate that, contrary to previous conclusions [10, 13], the humoral coagulation pathways play a crucial

role in achieving rapid hemostasis and can play a dramatic role in the formation of clots when nanofibers contact blood.

5.3.4 Complement C3a Activation

Biomaterials are known to be potential agonists for complement activation, where complement is known to play a vital role in the body's defence mechanism against infection and foreign entities [34]. Moreover, the complement system is interlinked with the coagulation cascade and platelet activation. Complement activation products (such as C3b) are directly known to enhance intravascular coagulation by fibrin deposition [35].

Complement activation is also known to be responsible for procoagulant activities, such as platelet activation, tissue factor expression [36], and modification of the activity of mast cells [37] and basophils [38]. Therefore, the material's interaction with complement is considered a very important aspect of its hemocompatibility [18]. It is believed that three distinct pathways can initiate the complement system: the classical pathway (CP), the alternative pathway (AP), and the Lectin pathway (LP). All three pathways ultimately converge to generate the same central effector molecule C3b, *via* the activity of C3-convertases and the C3-activating enzyme complexes [39, 40]. Complement activation can be marked by an array of anaphylatoxins released [41]. The anaphylatoxin C3a itself is very short lived and is cleaved rapidly to the more stable C3a-desArg, which was quantified conducting an enzyme immunoassay [42]. As an anaphylatoxin, C3a has a broad proinflammatory impact on cells such as cytokine expression and chemotaxis [43, 44], as well as it plays a crucial role in both the coagulation and complement cascades [45].

Interestingly, a previous study revealed a significant increase in complement activation by coatings containing several functional groups, such as COOH, NH$_2$, OH [46-48]. Thus, (RADA)$_4$ may be expected to significantly activate complement due to the abundance of aspartic acid residues. However, upon increasing (RADA)$_4$ concentration from 1.0 to 3.0% (w/v), low C3a amounts of ~3 to ~8 µg/ml were observed when compared with the PBS control of ~3 µg/ml (Figure 3). For the 0.5%(w/v) (RADA)$_4$ hydrogel the amount of C3a generated fell below the sensitivity of the assay and could not be measured. Although the C3a generation range for (RADA)$_4$ varied at different concentrations, no clear trend in dose dependency of C3a generation was observed. The data suggests that C3a formation is less dependent on the peptide concentration compared to the clotting kinetics.

Remarkably, C3a activation mediated by these nanofibers is less than that of widely used polymers considered to be biocompatible (such as dextran, hetastarch, and PEG). For these polymers, C3a generation was found to be between ~11 and ~25 µg/ml when incubated in plasma at the highest concentrations and longest incubations tested. Furthermore, recent studies have indicated that the initial complement activation is primarily mediated *via* the classical pathway, whereas the alternative pathway acts as an amplification loop, where complement proteins are associated with the already adsorbed plasma proteins and not to the underlying surface itself [49, 50]. Hence, C3a generation may be dictated by the nature of the adsorbed proteins onto the (RADA)$_4$ nanofibers, rather than the fibers themselves.
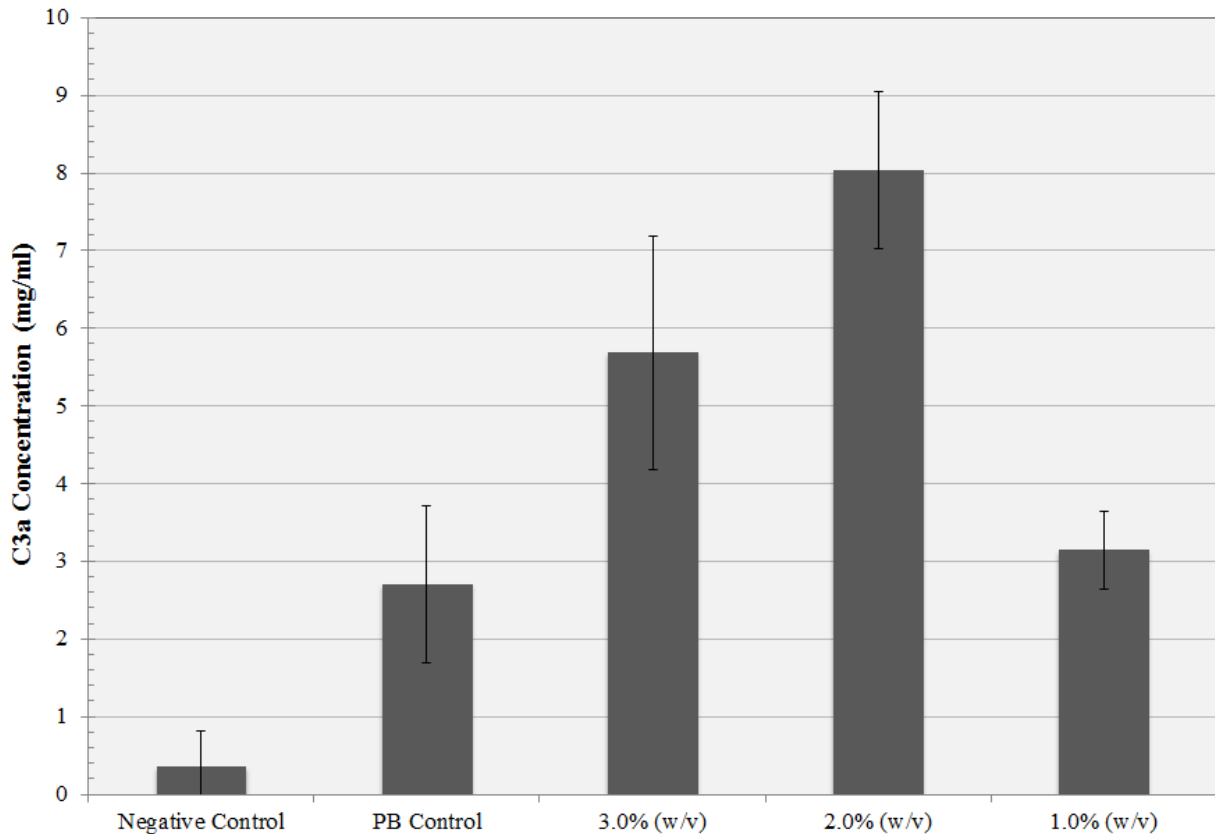
Figure 5.3 C3a-desArg in human platelet poor plasma (PPP) exposed to (RADA)₄ hydrogel systems

Release of C3a-desArg in human platelet poor plasma (PPP) exposed to (RADA)₄ hydrogel systems in PB (pH 7.4). Human PPP incubated with PB (pH 7.4) is used as a control. The negative control indicates background signal obtained with buffer blank. Experiments were repeated two times for each system using the same-pooled plasma from three healthy unmedicated donors.

5.3.5 Platelet activation

The platelet response to biomaterials gives an indication of material thrombogenicity, and influences various aspects of the inflammatory response [51]. Though there are numerous *in-vitro* methods available to evaluate platelet activation [52], no single assay is deemed sufficiently

robust [53], thus both expressions of the platelet surface receptor CD62P as well as platelet morphology for platelets upon incubation with the hydrogels for 30 min was used to characterize the material-induced activation of platelets.

Platelet activation results for CD62P expression are summarized in Figure 5.4 for all (RADA)$_4$ systems and controls. It was observed (Figure 5.4) that donor-to-donor variability was high, as expected, and when comparing all of these trends using one-way ANOVA statistics, no significant trend was observed between peptide concentration and platelet expression of CD62P ($p>0.05$). However, when excluding donor 1, which showed higher basal platelet activity in the controls, both Donors 2 and 3 seemed to show a dose dependence on CD62P expression as peptide concentration increased, and values that were definitely higher on average when compared to PBS controls. For example, Donor 2 showed an increasing trend in CD62P up to 2.0%(w/v), whereas Donor 3 showed a similar increasing trend up to 3.0%(w/v). Overall, it is likely that the fact these systems are highly hydrated, as well as having a net zero charge, results in the relatively low platelet activation for all the systems of interest.

The low CD62P activation, along with clot formation in platelet-poor plasma solutions (Figure 5.3), further confirm that platelets are not dictating the rapid and complete hemostasis mechanism of (RADA)$_4$ peptide; this result is further confirmed by platelet morphology.
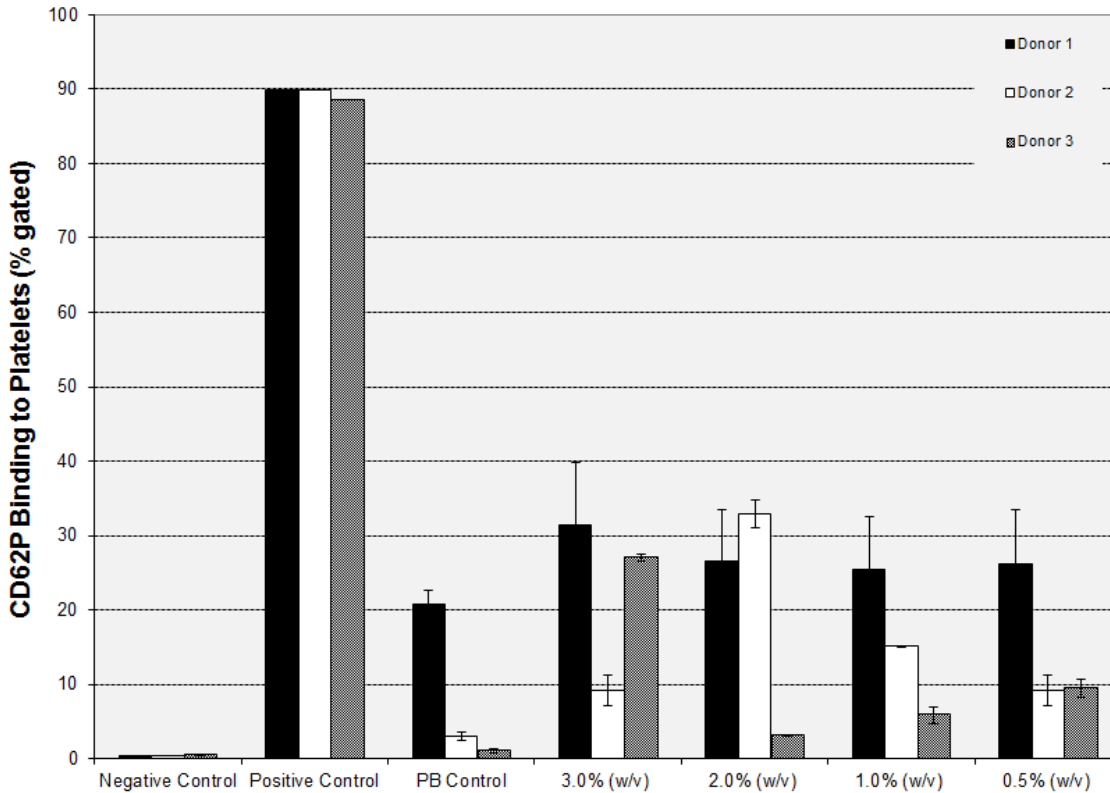
Figure 5.4 CD62P expression as a function of (RADA)$_4$ peptide concentration

Expression of platelet activation marker CD62P in Platelet Rich Plasma (PRP), collected from three unmedicated healthy blood donors. PRP was incubated with (RADA)$_4$ hydrogels in PB (pH 7.4) at 37°C for 30 min prior to data collection. PRP incubated with PB (pH 7.4) is used as a control, and the negative control indicates the background signal obtained with isotype control antibody. Experiments were repeated two times for each system using the same-pooled PRP from three healthy unmedicated donors Data represent percent of 5000 platelets counted. p>0.05 (one way ANOVA for PB control and 0.5%, 1.0%, 2.0% and 3.0% (RADA)$_4$ peptides).

5.3.6 Platelet morphology

Platelets are known to respond to external stimuli (such as, foreign particles and surfaces) by altering their shape from the resting, normal discoid form, into more rounded structures

possessing blebs and multiple pseudopodia [54]. Platelet morphology was assessed using a modified Kunicki scoring system [27], where platelets are categorized by shape as discoid, spiny spheres, or balloons. Figure 5.5 illustrates all three morphological states present in the PBS control as discussed in the materials section. A Kunicki morphology score above 385 was achieved for all the systems (Table I); a score of less than 200 implies poor retention of morphological characteristics associated with platelets that are activated. Our data suggest that the majority of platelets retain a discoid shape, and as such are not activated upon interacting with $(RADA)_4$-hydrogels [27]. Moreover, similar to a previous study [10], platelet adhesion was observed in the case of $(RADA)_4$ systems when compared with the PBS control, which is likely due to the presence of solid surface of nanofibers for platelet interaction (Figure 5.6). Hence, low platelet activation in combination with the morphological analysis (Figure 5.5 and Figure 5.6) suggests that the platelets are only marginally perturbed from their quiescent state.
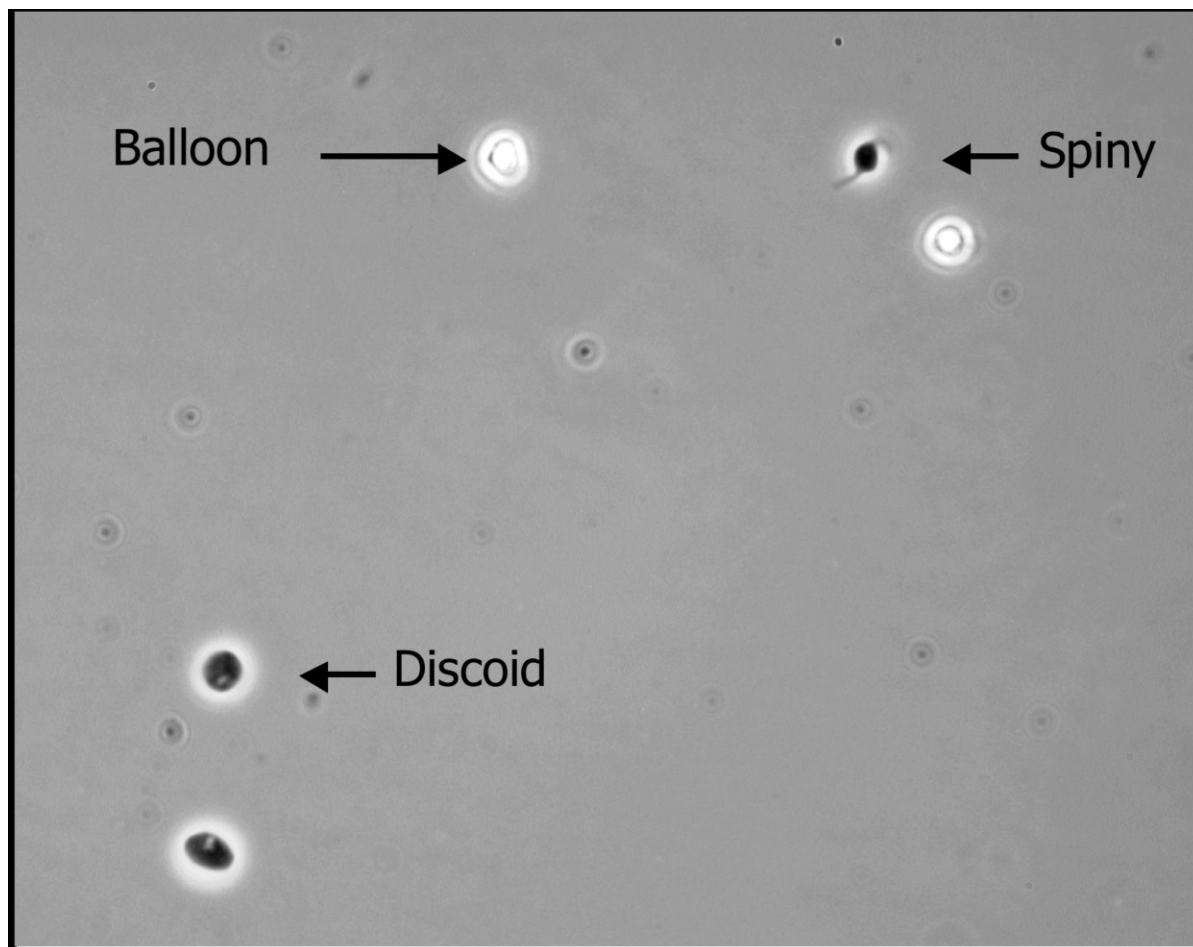
Figure 5.5 Three categories of platelets present in the systems upon PRP incubation with (RADA)₄.

Three different kinds of platelets present in the systems upon PRP incubation with (RADA)$_4$ at 37°C for 30 mins. The microscopy was performed at room temperature. The image shows the various platelet shapes that were found upon incubating with the hydrogel systems: discoid, spiny and balloon forms.

5.4   Proposed Coagulation Mechanism for (RADA)$_4$ Peptide

Based upon these results it seems that platelets are minimally involved in (RADA)$_4$ based hemostasis. This is due to the fact that only marginal platelet activation was witnessed in (RADA)$_4$ systems when compared with the control (Figure 4), but platelet-poor plasma with (RADA)$_4$ was able to achieve clotting itself (Figure 2). This conclusion is further supported by the earlier observations [13] where no red blood cells (RBC) or platelet lesions were found after achieving complete hemostasis with (RADA)$_4$ nanofibers.

The observed hemostasis [13] cannot be fully explained using a mechanical inhibition of blood flow; as upon testing a stiffer gel than (RADA)$_4$ (from the same family as (RADA)$_4$ peptide), the modified gel failed to arrest bleeding [10]. However, we report an overall dose dependency of clotting kinetics on the (RADA)$_4$ concentration; suggesting the significance of peptide concentration for clot formation. It is likely that the non-covalent interactions of the nanofiber stabilize a "mesh-network", which provides a molecular level barrier to bleeding. Our lab has previously shown that even though the total amount of water present decreases upon the increase in (RADA)$_4$ concentration (from 0.5%(w/v) to 3.0% (w/v)), the non-frozen bound water content increases significantly [24]. Current work has shown that higher (RADA)$_4$ concentration systems achieved more arrested bleeding when compared with 1.0% (w/v) (RADA)$_4$ [10]. Compiling these results with the clotting cascade, it may be that the increase in bound water promotes the hemostatic mechanism of the (RADA)$_4$ peptide. Although further studies need to be conducted to reveal the exact underlying mechanism for this rapid clot formation, and the potential role hydration may have on plasma protein based clotting mechanisms.   Herein, however, it seems that protein based clotting mechanisms are largely responsible for this

hemostasis and requires minimal involvement of either complement (Figure 5.3) or platelet activation (Figure 5.4)

Table 5.1 Morphology score computed *via* Kunicki scoring system [27], n>3.

(RADA)$_4$ (% w/v)	Morphology Score (MS)
PBS Control	397 ± 1
3.0	389 ± 4
2.0	392 ± 2
1.0	396 ± 3
0.5	393 ± 6
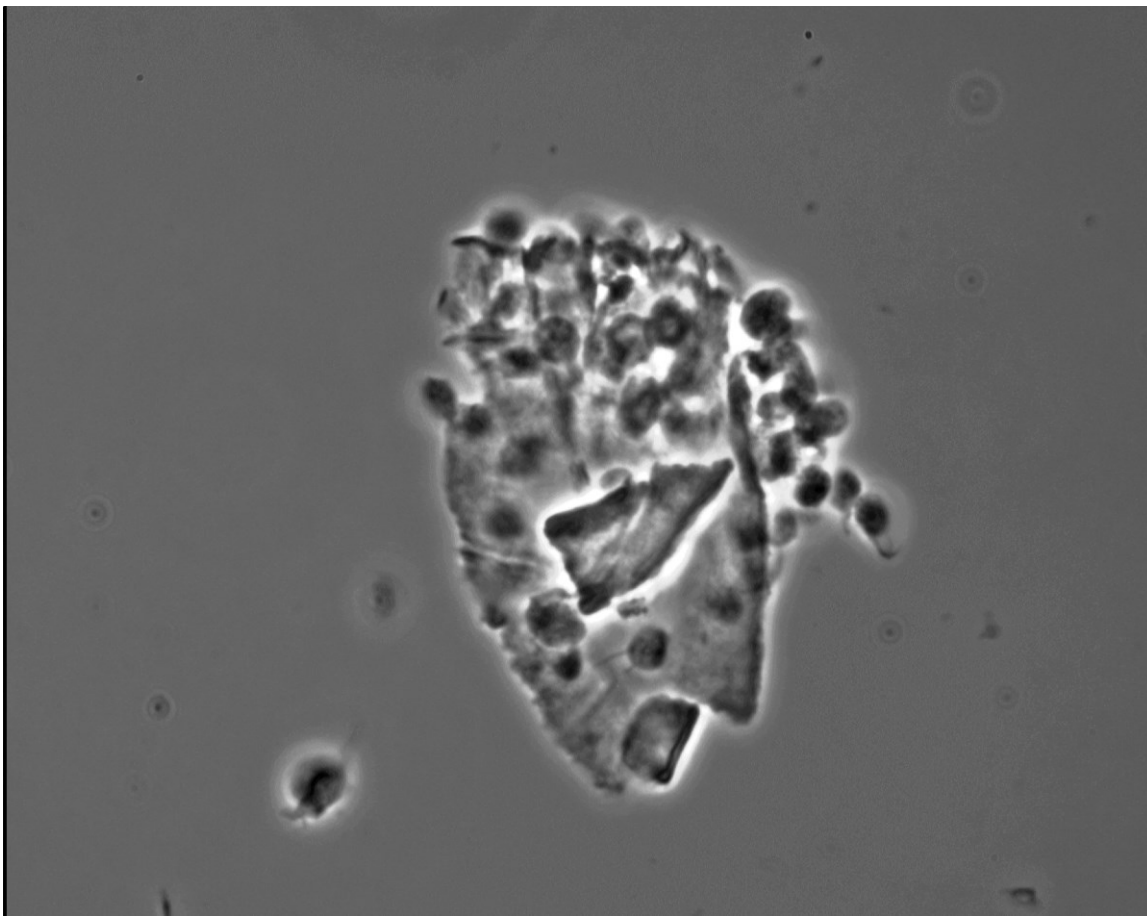
Figure 5.6 Microscopy image showing the interaction of (RADA)$_4$ hydrogel with platelets.

Representative light microscopy image showing the interaction of (RADA)$_4$ hydrogel with platelets. The (RADA)$_4$ at 0.5% (w/v) was incubated with PRP at 37ºC for 30 min. The microscopy was performed at room temperature.

5.5   Concluding remarks

The present study demonstrated that the self-assembling peptide $(RADA)_4$ can form higher ordered peptide nanofiber hydrogels at various concentrations. *In-vitro* biocompatibility assays are vital for the design of any blood contacting biomaterial. We investigated both complement and platelet activation upon incubation of human blood with the $(RADA)_4$ based hydrogels. The complement activation studies indicated that the presence of $(RADA)_4$ hydrogels resulted in more complement activation (up to ~8 μg/ml) when compared with the control (~3 μg/ml), potentially due to the presence of COOH and NH_2 groups. However, the values were significantly less than the widely used polymers known to be biocompatible (11 and 25 μg/ml). The data suggests that C3a formation was less dependent on the nanofiber concentration. CD62P expression on the platelets also revealed a lack of dependency on the nanofiber concentration. Moreover, a high morphology score of 385 and above for all the systems, indicated a low platelet activation upon the treatment with hydrogels. Previous studies have shown the rare and novel complete hemostatic ability of the $(RADA)_4$ peptide nanofibers; however, to our knowledge the underlying mechanism of hemostasis has not yet been identified. Here, we have tested and evaluated some proposed theories of the hemostasis. The hemostatic ability of the peptide was tested using a plasma clotting assay where immediate hemostasis was achieved with $(RADA)_4$ hydrogels in a dose dependent manner. The overall *in-vitro* evaluation of the peptide along with the clotting analysis provides an insight into the further development of nano-biomaterials. This polymer is not only biocompatible but also shows great promise as a means of achieving immediate hemostasis, and could potentially revolutionize controlled bleeding in surgical procedures.

Acknowledgements

Conflicts of interest

The authors have no conflicts of interest to declare.

References

[1] Johnson TD, Christman KL. Injectable hydrogel therapies and their delivery strategies for treating myocardial infarction. Expert Opinion on Drug Delivery 2013;10:59-72.

[2] Zhao X, Nagai Y, Reeves PJ, Kiley P, Khorana HG, Zhang S. Designer short peptide surfactants stabilize G protein-coupled receptor bovine rhodopsin. Proceedings of the National Academy of Sciences of the United States of America 2006;103:17707-12.

[3] Gelain F, Bottai D, Vescovi A, Zhang S. Designer Self-Assembling Peptide Nanofiber Scaffolds for Adult Mouse Neural Stem Cell 3-Dimensional Cultures. Plos One 2006;1.

[4] Semino CE, Kasahara J, Hayashi Y, Zhang SG. Entrapment of migrating hippocampal neural cells in three-dimensional peptide nanofiber scaffold. Tissue Engineering 2004;10:643-55.

[5] Ellis-Behnke RG, Liang YX, You SW, Tay DKC, Zhang SG, So KF, *et al*. Nano neuro knitting: Peptide nanofiber scaffold for brain repair and axon regeneration with functional return of vision. Proceedings of the National Academy of Sciences of the United States of America 2006;103:5054-9.

[6] Guo JS, Leung KKG, Su HX, Yuan QJ, Wang L, Chu TH, *et al*. Self-assembling peptide nanofiber scaffold promotes the reconstruction of acutely injured brain. Nanomedicine-Nanotechnology Biology and Medicine 2009;5:345-51.

[7] Segers VFM, Lee RT. Local delivery of proteins and the use of self-assembling peptides. Drug Discovery Today 2007;12:561-8.

[8] Ye ZY, Zhang HY, Luo HL, Wang SK, Zhou QH, Du XP, *et al*. Temperature and pH effects on biophysical and morphological properties of self-assembling peptide RADA16-1. Journal of Peptide Science 2008;14:152-62.

[9] Zhang SG, Lockshin C, Cook R, Rich A. Unusally stable beta-sheet formation in an ionic self-complementary oligopeptide. Biopolymers 1994;34:663-72.

[10] Ellis-Behnke RG, Liang Y-X, Tay DKC, Kau PWF, Schneider GE, Zhang S, *et al*. Nano hemostat solution: immediate hemostasis at the nanoscale. Nanomedicine : nanotechnology, biology, and medicine 2006;2:207-15.

[11] Zwischenberger JB, Brunston RL, Swann JR, Conti VR. Comparison of two topical collagen-based hemostatic sponges during cardiothoracic procedures. Journal of Investigative Surgery 1999;12:101-6.

[12] Sabel M, Stummer W. The use of local agents: Surgicel and Surgifoam. European Spine Journal 2004;13:S97-S101.

[13] Wang T, Zhong XZ, Wang ST, Lv F, Zhao XJ. Molecular Mechanisms of RADA16-1 Peptide on Fast Stop Bleeding in Rat Models. Int J Mol Sci 2012;13:15279-90.

[14] Tirrell M, Kokkoli E, Biesalski M. The role of surface science in bioengineered materials. Surface Science 2002;500:61-83.

[15] Werner C, Maitz MF, Sperling C. Current strategies towards hemocompatible coatings. J Mater Chem 2007;17:3376-84.

[16] Ostuni E, Chapman RG, Holmlin RE, Takayama S, Whitesides GM. A survey of structure-property relationships of surfaces that resist the adsorption of protein. Langmuir 2001;17:5605-20.

[17] Hayashi K, Fukumura H, Yamamoto N. *In-vivo* thrombus formation induced by complement activation on polymer surfaces. J Biomed Mater Res 1990;24:1385-95.

[18] Gorbet MB, Sefton MV. Biomaterial-associated thrombosis: roles of coagulation factors, complement, platelets and leukocytes. Biomaterials 2004;25:5681-703.

[19] Body SC. Platelet activation and interactions with the microvasculature. Journal of Cardiovascular Pharmacology 1996;27:S13-S25.

[20] Shattil SJ, Cunningham M, Hoxie JA. Detection of activated platelets in whole blood using activation dependent monoclonal antibodies and flow cytometry. Blood 1987;70:307-15.

[21] Friedman LI, Grabowsk.Ef, Leonard EF, Liem H, McCord CW. Inconsequentiality of surface properties for initial platelt adhesion. Transactions American Society for Artificial Internal Organs 1970;16:63-73.

[22] Gemmell CH. Activation of platelets by *in vitro* whole blood contact with materials: Increases in microparticle, procoagulant activity, and soluble P-selectin blood levels. J Biomater Sci-Polym Ed 2001;12:933-43.

[23] Thaler U, Deusch E, Kozek-Langenecker SA. In vitro effects of gelatin solutions on platelet function: a comparison with hydroxyethyl starch solutions. Anaesthesia 2005;60:554-9.

[24] Saini AK, K and Unsworth, L.D. . Effect of Peptide Concentration on Water Structure, Morphology, and Thermal Stability of Self-Assembling (RADA)$_4$ Peptide Matrices. Journal of Biomaterials and Tissue Engineering 2014;In Print.

[25] Abraham S, So A, Unsworth LD. Poly(carboxybetaine methacrylamide)-Modified Nanoparticles: A Model System for Studying the Effect of Chain Chemistry on Film Properties, Adsorbed Protein Conformation, and Clot Formation Kinetics. Biomacromolecules 2011;12:3567-80.

[26] Levin E, Jenkins C, Culibrk B, Gyongyossy-Issa MIC, Serrano K, Devine DV. Development of a quality monitoring program for platelet components: a report of the first four years' experience at Canadian Blood Services. Transfusion;52:810-8.

[27] Kunicki TJ, Tuccelli M, Becker GA, Aster RH. Study of variables affecting quality of platelets stored at room-temperature. Transfusion 1975;15:414-21.

[28] Zhang S, Holmes T, Lockshin C, A. R. Spontaneous assembly of a self-complementary oligopeptide to form a stable macroscopic membrane. Proceedings of the National Academcy of Sciences USA 1993;90:3334-8.

[29] Zhang SG, Holmes TC, Dipersio CM, Hynes RO, Su X, Rich A. Self-complementary oligopeptide matrices support mammalian-cell attachment. Biomaterials 1995;16:1385-93.

[30] Arosio P, Owczarz M, Wu H, Butte A, Morbidelli M. End-to-End Self-Assembly of RADA 16-I Nanofibrils in Aqueous Solutions. Biophys J 2012;102:1617-26.

[31] Basmadjian D, Sefton MV, Baldwin SA. Coagulation on biomaterials in flowing blood: some theoretical considerations. Biomaterials 1997;18:1511-22.

[32] Vogler EA, Siedlecki CA. Contact activation of blood-plasma coagulation. Biomaterials 2009;30:1857-69.

[33] Decaterina R, Lanza M, Manca G, Strata GB, Maffei S, Salvatore L. Bleeding-time and bleeding- An analysis of the relationship of the bleeding-time test with parameters of surgical bleeding. Blood 1994;84:3363-70.

[34] Gorbet MB, Sefton MVMV. Biomaterial-associated thrombosis: roles of coagulation factors, complement, platelets and leukocytes. Biomaterials 2004;25:5681-703.

[35] Nangaku M, Couser WG. Mechanisms of immune-deposit formation and the mediation of immune renal injury. Clinical and experimental nephrology 2005;9:183-91.

[36] Esmon CT. The impact of the inflammatory response on coagulation. Thrombosis Research 2004;114:321-7.

[37] Wojta J, Huber K, Valent P. New aspects in thrombotic research: Complement induced switch in mast cells from a profibrinolytic to a prothrombotic phenotype. Pathophysiology of Haemostasis and Thrombosis 2003;33:438-41.

[38] Wojta J, Kaun C, Zorn G, Ghannadan M, Hauswirth AW, Sperr WR, et al. C5a stimulates production of plasminogen activator inhibitor-1 in human mast cells and basophils. Blood 2002;100:517-23.

[39] Walport MJ. Advances in immunology: Complement (First of two parts). N Engl J Med 2001;344:1058-66.

[40] Walport MJ. Advances in immunology: Complement (Second of two parts). N Engl J Med 2001;344:1140-4.

[41] Chenoweth DE. Complement Activation Produced by Biomaterials. Artificial Organs 1988;12:508-10.

[42] Berger M, Broxup B, Sefton MV. Using ELISA to evaluate complement activation by reference biomaterials. Journal of Materials Science-Materials in Medicine 1994;5:622-7.

[43] Sayah S, Ischenko AM, Zhakhov A, Bonnard AS, Fontaine M. Expression of cytokines by human astrocytomas following stimulation by C3a and C5a anaphylatoxins: Specific increase in interleukin-6 mRNA expression. Journal of Neurochemistry 1999;72:2426-36.

[44] Takabayashi T, Vannier E, Clark BD, Margolis NH, Dinarello CA, Burke JF, et al. A new biologic role for C3a and C3a desArg - Regulation of TNF-alpha and IL-1 beta synthesis. Journal of Immunology 1996;156:3455-60.

[45] Amara U, Rittirsch D, Flierl M, Bruckner U, Klos A, Gebhard F, et al. Interaction Between the Coagulation and Complement System. In: Lambris JD, editor. Current Topics in Complement Ii2008. p. 71-9.

[46] Golander CG, Lassen B, Nilssonekdahl K, Nilsson UR. RF-Plasma-modified polystyrene surfaces for studying complement activation. J Biomater Sci-Polym Ed 1992;4:25-30.

[47] Frautschi JR, Eberhart RC, Hubbell JA, Clark BD, Gelfand JA. Alkylation of cellulosic membranes results in reduced complement activation. J Biomater Sci-Polym Ed 1996;7:707-14.

[48] Bahulekar R, Tamura N, Ito S, Kodama M. Platelet adhesion and complement activation studies on poly(N-alkyl mono and disubstituted) acrylamide derivatives. Biomaterials 1999;20:357-62.

[49] Wettero J, Askendal A, Bengtsson T, Tengvall P. On the binding of complement to solid artificial surfaces in vitro. Biomaterials 2002;23:981-91.

[50] Andersson J, Ekdahl KN, Lambris JD, Nilsson B. Binding of C3 fragments on top of adsorbed plasma proteins during complement activation on a model biomaterial surface. Biomaterials 2005;26:1477-85.

[51] Motlagh D, Yang J, Lui KY, Webb AR, Ameer GA. Hernocompatibility evaluation of poly(glycerol-sebacate) in vitro for vascular tissue engineering. Biomaterials 2006;27:4315-24.

[52] Rock G, Freedman M, Hamilton C, Bormanis J. New methods showing in vitro changes of platelets. Transfusion and Apheresis Science 2006;35:145-9.

[53] Kainthan RK, Hester SR, Levin E, Devine DV, Elliott BD. In vitro biological evaluation of high molecular weight hyperbranched polyglycerols. Biomaterials 2007;28:4581-90.

[54] Goodman SL. Sheep, pig, and human platelet-material interactions with model cardiovascular biomaterials. Journal of Biomedical Materials Research 1999;45:240-50.

Chapter 6

Effect of End Group on Nanofiber Self Assembly and Vicinal Water Structure

[a] *Department of Chemical and Materials Engineering, Faculty of Engineering, University of Alberta, Edmonton, Alberta, Canada T6G 2G6*

[b] *National Research Council, National Institute for Nanotechnology, Edmonton, Alberta, Canada T6G 2M9*

[c] *Department of Chemistry 2500 University Drive NW, University of Calgary, Alberta, Canada T2N 1N4*

[1] Corresponding author info:

Phone: 780-492-6020

Fax: 780-492-2881

E-mail: larry.unsworth@ualberta.ca

Abstract

In order to elucidate the design principles for peptide-based nanofibers, we investigate $(RADA)_4$ oligopeptide which self-assembles to form an antiparallel β-sheet rich nanofiber that further assembles into a viscoelastic 3D matrix in aqueous solution. Despite the on-going advances to explore applicative capabilities of this peptide, the molecular level interactions responsible for its self-assembly are not fully understood. Three types of peptides, RADARADARADARADA $(RADA)_4$, RADARADARADARADASSSSS $(RADA)_4S_5$, and RADARADARADARADAKKKKK $(RADA)_4K_5$, were investigated for nanostructure formation *via* self-assembling mechanism. Circular Dichroism (CD) investigated the propensity of nanofiber formation; both $(RADA)_4$ and $(RADA)_4S_5$ peptides showed successful β-sheet formation, which are prerequisites for nanofiber self-assembly. Solution containing $(RADA)_4K_5$ did not show β-sheet formation. Peptide $(RADA)_4$ was then added to $(RADA)_4K_5$ with the goal of determining the critical self-assembling concentration for the $(RADA)_4K_5$ peptide, which was found to be at 25% $(RADA)_4K_5$ and below. Single-molecule Florescence Correlation Spectroscopy (FCS) was used to confirm the molecular interaction of the pristine $(RADA)_4$ nanofibers with 25% $(RADA)_4K_5$. The results showed that the 3D nanostructures formed by the peptides are dependent on the amino acid sequence as well as the temperature of the peptide solution. Moreover, differential scanning Calorimetry (DSC) proved the vital role of hydration on the self-assembly of $(RADA)_4$ peptides and its variants. Molecular level understanding provided in our research would not only aid in the understanding of peptide self-assembly, but would allow modifications to the existing peptides to yield desirable material properties.

189

6.1 Introduction

Hydrogel materials are considered to be ideal for many tissue-engineering applications [1-3]. Their successful implementation, however, has been largely inhibited due lack of full understanding of their self-assembling mechanisms. The bottom-up approach to material design provides a novel method for understanding how molecular level architecture affects events central to the host response. For example, how the physical and chemical properties of nanofibers formed from self-assembled peptides affect water structure when in a hydrogel environment. Also, hydrogels formed through molecular self-assembly mechanisms retain the advantages of polymeric hydrogels, whilst negating the use of cytotoxic cross-linkers. In this case the programmability of the peptide sequence is an innate attribute, potentially allowing a means of controlling the nanofiber properties at the molecular level. This programmability may provide a means for peptide engineering that significantly affects the hydrogel-matrix structure.

Self-assembling peptides, *viz*., (RADA)$_4$ have been shown to form nanofibers in physiologically relevant solutions, with traits that make them amenable for soft-tissue applications [4, 5]: applicable to minimally invasive therapies (i.e. injectable), able to respond to external stimuli under physiological conditions, facilitate 3-D cellular activities, while maintaining an internal hydration of up to 99.5 % (w/v) water [6-8]. The latter feature suggests that these self-assembling nanofiber systems are able to dramatically affect the surrounding aqueous solution, and perhaps dictate the various water phases within the hydrogel environment itself (i.e. frozen vs. non-frozen water content). The characteristic amphiphillic nature of (RADA)$_4$ (R, arginine; A, alanine; D, aspartic acid; acetylated and amidated N- and C-termini, respectively) is thought to be responsible for the peptide's structural stabilization as higher three

dimensional structures. The alternating hydrophobic and hydrophilic components, including positive and negative charged residues lead to stable nanofiber formation. The hydrogen bonding between neighboring peptide backbones, and ionic bonding among intra- and inter-peptide and water are believed to play a critical role in stabilizing a possible cross-β- structural motif [7]. Determining the self-assembly forces dictating the 3D structure stabilization would provide the means to control the mechanical characteristics of these peptide by tailoring its underlying physiochemical structure. We have previously reported the effect of concentration on $(RADA)_4$ nanofiber formation, with an ultimate goal of understanding the self-assembling mechanism of this peptide. Here, we have systematically varied the C-terminus of the $(RADA)_4$ peptide by appending five uncharged and polar serine residues, as well as electrically charged lysine residues.

Here, the presence of this β-structural motif is confirmed *via* Circular Dichroism (CD). Furthermore, the effect of end group chemistries on $(RADA)_4$ on the underlying secondary structure of the peptide was analyzed by computational spectral analysis *via* Contin. Nanofiber assembly is affected by moisture and change in temperature, as these factors would dictate the movement of individual fibers and the availability of the area for inter- and intra- molecular bonds for secondary structure formation. Hydration state analysis was conducted using Differential Scanning Calorimetry (DSC) to determine the effect of vicinal water on the intermolecular order of the $(RADA)_4$ peptide, and Circular Dichroism (CD) was used to determine the secondary structure transition in the nanofibers upon heating and the reversibility of the secondary structure upon cooling. Results indicate that the presence of non-frozen bound

191

water assists in the structural transformation of the α-helices to more stabilized β-sheet structures at higher peptide concentration.

The ability of these peptides to self-assemble into β-sheets and stack to form nanofibers can be utilized to establish model systems in which systematic exchange of individual amino acids within the peptide primary structure can be studied.

6.2 Materials and Methods:

6.2.1 Peptide Synthesis:

Self-assembling peptides, $(RADA)_4$ ([COCH$_3$]-RADARADARADARADA-[CONH$_2$]), $(RADA)_4K_5$ ([COCH$_3$]-RADARADARADARADAKKKKK-[CONH$_2$]) and $(RADA)_4S_5$ ([COCH$_3$]-RADARADARADARADASSSSS-[CONH$_2$]) were commercially synthesized and purified by SynBioSci (Livermore, CA) using FMOC amino acid derivatives. High Performance Liquid Chromatography (HPLC) and Mass Spectrometry (MS) were used to determine peptide purity and molecular weight (MW). Attained peptide purity was $\geq$ 95% for all the three peptides, with a calculated MW of 1713.2 for $(RADA)_4$, 2354.7 for $(RADA)_4K_5$ and 2149.3 for $(RADA)_4S_5$, which was very similar to their theoretical molecular weights. These peptides were used without any further purification.

6.2.2 Hydrogel Preparation:

Peptide solution was prepared by dissolving $(RADA)_4$ peptide powder in syringe filtered (0.2 μm) MilliQ water. These solutions were stored at 4ºC. Hydrogels were prepared by

sonicating the aqueous peptide stock solution (2510 Branson sonicator, Crystal Electronics, Newmarket, ON) for 15 min at 25°C. Stock solutions were diluted using syringe filtered (0.2 μm) MilliQ water to obtain 5 mg/mL, 6.271 mg/mL, and 6.869 mg/mL concentrations for (RADA)$_4$, (RADA)$_4$S$_5$, and (RADA)$_4$K$_5$, respectively. These amounts correspond to 0.5% (w/v) of (RADA)$_4$ in each gel. These solutions were sonicated again for 30 min. Peptides were allowed to self-assemble at 37°C for 30 min, and stored at 4°C.

The 25% (RADA)$_4$K$_5$ peptide mixture was made by pipetting, mixing, and vortexing 25% volume (RADA)$_4$K$_5$ and 75% volume (RADA)$_4$. Hydrogel formation was carried out by following the protocol stated above. Hydrogels of other percentages of (RADA)$_4$K$_5$ were formed similarly.

6.2.3 Circular Dichroism:

CD spectra were collected (Jasco J-810 spectropolarimeter) over the wavelength range of 180-300 nm. CD protocol was followed as described elsewhere,[9] except for the changes mentioned below: Criterion for low wavelength cut-off was kept at HT(V) value of 500 or lower. The spectra were collected on samples prepared by diluting stock peptide solution in water to a working concentration of 0.5% (w/v) with respect to (RADA)$_4$, and analyzed at room temperature. The structural contents of the peptides in solution were determined using a demountable quartz cuvette (Folio Instruments, Kitchener, ON). The quartz cuvette had a path length of 0.10 mm path length. Spectropolarimeter's scan mode was set to continuous and data pitch of 0.5 nm. Each spectrum taken was the average of ten scans.

$$[\Theta] = \frac{\Theta \times MRW}{c \times l \times 10}$$ **Equation 6.1**

Where $[\Theta]$ is the molar ellipticity (deg·cm^2/dmol), Θ is the raw ellipticity (m.deg), c is the sample concentration (g/mL), l is the optical path length (cm), and MRW is the mean residue molecular weight (Da). The three simultaneous data acquisition signals were: HT (V), Absorbance and CD (Θ). Background was subtracted from the sample signal, and the resulting CD signal converted to Molar Ellipticity as described elsewhere [10]; the mean residue molecular weight (Da) was obtained by dividing of sample molecular mass in Da with the number of amino acid residues present. The Molar Ellipticity was plotted against Wavelength (nm) for further data analysis.

To determine the quantitative aspects of the conformation changes in (RADA)$_4$, the approximate α helix, β turns and β sheet content was determined using de-convolution program Contin, which computes the secondary structure of a protein from its far-UV CD spectra, as provided by Dr. W.C. Johnson (Corvallis, OR) and accessed on the DICHROWEB server (located at http://www.cryst.bbk.ac.uk/cdweb). Measured CD spectra are first broken into several basic spectra, and these basis spectra are compared to a reference library of CD spectra (containing 7 reference data sets (IBasis7 λ = 240-190 nm)) composed of standard proteins with well-known structures *via* X-Ray crystallography. The relative fractions of secondary structure (such as α-helix and β-sheet) are given as output from Contin. A graphical output of the experimental and reconstructed data is also provided. NRMSD (normalized mean root square deviation) values less than 0.5 indicating that the Contin program and the reference selected are suitable for CD analysis for (RADA)$_4$ peptide. The secondary structures are composed of six categories: H(r) is regular α-helix; H(d) is distorted α -helix; S(r) is regular β-strand; S(d) is distorted β-sheets; β-sheet Turn; Unordered. The average length pertains to the number of

residues of α-helical and β-segments. The average length of α-helical segments in the reference proteins is 9.24 residues, and that of a β-strand segments is 5.02 residues.

6.2.4 Differential Scanning Calorimetry (DSC)

DSC (TA DSC/TGA Q 2000 Thermal Analyzer, TA Instruments, Grimsby, ON) was conducted on hydrogels in 150mM PBS working concentrations of 0.5% (w/v) of (RADA)$_4$ in all the peptides. Hermatic pans were purchased from TA Instruments (Grimsby, ON). Samples were cooled to -40°C at the rate of 5°C/min and then heated to 50°C, at the same rate, under a nitrogen atmosphere. In order to determine the total water of the system, the before DSC weights and the mass of dried peptide were used.

Non-frozen water contents were obtained from the difference between the equilibrium water content of the hydrogels and the calculated frozen water Equation 6.2 [11].

$$EWC = \frac{Wh - Wd}{Wh} \times 100 \qquad \textbf{Equation 6.2}$$

Where EWC is the Equilibrium Water Content (%), Wh is the weight of hydrated water sample (mg), and Wd is the weight of dry water sample (mg).

The three kinds of water present in any polymer can be represented by the following equation [11]:

$$EWC\ (wt\%) = Wnf\ (wt\%) + Wfb\ (wt\%) + Wf\ (wt\%) \qquad \textbf{Equation 6.3}$$

Where W_{nf} is the non-frozen water content (mg), W_{fb} is the frozen, bound water content (mg), and W_f is the free water content (mg).

195

Frozen and non-frozen water contents were determined by using the area under the resulting thermograms along with equilibrium water content. The frozen water content was calculated by the equation given below, where melting enthalpy of the bulk water was taken to be 334 J/g [11]:

$$W_{frozen} = \frac{\Delta H}{\Delta H^0} \, X \, 100$$ **Equation 6.4**

Where W_{frozen} is the weight of frozen water present in the sample (%), ΔH is the melting enthalpy of the sample (J/g), and ΔH^o Melting enthalpy of the bulk water (J/g).

6.2.5 Fluorescence Correlation Spectroscopy (FCS)

Alexa Fluor® 488 dye was purchased from Invitrogen (Burlington, ON), and was used without further purification. Aqueous solutions were prepared using deionizing water from a Milli-Q water purification system (Millipore, ON).

Data for fluorescence correlation spectroscopy were collected by following the previously established protocol [12]. Briefly, raw data was collected on an integrated imaging and spectroscoping platform LSM 510 MMeta –ConfoCor 2, purchased from Carl Zeiss Canada Ltd. (North York, ON). The fluorescence was collected above 605 nm. For each histogram the procedure yielded four parameters: counts per mol, the number of particles (N), diffusion time (τ_{diff}), and geometrical parameter reflecting the shape of the excitation volume (S). The value of S should fall in between zero to one, indicating the reliability and reproducibility of the analysis.

The autocorrelation functions were fitted to a theoretical model derived for free 3-D diffusion under the assumption that the detection volume is well approximated by a 3D Gaussian

function, prior to building it on the software. The correlation analyses were conducted in the software package provided by Carl-Zeiss with the system. Goodness of fit was determined by χ_0^2, with the inbuilt software. The absorption spectra of Alexa Fluor® 488 were recorded on UV-vis spectrophotometer Agilent 8453. The fluorescence spectra of Alexa Fluor® 488 were recorded on Photon Technology International (PTI) MP1 Fluorescence System.

6.3 Results and Discussion:

6.3.1 Nanofiber Assembly

Physicochemically there are three major inter- and intra-molecular forces driving self-assembly process: hydrogen bonding, hydrophobic and electrostatic interactions [13]. Figure 6.1 shows the three dimensional structures of $(RADA)_4$, $(RADA)_4S_5$, $(RADA)_4K_5$, using marvinSketch based on energy minimization [14]. Hydrophilic amino acids (Arginine, and Aspartic Acid) are located on one side of the peptide chain, whereas the hydrophobic residues (Alanine) are on the other side; resulting in two distinct faces of the nanofiber, which consequently lead to the β-conformation in the first stage of self assembly. Formation of stable β-sheets in the $(RADA)_4$ based peptides were investigated using CD. Previous studies consider the formation of strong secondary β-sheet structure formation in $(RADA)_4$, imperative for its self-assembling into nanofibers [15, 16]. The resulting three-dimensional structure from these peptides is expected to have diameters of 10-20 nm, with 5-200 nm pore size [15, 17-20], though these measurements expected to vary with peptide concentration.

197
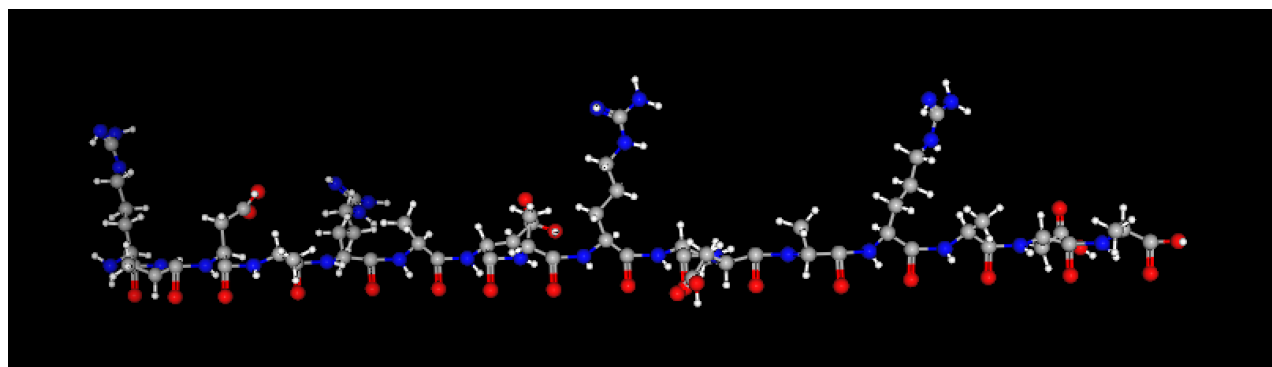
(A)
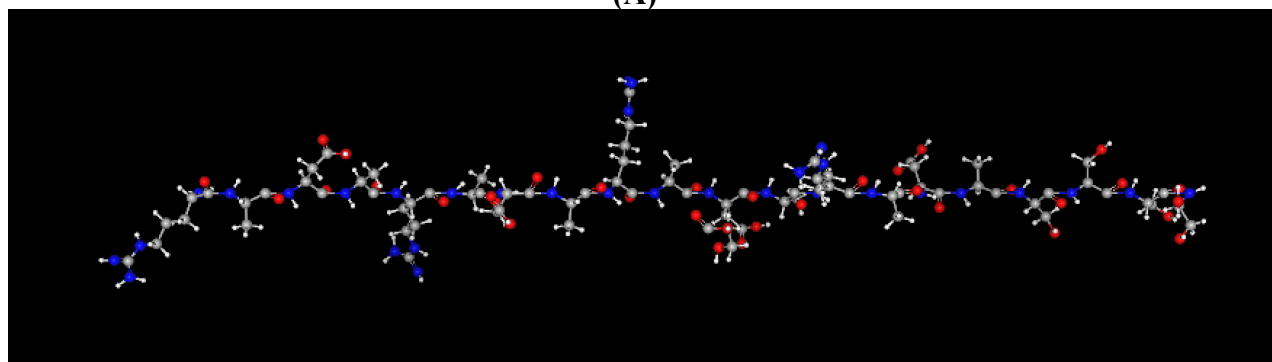
(B)
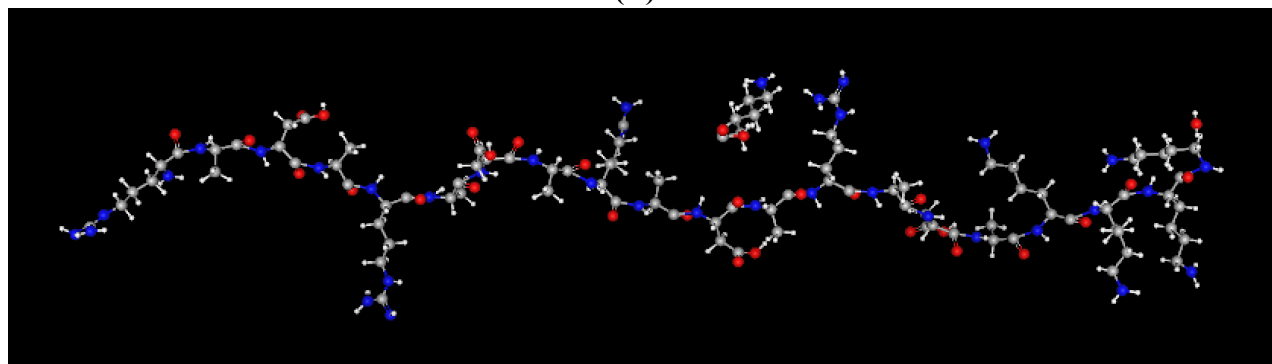
(C)

Figure 6.1: Schematic representation of the three dimensional molecular structure of (A) (RADA)₄, (B) (RADA)₄S₅, and (C) (RADA)₄K₅.

Carbon atoms are gray, oxygen atoms are red, nitrogen atoms are blue, and hydrogen atoms are white. The theoretical isoelectric point (pI) for (RADA)₄, (RADA)₄S₅, and (RADA)₄K₅ is 7.14, 6.84, and 11.07, respectively.

For a stable β-structure to form, all the hydrophobic alanine side chains face in one direction, and all the aspartic acid and arginine side chains face in another direction to create two distinct faces.

The chemical characteristics of the three peptides used in the study are given in Table 6.1. The (RADA)$_4$ peptide is a characteristic amphiphillic peptide with an alternating charge of $+ - + -$, whereas (RADA)$_4$K$_5$ has a net positive charge, and (RADA)$_4$S$_5$ is polar yet uncharged at the physiological pH. CD spectrum obtained in this study were compared with that of poly-L-lysine containing varying composition of three standard conformations of secondary structures: α, β and random coil. Whereas, the computed spectra of poly-L-lysine were compared with the experimentally obtained spectra of several proteins through X-ray diffraction studies [21]. A typical spectrum for β-sheet structure [21] is characterized with minimum mole residue ellipticity (deg cm^2/ decimole) at 216-218 nm and for backbone twist [18] a maximum mole ellipticity at around 195 nm. Figure 6.2 summarizes the molar ellipticity profile of (RADA)$_4$, (RADA)$_4$S$_5$, and (RADA)$_4$K$_5$ solutions as a function of wavelength. The CD spectrum observed for 100% (RADA)$_4$ shows a typical CD curve of the peptide [18], with a peak at around 195 nm and a minimum molar ellipticity 215 nm, indicating the presence of backbone twists and β-sheets. Since the peptide contains four alkaline arginine residues (pI = 10.76), four acidic aspartic acid residues (pI = 2.77), and eight alanine residues (pI = 6.00), its overall calculated pI is 7.20, which has also been experimentally confirmed [7]. Hence, the peptide is found to electrically neutral at physiological pH of 7.4, carrying partial positive and negative charges, and is expected to be positively charged in diH$_2$O.

Table 6.1: Chemical characteristics of (RADA)₄ peptide and it's variants. The purity analyzed by high-performance liquid chromatography (HPLC) had a ±2% deviation for peptides ≤ 95%. The accuracy of observed mass was ± 0.1%, as provided by the manufacturer.

Peptide	Theoretical Mass	Net Charge	Hydrophobicity
(RADA)$_4$	1670.81	0	33.7 Kcal*mol^{-1}
(RADA)$_4$S$_5$	2105.98	0	36.0 Kcal*mol^{-1}
(RADA)$_4$K$_5$	2311.28	5	47.7 Kcal*mol^{-1}

(RADA)$_4$ peptide is known to assemble into β-sheets in physiological relevant solutions, which are considered a prerequisite for self-assembling into nanofibers [7, 22]. We have previously reported that this peptide's strong β-sheet structure increases with the increase in concentration [23]. Here, we modified the (RADA)$_4$ in order to understand the effect of end groups on the overall nature of peptide formation. These (RADA)$_4$ variants were made by extending the original (RADA)$_4$ peptide at the C-terminus *via* solid phase synthesis by adding five serine and lysine residues to the peptide. Visual inspection of the solubilized peptides (in deionized water), revealed a transparent/translucent viscous solution for both (RADA)$_4$ and (RADA)$_4$S$_4$, but (RADA)$_4$K$_5$ resulted in relatively a more opaque viscous solution. All the solutions were made by keeping the (RADA)$_4$ content constant to 0.5% (w/v).

It can be expected that appending amino acids with various physicochemical properties would alter the interactions between amino acid residues within the peptide nanofiber, as well as would affect the packing propensity, resulting in a different three dimensional structure.

Similarly, the effect of appending hydrophilic uncharged Serine residues (-CH$_2$OH) and electrically charged Lysine residues ((CH$_2$)$_4$NH$_3$) on the (RADA)$_4$ peptide can provide insight into the higher dimensional physiologically relevant structures.

Herein, by appending five polar residues of Serine, consisting of a smaller side chain (Figure 6.1 B), an increase in the β-sheet content of the peptide was observed (Figure 6.2), when compared to the pristine (RADA)$_4$ peptide. However, the secondary structure evaluation of the peptides (Figure 6.2 (A)) resulted in the β-sheet content (S(r) + S(d)) for (RADA)$_4$ is 0.636, whereas for (RADA)$_4$S$_5$ is 0.476. It is likely that the intermolecular interactions between the serine side chains are much weaker than that of (RADA)$_4$ [24]. Moreover, the presence of the smaller side chain is not expected to impede in the nanofiber stacking. Also, it should be noted that most of the β-strand based biologically evolved proteins consist of three to ten amino acids in length [25], whereas we have demonstrated a successful β-strand based nanofiber formation with this 21 amino acid long peptide. It has been postulated before that in the case of peptides longer than ten residues in length, they have the tendency to fold over upon themselves, and interact as if they were the shorter moiety [26]; hence, possibly promoting the formation of more β-sheet based nanofibers. This is evident in (Figure 6.2(B)), as even though (RADA)$_4$S$_5$ consists of five more amino acid residues than (RADA)$_4$, its average strand length is less than half when compared with that of (RADA)$_4$.
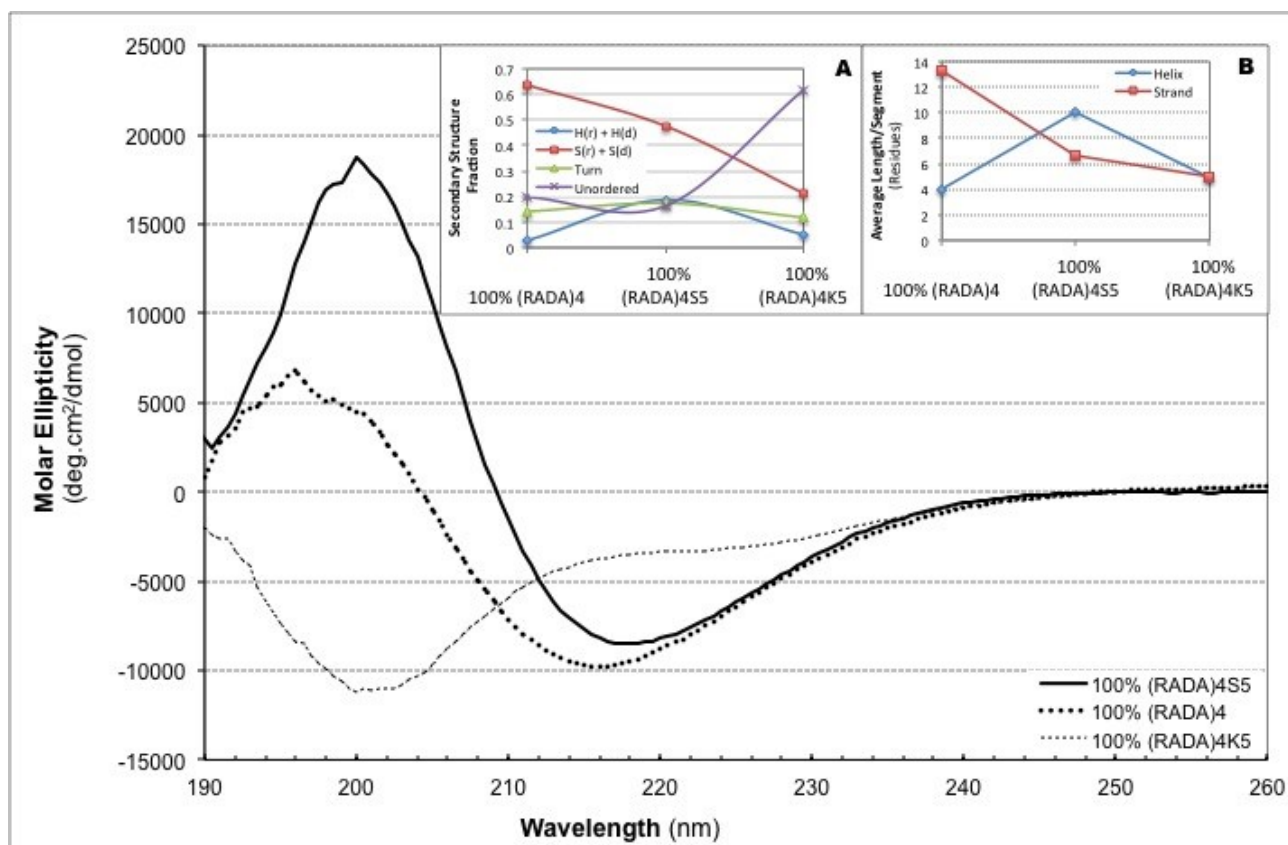
Figure 6.2: CD spectra for 100% solutions of (RADA)4, of (RADA)4K5, and (RADA)4S5 at 25°C, such that the final concentration of the (RADA)4 content in all the solutions was 0.5% (w/v).

The peptides (RADA)4, and (RADA)4S5 displayed a typical β-sheet structure (minimum at 215-216 nm and maximum at ~195-196 nm), whereas the secondary structure for (RADA)4K5 displayed the presence of disordered structures (minimum at 222 nm and 208 nm, and maximum at 190-193 nm). Data represents the average of five scans, with HT(V) values<500. Inset: (A) Estimated secondary structure composition of (RADA)4, of (RADA)4K5, and (RADA)4S5;(B) Estimated average length per segment of the three peptides.

The secondary structures are composed of six categories: H(r) is regular α-helix; H(d) is distorted α -helix; S(r) is regular β-strand; S(d) is distorted β-sheets; β-sheet Turn; Unordered. The average length pertains to the number of residues of α -helical and β-segments.

In a similar fashion when five residues of Lysine amino acid (with long and ionisable side chains) were appended to the C terminus of the peptide, no β-sheet presence was detected in CD (Figure 6.2). However, the observed minima at 222 and 208 nm and the maxima at 190-193 nm were directly related to the presence of random coils in the solution [9]. Further secondary structure analysis of the $(RADA)_4K_5$ peptide showed total β-sheet content $(S(r) + S(d))$ of merely 0.213 units, where 0.085 units pertain to the distorted β-sheet (Figure 6.2(A)). Contrary to our results, previous studies [26] postulate that the presence of ionisable species further stabilizes the nanofiber structure of the peptide, by stabilizing the hydrogen bonds as well as ionic salt bridges. However, our study suggests, the length of the Lysine side chains (Figure 6.1(C)) rather impedes with the stacking ability of the nanofiber (Figure 6.2). Moreover, we believe that the charged part of the Lysine residues does promote interactions with the other side chains, and forms β-sheet to some extent. To evaluate this, the critical concentration for self-assembly of $(RADA)_4K_5$ was evaluated. It was found that the concentrations $25\%(RADA)_4K_5$ (and below) with $(RADA)_4$ peptides, does form successful nanofibers (as indicative of the presence of β-sheets). Also, the β-sheet formation increases with the increase of $(RADA)_4$ in the solution (Figure 6.3).
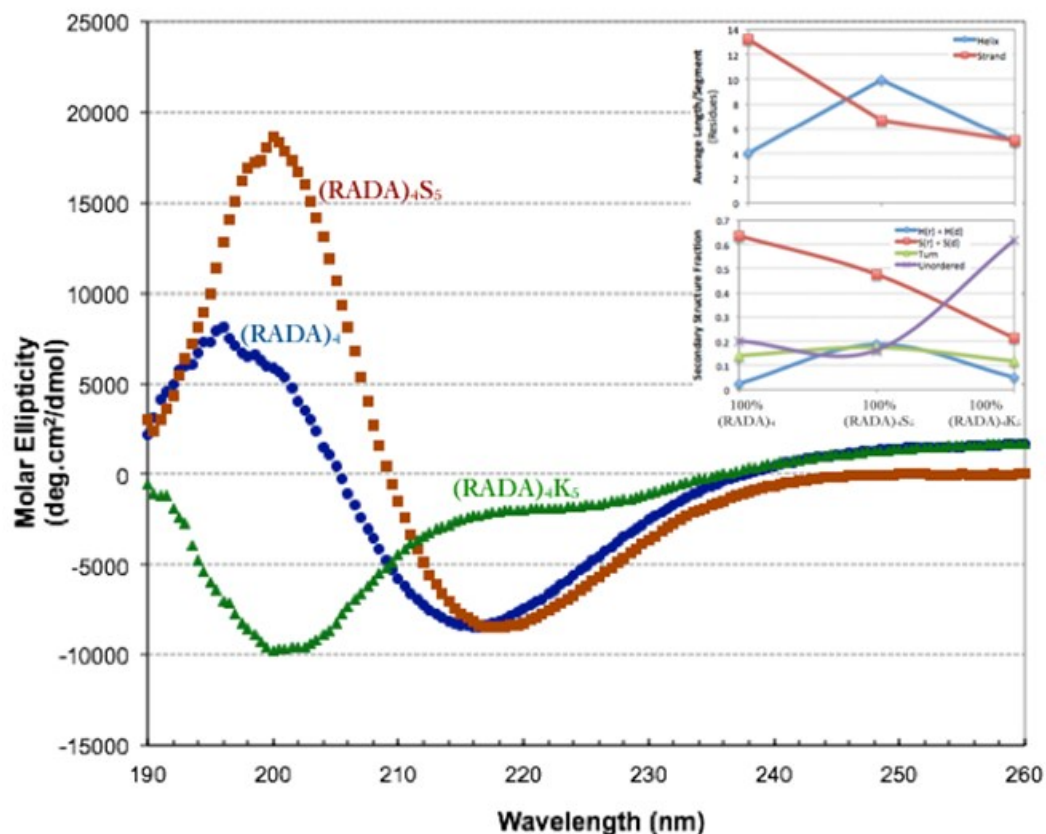
Figure 6.3: CD spectra of 0.5% (w/v) (RADA)₄ with various concentrations of (RADA)₄K₅, as accumulated at 25ºC in diH₂O.

The pristine (RADA)$_4$K$_5$ peptide mixture displayed disordered structure, indicated by a minima at ~200 nm and maxima~ 215 nm, whereas a typical β-sheet structure at lower concentrations of (RADA)$_4$K$_5$ peptide was observed. Data represents the average of five scans, with HT(V) values<500. Inset: (A) Estimated secondary structure composition of (RADA)$_4$, of (RADA)$_4$K$_5$, and (RADA)$_4$S$_5$;(B) Estimated average length per segment of the three peptides.

The secondary structures are composed of six categories: H(r) is regular α-helix; H(d) is distorted α -helix; S(r) is regular β-strand; S(d) is distorted β-sheets; β-sheet Turn; Unordered. The average length pertains to the number of residues of α -helical and β-segments.

6.3.2 **Hydration State Analysis:**

Despite these materials being studied for several decades, and their interesting properties regarding hydrogel formation at low (0.5%, w/v) concentration, there is a dearth in the literature regarding how these nanofiber structures interact with water. Not only is it thought that water interaction is crucial for nanofiber formation itself through a hydrophobic effect [22], it is also thought that water-nanofiber interactions may affect secondary phenomena like peptide packing, and protein adsorption. Where it is believed that water adsorption to a biomaterial precedes protein biomaterial interaction, and hence determines the fate of subsequent events [27].

Differential Scanning Calorimetry (DSC) was performed to estimate the content of different types of water present in these hydrogels as a function of peptide concentration. Both, frozen and non-frozen water are known to be present in swollen hydrogels and are believed to influence protein adsorption and platelet activation properties of the hydrogels [28]. Water that easily freezes (i.e.-frozen water) is loosely adsorbed to the nanofiber. Non-frozen water, however, is thought to be very tightly bonded to the nanofiber that it shows no freezing/melting transition. Here, it is possible to indirectly quantify the amount of non-frozen water present in the samples and how peptide chemistry affects the vicinal water structure; correlation of which to protein adsorption and platelet activation is thought to be extremely novel. Here, the state of water is examined with the increase in peptide concentration. Frozen and non-frozen water content was determined from the area enclosed by a DSC peak and a base line. The Equilibrium Water Content (EWC) in in $(RADA)_4$ is comparable to ones in $(RADA)_4S_5$ and $(RADA)_4K_5$, even at varying compositions (Table 6.2). The content of non-frozen bound water increased (Table 6.2) upon appending either Lysine or Serine residues to the $(RADA)_4$ peptide. However,

upon examining the bound water content of those compositions forming successful β-sheets, it can be concluded that the content of non-frozen water is highly dose dependent. It is thought that this dose dependency pertains directly to the level of surface area present in the nanofiber sample; the more peptide, the more surface area that the water can interact with. Moreover, it is thought that the serine residues consisting of a free hydroxyl group, facilitates this increase in non-frozen waters due to a stronger interaction between the polar side chain and the vicinal water.

Table 6.2: Differential Scanning Calorimetry analysis of the various water phases present in (RADA)$_4$, (RADA)$_4$S$_5$ and (RADA)$_4$K$_5$ hydrogels as a fraction of peptide concentration.

The (RADA)$_4$S$_5$ and (RADA)$_4$K$_5$ peptide solutions were made such that the final concentration of the (RADA)$_4$ content in all the solutions was 0.5% (w/v). Frozen and non-frozen water content representing loosely adsorbed and tightly bound water contents on the peptide. Data represent average $\pm$ 1 SD, n>5.

Peptide	Equilibrium Water Content (%)	Frozen Water Content (%)	Non-frozen Water Content (%)
100% (RADA)$_4$	98.70 $\pm$ 0.37	90.19 $\pm$ 0.76	8.51 $\pm$ 0.75
100% (RADA)$_4$S$_5$	98.58 $\pm$ 1.22	83.34 $\pm$ 2.39	15.24 $\pm$ 1.29
25% (RADA)$_4$S$_5$	97.85 $\pm$ 0.10	88.74 $\pm$ 3.99	9.10 $\pm$ 4.06
10% (RADA)$_4$S$_5$	98.94 $\pm$ 0.05	82.30 $\pm$ 14.30	16.63 $\pm$ 14.30
5% (RADA)$_4$S$_5$	98.99 $\pm$ 0.02	89.61 $\pm$ 1.61	9.38 $\pm$ 1.60
100% (RADA)$_4$K$_5$	98.62 $\pm$ 0.61	88.52 $\pm$ 6.29	10.09 $\pm$ 6.57
25% (RADA)$_4$K$_5$	97.17 $\pm$ 0.55	82.31 $\pm$ 4.42	14.86 $\pm$ 4.92
10% (RADA)$_4$K$_5$	98.89 $\pm$ 0.72	87.73 $\pm$ 2.70	11.15 $\pm$ 2.59
5% (RADA)$_4$K$_5$	98.31 $\pm$ 0.59	88.89 $\pm$ 2.59	9.42 $\pm$ 2.59

The CD data shown above indicates that the observed secondary structure of (RADA)$_4$ is associated with the structural transition from α-helices to β-sheet dominated conformations, and the given hydration studies reveal that the structural transition is driven by the presence of intermolecular bound water, acting as plasticizers on the nanofibers. Non-frozen bound water is known to enhance the mobility of the polymers by expanding its conformational space by

decreasing its inter- and intra-molecular friction and in this case, acting as a plasticizer to decrease the effective barrier heights for conformational change from α-helices to β-sheets [29].

6.3.3 **(RADA)$_4$K$_5$ in (RADA)$_4$:**

We first analysed the behaviour of (RADA)$_4$ in aqueous solution at constant dye concentration and different (RADA)$_4$ concentration. The results of the FCS analysis are presented in Figure 6.4. Our results showed that the smaller the concentration of the (RADA)$_4$ nanofibers the higher the number of particles in diffusion. Moreover, the diffusion time (t_{diff}) immediately increases (Figure 6.4) to 31.2-37.7 μs, and reaches the maximum value of 38.7 μs and plateaus, displaying that the nanofibers do not restrict the motion of dye (even for well above the CAC (critical assembly concentration) of nanofiber formation at 0.3 μM). Above the CAC of (RADA)$_4$ diffusion time was measured to be 38.7 μs, and attained plateau even at a much higher concentration of the peptide. Upon establishing the typical t_{diff} of fluorescent dye (~30 μs), τ_{diff} of the (RADA)$_4$K$_5$ peptide labelled with the dye was found (~62 μs).
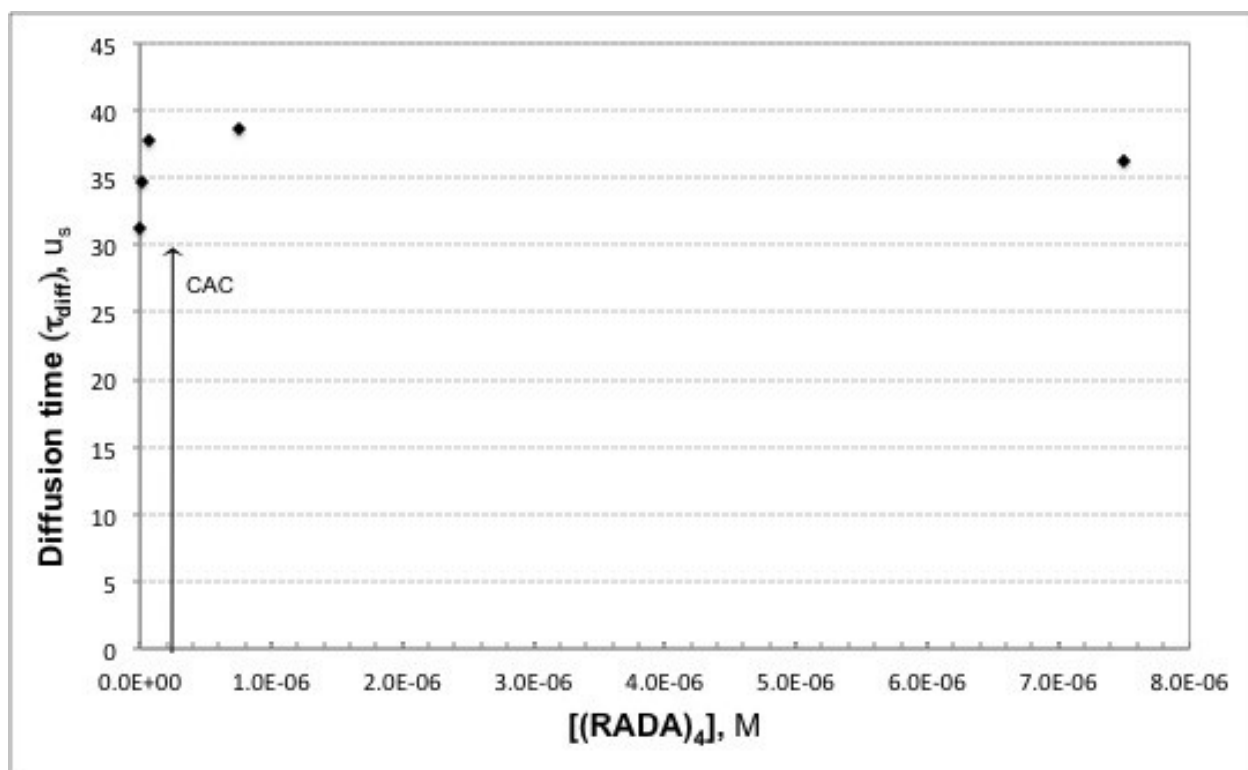
Figure 6.4: Mean diffusion time (τ_{diff}) of Alexa488® measured as the decter count rate in the presence of increasing (RADA)$_4$ concentrations in aqueous solution.
The critical assembly concentration (CAC) for the (RADA)$_4$ peptide is indicated.

The results of the FCS analysis are presented in (Table 6.3) At 0.75 x 10^{-6} M, which is above the CAC of (RADA)$_4$ peptide diffusion time was measured to be as high as 7652.3 µs, which is well above the τ_{diff} value for (RADA)$_4$K$_5$.

Fluorescence traits labelled peptide fraction of (RADA)$_4$K$_5$ was added along with unlabelled (RADA)$_4$ peptide (above the CAC) to test if (RAD)$_4$K$_5$ is incorporated in the pristine (RADA)$_4$ upon nanofiber formation. The experimental values deduced for diffusion coefficients with the standard single molecule FCS are prone to several experimental errors [30], hence, only relative values for count rates and diffusion times should be considered. Therefore, several

repeats were conducted at each concentration of $(RADA)_4$ peptide to determine the overall trend of diffusion. At the peptide concentration higher than 0.75×10^{-6} M, not only the τ_{diff} increased substantially, but also the count rate per mol (kHz), remained low, indicating a stronger association of $(RADA)_4K_5$ with the $(RADA)_4$ peptide, especially during nanofiber formation.

Table 6.3: Single molecule Fluorscence Correlation Spectroscopy analysis of (RADA)$_4$ interaction with (RADA)$_4$K$_5$ peptide, at a constant Alexa488® dye concentration.

(RADA)$_4$ Peptide Concentration (M)	Experimental Runs	Count rate (kHz)	Correlation	Counts per mol. (kHz)	N	$t_{diffusion}$ (ms)	S
0	1	2.318	6.14	11.916	0.195	135.636	0.998
	2	2.257	6.202	11.739	0.192	62.46	3.564
	3	2.245	7.463	14.509	0.155	50.138	8.059
	4	2.202	6.373	11.83	0.186	68.573	35.041
	5	2.284	5.867	11.113	0.205	85.912	2.906
	6	2.341	5.837	11.321	0.207	88.197	5.33
	7	2.141	3.709	5.8	0.369	261.458	2.13
	8	2.217	7.263	13.888	0.16	58.455	9.362
	9	2.177	6.727	12.465	0.175	56.7	6.966
	10	2.179	6.318	11.588	0.188	87.831	2.064
	Average	**2.236**	**6.735**	**12.824**	**0.174**	**62.169**	**6.839**
0.75 x 10^{-6}	1	1.932	7.311	12.193	0.158	61.376	3.393
	2	1.887	3.487	4.693	0.402	327.756	1
	3	1.772	2.994	3.533	0.501	298.535	1.005
	4	38.936	1.159	6.178	6.302	7652.28	5.5
	5	1.809	4.429	6.204	0.292	227.028	0.988
	6	1.88	6.416	10.179	0.185	73.774	6.987
	7	1.918	7.059	11.624	0.165	125.503	1
	8	1.876	8.658	14.37	0.131	55.854	25631245.49
	9	1.812	5.928	8.931	0.203	257.224	0.501
	10	1.771	5.281	7.582	0.234	167.569	0.999
	Average	**1.851**	**7.465**	**11.966**	**0.155**	**58.246**	**5.349**
0.75 x 10^{-5}	1	1.83	5.647	8.505	0.215	68.679	17104264.85
	2	1.8	3.155	3.878	0.464	680.664	57578.386
	3	1.745	6.068	8.845	0.197	61.237	3.349
	4	1.72	6.087	8.751	0.197	65.782	8.345
	5	1.732	3.628	4.552	0.381	326.842	1.001
	6	1.65	6.48	9.042	0.182	52.777	9.586
	7	1.558	6.993	9.335	0.167	91.503	1.003
	8	1.652	4.257	5.379	0.307	358.008	1.001
	9	1.634	7.47	10.57	0.155	60.392	3.994
	10	1.971	4.729	7.351	0.268	2619.65	3.629
	Average	**1.729**	**3.589**	**4.477**	**0.386**	**292.228**	**17030.903**
0.75 x 10^{-4}	1	2.703	1.253	0.683	3.957	5503621	0.103
	2	1.719	3.029	3.488	0.493	357.464	1.001
	3	1.744	6.042	8.791	0.198	61.364	6.004
	4	1.73	6.077	8.785	0.197	50.989	34.043
	5	2.207	3.905	6.41	0.344	67.881	1853160344
	6	1.736	4.361	5.836	0.298	212.097	1
	7	1.675	6.127	8.589	0.195	151.532	0.839
	8	1.706	4.089	5.271	0.324	197.709	1.001
	9	1.775	3.369	4.204	0.422	308.935	1.003
	10	1.643	2.161	1.909	0.861	376.65	1.002
	Average	**1.771**	**5.639**	**8.214**	**0.216**	**64.475**	**5.92**

6.3.4 **Effect of Heating on Nanofiber Formation:**

In our quest to understand self-assembly of (RADA)$_4$ peptide, we have previously studied [23] the effect of concentration of (RADA)$_4$ as a function of temperature. Our study concluded that upon increasing the (RADA)$_4$ peptide concentration from 0.5% (w/v)-3.0% (w/v) a structural transition from α-helices to more stable β-sheets was evident; which was also partially due to the presence of bound water content. Also, we found the peptide maintained stability up till 80°C, at all the concentrations tested.

Our present study entails variable temperature experiments performed on the (RADA)$_4$ variants in order to gain further insight into the role of heating on structural transformations, with respect to different end group chemistries. Thermal transitions corresponding to the secondary structure transitions of (RADA)$_4$, (RADA)$_4$S$_5$, and (RADA)$_4$K$_5$ could also provide more information regarding the role of bound water on the self-assembly of peptides. Heat is thought to denature the peptide secondary structure of (RADA)$_4$ by destroying its non-covalent interactions such as hydrogen or electrostatic bonds [7]. Moreover, the increase in temperature is known to accelerate the Brownian motion of the individual molecules in the peptide, decreasing the chances of the peptides to associate with each other *via* inter and intra molecular interactions [7]. Temperature was increased from 20 to 80°C, and spectra was accumulated every 5°C to monitor changes in the secondary structure of the peptides. Qualitative analysis of the spectra was done by the collected spectra whereas a quantitative analysis of the secondary structures present was conducted *via* deconvulation method contin using a web server DICHROWEB.

It is evident from Figure 6.5, that even though the β-sheet content decreases upon the increase in temperature, the (RADA)$_4$ peptide maintains overall structural integrity, as asserted by the deconvolution analysis of the secondary structures where the overall β-sheet content (S(R)+S(d)) not only remain higher than other secondary structures present, but are also consistent throughout the thermal transition of the peptide (Figure 6.5(A)). The overall average β-strand length also remains higher than the α-helix length, throughout the change in temperature from 80 to 20°C for (RADA)$_4$ peptide.
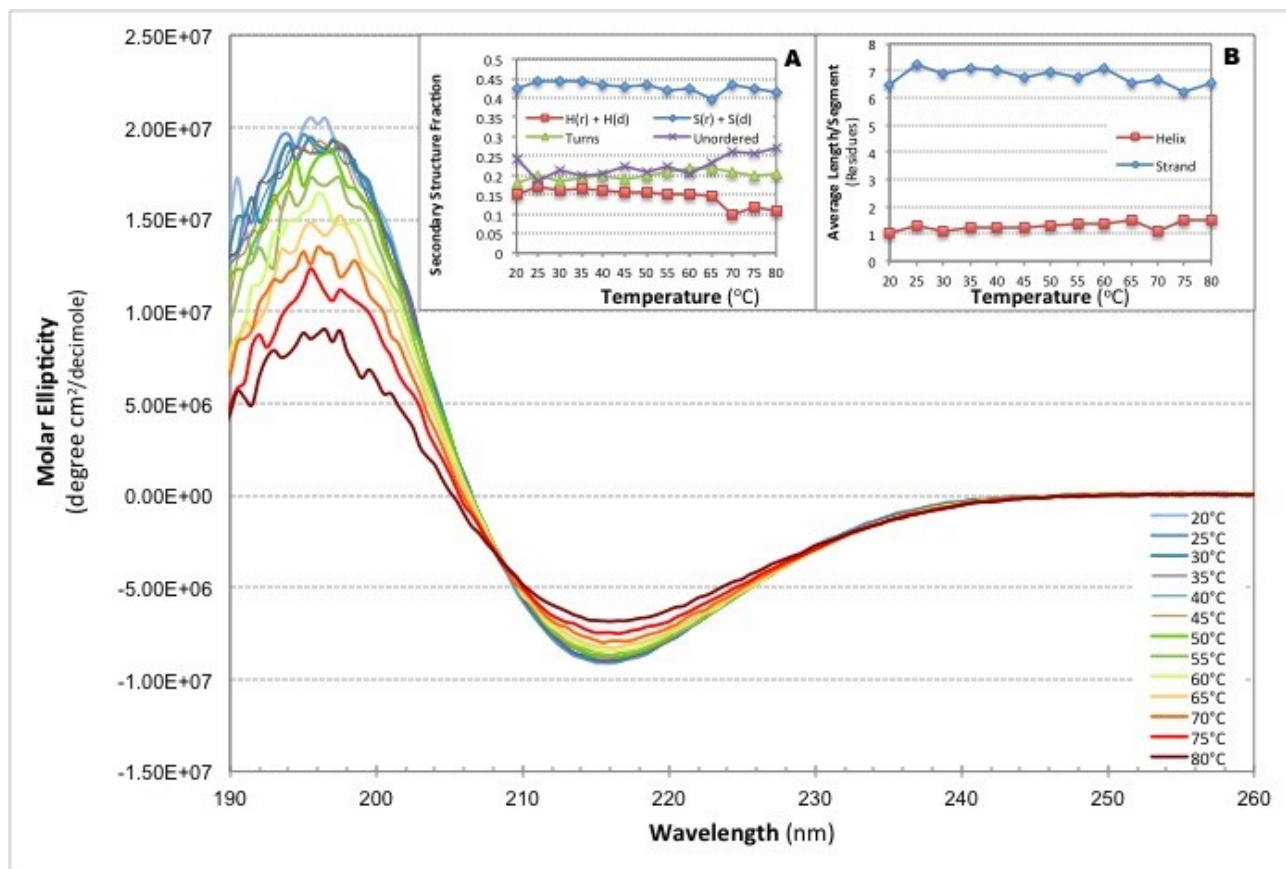
Figure 6.5: CD spectra of 0.5% (w/v) (RADA)$_4$ at various temperatures in diH$_2$O.

Data represents the average of five scans, with HT(V) values<500. Inset: (A) Estimated secondary structure composition of (RADA)$_4$;(B) Estimated average length per segment of the peptide.

213

The secondary structures are composed of six categories: H(r) is regular α-helix; H(d) is distorted α -helix; S(r) is regular β-strand; S(d) is distorted β-sheets; β-sheet Turn; Unordered. The average length pertains to the number of residues of α -helical and β-segments.

Our primary CD analysis involving the end group variations of (RADA)$_4$ peptide showed a more stable β-sheet structure with (RADA)$_4$S$_5$ peptide (Figure 6.2). The results might be associated with the high hydration of the peptide (Table 6.2). It has been postulated earlier that the presence of serine residue results in a significant decrease in the α-helical content [31]. Upon increasing the temperature from 20-80°C, the stability of the β-sheets in the (RADA)$_4$S$_5$ peptide is reduced; however the peptide's overall structure remains consistent. It is also evident from the deconvolution analysis that even though the overall β-sheet content of the peptide is decreased with the increase in temperature, so is the α-helix content. Interestingly, with the increase in the temperature the peak of the spectra shifts towards a higher wavelength, whereas the minima remains same at ~215 nm, this phenomenon could be the result in an increase in the unordered content of secondary structure (Figure 6.5(A)), as well as an increase in the overall average length of β-sheet strands, possibly due to the stabilization of the side chain of serine residues.
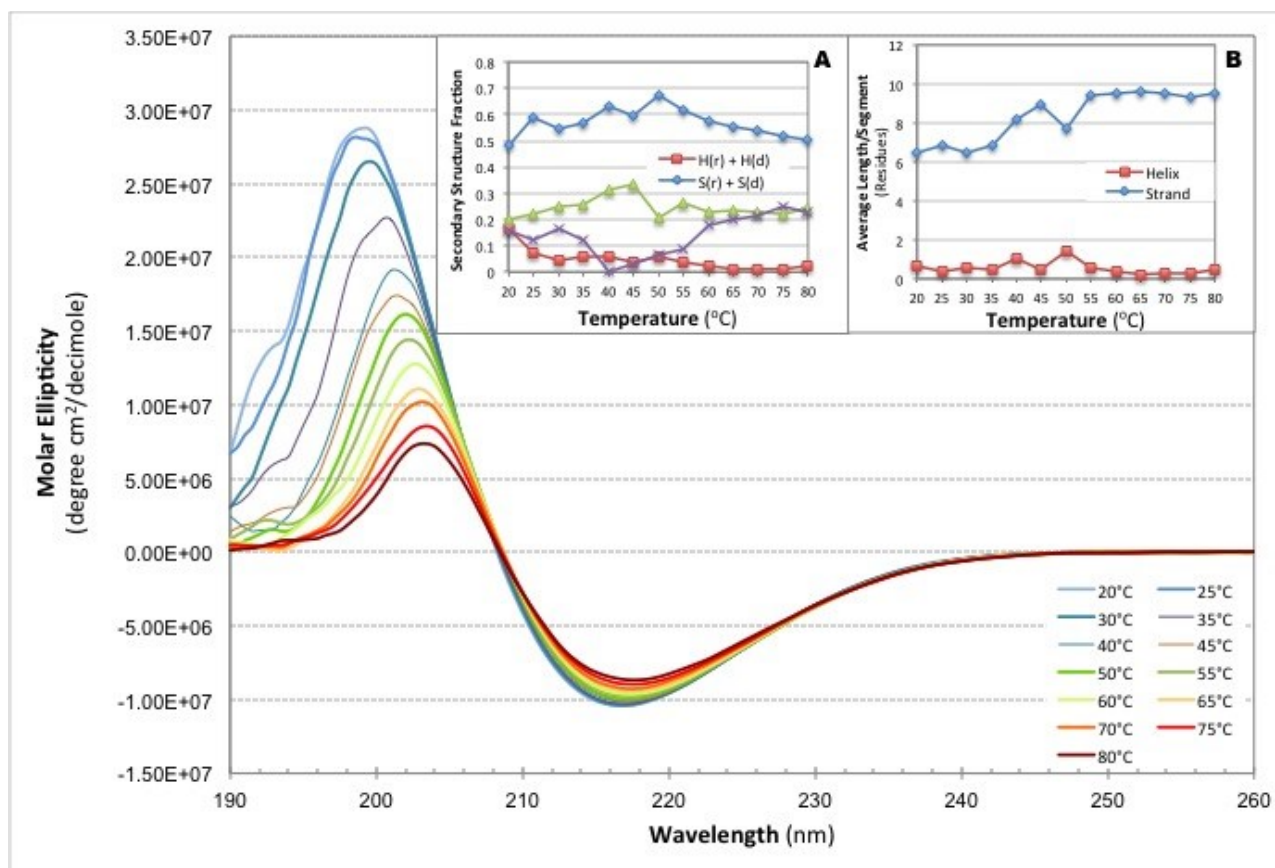
Figure 6.6: CD spectra of 0.5% (w/v) (RADA)₄S₅ at various temperatures in diH₂O.

Data represents the average of five scans, with HT(V) values<500. Inset: (A) Estimated secondary structure composition of the peptide ;(B) Estimated average length per segment of (RADA)$_4$S$_5$.

The secondary structures are composed of six categories: H(r) is regular α-helix; H(d) is distorted α -helix; S(r) is regular β-strand; S(d) is distorted β-sheets; β-sheet Turn; Unordered. The average length pertains to the number of residues of α -helical and β-segments.
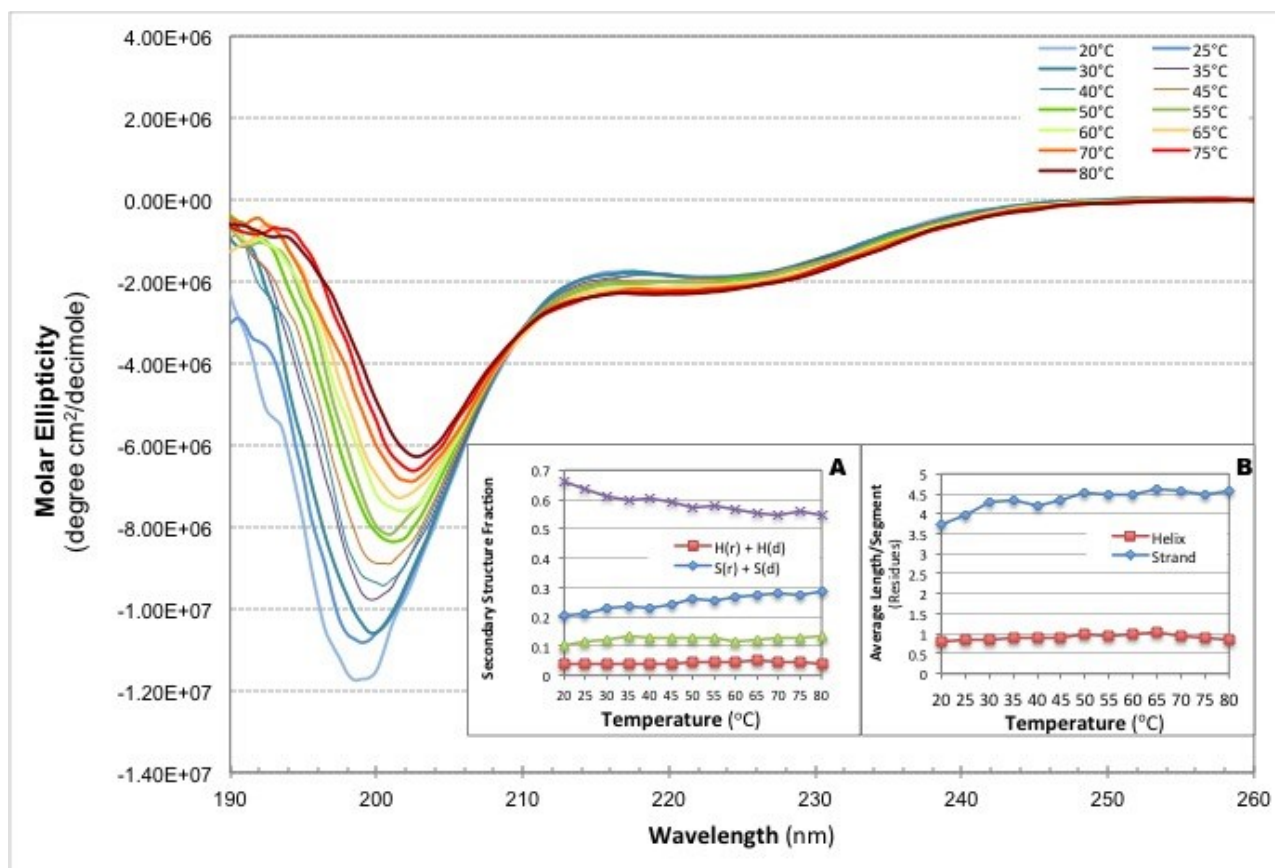
Figure 6.7: CD spectra of 0.5% (w/v) (RADA)₄K₅ with various temperatures in diH₂O.

Data represents the average of five scans, with HT(V) values<500. Inset: (A) Estimated secondary structure composition of (RADA)₄K₅ ;(B) Estimated average length per segment of the peptide.

The secondary structures are composed of six categories: H(r) is regular α-helix; H(d) is distorted α -helix; S(r) is regular β-strand; S(d) is distorted β-sheets; β-sheet Turn; Unordered. The average length pertains to the number of residues of α -helical and β-segments.

It was evident from the primary analysis of the secondary structure of the peptides that the shorter side chain of the uncharged polar serine residues assisted in the stabilization of (RADA)₄ peptide *via* β-sheet formation; whereas the longer side chain of positively charged lysine residues

(Figure 6.1) impeded with the overall self-assembly of the $(RADA)_4$ peptide (Figure 6.2). With the knowledge that the pristine $(RADA)_4K_5$ primarily forms disordered structures (perhaps due to the serine hindrance of the electrically charged side chains), the disordered structures remained consistent, even upon the increase in temperature of the peptides from 20-80°C. These results are also supported by further deconvolution analysis, which concluded the presence of primarily unordered structures for $(RADA)_4K_5$ (Figure 6.7(A)). However, the overall decrease in the unordered structure of the $(RADA)_4K_5$ peptide is accompanied by a surprising increase in the overall beta strands (S(r) +S(d)) (Figure 6.7 (A)), and an increase in the average length of the β-sheet residues as well (Figure 6.7(B)).

Our present investigation concluded that the successful nanofiber formation (resulting from the stable β-sheet structure) with $(RADA)_4K_5$ can be achieved at the 25% content of $(RAD)_4K_5$ (or/and lower), when combined with $(RADA)_4$. Even though the single molecule FCS results (Table 6.3) conclude the active participation of $(RADA)_4K_5$ nanofibers with those of $(RADA)_4$, apparently this inter nanofiber association does not seem to sustain the increase in thermal energy. A very low signal to noise ratio (Figure 6.8) implies the possible dissociation of these two peptides upon heating, and the resulting interference with each other while the measurements of the secondary structure. Even though the content of various secondary structure moieties as well as the average lengths of α-helix and β-strand segment seems consistent while varying the temperature, this data is possibly an accumulation of the overall structures present, rather than the transition itself.
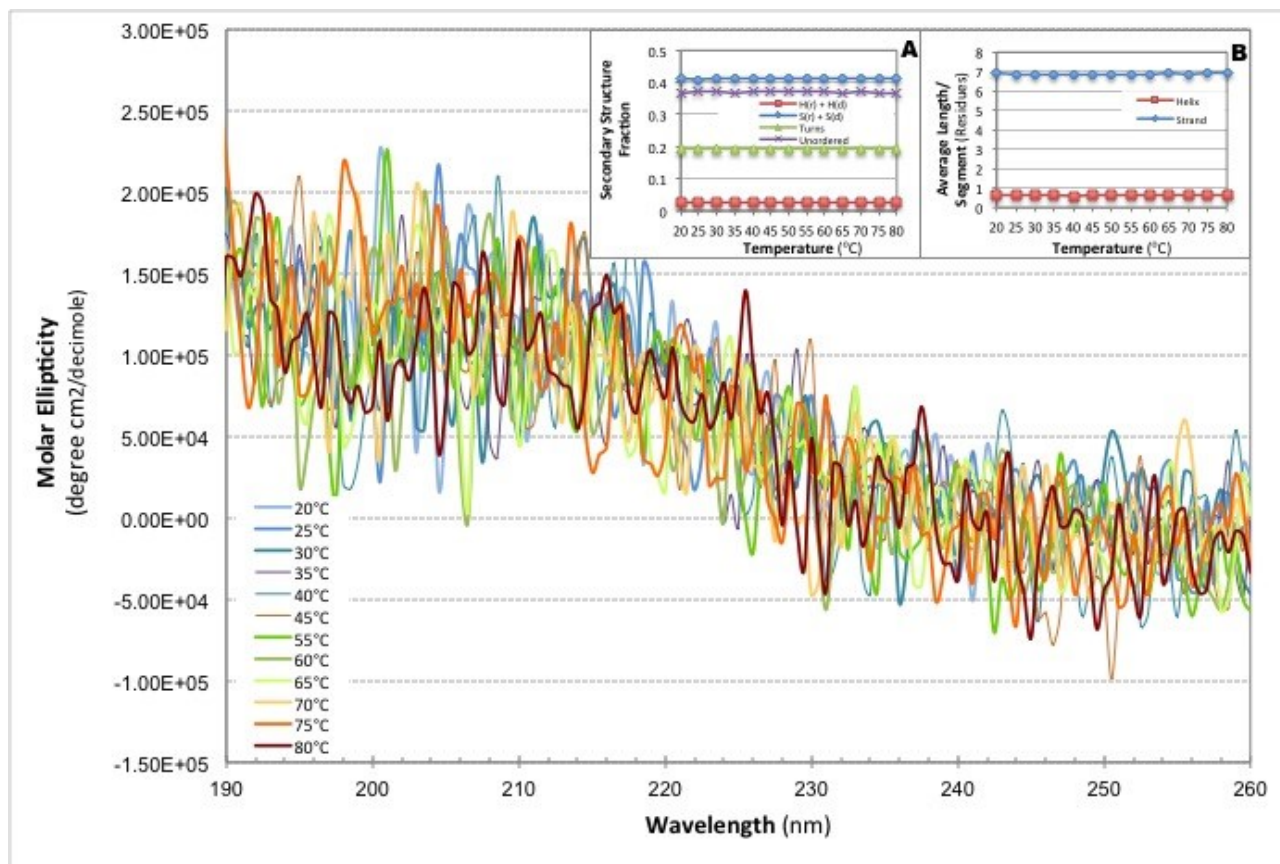
Figure 6.8: CD spectra of 0.5% (w/v) (RADA)₄K₅ at various temperature in diH₂O.

Data represents the average of five scans, with HT(V) values<500. Inset: (A) Estimated secondary structure composition of 25%(RADA)₄K₅ ;(B) Estimated average length per segment of the peptide mixture.

The secondary structures are composed of six categories: H(r) is regular α-helix; H(d) is distorted α -helix; S(r) is regular β-strand; S(d) is distorted β-sheets; β-sheet Turn; Unordered. The average length pertains to the number of residues of α -helical and β-segments.

6.4 Conclusion

Our study provides significant insight into the self-assembly process of (RADA)₄ peptide and its two variants; (RADA)₄S₅, and (RADA)₄K₅. Analysis of the CD measurement showed that

(RADA)$_4$ retains its characteristic β-sheet structure (presented by the trough at 210-218 nm and a peak at 195-206 nm). The β-sheet structure is further strengthened by the addition of five uncharged and polar serine residues, whereas it is hindered when five electrically charged lysine residues are appended. Successful β-sheet formation was achieved with (RADA)$_4$K$_5$ at the concentration of equal to or below 25%. The results suggest that the (RADA)$_4$ self-assembly is enabled by a structural transition from α-helices to β-sheet structures; this transition is also seeming to be dictated by the presence of frozen bound water content in the peptides. Further analysis of temperature sensitivity revealed an overall stable structure with all the three peptides, however the mixture of (RADA)$_4$ with that of (RADA$_4$K$_5$ did not seem to retain the structural integrity upon heating. Our research provides significant insight into the self-assembly of ionic complementary peptides, and has direct applications in clinical and medical nano-biotechnology.

Acknowledgements

References

[1] Johnson TD, Christman KL. Injectable hydrogel therapies and their delivery strategies for treating myocardial infarction. Expert Opinion on Drug Delivery 2013;10:59-72.

[2] Haugh MG, Thorpe SD, Vinardell T, Buckley CT, Kelly DJ. The application of plastic compression to modulate fibrin hydrogel mechanical properties. Journal of the Mechanical Behavior of Biomedical Materials 2012;16:66-72.

[3] Buenger D, Topuz F, Groll J. Hydrogels in sensing applications. Progress in Polymer Science 2012;37:1678-719.

[4] Janssen I, Koene M, Lischer C. Intraarticular applikation of polyacrylamide hydrogel as a treatment of osteoarthritis in the distal interphalangeal joint: case series with 12 horses. Pferdeheilkunde 2012;28:650-6.

[5] Uchida Y, Fukuda K, Murakami Y. The hydrogel containing a novel vesicle-like soft crosslinker, a "trilayered" polymeric micelle, shows characteristic rheological properties. Journal of Polymer Science Part B-Polymer Physics 2013;51:124-31.

[6] Segers VFM, Lee RT. Local delivery of proteins and the use of self-assembling peptides. Drug Discovery Today 2007;12:561-8.

[7] Ye ZY, Zhang HY, Luo HL, Wang SK, Zhou QH, Du XP, *et al*. Temperature and pH effects on biophysical and morphological properties of self-assembling peptide RADA16-1. Journal of Peptide Science 2008;14:152-62.

[8] Zhang SG, Lockshin C, Cook R, Rich A. Unusally stable beta-sheet formation in an ionic self-complementary oligopeptide. Biopolymers 1994;34:663-72.

[9] Greenfield NJ. Using circular dichroism spectra to estimate protein secondary structure. Nature Protocols 2006;1:2876-90.

[10] Snatzke G. Circular Dichroism: Principles and Applications. New York: VCH Publishers; 1994. p. 59-84.

[11] Mequanint. K S, H. 2-Methacryloyloxyethyl N-butylcarbamate: A new comonomer for hydrogel syntheses with improved hydrophilicity and mechanical properties for ophthalmic applications. Journal of Biomaterials Science, Polymer Edition 2005;16:1303-18.

[12] Elson EL, Magde D. Fluorescense correlation spectrospcoy.1. Conceptual basis and theory. Biopolymers 1974;13:1-27.

[13] Hong YS, Legge RL, Zhang S, Chen P. Effect of amino acid sequence and pH on nanofiber formation of self-assembling peptides EAK16-II and EAK16-IV. Biomacromolecules 2003;4:1433-42.

[14] ChemAxon. Cheminformatics platforms and desktop applications, http;//chemaxon.com. 2015.

[15] Zhang S, Holmes T, Lockshin C, A. R. Spontaneous assembly of a self-complementary oligopeptide to form a stable macroscopic membrane. Proceedings of the National Academcy of Sciences USA 1993;90:3334-8.

[16] Zhang SG, Holmes TC, Dipersio CM, Hynes RO, Su X, Rich A. Self-complementary oligopeptide matrices support mammalian cell attachment. Biomaterials 1995;16:1385-93.

[17] Zhang S, Holmes T, DiPersio M, Hynes RO, Su X, A. R. Self-complementary oligopeptide matrices support mammalian cell attachment. Biomaterials 1995;16:1385-93.

[18] Yokoi H, Kinoshita T, Zhang S. Dynamic reassembly of peptide RADA16 nanofiber scaffold. Proceedings of the National Academy of Sciences 2005;102:8414-9.

[19] Gelain F, Bottai D, Vescovi A, Zhang S. Designer Self-Assembling Peptide Nanofiber Scaffolds for Adult Mouse Neural Stem Cell 3-Dimensional Cultures. Public Library of Science 2006:1-11.

[20] Holmes T, De Lacalle S, Su X, Liu G, Rich A. Extensive neurite outgrowth and active synapse formation on self-assembling peptide scaffolds. Proceedings of the National Academcy of Sciences USA 2000;97:6728-33.

[21] Greenfield N, Fasman GD. Computed circular dichroism spectra for the evaluation of protein conformation. Biochemistry 1969;8:4108-16.

[22] Zhang SG, Lockshin C, Cook R, Rich A. Unusually stable beta-sheet formation in an ionic self-complementary oligopeptide. Biopolymers 1994;34:663-72.

[23] Saini AK, K and Unsworth, L.D. Effect of Peptide Concentration on Water Structure, Morphology, and Thermal Stability of Self-Assembling (RADA)4 Peptide Matrices. Journal of Biomaterials and Tissue Engineering 2014; ;4:895-905..

[24] Maude S, Miles DE, Felton SH, Ingram J, Carrick LM, Wilcox RK, *et al*. De novo designed positively charged tape-forming peptides: self-assembly and gelation in physiological solutions and their evaluation as 3D matrices for cell growth. Soft Matter 2011;7:8085-99.

[25] E CT. Proteins: Structure and Molecular Properties. 2nd ed. New York: Freeman W H; 1993.

[26] Caplan R, Moore N, Zhang S, Kamm D, Lauffenburger A. Biomacromolecules 2000;1:627.

[27] Tsuruta T. Contemporary topics in polymeric materials for biomedical applications. Biopolymers liquid crystalline polymers phase emulsion1996.

[28] Tanaka M, Mochiziki A, Ishii N, Motomura T, Hatekeyama T. Study of blood compatibility with poly(2-methoxyethyl acrylate). Relationship between water structure and platelet compatibility in poly(2-methoxyethylacrylate-co-2-hydroxyethylmethacrylate). . Biomacromolecules 2002;3:36-41.

[29] Hu X, Kaplan D, Cebe P. Dynamic protein-water relationships during beta-sheet formation. Macromolecules 2008;41:3939-48.

[30] Enderlein J, Gregor I, Patra D, Dertinger T, Kaupp UB. Performance of fluorescence correlation spectroscopy for measuring diffusion and concentration. Chemphyschem 2005;6:2324-36.

[31] Schneider JP, Kelly JW. Templates that induce alpha-helical, beta-sheet, and loop conformations. Chemical Reviews 1995;95:2169-87.

Chapter 7

Effect of Physiochemical Characteristics of Self-assembling (RADA)$_4$ Based Peptide Nanofibers on their *In-vitro* Biological Evaluation

Aditi Saini[a,b], Katherine Serrano[c], Theodore Ng[a,b], and Larry D. Unsworth[a,b] *

[a] Department of Chemical and Materials Engineering, Faculty of Engineering, University of Alberta, Edmonton, Alberta, Canada T6G 1H9

[b] National Research Council, National Institute for Nanotechnology, Edmonton, Alberta, Canada T6G 2M9

[c] Canadian Blood Services, Centre for Blood Research, 2350 Health Sciences Mall, University of British Columbia, Vancouver, British Columbia, Canada V6T 1Z3

* Corresponding author info:

Phone: 780-492-6020

Fax: 780-492-2881

E-mail: larry.unsworth@ualberta.ca

222

Abstract

(RADA)$_4$ based peptides are promising biomaterials due to their non-immunogenic biodegradability, high hydration (<99.5% (w/v)), and their ability to respond to external stimuli, as well as complete and rapid (~15 seconds) hemostasis when applied directly to wounds. The hemocompatibility of (RADA)$_4$ peptide; a prerequisite for its application as a blood contacting biomaterial, was investigated by determining the host response to the (RADA)$_4$ based peptides. We have created two variants of the (RADA)$_4$ peptide by appending five Lysine and Serine residues to its C terminus, for studying the effect of electrically charged and polar uncharged side chains on the otherwise amphiphilic peptide. Specifically, western blot analysis, C3a immunoassay, flow cytometry and platelet morphology studies were employed to understand the complement and platelet response to the peptide, and hence general hemocompatibility. Our study revealed low platelet, and C3a activation upon incubation with human blood, at physiological conditions. These results strongly support further development of (RADA)$_4$ peptide based biomaterials.

7.1 Introduction

Uncontrolled blood loss, or haemorrhaging is the second leading cause of death and is the leading cause of preventable deaths after hospital admission [1, 2]. More than 90% of military deaths on the battlefield are due to uncontrolled haemorrhaging [2, 3]. Blood loss is also most common cause of mortality during orthopaedic, cardiovascular, hepatic and spinal surgeries [1, 2, 4]. Blood consumption in surgeries is also a limiting factor, and blood donation is always in

223

demand, hence strategies to minimize the use limited resources (such as blood products) are imperative. Most of the commonly used hemostatic agents have met with certain limitations due to thrombotic complications, difficulty of application, and potential toxic effects.

A novel method to arrest bleeding involves the application of a self-assembling biodegradable and biocompatible peptide $(RADA)_4$, which forms nanofiber barrier by incorporating itself as a part of extracellular matrix (ECM) [5]. This method to stop bleeding does not employ any of the commonly used therapies such as applying pressure, cauterization, vasoconstriction, coagulation and cross-linked adhesives. These therapies have met with certain challenges, such as not being able to target specific tissue [6-8], unlike body's physiological environment requiring dry atmosphere [9], creating undesired immune response [8-11], having a short shelf-life [12, 13] or being unresponsive in uncontrolled environments [7-9, 14, 15]. Unlike the hemostatic agents involved in these therapies, self-assembling $(RADA)_4$ peptide has shown no pyrogenicity or systemic coagulation, has responded well in the wet physiological environment of the body, and has potential biodegradable by-products (L-amino acids). The $(RADA)_4$ peptide induced rapid (in less than 15 seconds) and complete hemostasis was achieved in a variety of tissues with varying degree of blood flow and underlying physiochemical environments (such as pH) [5]. Moreover, preliminary studies with $(RADA)_4$ peptides have been shown to lack inflammatory response, as well as non-thrombogenicity [16, 17]. However, there lacks a systematic evaluation of the effect of hemocompatibility with the $(RADA)_4$ based peptides, nor there has been any investigations with respect to protein adsorption onto these surfaces. Information gained through these experiments would not only provide insight into the

observed hemostatic mechanism of the peptide, but would aid in designing further blood contacting peptide-based biomaterials.

(RADA)$_4$ peptide is a member of designed ionic self-assembling peptides. The primary sequence of the peptide is [COCH$_3$]-RADARADARADARADA-[CONH$_2$], where the alternating hydrophilic and hydrophobic residues gives rise to a β-sheet formation, resulting in the complementary ionic bonds on the hydrophilic surface. The (RADA)$_4$ monomer is experimentally shown to be ~1.3 nm wide, ~ 5 nm long and ~0.8 nm thick in dimensions [18-20], monomers can spontaneously assemble nanofibers ranging from a few hundred nanometers to a few microns in length, subsequently forming higher order interweaving nanofiber scaffolds: hydrogels, possessing a very high hydration (up to 99.5%).

We have previously reported the β-sheet forming capabilities of (RADA)$_4$ peptide and its variants: (RADA)$_4$S$_5$, and 25%(RADA)$_4$K$_5$. We have also established biocompatibility of the (RADA)$_4$ peptide [21], as well as the stability of its structure at extreme temperatures [22]. In the present study we have reported the effect of end groups (lysine and serine residues) on the overall hemocompatibility of the (RADA)$_4$ peptide with the ultimate goal of designing ((RADA)$_4$ based blood contacting biomaterials.

Protein adsorption is the first event following any blood-material interaction [23]. This is followed by various complex and adverse responses [24], such as, coagulation, complement activation, platelet adhesion and activation leading to thrombosis, leukocyte adhesion, and red cell interactions leading to hemolytic damage. This in turn can lead to coagulation and thrombosis, which can grossly affect the bioactivity of a material. Hence, protein interactions should be controlled for designing a functional biomaterial; that is the non-specific protein

adsorption should be inhibited [25], whereas specific protein adsorption aiding in the material's bioactivity should be promoted [23]. The primary step in assessing protein interaction with any biomaterial is to evaluate total protein adsorption onto the surfaces.

Complement activation is an important parameter to evaluate a material's hemocompatibility [26]. Complement plays an important role in procoagulant activities, such as platelet activation, tissue factor expression [27], and modification of the activity of mast cells [28] and basophils [29]. Three distinct pathways are known to initiate the complement system: the classical pathway (CP), the alternative pathway (AP), and the lectin pathway (LP). The activation of complement *via* a biomaterial is thought to be induced by the AP pathway, whereas the contact with negatively charged surfaces or the use of certain drugs (such as protamine sulfate), may result in the activation of complement through the CP [30]. All three pathways ultimately converge to generate the same central effector molecule C3b, *via* the activity of C3-convertases and the C3-activating enzyme complexes, subsequently forming an anaphylatoxin C5 convertase splitting C5 [31, 32]. All the pathways ultimately culminate at the membrane attack complex (MAC), responsible for the cell damage and lysis [26].

Platelets are critical to ascertain overall hemocompatibility of any biomaterial due to their capability of adhering, aggregating and subsequently releasing their granule contents, altering their surface characteristics to support blood coagulation. There are several platelet activation markers used to assess *in-vitro* evaluation of biomaterials, such as CD63, CD40L, annexin V, CD62P and PAC-1 [33]. However, activation of platelets is usually assessed *via* expression of P-selectin (*via* CD62P) and glycoprotein (GP) IIb/IIIa (*via* PAC-1) [33]. P-selectin is stored in the inner walls of α-granules of the platelets, and is translocated to the plasma membrane upon

induction of inflammation. This protein plays in important role in the recruitment and aggregation of platelets at areas of vascular injury. Platelet activation (*via* the agonists, such as thrombin, $Ca^{2+,}$ ADP (adenosine diphosphate), and Type II collagen) leads to the release and exposure of α and dense granules, resulting in the platelet aggregation though platelet-fibrin and platelet-platelet binding. Therefore, P-selectin expression is specific only to the activated platelets, and not to quiescent platelets [34]. The integrin GPIIb/IIIa plays a major role in the regulation of platelet adhesion and aggregation during hemostasis. Platelet activation results in the conformational change within the GPIIb/IIa, which increases the affinity of the receptors for fibrinogen. Bound fibrinogen not only facilitates the interaction of adjacent platelets but also accelerates the platelet aggregation process [35].

Our goal is to study the hemocompatibility of $(RADA)_4$ and comparing it with it's successful nanofiber forming variants: $100\%(RADA)_4S_5$ and $25\%(RADA)_4K_5$. The *in-vitro* biological response of these peptides may be different from their pristine $(RADA)_4$ peptide, as the appended amino acids may sterically hinder the nanofiber packing, or the physicochemical characteristics of these peptides may affect interactions with the biomolecules compared to that of the $(RADA)_4$ peptide. The results will be compared with those of some of the common hemocompatible polymers currently approved for clinical use. *In-vitro* biological evaluation of these peptides involves, western blotting, complement activation, platelet activation and morphology analysis.

7.2 Materials and methods

All chemicals (including proteins) were purchased from Sigma-Aldrich, unless otherwise stated. Platelet poor plasma was obtained from Canadian Blood Services (CBS) Research Division and kept at -80°C prior to use. Blood was collected using research ethics board approved protocols, and all plasma was pooled prior to being distributed from the CBS Division. Briefly, whole blood was collected from healthy unmedicated donors, who provided informed consent in accordance with the current CBS and National Ethics Board standards. Blood collected in this manner was used for all subsequent plasma related assays, as described in the respective sections.

7.2.1 Peptide synthesis

The three self-assembling peptides: $(RADA)_4$ ([COCH$_3$]-RADARADARADARADA-[CONH$_2$]), $(RADA)_4K_5$ ([COCH$_3$]-RADARADARADARADAKKKKK-[CONH$_2$]) and $(RADA)_4S_5$ ([COCH$_3$]-RADARADARADARADASSSSS-[CONH$_2$]) were commercially synthesized and purified by SynBioSci (Livermore, CA) using FMOC amino acid derivatives. High Performance Liquid Chromatography (HPLC) and Mass Spectrometry (MS) were used to determine peptide purity and molecular weight (MW). Attained peptide purity was $\geq$ 95% for all the three peptides, with a calculated MW of 1713.2 for $(RADA)_4$, 2354.7 for $(RADA)_4K_5$ and 2149.3 for $(RADA)_4S_5$, which was very similar to their theoretical molecular weights. These peptides were used without any further purification.

7.2.2 Hydrogel preparation

Peptide solution was prepared by dissolving (RADA)$_4$ peptide powder in syringe-filtered (0.2 μm) MilliQ water. Hydrogels were prepared by sonicating the aqueous peptide stock solution (2510 Branson sonicator, Crystal Electronics, Newmarket, ON) for 15 min at 25°C. Stock solutions were diluted using syringe filtered (0.2 μm) MilliQ water to obtain 5 mg/mL, 6.271 mg/mL, and 6.869 mg/mL concentrations for (RADA)$_4$, (RADA)$_4$S$_5$, and (RADA)$_4$K$_5$, respectively, corresponding to 0.5% (w/v) of (RADA)$_4$ in each gel. Aqueous peptide solutions were diluted with syringe filtered, 10x phosphate buffer (Sigma-Aldrich P7059, pH 7.4), and a final 1x PB (150 mM) solution was obtained. Peptides were allowed to self-assemble at 37°C for 30 min, and stored at 4°C. Prior to use, peptide solutions were sonicated for 30 min at 37°C, pipetted as needed, and rested for at least 30 min to allow time for complete self-assembly [22]. The 25% (RADA)$_4$K$_5$ peptide mixture was made by pipetting, mixing, and lightly vortexing 25% volume (RADA)$_4$K$_5$ and 75% volume (RADA)$_4$. The resulting mixtures were then set undisturbed for at least one hour to ensure successful hydrogel formation. Hydrogels of other percentages of (RADA)$_4$K$_5$ and (RADA)$_4$S$_5$ were formed similarly.

7.2.3 Circular Dichroism

CD spectra were collected (Jasco J-810 spectropolarimeter) over the wavelength range of 180-300 nm. CD protocol was followed as described elsewhere [36], except for the changes mentioned below: Criterion for low wavelength cut-off was kept at HT(V) value of 500 or lower. The spectra were collected on samples prepared by diluting stock peptide solution in water to a working concentration of 0.5% (w/v) with respect to (RADA)$_4$, and analyzed at room

temperature. The structural contents of the peptides in solution were determined using a demountable quartz cuvette (Folio Instruments, Kitchener, ON). The quartz cuvette had a path length of 0.10 mm path length. Spectropolarimeter's scan mode was set to continuous and data pitch of 0.5 nm. Each spectrum taken was the average of ten scans.

$$[\Theta] = \frac{\Theta \times MRW}{c \times l \times 10}$$

Equation 7.1

Where $[\Theta]$ is the molar ellipticity (deg·cm^2/dmol), Θ is the raw ellipticity (m.deg), c is the sample concentration (g/mL), l is the optical path length (cm), and MRW is the mean residue molecular weight (Da). The three simultaneous data acquisition signals were: HT (V), Absorbance and CD (Θ). Background was subtracted from the sample signal, and the resulting CD signal converted to Molar Ellipticity as described elsewhere [37]; the mean residue molecular weight (Da) was obtained by dividing of sample molecular mass in Da with the number of amino acid residues present. The Molar Ellipticity was plotted against Wavelength (nm) for further data analysis.

7.2.4 Plasma Incubation and Total Protein Assay

Each sample was prepared and sonicated at room temperature for 30 minutes to disperse nanofibers. The samples were incubated with one millilitre of 100% plasma in a mechanical agitation bath for two hours at 37°C. Upon completion of incubations, the samples were centrifuged for ten minutes at 15000 rpm and washed three times with one millilitre Phosphate buffer saline for 20 mins on a rocking platform twice. Proteins were eluted off the surface of the

sample using 100 µl of phosphate buffer with two per cent sodium dodecyl sulfate at 50°C for two hours in a mechanical agitation bath.

7.2.5 Total Protein Assay

Proteins concentrations from the elution were determined using Bio-Rad DC Protein Assay Kit (Hercules, CA). Aliquots of five microliters of each eluted protein sample and standard curve sample solutions were prepared and analyzed, in triplicate, at 740 nm (UV/vis).

7.2.6 SDS-PAGE and Immunoblotting

Plasma protein samples were identified using reduced SDS polyacrylamide gel electrophoresis (SDS-PAGE) and immunoblot methods. All equipment was purchased from Bio-Rad (Hercules, CA). Using concentrations, previously determined in the Total Protein Assay, the samples were prepared with 30 µg of proteins per sample, calculated from the total protein assay and the proteins were denatured using 0.5 M β-mercaptoethanol and two per cent SDS. The sample and sample buffer was heated on a heat block for five minutes at 95°C. The samples were run through a 12% separating gel for ~45 minutes at 200 V and 400 mA.

The gel was equilibrated with a transfer buffer (Tris, glycine, methanol and water) for 20 minutes on a rocking platform. A 0.2 µm Immuno-Blot PVDF membrane was cut and also equilibrated for 15 minutes on the rocking platform. Due to the hydrophobicity of the membrane, it was immersed in methanol until the colour was uniform, then rinsed in water three times before put in the transfer buffer. A semidry transfer at 100 V and 200 mA was run for one hour. Membranes were cut into strips for antibody incubations or and the ladders for colloidal gold

staining. The strips were blocked overnight with two millilitres of 10% skim milk powder in 0.3 μl/mL Tween-20 in 0.15 M Tris Buffer Saline (TTBS).

Strips were washed for three times with 0.1% skim milk powder in 0.15 M Tris Buffer Saline (TBS). The strips were then incubated in antibodies (Table 7.1), which were used at concentrations of 1:1000. The colour-developing reagent used was 350 μl of stabilized TMB substrate (Promega, Madison, WI) per strip. The reaction was carried for ten minutes before being quenched by two millilitre of Milli-Q water.

Ladders were blocked on a petri dish with TTBS on a rocking platform for 20 minutes for three separate times. This was followed by two minutes of washing using Milli-Q water. Colloidal Gold Total Protein stain was used to stain the ladders until protein strips became visible. The reaction was allowed to take place, under close observation for one hour on a rocking platform, and then was quenched with Milli-Q water for three separate times for one minute.

7.2.7 Complement C3a activation

Complement C3a studies were performed using platelet-poor human plasma [21]. Plasma (5 μl) was incubated at 37°C with an equal volume of hydrogel for 30 min and then ethylenediaminetetraacetic acid (EDTA at pH 7.4) was added to a final concentration of 18.5 μM for quenching the reaction. 1X PB (pH 7.4) was used as control for the experiments. The samples were stored at -80°C. The samples were thawed briefly at 37°C prior to the assay.

The activation state of complement C3 was investigated using a commercial C3a enzyme immunoassay kit (Quidel, San Diego, CA), following manufacturer's protocols. The assay was

analyzed using a four-parameter curve fit. The experiment was conducted in duplicates and the values are given as the average of two measurements.

7.2.8 **Platelet activation**

Platelet activation studies were carried out as described elsewhere [21, 38]. Blood was drawn using a ten cc syringe into an acid citrate dextrose (ACD) tube (11.5 mM citric acid monohydrate, 88.5 mM trisodium citrate dihydrate, 111 mM dextrose, pH 6.0, anticoagulant at a ratio of 1:9), purchased from Beckton Dickinson (Franklin Lakes, NJ). Platelets were analyzed within two hours. Platelet-rich plasma (PRP) was isolated by centrifuging whole blood at room temperature for 15 min, at 146 X g (Beckman Coulter, Mississauga, ON). PRP (20 μl) was incubated at 37°C with an equal volume of hydrogel for 30 min. The experimental control being platelets exposed to a 1X PBS (pH 7.4) solution. The experiment was conducted in duplicates and the values are given as the average of two measurements (as per the well established CBS protocols).

Platelet activation state was investigated using a Beckman Coulter fluorescence flow cytometer EPICS XL-MCL model (Miami, FL). Five microliters of a platelet agonist such as, thrombin or adenosine diphosphate (ADP) were added to activate platelets as a positive control with five microliters of phycoerythrin (PE) conjugated anti-CD62P antibodies (Immunotech Coulter, Mississauga, ON), and Fluorescein Isothiocynate (FITC) conjugated PAC-1 (Becton Dickinson Immunocytometry Systems, San Jose, CA), respectively. The positive controls also had three microliters of fibrin polymerization inhibitor peptide, GPRP. Three microliters of anti-CD42-PE or anti-CD42-FITC antibodies were used as pan platelet markers. Mouse IgG and IgM

isotypes conjugated to the same chromophore (PE or FITC) were used as the non-specific binding controls. Lastly, 1X PB (pH 7.4) was added to the samples to achieve a final volume of 50 μl, followed by a 30 min incubation in the dark at room temperature. Subsequently, the samples were diluted with one microliter of 1X PB (pH 7.4) for flow cytometric analysis.

Single populations of platelets were substantiated and the gate for the underlying area was selected on the basis of platelet forward scatter (FSC) versus side scatter characteristics (SSC). Five thousand platelet events were collected. Events positive for CD42a or CD42b were monitored to confirm the identity of the platelets. The fluorescence measurement gates were adjusted to include the upper five per cent of signals obtained with the isotype control antibodies. The signals collected within the gates for the test samples were counted as positive events for the antibody marker. Data is reported as the percentage of positive events.

7.2.9 Platelet morphology

Platelet morphology was performed by isolating Platelet Rich Plasma (PRP) as described previously [38]. PRP (15 μl) was incubated at 37°C with an equal volume of hydrogel for 30 minutes. To fix the samples, 30 μl of four per cent paraformaldehyde was added and samples stored at room temperature and analyzed by phase contrast microscopy (Nikon, Mississauga, ON) using a 1000X oil immersion lens. The sample size for analysis was 100 platelets and values were reported as the average of three sets totalling 300 platelets. The platelets were categorized by shape as, discoid, spiny sphere, and balloons [39]. The morphology score was calculated by the modified Kunicki scoring system [39], described in Equation 7.2 below:

$$MS = [(D \times 4) + (S \times 2) + (B \times 1)] \qquad \textbf{Equation 7.2}$$

Where, MS is the morphology score, D is the number of discoid shaped platelets, S is the number of spiny sphere shaped platelets and B is the number of balloon shaped platelets.

7.2.10 **Statistical analysis**

Statistical analyses were performed using VassarStats: Website for Statistical Computation (http://vassarstats.net/). Results are presented as a mean $\pm$ SD. Multiple comparisons between groups were performed by one-way ANOVA followed with Tukey's HSD *post hoc* analysis. Differences were reported as statistically significant at $p<0.05$, and $p<0.01$.

7.3 **Results and Discussion**

7.3.1 **Nanofiber Assembly**

Schematic representation of the $(RADA)_4$ and the two variants used in the study are given in Figure 7.1. Whereas the ionic complementary of the $(RADA)_4$ peptide has been known to form stable secondary structure (β-sheets) of the peptides, imperative for the self-assembling into nanofibers [19, 40], we have previously reported that these secondary structures maintain their integrity at extreme temperatures [22]. We have also reported in-depth biocompatibility analysis of the $(RADA)_4$ peptide at various concentrations [21]. Work done in our lab has also shown that appending five serine residues does lead to similar β-sheet formation, and nanofiber formation as the pristine $(RADA)_4$ peptide, but not $(RADA)_4K_5$ (Figure 7.2). Single molecular studies and circular dichroism concluded that upon combining 75%$(RADA)_4$ with 25%$(RADA)_4K_5$, not only successful nanofiber formation was witnessed, but also $(RADA)_4K_5$ nanofibers interacted with

the (RADA)$_4$ for the formation of higher ordered structure. After establishing successful nanofiber formation with the two variants of (RADA)$_4$ peptide, we are reporting the hemocompatibility assessment of these peptides with the intention of studying the effect of end group chemistry for designing blood contacting biomaterials.
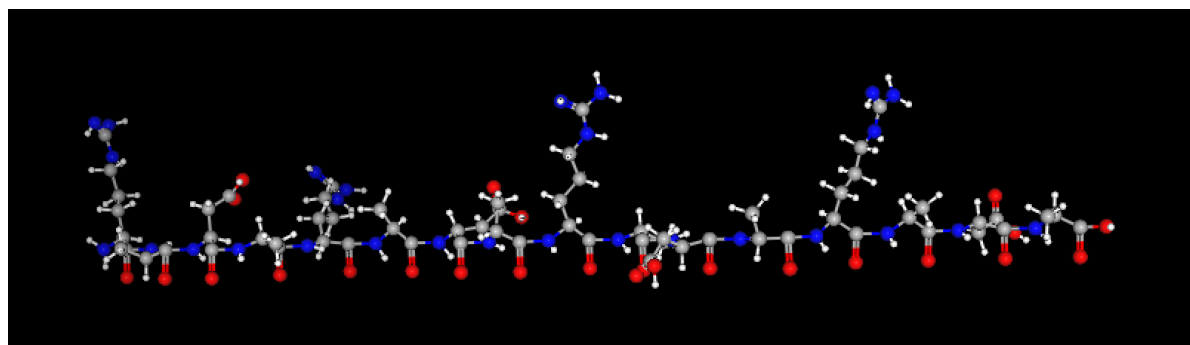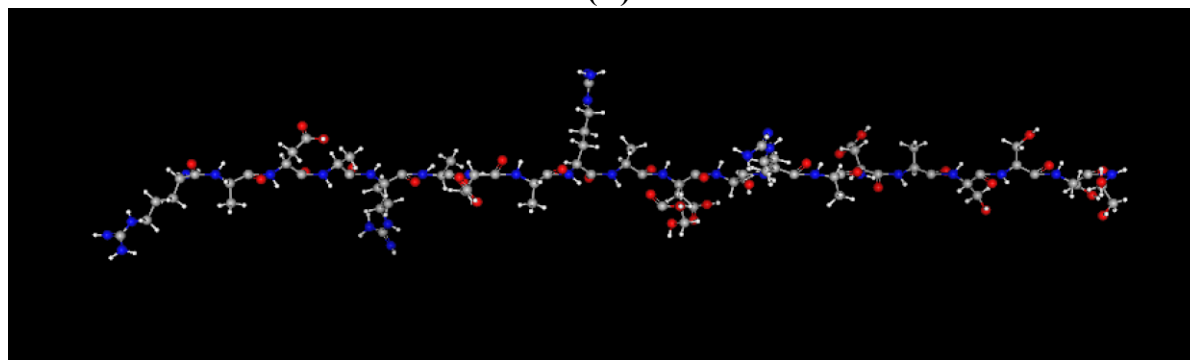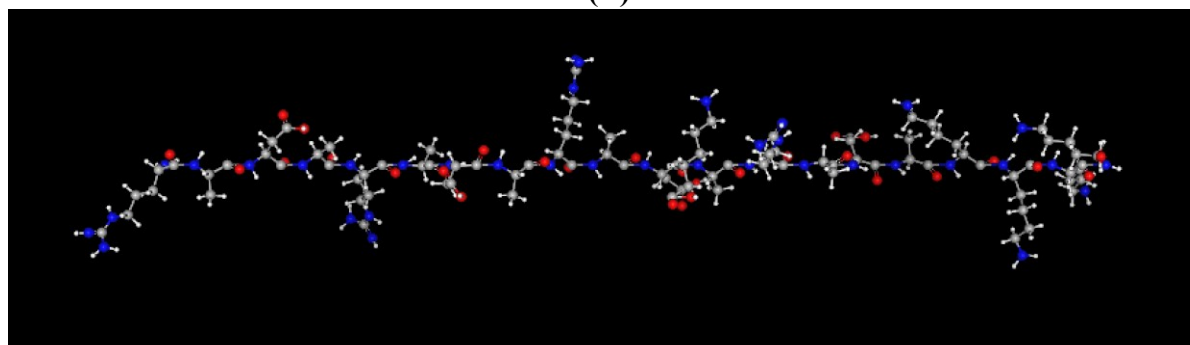
Figure 7.1: Schematic representation of the three dimensional molecular structure of (A) (RADA)₄, (B) (RADA)₄S₅, and (C) (RADA)₄K₅.

Carbon atoms are gray, oxygen atoms are red, nitrogen atoms are blue, and hydrogen atoms are white. The theoretical isoelectric point (pI) for $(RADA)_4$, $(RADA)_4S_5$, and $(RADA)_4K_5$ is 7.14, 6.84, and 11.07, respectively. For a stable β-structure to form, all the hydrophobic alanine side chains face in one direction, and all the aspartic acid and arginine side chains face in another direction to create two distinct faces.
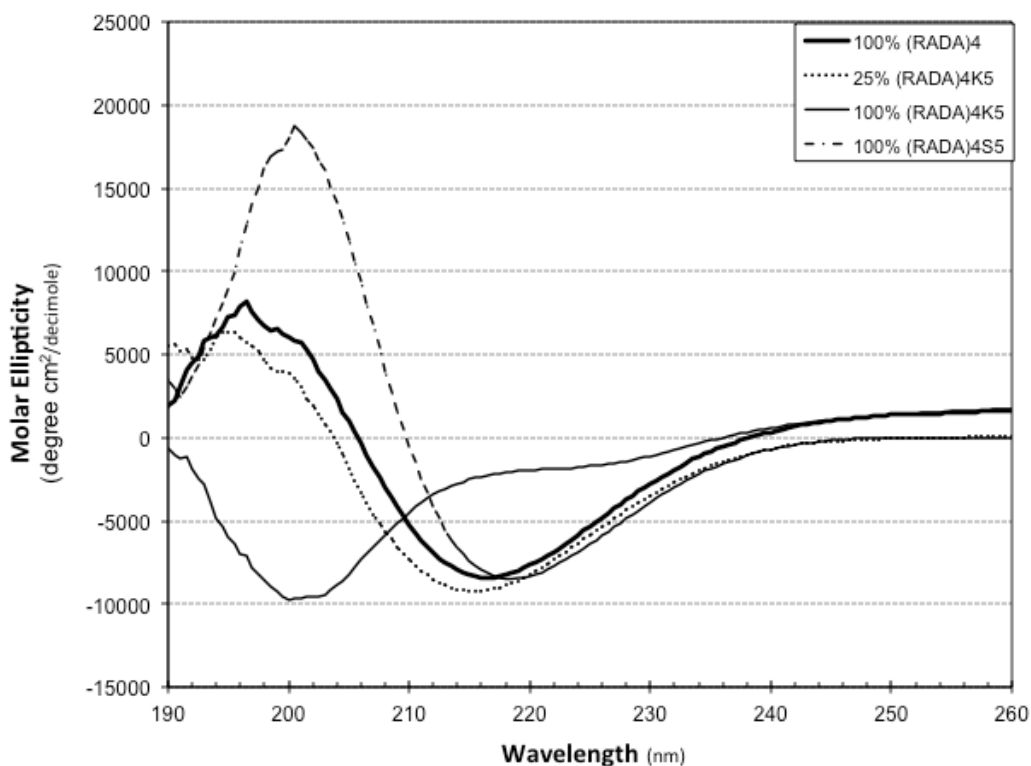
Figure 7.2: CD spectra for peptide solutions of 100% (RADA)₄, 100% and 25%(RADA)₄K₅, and (RADA)₄S₅ at 25°C, such that the final concentration of the (RADA)₄ content in all the solutions was 0.5% (w/v).

The peptides (RADA)$_4$, and (RADA)$_4$S$_5$ displayed a typical β-sheet structure (minimum at 215-216 nm and maximum at ~195-196 nm), whereas the secondary structure for (RADA)$_4$K$_5$ displayed the presence of disordered structures (minimum at 222 nm and 208 nm, and maximum at 190-193 nm). The critical concentration of (RADA)$_4$K$_5$ for successful nanofiber formation is determined as 25%. Data represents the average of five scans, with HT(V) values<500.

7.3.2 *In-vitro* Hemocompatibility Assessment

7.3.2.1 Plasma Protein Adsorption

In order to understand the protein adsorption onto the $(RADA)_4$ and its derivatives total protein adsorption studies were conducted by incubating the $(RADA)_4$, $(RADA)_4K_5$, and $(RADA)_4S_5$ hydrogels with 100% platelet poor plasma for two hours and the total adsorbed proteins were eluted off and determined using the Bio-Rad DC assay. The results showed that all the three peptides demonstrated affinity to certain antibodies. In total, 11 antibodies were detected upon incubation with $(RADA)_4$, while an identical set of 13 antibodies were identified for both $(RADA)_4S_5$, and $(RADA)_4K_5$ peptides. While both the variants of $(RADA)_4$: $(RADA_4K_5$ and $(RADA)_4S_5$ displayed the presence of similar antibodies, the intensity of the bands varied between the samples. For example, the bands for human albumin have a smaller intensity for $(RADA)_4K_5$, whereas larger for $(RADA)_4S_5$.

It can also be concluded from the total protein assay that $(RADA)_4K_5$ resulted in the elution of the least amount of protein, whereas $(RADA)_4S_5$ had the most. The complete list of plasma proteins screened for are listed in Table 7.2. It should be noted that these immunoblotting technique could determine the presence or absence of the protein; but not the conformation. It has been proven that along with the presence of a protein, its conformation significantly affects its cellular interactions [41].

Table 7.1: Antibodies investigated during immunoblotting

Antibody	Host	Protein MW (kDa)	Source
Kininogen (light chain)	Mouse	50	US Biological, Swampscott, MA, USA
Kininogen (heavy chain)	Mouse	88-120	US Biological, Swampscott, MA, USA
Factor I	Mouse	88	Cedarlane Laboratories, Hornby, Ontario, Canada
Fibrinogen	Rabbit	340	Calbiochem, Gibbstown, NJ, USA
Fibronectin	Rabbit	440	Cedarlane Laboratories, Hornby, Ontario, Canada
Hemoglobin	Rabbit	68	Sigma-Aldrich, St. Louis, MO, USA
a_1-Antitrypsin	Sheep	47	Cedarlane Laboratories, Hornby, Ontario, Canada
Thrombin	Sheep	36	Cedarlane Laboratories, Hornby, Ontario, Canada
Prothrombin	Sheep	72	Cedarlane Laboratories, Hornby, Ontario, Canada
Protein C	Sheep	62	Cedarlane Laboratories, Hornby, Ontario, Canada
Vitronectin	Sheep	75	Cedarlane Laboratories, Hornby, Ontario, Canada
Protein S	Sheep	69	Cedarlane Laboratories, Hornby, Ontario, Canada
Prekallikrein	Sheep	85	Cedarlane Laboratories, Hornby, Ontario, Canada
Antithrombin	Sheep	53	Cedarlane Laboratories, Hornby, Ontario, Canada
IgG	Goat	174	Sigma-Aldrich, St. Louis, MO, USA
Human Albumin	Goat	66	OEM Concepts, Saco, ME, USA
Plasminogen	Goat	90	Cedarlane Laboratories, Hornby, Ontario, Canada
Complement Factor 3 (C3)	Goat	185	Calbiochem, Gibbstown, NJ, USA
Factor XII	Goat	80	Cedarlane Laboratories, Hornby, Ontario, Canada
Factor XI	Goat	160	Cedarlane Laboratories, Hornby, Ontario, Canada
Apolipoprotein A1	Goat	28	Sigma-Aldrich, St. Louis, MO, USA
Transferrin	Goat	77	Sigma-Aldrich, St. Louis, MO, USA
a_1-Macroglobulin	Goat	718	Sigma-Aldrich, St. Louis, MO, USA

Table 7.2: Total protein assay and western blotting analysis

	(RADA)$_4$	25% (RADA)$_4$K$_5$	25% (RADA)$_4$S$_5$
Amount of Eluted Protein (µg)	108 $\pm$ 6	90.6 $\pm$ 3	129 $\pm$ 2
Proteins Detected	Fibrinogen	Fibrinogen	Fibrinogen
	Prothrombin	Prothrombin	Prothrombin
	Vitronectin	Vitronectin	Vitronectin
	Antithrombin	Antithrombin	Antithrombin
	IgG	IgG	IgG
	Human Albumin	Human Albumin	Human Albumin
	C3	C3	C3
	Factor XI	Factor XI	Factor XI
	β-Lipoprotein	β-Lipoprotein	β-Lipoprotein
	Transferrin	Transferrin	Transferrin
	α$_2$-Macroglobulin	α$_2$-Macroglobulin	α$_2$-Macroglobulin
		α$_1$-Antitrypsin	α$_1$-Antitrypsin
		Plasminogen	Plasminogen

The difference in adsorption of these peptides can be influenced by a variety of factors, primarily based on their different end group chemistries. Two proteins (plasminogen and α$_1$-Antitrypsin) which were eluted upon exposure to 25%(RADA)$_4$K$_5$ and 25%(RADA)$_4$S$_5$, were absent in the pristine (RADA)$_4$ peptide. We hypothesize that this difference is due to the packing density

variation of the peptide, as 25%(RADA)$_4$S$_5$ and (RADA)$_4$ share the same net charge, and similar

secondary structure formation. Moreover, lysine is a well-known ligand for both tissue

plasminogen activator (t-PA), and plasminogen [42], whereas the later has the potential for clot

dissolution if converted to plasmin. The basic mechanism of fibrinolysis consists of binding of

plasminogen and t-PA to fibrin by interactions with terminal lysine residues (as found in

(RADA)$_4$K$_5$), where plasminogen, t-PA, and fibrin form a ternary complex [43]. The t-PA

induced plasminogen to plasmin conversion occurs 1000 times faster on the surface of fibrin than

in plasma [44], which is thought to be due to specific interactions with lysine residues [23]. In

this initial work assessing total protein adsorption to (RADA)$_4$ hydrogels, we found plasmin

adsorption to the (RADA)$_4$S$_5$ hydrogels as well. Further quantitative plasminogen adsorption

analysis should be conducted to assess lysine interaction with the (RADA)$_4$ based hydrogels.

Control release kinetics [45] of various proteins with different molecular weights loaded

onto the (RADA)$_4$ hydrogels concluded that the release was governed by diffusion, where the

diffusion coefficients were dependent on the molecular weight of proteins and the concentration

of peptide used to form the geometrically uniform hydrogel. Even though the study used a higher

concentration of the (RADA)$_4$ peptide (1.0%(w/v)), it was observed that the proteins with a high

molecular weight (IgG, MW: 150 kDa), was released more slowly than with a lower molecular

weight (Lysozyme, MW: 14.5 kDa). The study also concluded that the charge interaction

between proteins and the peptide scaffolds did not play a major role in the release kinetics of the

entrapped proteins [45], and the present study also suggests that the protein adsorption is not

dependent on the peptide charge (Table 7.2). The current knowledge provided *via* these

experiments would provide information on how proteins react to these self-assembling peptides,

when they are presented in the human system. This information along with platelet and complement activation will provide combined deimmunization, which can be applied to better designing these peptides with the goal to reduce potential immune responses without losing the efficacy of these peptides.

7.3.2.2 Complement C3a Activation

Along with platelet activation, complement activation plays an important role in directing body's defence mechanism. Free hydroxyl groups are attributed to high complement activation [46], and it has been suggested [47] that the hydroxyl group activates complement *via* the alternative pathway. The proposed and well accepted activation mechanism [48] of the complement system on surfaces bearing –OH groups are as following: Upon C3 hydrolysis to C3a in plasma, the thioester group in the C3b molecule is exposed to its surface, consequently reacting with the nucleophilic hydroxyl group on the surface. This process further amplifies the complement activation and triggers the complement loop activation *via* the alternative pathway. However, the studies in our lab showed $(RADA)_4$ peptide consisting of (-OH containing) serine groups elicited comparably higher C3a activation when compared with pristine $(RADA)_4$ ($p>0.05$), but was statistical significantly lower than $(RADA)_4K_5$ ($p<0.05$). Hence, consistent with the previous studies [47], despite the donor to donor variability the free hydroxyl groups appended to the $(RADA)_4$ peptide activated more C3a, than the pristine peptide. However, the difference was not statistically significant.
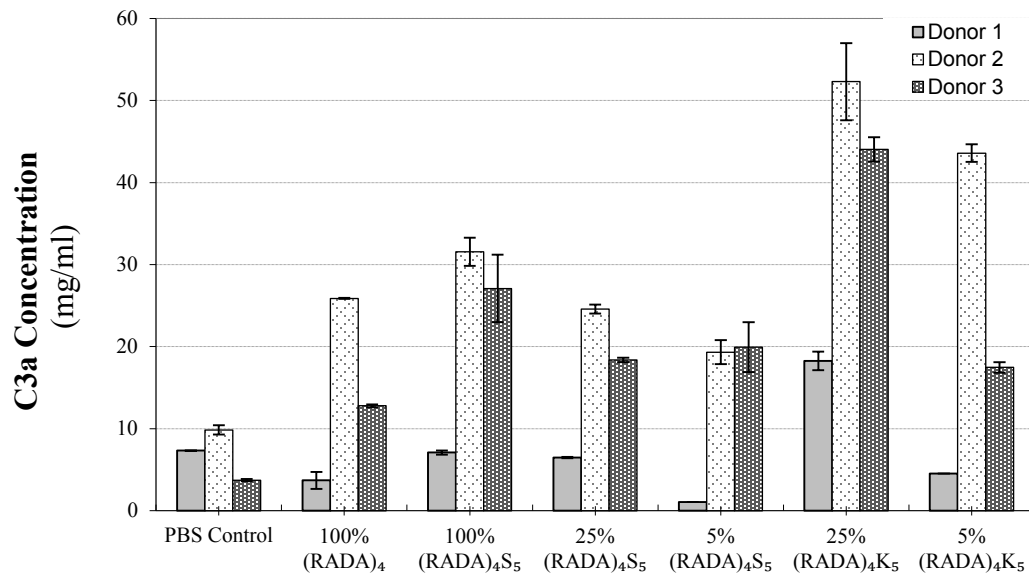
Figure 7.3: Release of C3a-desArg in human platelet poor plasma (PPP) exposed to (RADA)₄ based hydrogels systems in PB (pH 7.4).

Human PPP incubated with PBS (pH 7.4) is used as a control. The PBS control indicates background signal obtained with buffer blank. Experiments were repeated two times for each system using the same-pooled plasma from three healthy unmedicated donors, as per the standard CBS protocols.

It can be postulated that despite the presence of –OH groups, the different underlying polymer structures in both of the studies played a role in activating complement to different levels. In agreement with our theory, Labarre and colleagues [49] also found that not only the density of the –OH surface groups plays an important part in complement activation, but the underlying polymer also plays an important part. Further studies have explored the effect of amino ($-NH_2$), methyl ($-CH_3$), and carboxyl (-COOH), in addition to the hydroxyl (-OH) group have on the activating complement. It was found that among these groups –OH group elicited the

most complement, whereas all the other functional groups had low complement activation *via* either the classical or the alternative pathways.

It was postulated that the $-NH_3$ group, would elicit similar level of complement activation as the $-OH$ group, as both share nucleophilic characteristics. Low molecular weight amines in blood were found to react with thioester group of C3 [50], and C3b [51]. Studies in our lab also showed significantly high complement activation with $(RADA)_4$ consisting of $-NH_3$ group bearing lysine residues. Consistent with these observations (despite donor to donor variability) the present study resulted in an overall trend for C3a activation as: $(RADA)_4K_5 >> (RADA)_4S_5 > (RADA) >$ PBS control

Arima and colleagues [47] found that amount of C3a released into serum after exposure to amine group bearing self-assembling monolayer was much lower than the one with $-OH$ group. Toda and colleagues [52] also found no complement activation with amine groups. The authors [52] proposed that under physiological pH the positively charged amino group attracts various negatively charged serum proteins (such as albumin), forming a layer of proteins adsorbed to the surface through electrostatic interactions. The protein layer interrupts access of C3b to the surface amino groups, and hence, failing in the formation of C3 convertase. It has been concluded that the behaviour of complement system in the presence of the amino groups is still poorly understood; and hence, more systematic study with one consistent underlying polymer needs to be conducted to investigate the complement response further.

7.3.2.3 Platelet Activation

Platelet activation is one of the initial steps for thromboembolic complications in blood-contacting biomaterials. Presently, there is no single commonly accepted testing method to assess platelet activation with biomaterials *in-vitro*. In this study, two commonly used platelet activation marker antibodies, CD62P (platelet surface P-selectin) and PAC-1 (activated GPIIb/IIIa) were studied using flow cytometry.

Platelet driven physiologic hemostasis plays a critical role in pathological thrombosis [53, 54], ultimately leading to the blood contacting device malfunction. Flow cytometry is a gold standard hemocompatibility method to monitor platelet activation in whole blood [15], through the measurement of platelet microparticle generation, CD62P (platelet surface P-selectin) expression, and activated glycoprotein (GP) IIb/IIIa expression [33].

The effect of changing the end-group chemistries on the expression of two-platelet activation markers (CD62P and PAC-1) *in-vitro* is presented in Figure 7.4 and Figure 7.5. With both CD62P and PAC-1 expression, the negative control reported the lowest platelet activation, whereas the positive controls had the highest, proving the viability of the assay itself.
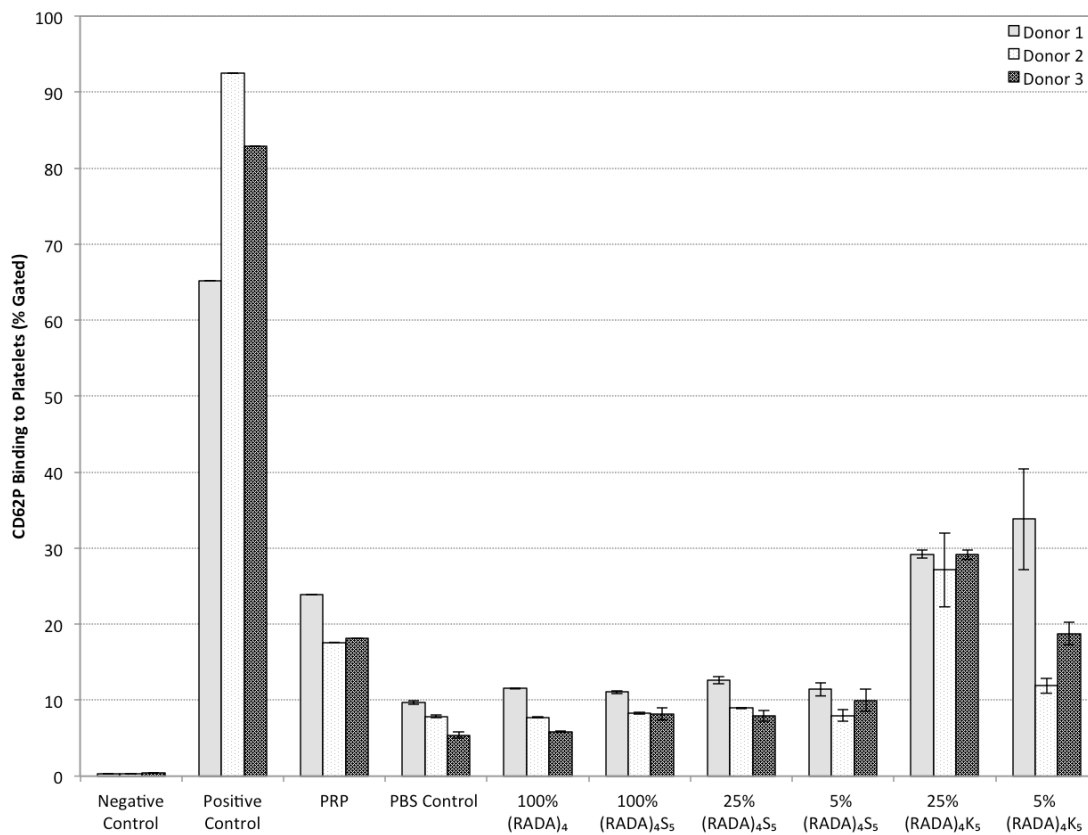
Figure 7.4: Platelet activation markers CD62P for the (RADA)₄ hydrogels based systems.

Data represent percentage of 5000 platelet count.
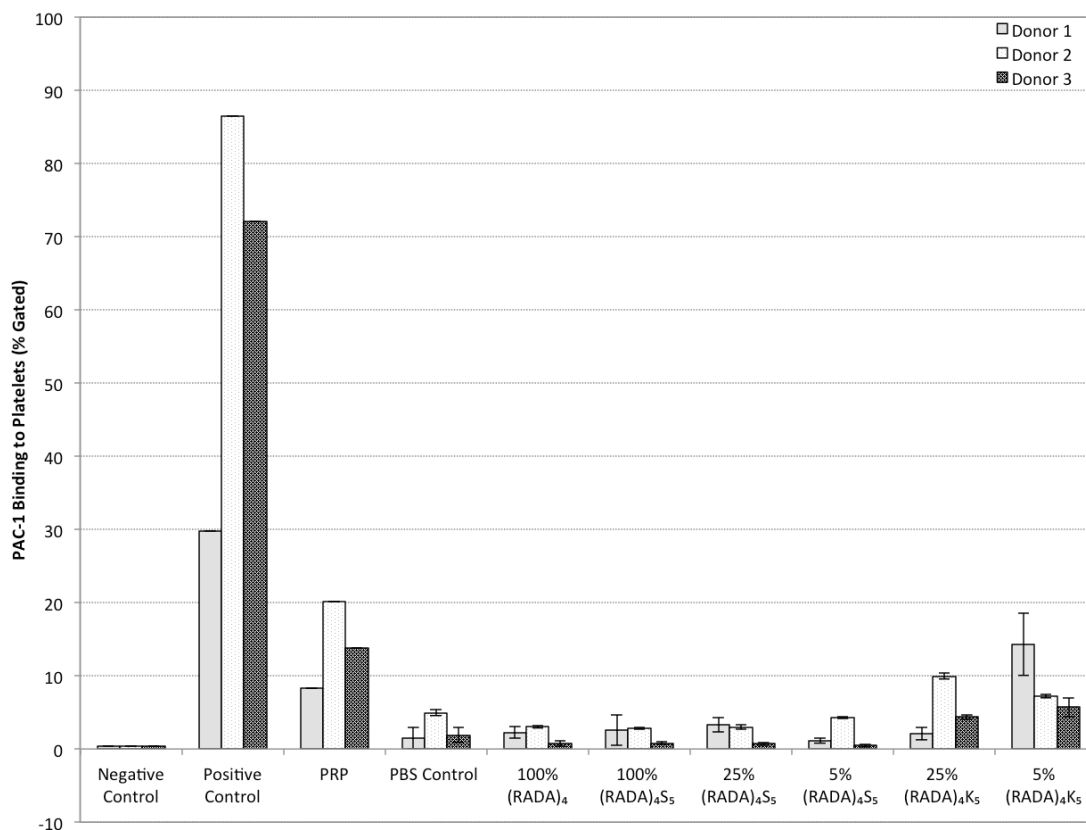
Figure 7.5: Platelet activation markers PAC-1 for the (RADA)$_4$ hydrogels based systems.
Data represent percentage of 5000 platelet count.

CD62P activation upon exposure to (RADA)$_4$ and its variants are reported in Figure 7.4. All the peptides, except for (RADA)$_4$K$_5$ elicited comparable and spastically insignificant CD62P exposure as with the PBS control. No dose dependency can be seen with either the (RADA)$_4$K$_5$ or with (RADA)$_4$S$_5$ peptides. Despite donor to donor variability the overall trend for CD62P expression is as following: (RADA)$_4$K$_5$> (RADA)$_4$S$_5$ > (RADA)$_4$ (Tukey post hoc P<0.01), whereas the platelet activation with respect to (RADA)$_4$ and PBS control was not statistically different.

The PAC-1 expression (Figure 7.5) of the peptides revealed an overall trend similar to that of CD62P: $(RADA)_4K_5 > (RADA)_4S_5 > (RADA)_4$ however, statistics proved no significant difference among platelet activation detected by PAC-1 ($P>0.05$). It should be noted that the overall trend of the platelet activation is similar with both of the activation markers, however PAC-1 expression is known to show high variability, and is considered lesser attractive choice while analyzing platelet activation [55].

7.3.2.4 Platelet Morphology

Platelets respond to external stimuli (such as biomaterials) by altering their shape from the resting, normal discoid form, into more rounded structures possessing blebs and multiple pseudopodia [56]. Platelet morphology was assessed using a modified Kunicki scoring system [57], where platelets are categorized by shape as discoid, spiny spheres, or balloons. An overall Kunicki morphology score of above 385 was achieved for the all peptides (Table 7.3), where a score of less than 200 represent poor retention of morphological characteristics associated with platelets that are activity. Low platelet activation (Figure 7.4, and Figure 7.5), and platelet morphology score (Table 7.3), together suggest that the platelets are only marginally perturbed from their quiescent state with respect to all the peptide systems.

Table 7.3: Kunicki morphology score for the (RADA)$_4$ based hydrogel systems

Gel Type	Morphology Score (MS)
PBS Control	397.33 ± 1.2
100% (RADA)$_4$	393.33 ± 6.4
100% (RADA)$_4$S$_5$	386.33 ± 7.4
25% (RADA)$_4$S$_5$	396.00 ± 2.0
5% (RADA)$_4$S$_5$	393.67 ± 4.5
25% (RADA)$_4$K$_5$	392.00 ± 2.0
5% (RADA)$_4$K$_5$	395.67 ± 1.2
PBS Control	397.33 ± 1.2

7.4 Concluding Remarks

The present study provided the *in-vitro* hemocompatibility assessment of (RADA)$_4$ peptide and its variants. (RADA)$_4$K$_5$ peptide displayed a significant difference in complement activation, when compared to both (RADA)$_4$S$_5$, and pristine (RADA)$_4$ peptide. The high complement activation may pertain to the free NH$_3$ groups present in the (RADA)$_4$K$_5$ peptides, as well as due to the steric hindrance provided by the long side chain of this peptide in nanofiber packing. While the *in-vitro* measurements of PAC-1 and CD62P binding has provided valuable information regarding the (RADA)$_4$ based nanofibers, further studies are needed to further establish the correlation between *in-vitro* platelet activation and (RADA)$_4$ induced *in-vivo* thrombosis. Even though the CD62P and PAC-1 showed different levels of platelet activation, overall the trend remained consistent: (RADA)$_4$K$_5$ activated the platelets to the highest, whereas (RADA)$_4$S$_5$, and (RADA)$_4$ showed comparable platelet activation. However, it should be noted that both the platelet and complement activation by these peptides was lower than the already considered hemocompatible biopolymers. Hence, (RADA)$_4$ based hydrogels are not only

hemocompatible, but have also displayed a great promise as means of achieving hemostasis without any potential side effects; and hence can potentially revolutionize controlled bleeding in surgical procedures.

Acknowledgements

Conflicts of interest

The authors have no conflicts of interest to declare.

References

[1] Evans JA, van Wessem KJP, McDougall D, Lee KA, Lyons T, Balogh ZJ. Epidemiology of Traumatic Deaths: Comprehensive Population-Based Assessment. World JSurg 2010;34:158-63.

[2] Bellamy RF. The causes of death in conventional land warfare- implications for combat casualty care research. Military Medicine 1984;149:55-62.

[3] Sauaia A, Moore FA, Moore EE, Moser KS, Brennan R, Read RA, et al. Epidemiology of trauma deaths - a reassessment. J Trauma-Injury Inf Crit Care 1995;38:185-93.

[4] Mannucci PM, Levi M. Drug therapy: Prevention and treatment of major blood loss. N Engl J Med 2007;356:2301-11.

[5] Ellis-Behnke R. At the nanoscale: nanohemostat, a new class of hemostatic agent. Wiley Interdisciplinary Reviews: Nanomedicine and Nanobiotechnology 2011;3:70-8.

[6] Wortham L. Hemorrhage control in the battlefield: role of new hemostatic agent. Military medicine 2005;170:1004-ii; author reply ii, .

[7] Schonauer C, Tessitore E, Barbagallo G, Albanese V, Moraci A. The use of local agents: bone wax, gelatin, collagen, oxidized cellulose. European Spine Journal 2004;13:S89-S96.

[8] Hoffman M. The cellular basis of traumatic bleeding. Military medicine 2004;169:5-4.

[9] Petersen B, Barkun A, Carpenter S, Chotiprasidhi P, Chuttani R, Silverman W, et al. Tissue adhesives and fibrin glues. Gastrointest Endosc 2004;60:327-33.

[10] Alam HB, Koustova E, Rhee P. Combat casualty care research: From bench to the battlefield. World JSurg 2005;29:S7-S11.

[11] Farrior E, Ladner K. Platelet Gels and Hemostasis in Facial Plastic Surgery. Facial Plast Surg 2011;27:308-14.

[12] Konturek SJ, Pawlik W. Physiology and pharmacology of prostaglandins. Dig Dis Sci 1986;31:S6-S19.

[13] Greer IA. Therapeutic progress review .28. Platelet function and calcium channel blocking agents. J Clin Pharm Ther 1987;12:213-22.

[14] Pallapies D. Vasoactive drugs affecting the prostaglandin systems. Wien Klin Wochen 1992;104:521-5.

[15] Alam HB, Burris D, DaCorta JA, Rhee P. Hemorrhage control in the battlefield: Role of new hemostatic agents. Military Medicine 2005;170:63-9.

[16] Ellis-Behnke RG, Liang Y-X, David KC, Kau PWF, Schneider GE, Zhang S, et al. Nano hemostat solution: immediate hemostasis at the nanoscale. Nanomedicine-Nanotechnology Biology and Medicine 2006;2:207-15.

[17] Zou Z, Zheng Q, Wu Y, Guo X, Yang S, Li J, et al. Biocompatibility and bioactivity of designer self-assembling nanofiber scaffold containing FGL motif for rat dorsal root ganglion neurons. Journal of Biomedical Materials Research Part A 2010;95A:1125-31.

[18] Ye Z, Zhang H, Luo H, Wang S, Zhou Q, Du X, et al. Temperature and pH effects on biophysical and morphological properties of self-assembling peptide RADA16-1. Journal of Peptide Science 2008;14:152-62.

[19] Zhang S, Holmes T, Lockshin C, Rich A. Spontaneous assembly of a self-complementary oligopeptide to form a stable macroscopic membrane. Proceedings of the National Academy of Sciences 1993;90:3334-8.

[20] Zhang SG, Lockshin C, Cook R, Rich A. Unusually stable beta-sheet formation in an ionic self-complementary oligopeptide. Biopolymers 1994;34:663-72.

[21] Saini A, Serrano K, Koss K, Unsworth LD. Evaluation of the hemocompatibility and rapid hemostasis of (RADA)4 peptide-based hydrogels. Acta Biomaterialia 2016;31:71-9.

[22] Saini A, Koss K, Unsworth LD. Effect of Peptide Concentration on Water Structure, Morphology, and Thermal Stability of Self-Assembling (RADA)(4) Peptide Matrices. Journal of Biomaterials and Tissue Engineering 2014;4:895-905.

[23] Brash JL. Exploiting the current paradigm of blood-material interactions for the rational design of blood-compatible materials. J Biomater Sci-Polym Ed 2000;11:1135-46.

[24] Haycox CL, Ratner BD. In-vitro platelet interactsions in the whole human blood exposed to biomaterial sufraces - insights on blood compatibility. Journal of Biomedical Materials Research 1993;27:1181-93.

[25] Ratner BD, Hoffmann A, Schoen F J, Lemons JE. Biomaterials Science, An Introduction to Materials in Medicine. 2nd ed2004.

[26] Sefton MV, Gemmell CH, Gorbet MB. What really is blood compatibility? Journal of Biomaterials Science-Polymer Edition 2000;11:1165-82.

[27] Esmon CT. The impact of the inflammatory response on coagulation. Thrombosis Research 2004;114:321-7.

[28] Wojta J, Huber K, Valent P. New aspects in thrombotic research: Complement induced switch in mast cells from a profibrinolytic to a prothrombotic phenotype. Pathophysiology of Haemostasis and Thrombosis 2003;33:438-41.

[29] Wojta J, Kaun C, Zorn G, Ghannadan M, Hauswirth AW, Sperr WR, *et al*. C5a stimulates production of plasminogen activator inhibitor-1 in human mast cells and basophils. Blood 2002;100:517-23.

[30] Janatova J. Activation and control of complement, inflammation, and infection associated with the use of biomedical polymers. Asaio J 2000;46:S53-S62.

[31] Walport MJ. Advances in immunology: Complement (Second of two parts). N Engl J Med 2001;344:1140-4.

[32] Walport MJ. Advances in immunology: Complement (First of two parts). N Engl J Med 2001;344:1058-66.

[33] Daugirdas JT, Bernardo AA. Hemodialysis effect on platelet count and function and hemodialysis-associated thrombocytopenia. Kidney International 2012;82:147-57.

[34] Savi P, Chong BH, Greinacher A, Gruel Y, Kelton JG, Warkentin TE, *et al*. Effect of fondaparinux on platelet activation in the presence of heparin-dependent antibodies: a blinded comparative multicenter study with unfractionated heparin. Blood 2005;105:139-44.

[35] Calvete JJ. Clues for understanding the structure and function of a prototypic human integrin- the platelet glycoprotein IIB/IIIA complex. Thrombosis and haemostasis 1994;72:1-15.

[36] Greenfield NJ. Using circular dichroism spectra to estimate protein secondary structure. Nature Protocols 2006;1:2876-90.

[37] Snatzke G. Circular Dichroism: Principles and Applications. New York: VCH Publishers; 1994. p. 59-84.

[38] Levin E, Jenkins C, Culibrk B, Gyongyossy-Issa MIC, Serrano K, Devine DV. Development of a quality monitoring program for platelet components: a report of the first four years' experience at Canadian Blood Services. Transfusion;52:810-8.

[39] Kunicki TJ, Tuccelli M, Becker GA, Aster RH. Study of variables affecting quality of platelets stored at room-temperature. Transfusion 1975;15:414-21.

[40] Zhang SG, Holmes TC, Dipersio CM, Hynes RO, Su X, Rich A. Slef complementary oligopeptide matrices support mammalian-cell attachment. Biomaterials 1995;16:1385-93.

[41] Sivaraman B, Latour RA. The Adherence of platelets to adsorbed albumin by receptor-mediated recognition of binding sites exposed by adsorption-induced unfolding. Biomaterials 2010;31:1036-44.

[42] Deutsch DG, Mertz ET. Plasminogen-purification from human plasma by affinity chromatography. Science 1970;170:1095.

[43] Collen D, Lijnen HR. Molecular basis of fibrinolysis as relevant for thrombolytic therapy. Thrombosis and Haemostasis 1995;74:167-71.

[44] Hoylaerts M, Rijken DC, Lijnen HR, Collen D. Kinetics of the activation of plasminogen by human tissue plasminogen actibator - role of fibrin. Journal of Biological Chemistry 1982;257:2912-9.

[45] Koutsopoulos S, Unsworth LD, Nagai Y, Zhang S. Controlled release of functional proteins through designer self-assembling peptide nanofiber hydrogel scaffold. Proceedings of the National Academy of Sciences 2009;106:4623-8.

[46] Sperling C, Schweiss RB, Streller U, Werner C. In vitro hemocompatibility of self-assembled monolayers displaying various functional groups. Biomaterials 2005;26:6547-57.

[47] Arima Y, Toda M, Iwata H. Surface plasmon resonance in monitoring of complement activation on biomaterials. Advanced Drug Delivery Reviews 2011;63:988-99.

[48] Nilsson B, Ekdahl KN, Mollnes TE, Lambris JD. The role of complement in biomaterial-induced inflammation. Mol Immunol 2007;44:82-94.

[49] Labarre D, Laurent A, Lautier A, Bouhni S, Kerbellec L, Lewest JM, et al. Complement activation by substituted polyacrylamide hydrogels for embolisation and implantation. Biomaterials 2002;23:2319-27.

[50] Pangburn MK, Mullereberhard HJ. Relation of a putative thioester bond in C-3 to activation of the alternative pathway and the binding of the C3B to biological targets of complement. Journal of Experimental Medicine 1980;152:1102-14.

[51] Sim RB, Sim E. Autolytic gragmentation of complement components C-3 and C-4 and its relationship to covalent binding activity. Annals of the New York Academy of Sciences 1983;421:259-76.

[52] Toda M, Iwata H. Effects of Hydrophobicity and Electrostatic Charge on Complement Activation by Amino Groups. ACS Appl Mater Interfaces 2010;2:1107-13.

[53] Gresele P, Agnelli G. Novel approaches to the treatment of thrombosis. Trends Pharmacol Sci 2002;23:25-32.

[54] Snyder TA, Watach MJ, Litwak KN, Wagner WR. Platelet activation, aggregation, and life span in calves implanted with axial flow ventricular assist devices. Ann Thorac Surg 2002;73:1933-8.

[55] Lu Q, Malinauskas RA. Comparison of Two Platelet Activation Markers Using Flow Cytometry After In Vitro Shear Stress Exposure of Whole Human Blood. Artificial Organs 2011;35:137-44.

[56] Goodman SL. Sheep, pig, and human platelet-material interactions with model cardiovascular biomaterials. Journal of Biomedical Materials Research 1999;45:240-50.

[57] Kunicki TJ, Tuccelli M, Becker GA, Aster RH. Study of variables affecting quality of platelets stored at room-temperature. Transfusion 1975;15:414-21.

Chapter 8

Conclusion and Recommendations

8.1 Summary and outlook

The present chapter summarizes the significant findings in the experiments presented in the preceding chapters, as well as how the conclusions addressed the aforementioned hypothesis. In this dissertation, type I $(RADA)_4$ peptide (with alternating positive, and negative charges) was used, and its physicochemical characteristics were altered to generate hydrogels with varying characteristics. By pursuing this approach, the fundamental chemical forces responsible for this peptide's self-assembly were studied, as well as *in-vitro* behaviour of these peptides were investigated for the purpose of being used in regenerative medical applications.

The major conclusions from this work are:

- Successful nanofiber formation was observed in the $(RADA)_4$ and $(RADA)_4S_5$ but not in $(RADA)_4K_5$.

- Hydration state analysis revealed that the modified peptide with the lysine residues had the highest amount (15.2%) of non-freezing water content, suggesting that the bound

water content in the hydrogel may play a significant role in protein adsorption and platelet activation of the hydrogels.

- $(RADA)_4K_5$ displayed significant activation of the platelets in a dose dependent manner for both CD62 and PAC-1. Whereas, $(RADA)_4$ and $(RADA)_4S_5$ systems have comparable activity to negative control; possibly due to high hydration and a net zero surface charge.

- Morphology score of 385 and above was achieved for all the systems, implying a high platelet survival upon the treatment with hydrogels.

- In comparison with the negative controls, all the hydrogel systems displayed a high C3a activation. $(RADA)_4S_5$ activated more of C3a when compared with the rest; possibly due to the available free hydroxyl groups.

- Although work is on-going, it is apparent that peptide chemistry is pivotal in directing the self-assembly process, nanofiber hydration state, and platelet and complement activation.

8.2 Future Recommendations

Future studies involving the $(RADA)_4$ peptide should be conducted by systematically varying the composition and sequence of these amino acids to further enhance the knowledge of self-assembly in ionic-complementary peptides. As discussed in the section 3.9.1.3, several methodologies for the assessment of platelet function exist. Even though, flow cytometry is currently considered a gold standard to for the primary assessment of platelets, and provides relevant and significant *in-vitro* platelet analysis, the method is limited due to its physiological relevance (due to the lack of shear force). Hence, the future studies of platelet assessment using

the cone and plate technique (to mimic the shear forces occurring in the vascular bed) would provide additional complementary knowledge along with the current flow cytometry assays.

Since conducting the C3a ELISA with plasma and serum seems to provide different aspects of coagulation cascade; we recommend conducting the assay with serum (and comparing the results with that of plasma), as the serum environment can elucidate natural mechanism of interaction between the complement system and the nanofibers. Moreover, as the complement activation varies among different kind of nanofibers, it may have potential detrimental effects for the patients, hence animal *in-vivo* studies to assess their biocompatibility is imperative for their human blood applications.

Further studies to analyze inflammation markers upon the contact with these nanofiber systems should be conducted. Various cell lines can also be tested with the hydrogel systems to study the cell viability, and differentiation. More studies can be conducted to study the toxicity of the byproducts of all the three hydrogel systems mentioned here.

The work presented in this dissertation has contributed to expand the application of (RADA)$_4$ based peptide amphiphiles and the information gained can be transferred to engineer other biomaterials for blood contacting purposes. The thermodynamic analysis involving water interaction with these peptides has never been done before; hence this information would provide valuable insight in studying protein interaction with hydrated amphiphilic peptide based nanofibers. Also, till now there has not been any systematic study conducted to understand how these peptides interact with biological systems; therefore the present work not only provide in-depth hemocompatibility assessment of these peptides, but also provided knowledge base in

understanding how these systems interact with the human biological environment at a microscopic level. Continuing assessment of these self-assembling peptides, as well as *in-vivo* experiments are still required to explore their full potential.

All truths are easy to understand once they are discovered; the point is to discover them.

- Galileo Galilei

References

Abraham S, So A, Unsworth LD. Poly(carboxybetaine methacrylamide)-Modified Nanoparticles: A Model System for Studying the Effect of Chain Chemistry on Film Properties, Adsorbed Protein Conformation, and Clot Formation Kinetics. Biomacromolecules 2011;12:3567-80.

Aghdam RM, Najarian S, Shakhesi S, Khanlari S, Shaabani K, Sharifi S. Investigating the effect of PGA on physical and mechanical properties of electrospun PCL/PGA blend nanofibers. J. Appl. Polym. Sc.i 2012;124:123-31.

Ahmed TAE, Dare EV, Hincke M. Fibrin: A versatile scaffold for tissue engineering applications. Tissue Eng Part B-Rev 2008;14:199-215.

Alam HB, Burris D, DaCorta JA, Rhee P. Hemorrhage control in the battlefield: Role of new hemostatic agents. Military Medicine 2005;170:63-9.

Alam HB, Koustova E, Rhee P. Combat casualty care research: From bench to the battlefield. World JSurg 2005;29:S7-S11.

Allen P, Melero-Martin J, Bischoff J. Type I collagen, fibrin and PuraMatrix matrices provide permissive environments for human endothelial and mesenchymal progenitor cells to form neovascular networks. J Tissue Eng Regen Med 2011;5:E74-E86.

Allison DD, Grande-Allen KJ. Review. Hyaluronan: A powerful tissue engineering tool. Tissue Eng 2006;12:2131-40.

Alsberg E, Anderson KW, Albeiruti A, Franceschi RT, Mooney DJ. Cell-interactive alginate hydrogels for bone tissue engineering. J Dent Res 2001;80:2025-9.

Alsberg E, Anderson KW, Albeiruti A, Rowley JA, Mooney DJ. Engineering growing tissues. Proceedings of the National Academy of Sciences of the United States of America 2002;99:12025-30.

Altman GH, Diaz F, Jakuba C, Calabro T, Horan RL, Chen JS, *et al.* Silk-based biomaterials. Biomaterials 2003;24:401-16.

Amara U, Rittirsch D, Flierl M, Bruckner U, Klos A, Gebhard F, *et al.* Interaction Between the Coagulation and Complement System. In: Lambris JD, editor. Current Topics in Complement 2008. p. 71-9.

Andersson J, Ekdahl KN, Lambris JD, Nilsson B. Binding of C3 fragments on top of adsorbed plasma proteins during complement activation on a model biomaterial surface. Biomaterials 2005;26:1477-85.

Andrade JD, Lee HB, Jhon MS, Kim SW, Hibbs JB. Water as biomaterial. Transactions American Society for Artificial Internal Organs 1973;19:1-7.

Anfinsen CB, Haber E, Sela M, White FH. Kinetic of formation of native ribonuclease during oxidation of reduced polypeptide chain.Proceedings of the National Academy of Sciences of the United States of America 1961;47:1309.

Anirudhan TS, Divya PL, Nima J. Synthesis and characterization of novel drug delivery system using modified chitosan based hydrogel grafted with cyclodextrin. Chem. Eng. J. 2016;284:1259-69.

Annabi N, Mithieux SM, Weiss AS, Dehghani F. The fabrication of elastin-based hydrogels using high pressure $CO(2)$. Biomaterials 2009;30:1-7.

Arima Y, Toda M, Iwata H. Surface plasmon resonance in monitoring of complement activation on biomaterials. Advanced Drug Delivery Reviews 2011;63:988-99.

Arosio P, Owczarz M, Wu H, Butte A, Morbidelli M. End-to-End Self-Assembly of RADA 16-I Nanofibrils in Aqueous Solutions. Biophys J 2012;102:1617-26.

Asakura T, Sugino R, Okumura T, Nakazawa Y. The role of irregular unit, GAAS, on the secondary structure of Bombyx mori silk fibroin studied with C-13 CP/MAS NMR and wide-angle X-ray scattering. Protein Science 2002;11:1873-7.

Ashbaugh HS, Paulaitis ME. Effect of solute size and solute-water attractive interactions on hydration water structure around hydrophobic solutes. Journal of the American Chemical Society 2001;123:10721-8.

Azriel R, Gazit E. Analysis of the structural and functional elements of the minimal active fragment of islet amyloid polypeptide (IAPP) - An experimental support for the key role of the phenylalanine residue in amyloid formation. J Biol Chem 2001;276:34156-61.

Bahulekar R, Tamura N, Ito S, Kodama M. Platelet adhesion and complement activation studies on poly(N-alkyl mono and disubstituted) acrylamide derivatives. Biomaterials 1999;20:357-62.

Balakrishnan B, Mohanty M, Umashankar PR, Jayakrishnan A. Evaluation of an *in situ* forming hydrogel wound dressing based on oxidized alginate and gelatin. Biomaterials 2005;26:6335-42.

Balbach JJ, Ishii Y, Antzutkin ON, Leapman RD, Rizzo NW, Dyda F, *et al.* Amyloid fibril formation by A beta(16-22), a seven-residue fragment of the Alzheimer's beta-amyloid peptide, and structural characterization by solid state NMR. Biochemistry 2000;39:13748-59.

Barrow CJ, Yasuda A, Kenny PTM, Zagorski MG. Solution conformations and aggregational properties of synthetic amyloid beta-peptides of the alzhiemeres disease- analysis of circular dichroism spectra. J Mol Biol 1992;225:1075-93.

Basmadjian D, Sefton MV, Baldwin SA. Coagulation on biomaterials in flowing blood: some theoretical considerations. Biomaterials 1997;18:1511-22.

Basmadjian D. The effect of flow and mass transport in thrombogenesis. Annals of Biomedical Engineering 1990;18:685-709.

Behanna HA, Donners J, Gordon AC, Stupp SI. Coassembly of amphiphiles with opposite peptide polarities into nanofibers. Journal of the American Chemical Society 2005;127:1193-200. Bellamy RF. The causes of death in conventional land warfare- implications for combat casualty care research. Military Medicine 1984;149:55-62.

Benesch J, Svedhem S, Svensson SCT, Valiokas R, Liedberg B, Tengvall P. Protein adsorption to oligo(ethylene glycol) self-assembled monolayers: Experiments with fibrinogen, heparinized plasma, and serum. Journal of Biomaterials Science-Polymer Edition 2001;12:581-97.

Beniash E, Hartgerink JD, Storrie H, Stendahl JC, Stupp SI. Self-assembling peptide amphiphile nanofiber matrices for cell entrapment. Acta Biomaterialia 2005;1:387-97.

Berard DR, Attard P, Patey GN. Cavitation of a lennard-jones fluid between hard walls, and the possible relevance to the attraction measured between hydrophobic durfaces. Journal of Chemical Physics 1993;98:7236-44.

Berger M, Broxup B, Sefton MV. Using ELISA to evaluate complement activation by reference biomaterials. J Mater Sci-Mater Med 1994;5:622-7.

Bertolini F, Murphy S. A multicenter evaluatino of reproducibility of swirling in platelet concentrates. Transfusion 1994;34:796-801.

Beychok S. Poly-alpha-amino acids: Protein Models for Conformational Studies. New York: Marcel Dekker; 1968.

Bhattarai N, Gunn J, Zhang MQ. Chitosan-based hydrogels for controlled, localized drug delivery. Advanced Drug Delivery Reviews 2010;62:83-99.

Bippon WB, Chen HH, Walton AG. Spectroscopic characterization of poly(Glu-Ala). Journal of Molecular Biology 1973;75:369-75.

Blockmans D, Deckmyn H, Vermylen J. Platelet activation. Blood Reviews 1995;9:143-56.
Body SC. Platelet activation and interactions with the microvasculature. Journal of Cardiovascular Pharmacology 1996;27:S13-S25.

Bouhadir KH, Lee KY, Alsberg E, Damm KL, Anderson KW, Mooney DJ. Degradation of partially oxidized alginate and its potential application for tissue engineering. Biotechnol. Prog. 2001;17:945-50.

Brack A, Orgel LE. [beta] structures of alternating polypeptides and their possible prebiotic significance. Nature 1975;256:383-7.

Brack A, Orgel LE. Beta structures of alternating polypeptides and their possible prebiotic significance. Nature 1975;256:383-7.

Brannonpeppas L, Peppas NA. Equilibrium swelling behaviour of dilute ionic hydrogels in electrolytic solutions. Journal of Controlled Release 1991;16:319-30.

Brash JL. Exploiting the current paradigm of blood-material interactions for the rational design of blood-compatible materials. J Biomater Sci-Polym Ed 2000;11:1135-46.

Buenger D, Topuz F, Groll J. Hydrogels in sensing applications. Progress in Polymer Science 2012;37:1678-719.

Burdick JA, Prestwich GD. Hyaluronic Acid Hydrogels for Biomedical Applications. Advanced Materials 2011;23:H41-H56.

Buxton AN, Zhu J, Marchant R, West JL, Yoo JU, Johnstone B. Design and characterization of poly(ethylene glycol) photopolymerizable semi-interpenetrating networks for chondrogenesis of human mesenchymal stem cells. Tissue Eng 2007;13:2549-60.

Calvete JJ. Clues for understanding the structure and function of a prototypic human integrin - the platelet glycoprotein IIB/IIIA complex. Thrombosis and haemostasis 1994;72:1-15.

Campo GM, Avenoso A, Nastasi G, Micali A, Prestipino V, Vaccaro M, *et al.* Hyaluronan reduces inflammation in experimental arthritis by modulating TLR-2 and TLR-4 cartilage expression. Biochim Biophys Acta-Mol Basis Dis 2011;1812:1170-81.

Caplan MR, Moore PN, Zhang SG, Kamm RD, Lauffenburger DA. Self-assembly of a beta-sheet protein governed by relief of electrostatic repulsion relative to van der Waals attraction. Biomacromolecules 2000;1:627-31.

Caplan MR, Schwartzfarb EM, Zhang SG, Kamm RD, Lauffenburger DA. Control of self-assembling oligopeptide matrix formation through systematic variation of amino acid sequence. Biomaterials 2002;23:219-27.

Caplan R, Moore N, Zhang S, Kamm D, Lauffenburger A. Biomacromolecules 2000;1:627.
Carter D, Farid RS. Circular Dichroism (CD) Spectroscopy. Theory of Protein CD2003.

Castelletto V, Hamley IW, Harris PJF, Olsson U, Spencer N. Influence of the Solvent on the Self-Assembly of a Modified Amyloid Beta Peptide Fragment. I. Morphological Investigation. Journal of Physical Chemistry B 2009;113:9978-87.

Cen L, Liu W, Cui L, Zhang WJ, Cao YL. Collagen tissue engineering: Development of novel biomaterials and applications. Pediatr Res 2008;63:492-6.

Chen C, Pan F, Zhang S, Hu J, Cao M, Wang J, *et al.* Antibacterial Activities of Short Designer Peptides: a Link between Propensity for Nanostructuring and Capacity for Membrane Destabilization. Biomacromolecules 2010;11:402-11.

Chen K, Sahoo S, He P, Ng KS, Toh SL, Goh JCH. A Hybrid Silk/RADA-Based Fibrous Scaffold with Triple Hierarchy for Ligament Regeneration. Tissue Engineering Part A 2012;18:1399-409.

Chen SF, Li LY, Zhao C, Zheng J. Surface hydration: Principles and applications toward low-fouling/nonfouling biomaterials. Polymer 2010;51:5283-93.

Chen X, Shao ZZ, Marinkovic NS, Miller LM, Zhou P, Chance MR. Conformation transition kinetics of regenerated Bombyx mori silk fibroin membrane monitored by time-resolved FTIR spectroscopy. Biophys Chem 2001;89:25-34.

Chen YR, Gan HX, Tong YW. pH-Controlled Hierarchical Self-Assembly of Peptide Amphiphile. Macromolecules 2015;48:2647-53.

Chenoweth DE, Hugli TE. Demonstration of specific C5A receptor on intact human polymorphonuclear leukocytes. Proceedings of the National Academy of Sciences of the United States of America 1978;75:3943-7.

Chenoweth DE. Complement Activation Produced by Biomaterials. Artificial Organs 1988;12:508-10.

Cheung AK, Parker CJ, Janatova J, Brynda E. Modulation of complement aactivation on hemodialysis memebranes by immobilized heparin. Journal of the American Society of Nephrology 1992;2:1328-37.

Cheung AK, Parker CJ, Wilcox LA, Janatova J. Activation of complement by hemodialysis membranes - polyacrylonitrile binds more C3a than cuprophan. Kidney Int 1990;37:1055-9.

Cheung MS, Garcia AE, Onuchic JN. Protein folding mediated by solvation: Water expulsion and formation of the hydrophobic core occur after the structural collapse. Proceedings of the National Academy of Sciences of the United States of America 2002;99:685-90.

Chevallay B, Herbage D. Collagen-based biomaterials as 3D scaffold for cell cultures: applications for tissue engineering and gene therapy. Medical and Biological Engineering and Computing;38:211-8.

Cholakis CH, Sefton MV. *In-vitro* platelet interatctions with a heparin-polyvinyl alcohol hydrogel. J Biomed Mater Res 1989;23:399-415.

Chou KC, Nemethy G, Scheraga HA. Effect of amino acid composition on the twist and the relative stability of parallel and anti-parallel beta sheets. Biochemistry 1983;22:6213-21.

Chou PY, Fasman GD. Conformational parameters for amino-acid in helical, beta- sheet, and random coil regions calculated from proteins. Biochemistry 1974;13:211-22.

Chou PY, Fasman GD. Prediction of protein conformation. Biochemistry 1974;13:222-45.

Cigognini D, Satta A, Colleoni B, Silva D, Donega M, Antonini S, et al. Evaluation of Early and Late Effects into the Acute Spinal Cord Injury of an Injectable Functionalized Self-Assembling Scaffold. PLoS One 2011;6:15.

Cipitria A, Skelton A, Dargaville TR, Dalton PD, Hutmacher DW. Design, fabrication and characterization of PCL electrospun scaffolds-a review. Journal of Materials Chemistry 2011;21:9419-53.

Claessens CG, Stoddart JF. pi-pi interactions in self-assembly. Journal of Physical Organic Chemistry 1997;10:254-72.

Clement JM, Hofnung M. Gene sequence of the lambda receptor, an outer-membrane protein of Excherichia-coli K12. Cell 1981;27:507-14.

Cohen DL, Malone E, Lipson H, Bonassar LJ. Direct freeform fabrication of seeded hydrogels in arbitrary geometries. Tissue Eng 2006;12:1325-35.

Collen D, Lijnen HR. Molecular basis of fibrinolysis as relevant for thrombolytic therapy. Thrombosis and Haemostasis 1995;74:167-71.

Conio G, Patrone E, Salaris F. Conformational transitions of poly(L-Tyrosine) in mixed ethanol solvents. Macromolecules 1971;4:283.

Cook DA. Relation between amino acid sequence and protein conformation. Journal of Molecular Biology 1967;29:167.

Cormier AR, Ruiz-Orta C, Alamo RG, Paravastu AK. Solid State Self-Assembly Mechanism of RADA16-I Designer Peptide. Biomacromolecules 2012;13:1794-804.

Cui HG, Webber MJ, Stupp SI. Self-Assembly of Peptide Amphiphiles: From Molecules to Nanostructures to Biomaterials. Biopolymers 2010;94:1-18.

Danon D, Jerushalmy Z, Devries A. Incorporation of influenza birus in human blood *in-vitro* - electron microscopical observation. Virology 1959;9:719-22.

Daugirdas JT, Bernardo AA. Hemodialysis effect on platelet count and function and hemodialysis-associated thrombocytopenia. Kidney International 2012;82:147-57.

Decaterina R, Lanza M, Manca G, Strata GB, Maffei S, Salvatore L. Bleeding-time and bleeding-An analysis of the relationship of the bleeding-time test with parameters of surgical bleeding. Blood 1994;84:3363-70.

Degano IR, Quintana L, Vilalta M, Horna D, Rubio N, Borros S, *et al.* The effect of self-assembling peptide nanofiber scaffolds on mouse embryonic fibroblast implantation and proliferation. Biomaterials 2009;30:1156-65.

Deutsch DG, Mertz ET. Plasminogen-purification from human plasma by affinity chromatography. Science 1970;170:1095.

Dickerson MB, Sandhage KH, Naik RR. Protein- and Peptide-Directed Syntheses of Inorganic Materials. Chem Rev 2008;108:4935-78.

Dobson CM. Protein misfolding, evolution and disease. Trends in Biochemical Sciences 1999;24:329-32.

Doster W, Settles M. Protein-water displacement distributions. BBA-Proteins Proteomics 2005;1749:173-86.

Dubey VK, Shah A, Jagannadham MV, Kayastha AM. Effect of organic solvents on the molten globule state of procerain: beta-sheet to alpha-helix switchover in presence of trifluoroethanol. Protein and peptide letters 2006;13:545-7.

Dumortier G, Grossiord JL, Agnely F, Chaumeil JC. A review of poloxamer 407 pharmaceutical and pharmacological characteristics. Pharm Res 2006;23:2709-28.

Duncan AC, Sefton MV, Brash JL. Effect of C-4-, C-8- and C-18-alkylation of poly(vinyl alcohol) hydrogels on the adsorption of albumin and fibrinogen from buffer and plasma: limited correlation with platelet interactions. Biomaterials 1997;18:1585-92.

Einav S, Dewey CF, Hartenbaum H. Cone-and-plate apparatus - a compact system for studying well charactersized turbulant flow fields. Exp Fluids 1994;16:196-202.

Ellis-Behnke R. At the nanoscale: nanohemostat, a new class of hemostatic agent. Wiley Interdisciplinary Reviews: Nanomedicine and Nanobiotechnology 2011;3:70-8.

Ellis-Behnke RG, Liang Y-X, David KC, Kau PWF, Schneider GE, Zhang S, *et al.* Nano hemostat solution: immediate hemostasis at the nanoscale. Nanomedicine-Nanotechnology Biology and Medicine 2006;2:207-15.

Ellis-Behnke RG, Liang YX, You SW, Tay DKC, Zhang SG, So KF, *et al.* Nano neuro knitting: Peptide nanofiber scaffold for brain repair and axon regeneration with functional return of vision. Proceedings of the National Academy of Sciences of the United States of America 2006;103:5054-9.

Elson EL, Magde D. Fluorescense correlation spectrospcoy.1. Conceptual basis and theory. Biopolymers 1974;13:1-27.

Enderlein J, Gregor I, Patra D, Dertinger T, Kaupp UB. Performance of fluorescence correlation spectroscopy for measuring diffusion and concentration. Chemphyschem 2005;6:2324-36.
Engel J, Schwarz G. Cooperative conformational transitions of linear biopolymers. Angewandte Chemie-International Edition 1970;9:389.

Esmon CT. The impact of the inflammatory response on coagulation. Thrombosis Research 2004;114:321-7.

Evans JA, van Wessem KJP, McDougall D, Lee KA, Lyons T, Balogh ZJ. Epidemiology of Traumatic Deaths: Comprehensive Population-Based Assessment. World JSurg 2010;34:158-63.
Farrior E, Ladner K. Platelet Gels and Hemostasis in Facial Plastic Surgery. Facial Plast Surg 2011;27:308-14.

Favaloro EJ. Utility of the PFA-100 (R) for assessing bleeding disorders and monitoring therapy: a review of analytical variables, benefits and limitations. Haemophilia 2001;7:170-9.

Filippovich I, Sorokina N, Pierre LS, Flight S, de Jersey J, Perry N, *et al.* Cloning and functional expression of venom prothrombin activator protease from Pseudonaja textilis with whole blood procoagulant activity. British Journal of Haematology 2005;131:237-46.

Finkelst.Av, Ptitsyn OB. Statistical analysis of correlation among amino acid residues in helical, beta-structural and non-regulatar regions of globular proteins. Journal of Molecular Biology 1971;62:613.

Foreman KE, Vaporciyan AA, Bonish BK, Jones ML, Johnson KJ, Glovsky MM, et al. C5A-Induced expression of P-selectin in endothelial cells. Journal of Clinical Investigation 1994;94:1147-55.

Fraga S, Parker JMR. Modeling of peptide and protein structures. Amino Acids 1994;7:175-202.
Franco AT, Corken A, Ware J. Platelets at the interface of thrombosis, inflammation, and cancer. Blood 2015;126:582-8.

Frautschi JR, Eberhart RC, Hubbell JA, Clark BD, Gelfand JA. Alkylation of cellulosic membranes results in reduced complement activation. J. Biomater. Sci-Polym. Ed. 1996;7:707-14.

Freier T, Koh HS, Kazazian K, Shoichet MS. Controlling cell adhesion and degradation of chitosan films by N-acetylation. Biomaterials 2005;26:5872-8.

Freudenberg U, Hermann A, Welzel PB, Stirl K, Schwarz SC, Grimmer M, et al. A star-PEG-heparin hydrogel platform to aid cell replacement therapies for neurodegenerative diseases. Biomaterials 2009;30:5049-60.

Friedman LI, Grabowsk.Ef, Leonard EF, Liem H, McCord CW. Inconsequentiality of surface properties for initial platelet adhesion. Transactions American Society for Artificial Internal Organs 1970;16:63-73.

Galler KM, Aulisa L, Regan KR, D'Souza RN, Hartgerink JD. Self-assembling Multidomain Peptide Hydrogels: Designed Susceptibility to Enzymatic Cleavage Allows Enhanced Cell Migration and Spreading. Journal of the American Chemical Society 2010;132:3217-23.

Garreta E, Genove E, Borros S, Semino CE. Osteogenic differentiation of mouse embryonic stem cells and mouse embryonic fibroblasts in a three-dimensional self-assembling peptide scaffold. Tissue Eng. 2006;12:2215-27.

Gasic GJ. Role of plasma, platelets, and endothelial-cells in tubor metasis. Cancer and Metastasis Reviews 1984;3:99-116.

Gawryl MS, Simon MT, Eatman JL, Lint TF. An enzyme linked immunoabsorbent assay for the quantification of the terminal complement complex from cell-membranes or in activated human sera. J Immunol Methods 1986;95:217-25.

Gelain F, Bottai D, Vescovi A, Zhang S. Designer Self-Assembling Peptide Nanofiber Scaffolds for Adult Mouse Neural Stem Cell 3-Dimensional Cultures. Public Library of Science 2006:1-11.

Gemmell CH, Yeo EL, Sefton MV. Flow cytometric analysis of material-induced platelet activation in a canine model: Elevated microparticle levels and reduced platelet life span. J. Biomed. Mater. Res. 1997;37:176-81.

Gemmell CH. Activation of platelets by in vitro whole blood contact with materials: Increases in microparticle, procoagulant activity, and soluble P-selectin blood levels. J. Biomater. Sci-Polym. Ed 2001;12:933-43.

Ghosh A, Haverick M, Stump K, Yang XY, Tweedle MF, Goldberger JE. Fine-Tuning the pH Trigger of Self-Assembly. Journal of the American Chemical Society 2012;134:3647-50.

Ghoussoub A, Lehn J-M. Dynamic sol-gel interconversion by reversible cation binding and release in G-quartet-based supramolecular polymers. Chemical Communications 2005:5763-5.

Gillard RE, Raymo FM, Stoddart JF. Controlling self-assembly. Chemistry-a European Journal 1997;3:1933-40.

Golander CG, Lassen B, Nilssonekdahl K, Nilsson UR. RF-Plasma-modified polystyrene surfaces for studying complement activation. J. Biomater. Sci-Polym. Ed. 1992;4:25-30.

Goldsmith HL, Turitto VT. Rheological aspects of thrombosis and hemostasis - basic principals and applications -ICTH-report - Subcommittee on rheology of the international committee on thrombosis and hemostasis. Thrombosis and haemostasis 1986;55:415-35.

Goodman SL. Sheep, pig, and human platelet-material interactions with model cardiovascular biomaterials. Journal of Biomedical Materials Research 1999;45:240-50.

Gorbet MB, Sefton MVMV. Biomaterial-associated thrombosis: roles of coagulation factors, complement, platelets and leukocytes. Biomaterials 2004;25:5681-703.

Goto S, Handa S, Takahashi E, Abe S, Handa M, Ikeda Y. Synergistic effect of epinephrine and shearing on platelet activation. Thromb. Res. 1996;84:351-9.

Greenfield N, Fasman GD. Computed circular dichroism spectra for the evaluation of protein conformation. Biochemistry 1969;8:4108-16.

Greer IA. Therapeutic progress review .28. Platelet function and calcium channel blocking agents. J. Clin. Pharm. Ther. 1987;12:213-22.

Gref R, Domb A, Quellec P, Blunk T, Muller RH, Verbavatz JM, et al. The controlled intravenous delivery of drugs using PEG-coated sterically stabilized nanospheres. Advanced Drug Delivery Reviews 2012;64:316-26.

Gresele P, Agnelli G. Novel approaches to the treatment of thrombosis. Trends Pharmacol. Sci. 2002;23:25-32.

Guggenheim EA. The conceptions of electrical potential difference between two phases and the individual activities of ions. J Phys Chem 1929;33:842-9.

Guo HD, Cui GH, Wang HJ, Tan YZ. Transplantation of marrow-derived cardiac stem cells carried in designer self-assembling peptide nanofibers improves cardiac function after myocardial infarction. Biochem Biophys Res Commun 2010;399:42-8.

Guo HD, Cui GH, Yang JJ, Wang C, Zhu J, Zhang LS, *et al.* Sustained delivery of VEGF from designer self-assembling peptides improves cardiac function after myocardial infarction. Biochem Biophys Res Commun 2012;424:105-11.

Guo J, Su H, Zeng Y, Liang YX, Wong WM, Ellis-Behnke RG, *et al.* Reknitting the injured spinal cord by self-assembling peptide nanofiber scaffold. Nanomed-Nanotechnol Biol. Med. 2007;3:311-21.

Guo JS, Leung KKG, Su HX, Yuan QJ, Wang L, Chu TH, *et al.* Self-assembling peptide nanofiber scaffold promotes the reconstruction of acutely injured brain. Nanomedicine-Nanotechnology Biology and Medicine 2009;5:345-51.

Guo WH, Lampoudi S, Shea JE. Posttransition state desolvation of the hydrophobic core of the src-SH3 protein domain. Biophysical Journal 2003;85:61-9.

Gupta P, Vermani K, Garg S. Hydrogels: from controlled release to pH-responsive drug delivery. Drug Discovery Today 2002;7:569-79.

Habibi Y, Lucia LA, Rojas OJ. Cellulose Nanocrystals: Chemistry, Self-Assembly, and Applications. Chem. Rev. 2010;110:3479-500.

Hakim RM, Fearon DT, Lazarus JM. Biocompatibility of dialysis membranes - effects of chornic complement activaiton. I. Kidney Int. 1984;26:194-200.

Hanson SR, Harker LA, Ratner BD, Hoffman AS. *In vivo* evaluation of artificial surfaces with a non human primate model of arterial thrombosis. Journal of Laboratory and Clinical Medicine 1980;95:289-304.

Harper JD, Lansbury PT. Models of amyloid seeding in Alzheimier's disease and scrapie: Mechanistic truths and physiological consequences of the time-dependent solubility of amyloid proteins. Annual Review of Biochemistry 1997;66:385-407.

Hartgerink JD, Beniash E, Stupp SI. Peptide-amphiphile nanofibers: A versatile scaffold for the preparation of self-assembling materials. Proceedings of the National Academy of Sciences of the United States of America 2002;99:5133-8.

Hartgerink JD, Beniash E, Stupp SI. Self-Assembly and Mineralization of Peptide-Amphiphile Nanofibers. Science 2001;294:1684-8.

Haugh MG, Thorpe SD, Vinardell T, Buckley CT, Kelly DJ. The application of plastic compression to modulate fibrin hydrogel mechanical properties. Journal of the Mechanical Behavior of Biomedical Materials 2012;16:66-72.

Hauser CAE, Zhang S. Designer self-assembling peptide nanofiber biological materials. Chemical Society Reviews 2010;39:2780-90.

Hayashi K, Fukumura H, Yamamoto N. *In vivo* thrombus formation induced by complement activation on polymer surfaces. J. Biomed. Mater. Res. 1990;24:1385-95.

Haycox CL, Ratner BD. *In-vitro* platelet interactsions in the whole human blood exposed to biomaterial sufraces - insights on blood compatibility. Journal of Biomedical Materials Research 1993;27:1181-93.

He S, Antovic A, Blomback M. A simple and rapid laboratory method for determination of haemostasis potential in plasma II. Modifications for use in routine laboratories and research work. Thromb. Res. 2001;103:355-61.

Heitmann P. A model for sulfhydryl groups in proteins. Hydrophobic interactions of the cysteine side chain in micelles. Eur. J. Biochem. 1968;3:346.

Hemker HC, Giesen P, AlDieri R, Regnault V, de Smed E, Wagenvoord R, *et al.* The Calibrated Automated Thrombogram (CAT): A universal routine test for hyper- and hypocoagulability. Pathophysiol Haemost Thromb 2002;32:249-53.

Hern DL, Hubbell JA. Incorporation of adhesion peptides into nonadhesive hydrogels useful for tissue resurfacing. J. Biomed. Mater. Res. 1998;39:266-76.

Hess B. Periodic patterns in biology. Naturwissenschaften 2000;87:199-211.

Higuchi A, Aoki N, Yamamoto T, Miyazaki T, Fukushima H, Tak TM, *et al*. Temperature-induced cell detachment on immobilized pluronic surface. Journal of Biomedical Materials Research Part A 2006;79A:380-92.

Hilbich C, Kisterswoike B, Reed J, Masters CL, Beyreuther K. Aggregation and secondary structure of synthetic amyloid beta-A4 peptides of alzheimers- disease. Journal of Molecular Biology 1991;218:149-63.

Hodge RM, Bastow TJ, Edward GH, Simon GP, Hill AJ. Free volume and the mechanism of plasticization in water-swollen poly(vinyl alcohol). Macromolecules 1996;29:8137-43.

Hoffman M. The cellular basis of traumatic bleeding. Military medicine 2004;169:5-4.

Höhne G, Hemminger W, Flammersheim HJ. Differential scanning calorimetry: Berlin ; New York : Springer, c2003.

Holland TA, Tabata Y, Mikos AG. Dual growth factor delivery from degradable oligo(poly(ethylene glycol) fumarate) hydrogel scaffolds for cartilage tissue engineering. Journal of Controlled Release 2005;101:111-25.

Holme S, Moroff G, Murphy S. A multi-laboratory evaluation of *in vitro* platelet assays: the tests for extent of shape change and response to hypotonic shock. Transfusion 1998;38:31-40.

Holmes TC, de Lacalle S, Su X, Liu GS, Rich A, Zhang SG. Extensive neurite outgrowth and active synapse formation on self-assembling peptide scaffolds. Proceedings of the National Academy of Sciences of the United States of America 2000;97:6728-33.

Hong Y, Lau LS, Legge RL, Chen P. Critical self-assembly concentration of an ionic-complementary peptide EAK16-1. The Journal of Adhesion 2004;80:913-31.

Hong YS, Legge RL, Zhang S, Chen P. Effect of amino acid sequence and pH on nanofiber formation of self-assembling peptides EAK16-II and EAK16-IV. Biomacromolecules 2003;4:1433-42.

Horii A, Wang XM, Gelain F, Zhang SG. Biological Designer Self-Assembling Peptide Nanofiber Scaffolds Significantly Enhance Osteoblast Proliferation, Differentiation and 3-D Migration. PLoS One 2007;2:9.

Horn RG, Israelachvili JN, Marra J, Parsegian VA, Rand RP. Comparison of the forces measured between phosphatidylcholine bilayers. Biophysical Journal 1988;54:1185-6.

Hoylaerts M, Rijken DC, Lijnen HR, Collen D. Kinetics of the activation of plasminogen by human tissue plasminogen actibator - role of fibrin. Journal of Biological Chemistry 1982;257:2912-9.

Hu X, Kaplan D, Cebe P. Determining beta-sheet crystallinity in fibrous proteins by thermal analysis and infrared spectroscopy. Macromolecules 2006;39:6161-70.

Hu X, Kaplan D, Cebe P. Dynamic protein-water relationships during beta-sheet formation. Macromolecules 2008;41:3939-48.

Hu X, Kaplan D, Cebe P. Effect of water on the thermal properties of silk fibroin. Thermochim. Acta. 2007;461:137-44.

Hua L, Huang X, Liu P, Zhou R, Berne BJ. Nanoscale dewetting transition in protein complex folding. J. Phys. Chem. B 2007;111:9069-77.

Huang X, Margulis CJ, Berne BJ. Dewetting-induced collapse of hydrophobic particles (vol 100, pg 11953, 2003). Proceedings of the National Academy of Sciences of the United States of America 2006;103:19605.

Hummer G, Garde S. Cavity expulsion and weak dewetting of hydrophobic solutes in water. Phys. Rev. Lett. 1998;80:4193-6.

Hwang W, Zhang SG, Kamm RD, Karplus M. Kinetic control of dimer structure formation in amyloid fibrillogenesis. Proceedings of the National Academy of Sciences of the United States of America 2004;101:12916-21.

Hynes RO, Lander AD. Contact and adhesive specificities in the associations, migrations, and targeting of cells and axons. Cell 1992;68:303-22.

Ide M, Mori T, Ichikawa K, Kitano H, Tanaka M, Mochizuki A, et al. Structure of water sorbed into poly (MEA-co-HEMA) films as examined by ATR-IR spectroscopy. Langmuir 2003;19:429-35.

Isbister GK. Procoagulant Snake Toxins: Laboratory Studies, Diagnosis, and Understanding Snakebite Coagulopathy. Seminars in Thrombosis and Hemostasis 2009;35:93-103.

Israelachvili JN. Intermolecular and surface forces: Burlington, MA : Academic Press, 2011.

Jakubith S, Rotermund HH, Engel W, Vonoertzen A, Ertl G. Spatiotemporal concentration patterns in a surface-reaction - propagating and standing waves, totating spirals and turbulence. Phys Rev Lett 1990;65:3013-6.

Janatova J, Cheung AK, Parker CJ. Bio-medical polymers differ in their capacity to activate complement. Complement and Inflammation 1991;8:61-9.

Janatova J. Activation and control of complement, inflammation, and infection associated with the use of biomedical polymers. Asaio. J. 2000;46:S53-S62.

Janssen I, Koene M, Lischer C. Intraarticular applikation of polyacrylamide hydrogel as a treatment of osteoarthritis in the distal interphalangeal joint: case series with 12 horses. Pferdeheilkunde 2012;28:650-6.

Jayawarna V, Ali M, Jowitt TA, Miller AE, Saiani A, Gough JE, *et al.* Nanostructured hydrogels for three-dimensional cell culture through self-assembly of fluorenylmethoxycarbonyl-dipeptides. Advanced Materials 2006;18:611.

Jayawarna V, Richardson SM, Hirst AR, Hodson NW, Saiani A, Gough JE, *et al.* Introducing chemical functionality in Fmoc-peptide gels for cell culture. Acta Biomater 2009;5:934-43.

Jiang H, Guler MO, Stupp SI. The internal structure of self-assembled peptide amphiphiles nanofibers. Soft Matter. 2007;3:454-62.

Jin HJ, Kaplan DL. Mechanism of silk processing in insects and spiders. Nature 2003;424:1057-61.

Johnson TD, Christman KL. Injectable hydrogel therapies and their delivery strategies for treating myocardial infarction. Expert Opinion on Drug Delivery 2013;10:59-72.

Johnson WC, Tinoco I. Circular dichroism of polypeptide solutinos in vacuum ultravoilet. Journal of the American Chemical Society 1972;94:4389.

Jordine ESA. Specific interactions which need nonequilibrium particle/particle models. Journal of Colloid and Interface Science 1973;45:435-9.

Jorgensen L, Borchgrevink CF. Platelet plug in normal persons.2. Histological appearance of plug in secondary bleeding time test. Acta Pathologica Et Microbiologica Scandinavica 1963;57:427.

Jy WC, Mao WW, Horstman LL, Tao JG, Ahn YS. Platelet microparticles bind, activate and aggregate neutrophils in vitro. Blood Cells Molecules and Diseases 1995;21:217-31.

Kabiri M, Bushnak I, McDermot MT, Unsworth LD. Toward a Mechanistic Understanding of Ionic Self-Complementary Peptide Self-Assembly: Role of Water Molecules and Ions. Biomacromolecules 2013;14:3943-50.

Kainthan RK, Gnanamani M, Ganguli M, Ghosh T, Brooks DE, Maiti S, *et al*. Blood compatibility of novel water soluble hyperbranched polyglycerol-based multivalent cationic polymers and their interaction with DNA. Biomaterials 2006;27:5377-90.

Kainthan RK, Hester SR, Levin E, Devine DV, Elliott BD. *In vitro* biological evaluation of high molecular weight hyperbranched polyglycerols. Biomaterials 2007;28:4581-90.

Karfeld-Sulzer LS, Siegenthaler B, Ghayor C, Weber FE. Fibrin Hydrogel Based Bone Substitute Tethered with BMP-2 and BMP-2/7 Heterodimers. Materials 2015;8:977-91.

Kataoka K, Ito H, Amano H, Nagasaki Y, Kato M, Tsuruta T, et al. Minimized platelet interaction with poly(2-hydroxyethyl methacrylate-block-4-bis(trimethylsilyl)methylstyrene) hydrogel showing anomalously high free water content. Journal of Biomaterials Science-Polymer Edition 1998;9:111-29.

Khare AR, Peppas NA, Massimo G, Colombo P. Measurement of the swelling force in ionic polymeric networsk.1. Effect of pH and ionic content. Journal of Controlled Release 1992;22:239-44.

Khare AR, Peppas NA. Swelling and deswelling of anionic copolymer gells. Biomaterials 1995;16:559-67.

Kim SJ, Park SJ, Kim SI. Properties of smart hydrogels composed of polyacrylic acid/poly(vinyl sulfonic acid) responsive to external stimuli. Smart. Mater. Struct. 2004;13:317-22.

Kim YS, Dong LM, Hickner MA, Glass TE, Webb V, McGrath JE. State of water in disulfonated poly(arylene ether sulfone) copolymers and a perfluorosulfonic acid copolymer (nafion) and its effect on physical and electrochemical properties. Macromolecules 2003;36:6281-5.

King DJ, Kelton JG. Heparin-associated thrombocytopenia. Annals. of Internal Medicine 1984;100:535-40.

Kisiday J, Jin M, Kurz B, Hung H, Semino C, Zhang S, *et al*. Self-assembling peptide hydrogel fosters chondrocyte extracellular matrix production and cell division: Implications for cartilage tissue repair. Proceedings of the National Academy of Sciences of the United States of America 2002;99:9996-10001.

Kjaerheim A, Hovig T. Hemostatic blood platelet plugs in rabbits. Journal of Ultrastructure Research 1962;6:138.

Klinger MHF, Jelkmann W. Role of blood platelets in infection and inflammation. Journal of Interferon and Cytokine Research 2002;22:913-22.

Konturek SJ, Pawlik W. Physiology and pharmacology of prostaglandins. Dig Dis Sci 1986;31:S6-S19.

Kopesky PW, Vanderploeg EJ, Sandy JS, Kurz B, Grodzinsky AJ. Self-assembling peptide hydrogels modulate *in vitro* chondrogenesis of bovine bone marrow stromal cells. Tissue engineering Part A 2010;16:465-77.

Koutsopoulos S, Unsworth LD, Nagai Y, Zhang S. Controlled release of functional proteins through designer self-assembling peptide nanofiber hydrogel scaffold. Proceedings of the National Academy of Sciences 2009;106:4623-8.

Kuijpers AJ, Engbers GHM, Krijgsveld J, Zaat SAJ, Dankert J, Feijen J. Cross-linking and characterisation of gelatin matrices for biomedical applications. Journal of Biomaterials Science-Polymer Edition 2000;11:225-43.

Kumar M, Muzzarelli RAA, Muzzarelli C, Sashiwa H, Domb AJ. Chitosan chemistry and pharmaceutical perspectives. Chem Rev 2004;104:6017-84.

Kunicki TJ, Tuccelli M, Becker GA, Aster RH. Study of variables affecting quality of platelets stored at room-temperature. Transfusion 1975;15:414-21.

Labarre D, Laurent A, Lautier A, Bouhni S, Kerbellec L, Lewest JM, *et al.* Complement activation by substituted polyacrylamide hydrogels for embolisation and implantation. Biomaterials 2002;23:2319-27.

Lamba NMK, Courtney JM, Gaylor JDS, Lowe GDO. *In vitro* investigation of the blood response to medical grade PVC and the effect of heparin on the blood response. Biomaterials 2000;21:89-96.

Lazarus AH, Wright JF, Blanchette V, Freedman J. Analysis of platelets by flow cytometry. Transfusion Science 1995;16:353-61.

Lee KY, Mooney DJ. Alginate: Properties and biomedical applications. Progress in Polymer Science 2012;37:106-26.

Lee YS. Self-assembly and nanotechnology : a force balance approach: Hoboken, N.J. : John Wiley & Sons, c2008.; 2008.

Leininger RI. Polymers as surgical implants. CRC critical reviews in bioengineering 1972;1:333-81.

Leung GKK, Wang YC, Wu WT. Peptide nanofiber scaffold for brain tissue reconstruction. In: Duzgunes N, editor. Nanomedicine: Cancer, Diabetes, and Cardiovascular, Central Nervous System, Pulmonary and Inflammatory Diseases. San Diego: Elsevier Academic Press Inc; 2012. p. 177-90.

Levin E, Jenkins C, Culibrk B, Gyongyossy-Issa MIC, Serrano K, Devine DV. Development of a quality monitoring program for platelet components: a report of the first four years' experience at Canadian Blood Services. Transfusion;52:810-8.

Li XW, Katsanevakis E, Liu XY, Zhang N, Wen XJ. Engineering neural stem cell fates with hydrogel design for central nervous system regeneration. Prog Polym Sci 2012;37:1105-29.

Liedmann A, Rolfs A, Frech MJ. Cultivation of Human Neural Progenitor Cells in a 3-dimensional Self-assembling Peptide Hydrogel. J Vis Exp 2012:7.

Lin CC, Metters AT. Hydrogels in controlled release formulations: Network design and mathematical modeling. Advanced Drug Delivery Reviews 2006;58:1379-408.

Lin YS, Hlady V, Janatova J. Adsorption of complement proteins on surfaces with hydrophobicity gradient. Biomaterials 1992;13:497-504.

Liu G, Prabhakar A, Aucoin D, Simon M, Sparks S, Robbins KJ, et al. Mechanistic Studies of Peptide Self-Assembly: Transient alpha-Helices to Stable beta-Sheets. Journal of the American Chemical Society 2010;132:18223-32.

Liu J, Zhang L, Yang Z, Zhao X. Controlled release of paclitaxel from a self-assembling peptide hydrogel formed *in situ* and antitumor study *in vitro*. International Journal of Nanomedicine 2011;6:2143-53.

Liu L, Xu K, Wang H, Jeremy Tan PK, Fan W, Venkatraman SS, *et al*. Self-assembled cationic peptide nanoparticles as an efficient antimicrobial agent. Nat. Nano 2009;4:457-63.

Liu P, Huang XH, Zhou RH, Berne BJ. Observation of a dewetting transition in the collapse of the melittin tetramer. Nature 2005;437:159-62.

Llanos GR, Sefton MV. Immobilization of poly(ethylene glycol) onto a poly(vinyl alcohol) 2. Evaluation of thrombogenicity. J. Biomed Mater. Res. 1993;27:1383-91.

Lodish H. Cloning Expeditions: Risky but Rewarding. Mol Cell Biol 2013;33:4620-7.

Lu Q, Malinauskas RA. Comparison of Two Platelet Activation Markers Using Flow Cytometry After In Vitro Shear Stress Exposure of Whole Human Blood. Artificial Organs 2011;35:137-44.

Maher SA, Mauck RL, Rackwitz L, Tuan RS. A nanofibrous cell-seeded hydrogel promotes integration in a cartilage gap model. J. Tissue Eng. Regen. Med. 2010;4:25-9.

Mannucci PM, Levi M. Drug therapy: Prevention and treatment of major blood loss. N Engl J Med 2007;356:2301-11.

Markiewski MM, DeAngelis RA, Strey CW, Foukas PG, Gerard C, Gerard N, *et al*. The Regulation of Liver Cell Survival by Complement. Journal of Immunology 2009;182:5412-8.

Mart RJ, Osborne RD, Stevens MM, Ulijn RV. Peptide-based stimuli-responsive biomaterials. Soft Matter 2006;2:822-35.

Martinsen A, Storro I, Skjakbraek G. Alginate as immobilization material.3. Diffisuonal properties. Biotechnol Bioeng 1992;39:186-94.

Mata A, Hsu L, Capito R, Aparicio C, Henrikson K, Stupp SI. Micropatterning of bioactive self-assembling gels. Soft Matter. 2009;5:1228-36.

Maude S, Miles DE, Felton SH, Ingram J, Carrick LM, Wilcox RK, *et al*. De novo designed positively charged tape-forming peptides: self-assembly and gelation in physiological solutions and their evaluation as 3D matrices for cell growth. Soft Matter. 2011;7:8085-99.

Maurer-Spurej E, Chipperfield K. Past and Future Approaches to Assess the Quality of Platelets for Transfusion. Transfusion Medicine Reviews 2007;21:295-306.

Mayer MM. Complement. Historical perspectives and some current issues. Complement (Basel, Switzerland) 1984;1:2-26.

McEver RP, Martin MN. A monoclonal- antibody to a membrane glycoprotein binds only to the activated platelts. J. Biol. Chem. 1984;259:9799-804.

McGaughey GB, Gagne M, Rappe AK. pi-stacking interactions - Alive and well in proteins. J Biol Chem 1998;273:15458-63.

Mendez J, Annamalai PK, Eichhorn SJ, Rusli R, Rowan SJ, Foster EJ, *et al*. Bioinspired Mechanically Adaptive Polymer Nanocomposites with Water-Activated Shape-Memory Effect. Macromolecules 2011;44:6827-35.

Mequanint K, Patel A, Bezuidenhout D. Synthesis, swelling behavior, and biocompatibility of novel physically cross-linked polyurethane-block-poly(glycerol methacrylate) hydrogels. Biomacromolecules 2006;7:883-91.

Mequanint K, Sheardown H. 2-methacryloyloxyethyl N-butylcarbamate: a new co-monomer for synthesis of polyurethane hydrogels with improved mechanical properties for biomedical applications. Journal of Biomaterials Science-Polymer Edition 2005;16:1303-18.

Mickelson JK, Lakkis NM, Villarreal-Levy G, Hughes BJ, Smith CW. Leukocyte activation with platelet adhesion after coronary angioplasty: a mechanism for recurrent disease? Journal of the American College of Cardiology 1996;28:345-53.

Misawa H, Kobayashi N, Soto-Gutierrez A, Chen Y, Yoshida A, Rivas-Carrillo JD, et al. PuraMatrix (TM) facilitates bone regeneration in bone defects of calvaria in mice. Cell Transplant 2006;15:903-10.

Mitra RN, Shome A, Paul P, Das PK. Antimicrobial activity, biocompatibility and hydrogelation ability of dipeptide-based amphiphiles. Organic & Biomolecular Chemistry 2009;7:94-102.

Moll S, Demoerloose P, Reber G, Schifferli J, Leski M. Comparison of 2 hemodialysis memebranes, polyacrilonitrile and cellulose-acetate, on complement and coagulation systems. Int. J. Artif. Organs 1990;13:273-9.

Mollnes TE, Garred P, Bergseth G. Efffect of time, temperature, and anticoagulats on *in-vitro* complement activation - consequences for collection and preservation of samples to be examined for complement activation. Clinical and Experimental Immunology 1988;73:484-8.

Mollnes TE, Vandvik B, Lea T, Vartdal F. Intrathecal complement activvation in nurogical diseases evaluated by analysis of terminal complement complex. J. Neurol. Sci. 1987;78:17-28.

Motlagh D, Yang J, Lui KY, Webb AR, Ameer GA. Hernocompatibility evaluation of poly(glycerol-sebacate) in vitro for vascular tissue engineering. Biomaterials 2006;27:4315-24.

Motta A, Fambri L, Migliaresi C. Regenerated silk fibroin films: Thermal and dynamic mechanical analysis. Macromol Chem Phys 2002;203:1658-65.

Movat HZ, Mustard JF, Taichman NS, Uriuhara T. Platelet aggregation and release of ADP serotonin and histamine associated with phagocytosis of antigen-antibody complexes. Proceedings of the Society for Experimental Biology and Medicine 1965;120:232.

Movat HZ, Weiser WJ, Glynn MF, Mustard JF. Platelet phagocytosis and aggregation. Journal of Cell Biology 1965;27:531.

Mueller-Plathe F. Different states of water in hydrogels? Macromolecules 1998;31:6721-3.

Mustard JF, Rowsell HC, Murphy EA. Animal and laboratory techniques for evaluating blood coagulation1964.

Mustard JF, Rowsell HC, Murphy EA. platelet economy (platelet survival and turnover). British Journal of Haematology 1966;12:1.

Nagano K. logical analysis of mechanism of protein folding.1. Prediction of helices, loops, an beta-structures from primary structure. Journal of Molecular Biology 1973;75:401-20.

Nakahara H, Misawa H, Yoshida A, Hayashi T, Tanaka M, Furumatsu T, et al. Bone Repair Using a Hybrid Scaffold of Self-Assembling Peptide PuraMatrix and Polyetheretherketone Cage in Rats. Cell Transplant 2010;19:791-7.

Nangaku M, Couser WG. Mechanisms of immune-deposit formation and the mediation of immune renal injury. Clinical and experimental nephrology 2005;9:183-91.

Nilsson B, Ekdahl KN, Mollnes TE, Lambris JD. The role of complement in biomaterial-induced inflammation. Mol. Immunol. 2007;44:82-94.

Nishimura A, Hayakawa T, Yamamoto Y, Hamori M, Tabata K, Seto K, et al. Controlled release of insulin from self-assembling nanofiber hydrogel, PuraMatrix (TM): Application for the subcutaneous injection in rats. European Journal of Pharmaceutical Sciences 2012;45:1-7.

Oliveira JT, Reis RL. Polysaccharide-based materials for cartilage tissue engineering applications. J. Tissue Eng. Regen. Med. 2011;5:421-36.

Olsson P, Lagergren H, Larsson R, Radegran K. Prevention of platelet adhesion and aggregation by a glutardialdehyde-stabilized heparin surface. Thrombosis and haemostasis 1977;37:274-82.

Ossipov DA, Brannvall K, Forsberg-Nilsson K, Hilborn J. Formation of the first injectable poly(vinyl alcohol) hydrogel by mixing of functional PVA precursors. J. Appl. Polym. Sci. 2007;106:60-70.

Ostuni E, Chapman RG, Holmlin RE, Takayama S, Whitesides GM. A survey of structure-property relationships of surfaces that resist the adsorption of protein. Langmuir 2001;17:5605-20.

Pakala R, Waksman R. Currently available methods for platelet function analysis: advantages and disadvantages. Cardiovascular revascularization medicine: including molecular interventions 2011;12:312-22.

Pallapies D. Vasoactive drugs affecting the prostaglandin systems. Wien Klin Wochen 1992;104:521-5.

Panda JJ, Mishra A, Basu A, Chauhan VS. Stimuli responsive self-assembled hydrogel of a low molecular weight free dipeptide with potential for tunable drug delivery. Biomacromolecules 2008;9:2244-50.

Pangburn MK, Mullereberhard HJ. Relation of a putative thioester bond in C-3 to activation of the alternative pathway and the binding of the C3B to biological targets of complement. Journal of Experimental Medicine 1980;152:1102-14.

Paniccia R, Priora R, Alessandrello Liotta A, Abbate R. Platelet function tests: a comparative review. Vascular Health and Risk Management 2015;11:133-48.

Paramonov SE, Jun HW, Hartgerink JD. Self-assembly of peptide-amphiphile nanofibers: The roles of hydrogen bonding and amphiphilic packing. Journal of the American Chemical Society 2006;128:7291-8.

Park KE, Kang HK, Lee SJ, Min BM, Park WH. Biomimetic nanofibrous scaffolds: Preparation and characterization of PGA/chitin blend nanofibers. Biomacromolecules 2006;7:635-43.

Park KH. Improved long-term culture of hepatocytes in a hydrogel containing Arg-Gly-Asp (RGD). Biotechnol. Lett. 2002;24:1131-5.

Parsegian VA, Zemb T. Hydration forces: Observations, explanations, expectations, questions. Current Opinion in Colloid & Interface Science 2011;16:618-24.

Pascual M, TolkoffRubin N, Schifferli JA. Is adsorption an important characteristic of dialysis membranes? Kidney Int 1996;49:309-13.

Patenaude M, Hoare T. Injectable, Degradable Thermoresponsive Poly(N-isopropylacrylamide) Hydrogels. ACS Macro Letters 2012;1:409-13.

Pauling L, Corey RB, Branson HR. The structure of proteins - 2 Hydrogen bonded helical configurations of the polypeptide chain. Proceedings of the National Academy of Sciences of the United States of America 1951;37:205-11.

Pauling L, Corey RB. Configurations of polypeptide hcains with favoured orientations around single bonds. 2 new pleated sheets. Proceedings of the National Academy of Sciences of the United States of America 1951;37:729-40.

Payne MS, Horbett TA. Complement activation by hydroxyethymethacrylate-ethylmethacrylate copolymers. J. Biomed. Mater. Res. 1987;21:843-59.

Peggion E, Terbojev.M, Borin G, Cosani A. CConformational studies on polypeptides - effect of sodicum perchlorate on conformation of poly-L-Lysine and of random copolymers of L-lysine and L-phenylalanine in aqeous solution. Biopolymers 1972;11:633.

Pelesko JA. Self assembly. [electronic resource] : the science of things that put themselves together: Boca Raton : Taylor & Francis, 2007.; 2007.

Peppas NA, Hilt JZ, Khademhosseini A, Langer R. Hydrogels in biology and medicine: From molecular principles to bionanotechnology. Advanced Materials 2006;18:1345-60.

Petersen B, Barkun A, Carpenter S, Chotiprasidhi P, Chuttani R, Silverman W, *et al.* Tissue adhesives and fibrin glues. Gastrointest Endosc 2004;60:327-33.

Pierschbacher MD, Ruoslahti E. Cell attachment activity of a fibronectin can be duplicated by small synthetic fragments of the molecule. Nature 1984;309:30-3.

Plow EF, Ginsberg MH. Specific and saturable binding of plasma fibronectin to thrombin-stimulated human platelets. J. Biol. Chem. 1981;256:9477-82.

Plow EF, Marguerie G. Inhibition of fibrinogen binding to human platelets by the tetrapeptide glycyl-L-prolyl-Larginyl-L Proline. Proceedings of the National Academy of Sciences of the United States of America 1982;79:3711-5.

Pribic R, Vanstokkum IHM, Chapman D, Haris PI, Bloemendal M. Protein secondary structure from Fourier transform infrared and or circular dichroism spectra. Analytical Biochemistry 1993;214:366-78.

Prieto AL, Edelman GM, Crossin KL. Multiple integrins mediate cell attachment to cytotactin/tenascin. Proceedings of the National Academy of Sciences 1993;90:10154-8.

Ptitsyn OB. Stastical analysis of distribution of amino acid residues among helical and non-helical regions in glubular proteins. Journal of Molecular Biology 1969;42:501.

Rapp HJ, Borsos T. Molecular basis of complement activation. 1970.

Ratner BD, Hoffmann A, Schoen F J, Lemons JE. Biomaterials Science. An Introduction to Materials in Medicine. 2nd ed2004.

Reches M, Gazit E. Formation of closed-cage nanostructures by self-assembly of aromatic dipeptides. Nano Letters 2004;4:581-5.

Rendu F, Brohard-Bohn B. The platelet release reaction: granules' constituents, secretion and functions. Platelets 2001;12:261-73.

Ribeiro CC, Barrias CC, Barbosa MA. Calcium phosphate-alginate microspheres as enzyme delivery matrices. Biomaterials 2004;25:4363-73.

Rice CM, Strauss JH. Nucleotide-sequence of the 26S messenger-RNA of Sindbis virus and deduced sequence of the encoded virus structural proteins. Proceedings of the National Academy of Sciences of the United States of America-Biological Sciences 1981;78:2062-6.

Richardson JS. The anatomy and taxonomy of protein structure. Advances in protein chemistry 1981;34:167-339.

Ricklin D, Hajishengallis G, Yang K, Lambris JD. Complement: a key system for immune surveillance and homeostasis. Nature Immunology 2010;11:785-97.

Rinaudo M, Pavlov G, Desbrieres J. Influence of acetic acid concentration on the solubilization of chitosan. Polymer 1999;40:7029-32.

Rinder CS, Smith MJ, Rinder HM, Cortright DN, Brodbeck RM, Krause JE, et al. Leukocyte effects of C5a-receptor blockade during simulated extracorporeal circulation. Ann Thorac Surg 2007;83:146-52.

Rinder HM, Bonan JL, Rinder CS, Ault KA, Smith BR. Dynamics of leukocyte-platelet adhesion in whole-blood. Blood 1991;78:1730-7.

Rinder HM, Tracey JL, Rinder CS, Leitenberg D, Smith BR. Neutrophil but not monocyte activation inhibits P-selectin-mediated platelet adhesion. Thrombosis and haemostasis 1994;72:750-6.

Rock G, Freedman M, Hamilton C, Bormanis J. New methods showing in vitro changes of platelets. Transfusion and Apheresis Science 2006;35:145-9.

Rodríguez-Cabello JC, Arias FJ, Rodrigo MA, Girotti A. Elastin-like polypeptides in drug delivery. Advanced Drug Delivery Reviews 2016;97:85-100.

Rose GD, Gierasch LM, Smith JA. Turns in peptides and proteins. Advances in Protein Chemistry 1985;37:1-109.

Ruan L, Zhang H, Luo H, Liu J, Tang F, Shi Y-K, *et al*. Designed amphiphilic peptide forms stable nanoweb, slowly releases encapsulated hydrophobic drug, and accelerates animal hemostasis. Proceedings of the National Academy of Sciences of the United States of America 2009;106:5105-10.

Ruoslahti E, Vaheri A. Interaction of soluble fibroblast surface antigen with firbinogen and fibrin - Identitiy with cold insoluble globulin of human plasma. Journal of Experimental Medicine 1975;141:497-501.

Rusli R, Shanmuganathan K, Rowan SJ, Weder C, Eichhorn SJ. Stress-Transfer in Anisotropic and Environmentally Adaptive Cellulose Whisker Nanocomposites. Biomacromolecules 2010;11:762-8.

Sabel M, Stummer W. The use of local agents: Surgicel and Surgifoam. European Spine Journal 2004;13:S97-S101.

Saffer EM, Tew GN, Bhatia SR. Poly(lactic acid)-poly(ethylene oxide) Block Copolymers: New Directions in Self-Assembly and Biomedical Applications. Curr Med Chem 2011;18:5676-86.

Saini A, Koss K, Unsworth LD. Effect of Peptide Concentration on Water Structure, Morphology, and Thermal Stability of Self-Assembling (RADA)4 Peptide Matrices. Journal of Biomaterials and Tissue Engineering 2014;4:895-905.

Saini A, Serrano K, Koss K, Unsworth LD. Evaluation of the hemocompatibility and rapid hemostasis of (RADA)4 peptide-based hydrogels. Acta Biomaterialia 2016;31:71-9.

Sakariassen KS, Hanson SR, Cadroy Y. Methods and models to evaluate shear-dependent and surface reactivity-dependent antithrombotic efficacy. Thromb. Res. 2001;104:149-74.

Salzman EW, Merrill EW, Binder A, Wolf CF, Ashford TP, Austen WG. Protein-platelet interaction on heparinized surfaces. J. Biomed. Mater. Res. 1969;3:69-81.

Sanchez de Groot N, Parella T, Aviles FX, Vendrell J, Ventura S. Ile-Phe dipeptide self-assembly: Clues to amyloid formation. Biophysical Journal 2007;92:1732-41.

Santos MT, Valles J, Marcus AJ, Safier LB, Broekman MJ, Islam N, *et al*. Enhancement of platlet reactivity and modulation of eicosanoid production by intact erythrocytes - a new approach to platelet activation and recruitment. Journal of Clinical Investigation 1991;87:571-80.

Sargeant TD, Guler MO, Oppenheimer SM, Mata A, Satcher RL, Dunand DC, *et al.* Hybrid bone implants: Self-assembly of peptide amphiphile nanofibers within porous titanium. Biomaterials 2008;29:161-71.

Sauaia A, Moore FA, Moore EE, Moser KS, Brennan R, Read RA, *et al.* Epidemiology of trauma deaths - a reassessment. J. Trauma-Injury Inf. Crit. Care 1995;38:185-93.

Savage B, Saldivar E, Ruggeri ZM. Initiation of platelet adhesion by arrest onto fibrinogen or translocation on von Willebrand factor. Cell 1996;84:289-97.

Savi P, Chong BH, Greinacher A, Gruel Y, Kelton JG, Warkentin TE, *et al*. Effect of fondaparinux on platelet activation in the presence of heparin-dependent antibodies: a blinded comparative multicenter study with unfractionated heparin. Blood 2005;105:139-44.

Savin T, Doyle PS. Electrostatically tuned rate of peptide self-assembly resolved by multiple particle tracking. Soft Matter 2007;3:1194-202.

Sayah S, Ischenko AM, Zhakhov A, Bonnard AS, Fontaine M. Expression of cytokines by human astrocytomas following stimulation by C3a and C5a anaphylatoxins: Specific increase in interleukin-6 mRNA expression. Journal of Neurochemistry 1999;72:2426-36.

Schachner M. Neurobiology - Nervous engineering. Nature 2000;405:747-8.

Schense JC, Hubbell JA. Cross-linking exogenous bifunctional peptides into fibrin gels with factor XIIIa. Bioconjugate Chemistry 1999;10:75-81.

Schmaljohann D. Thermo- and pH-responsive polymers in drug delivery. Advanced Drug Delivery Reviews 2006;58:1655-70.

Schmedlen KH, Masters KS, West JL. Photocrosslinkable polyvinyl alcohol hydrogels that can be modified with cell adhesion peptides for use in tissue engineering. Biomaterials 2002;23:4325-32.

Schneider JP, Kelly JW. Templates that induce alpha-helical, beta-sheet, and loop conformations. Chemical Reviews 1995;95:2169-87.

Schneider JP, Pochan DJ, Ozbas B, Rajagopal K, Pakstis L, Kretsinger J. Responsive Hydrogels from the Intramolecular Folding and Self-Assembly of a Designed Peptide. Journal of the American Chemical Society 2002;124:15030-7.

Schnepp ZAC, Gonzalez-McQuire R, Mann S. Hybrid biocomposites based on calcium phosphate mineralization of self-assembled supramolecular hydrogels. Advanced Materials 2006;18:1869.

Schonauer C, Tessitore E, Barbagallo G, Albanese V, Moraci A. The use of local agents: bone wax, gelatin, collagen, oxidized cellulose. European Spine Journal 2004;13:S89-S96.

Schulz G, Schirmer RH. Patterns of Folding and Association of Polypeptide Chains. Principles of Protein Structure: Springer New York; 1979. p. 66-107.

Sefton MV, Gemmell CH, Gorbet MB. What really is blood compatibility? Journal of Biomaterials Science-Polymer Edition 2000;11:1165-82.

Segers VFM, Lee RT. Local delivery of proteins and the use of self-assembling peptides. Drug Discovery Today 2007;12:561-8.

Seipke G, Arfmann HA, Wagner KG. Synthesis and properties of alternating poly(lys-phe) and comparison with random copolymer poly (lys51, phe 49). Biopolymers 1974;13:1621-33.

Semino CE, Kasahara J, Hayashi Y, Zhang SG. Entrapment of migrating hippocampal neural cells in three-dimensional peptide nanofiber scaffold. Tissue Engineering 2004;10:643-55.

Setton LA, Elliott DM, Mow VC. Altered mechanics of cartilage with osteoarthritis: human osteoarthritis and an experimental model of joint degeneration. Osteoarthritis Cartilage 1999;7:2-14.

Shattil SJ, Cunningham M, Hoxie JA. Detection of activated platelets in whole blood using activation dependent monoclonal antibodies and flow cytometry. Blood 1987;70:307-15.

Shea JE, Onuchic JN, Brooks CL. Probing the folding free energy landscape of the src-SH3 protein domain. Proceedings of the National Academy of Sciences of the United States of America 2002;99:16064-8.

Shen CL, Murphy RM. Solvent effects on self-assembly of beta-amyloid peptide. Biophys. J. 1995;69:640-51.

Shenkman B, Savion N, Dardik R, Tamarin I, Varon D. Testing of platelet deposition on polystyrene surface under flow conditions by the cone and plate(let) analyzer: Role of platelet activation, fibrinogen and von Willebrand factor. Thromb Res 2000;99:353-61.

Shetty AS, Zhang JS, Moore JS. Aromatic pi-stacking in solution as revealed through the aggregation of phenylacetylene macrocycles. Journal of the American Chemical Society 1996;118:1019-27.

Shin H, Jo S, Mikos AG. Biomimetic materials for tissue engineering. Biomaterials 2003;24:4353-64.

Silva AK, Richard C, Bessodes M, Scherman D, Merten OW. Growth factor delivery approaches in hydrogels. Biomacromolecules 2009;10:9-18.

Sim RB, Sim E. Autolytic fragmentation of complement components C-3 and C-4 and its relationship to covalent binding activity. Annals of the New York Academy of Sciences 1983;421:259-76.

Simnick AJ, Lim DW, Chow D, Chilkoti A. Biomedical and biotechnological applications of elastin-like polypeptides. Polym. Rev. 2007;47:121-54.

Sims PJ, Wiedmer T. Induction of cellular procoagulant activity by the membrane attack complex of complement. Seminars in Cell Biology 1995;6:275-82.

Sipe JD, Cohen AS. Review: History of the amyloid fibril. Journal of Structural Biology 2000;130:88-98.

Sivaraman B, Latour RA. The Adherence of platelets to adsorbed albumin by receptor-mediated recognition of binding sites exposed by adsorption-induced unfolding. Biomaterials 2010;31:1036-44.

Skarja GA, KinloughRathbone RL, Perry DW, Rubens FD, Brash JL. Cone-and-plate device for the investigation of platelet biomaterial interactions. J. Biomed. Mater. Res. 1997;34:427-38.

Slack SM, Turitto VT. Flow chambers and their standardization for the use in studies of thrombosis - on behalf of the subcommittee on rheology. Thrombosis and haemostasis 1994;72:777-81.

Smith AM, Williams RJ, Tang C, Coppo P, Collins RF, Turner ML, *et al.* Fmoc-Diphenylalanine self assembles to a hydrogel via a novel architecture based on pi-pi interlocked beta-sheets. Advanced Materials 2008;20:37.

Snatzke G. Circular Dichroism: Principles and Applications. New York: VCH Publishers; 1994. p. 59-84.

Snell CR, Fasman GD. Kinetics and thermodynamics of alpha helix-/-beta transconfromation of poly(L-lysine) and L-leucine copilymers - Compensation phenomenon. Biochemistry 1973;12:1017-25.

Snyder TA, Watach MJ, Litwak KN, Wagner WR. Platelet activation, aggregation, and life span in calves implanted with axial flow ventricular assist devices. Ann Thorac Surg 2002;73:1933-8.

Solchaga LA, Yoo JU, Lundberg M, Dennis JE, Huibregtse BA, Goldberg VM, *et al.* Hyaluronan-based polymers in the treatment of osteochondral defects. J Orthop Res 2000;18:773-80.

Soto P, Griffin MA, Shea J-E. New insights into the mechanism of Alzheimer amyloid-beta fibrillogenesis inhibition by N-methylated peptides. Biophysical Journal 2007;93:3015-25.

Sperling C, Schweiss RB, Streller U, Werner C. *In vitro* hemocompatibility of self-assembled monolayers displaying various functional groups. Biomaterials 2005;26:6547-57.

Stephanopoulos N, Ortony JH, Stupp SI. Self-assembly for the synthesis of functional biomaterials. Acta Mater 2013;61:912-30.

Stile RA, Burghardt WR, Healy KE. Synthesis and characterization of injectable poly(N-isopropylacrylamide)-based hydrogels that support tissue formation *in vitro*. Macromolecules 1999;32:7370-9.

Stile RA, Healy KE. Poly(N-isopropylacrylamide)-based semi-interpenetrating polymer networks for tissue engineering applications. 1. Effects of linear poly(acrylic acid) chains on phase behavior. Biomacromolecules 2002;3:591-600.

Stokes KY, Granger DN. Platelets: a critical link between inflammation and microvascular dysfunction. Journal of Physiology-London 2012;590:1023-34.

Strzinar I, Sefton MV. Preparation and thrombogenicity of alkylated and polyvinyl alcohol coated tubing. J. Biomed. Mater. Res. 1992;26:577-92.

Stupp SI. Self-assembly and biomaterials. Nano. Lett. 2010;10:4783-6.

Suh JKF, Matthew HWT. Application of chitosan-based polysaccharide biomaterials in cartilage tissue engineering: a review. Biomaterials 2000;21:2589-98.

Sunde M, Blake CCF. From the globular to the fibrous state: protein structure and structural conversion in amyloid formation. Quarterly Reviews of Biophysics 1998;31:1.

Takabayashi T, Vannier E, Clark BD, Margolis NH, Dinarello CA, Burke JF, et al. A new biologic role for C3a and C3a desArg - Regulation of TNF-alpha and IL-1 beta synthesis. Journal of Immunology 1996;156:3455-60.

Takezawa T, Mori Y, Yoshizato K. Cell culture on a thermoresponsive polymer surface. Bio-Technology 1990;8:854-6.

Tanaka M, Mochiziki A, Ishii N, Motomura T, Hatekeyama T. Study of blood compatibility with poly(2-methoxyethyl acrylate). Relationship between water structure and platelet compatibility in poly(2-methoxyethylacrylate-co-2-hydroxyethylmethacrylate). Biomacromolecules 2002;3:36-41.

Tenidis K, Waldner M, Bernhagen J, Fischle W, Bergmann M, Weber M, et al. Identification of a penta- and hexapeptide of islet amyloid polypeptide (IAPP) with amyloidogenic and cytotoxic properties. Journal of Molecular Biology 2000;295:1055-71.

Thaler U, Deusch E, Kozek-Langenecker SA. *In vitro* effects of gelatin solutions on platelet function: a comparison with hydroxyethyl starch solutions. Anaesthesia 2005;60:554-9.

Tirrell M, Kokkoli E, Biesalski M. The role of surface science in bioengineered materials. Surface Science 2002;500:61-83.

Toda M, Iwata H. Effects of Hydrophobicity and Electrostatic Charge on Complement Activation by Amino Groups. ACS Appl. Mater. Interfaces 2010;2:1107-13.

Tokunaga M, Liu ML, Nagai T, Iwanaga K, Matsuura K, Takahashi T, et al. Implantation of cardiac progenitor cells using self-assembling peptide improves cardiac function after myocardial infarction. J. Mol. Cell Cardiol. 2010;49:972-83.

Toledano S, Williams RJ, Jayawarna V, Ulijn RV. Enzyme-triggered self-assembly of peptide hydrogels via reversed hydrolysis. Journal of the American Chemical Society 2006;128:1070-1.

Trudelle Y. Conformational study of the sequential (Tyr-Glu)n copolymer in aqueous solution. Polymer 1975;16:9-15.

Tsuruta T. Contemporary topics in polymeric materials for biomedical applications. Biopolymers liquid crystalline polymers phase emulsion1996.

Uchida Y, Fukuda K, Murakami Y. The hydrogel containing a novel vesicle-like soft crosslinker, a "trilayered" polymeric micelle, shows characteristic rheological properties. Journal of Polymer Science Part B-Polymer Physics 2013;51:124-31.

Uemura M, Refaat MM, Shinoyama M, Hayashi H, Hashimoto N, Takahashi J. Matrigel Supports Survival and Neuronal Differentiation of Grafted Embryonic Stem Cell-Derived Neural Precursor Cells. J Neurosci Res 2010;88:542-51.

Varon D, Dardik R, Shenkman B, KotevEmeth S, Farzame N, Tamarin I, *et al*. A new method for quantitative analysis of whole blood platelet interaction with extracellular matrix under flow conditions. Thromb Res 1997;85:283-94.

Venkatac.Cm. Stereochemical criteria for polypeptides and proteins.V. Conformation of a system of 3 linked peptide units. Biopolymers 1968;6:1425.

Verrecchia T, Spenlehauer G, Bazile DV, Murrybrelier A, Archimbaud Y, Veillard M. Non-steatlth poly(lactic acid albumin) and stealth polly(lactiv acid-polyethylene glycol) nanoparticles as injectable drug carriers. Journal of Controlled Release 1995;36:49-61.

Vogler EA, Siedlecki CA. Contact activation of blood-plasma coagulation. Biomaterials 2009;30:1857-69.

Wagner I, Musso H. New naturally occuring amino acids. Angewandte Chemie-International Edition in English 1983;22:816-28.

Wallace DG, Rosenblatt J. Collagen gel systems for sustained delivery and tissue engineering. Advanced Drug Delivery Reviews 2003;55:1631-49.

Wallqvist A, Berne BJ. Computer simulation of hydrophobic hydration forces on stacked plates at short range. J Phys Chem 1995;99:2893-9.

Walport MJ. Advances in immunology: Complement (First of two parts). N. Engl. J. Med. 2001;344:1058-66.

Walport MJ. Advances in immunology: Complement (Second of two parts). N. Engl. J. Med. 2001;344:1140-4.

Wang LJ, Sun N, Terzyan S, Zhang XJ, Benson DR. Histidine/tryptophan pi-stacking interaction stabilizes the heme-independent folding core of microsomal apocytochrome b(5) relative to that of mitochondrial apocytochrome b(5). Biochemistry 2006;45:13750-9.

Wang RLC, Kreuzer HJ, Grunze M. Molecular conformation and solvation of oligo(ethylene glycol)-terminated self-assembled monolayers and their resistance to protein adsorption. J. Phys. Chem. B 1997;101:9767-73.

Wang T, Zhong XZ, Wang ST, Lv F, Zhao XJ. Molecular Mechanisms of RADA16-1 Peptide on Fast Stop Bleeding in Rat Models. Int. J. Mol. Sci. 2012;13:15279-90.

Wang YD, Ameer GA, Sheppard BJ, Langer R. A tough biodegradable elastomer. Nature Biotechnology 2002;20:602-6.

Watt KWK, Cottrell BA, Strong DD, Doolittle RF. Amino acid sequence studies on the alpha-chain of human-fibrinogen - overlappign sequences providing the complete sequence. Biochemistry 1979;18:5410-6.

Webber MJ, Tongers J, Renault M-A, Roncalli JG, Losordo DW, Stupp SI. Development of bioactive peptide amphiphiles for therapeutic cell delivery. Acta Biomaterialia 2010;6:3-11.

Weinberg CB, Bell E. A blood-vessel model constructed from collagen and cultured vascular cells. Science 1986;231:397-400.

Werner C, Maitz MF, Sperling C. Current strategies towards hemocompatible coatings. J. Mater. Chem. 2007;17:3376-84.

Wettero J, Askendal A, Bengtsson T, Tengvall P. On the binding of complement to solid artificial surfaces in vitro. Biomaterials 2002;23:981-91.

Whitesides GM, Grzybowski B. Self-assembly at all scales. Science 2002;295:2418-21.

Wicken JS, Woody RW. Conformational changes in liver alcohol dehydrogenase upon nucleotide binding - detection by circular dichroism of dye complexes. Archives of Biochemistry and Biophysics 1974;162:12-6.

Wiedmer T, Sims PJ. Participation of protein-kinases in complement C5B-9-induced shedding of platelet plasma-membrane vesicles. Blood 1991;78:2880-6.

Wiradharma N, Khan M, Tong YW, Wang S, Yang YY. Self-assembled cationic peptide nanoparticles capable of inducing efficient gene expression *in vitro*. Advanced Functional Materials 2008;18:943-51.

Wiradharma N, Tong YW, Yang Y-Y. Self-assembled oligopeptide nanostructures for co-delivery of drug and gene with synergistic therapeutic effect. Biomaterials 2009;30:3100-9.

Wojta J, Huber K, Valent P. New aspects in thrombotic research: Complement induced switch in mast cells from a profibrinolytic to a prothrombotic phenotype. Pathophysiology of Haemostasis and Thrombosis 2003;33:438-41.

Wojta J, Kaun C, Zorn G, Ghannadan M, Hauswirth AW, Sperr WR, *et al*. C5a stimulates production of plasminogen activator inhibitor-1 in human mast cells and basophils. Blood 2002;100:517-23.

Wood SJ, Maleeff B, Hart T, Wetzel R. Physical, morphological and functional differences between pH 5.8 and 7.4 aggregates of the Alzheimer's amyloid peptide AP. J. Mol. Bio.l 1996;256:870-7.

Wortham L. Hemorrhage control in the battlefield: role of new hemostatic agent. Military medicine 2005;170:1004.

Xiong H, Buckwalter BL, Shieh HM, Hecht MH. Periodicity of polar and nonpolar amino acids is the major determinant of secondary structure in self-assembling oligomeric peptides. Proceedings of the National Academy of Sciences 1995;92:6349-53.

Yamada KM. Adhesive recognition sequences. J Biol Chem 1991;266:12809-12.

Yamaoka H, Asato H, Ogasawara T, Nishizawa S, Takahashi T, Nakatsuka T, *et al.* Cartilage tissue engineering chondrocytes embedded in using human auricular different hydrogel materials. Journal of Biomedical Materials Research Part A 2006;78A:1-11.

Yang F, Williams CG, Wang DA, Lee H, Manson PN, Elisseeff J. The effect of incorporating RGD adhesive peptide in polyethylene glycol diacrylate hydrogel on osteogenesis of bone marrow stromal cells. Biomaterials 2005;26:5991-8.

Yang ZM, Gu HW, Zhang Y, Wang L, Xu B. Small molecule hydrogels based on a class of antiinflammatory agents. Chemical Communications 2004:208-9.

Yang ZM, Xu KM, Wang L, Gu HW, Wei H, Zhang MJ, *et al*. Self-assembly of small molecules affords multifunctional supramolecular hydrogels for topically treating simulated uranium wounds. Chemical Communications 2005:4414-6.

Ye Z, Zhang H, Luo H, Wang S, Zhou Q, Du X, *et al*. Temperature and pH effects on biophysical and morphological properties of self-assembling peptide RADA16-1. Journal of Peptide Science 2008;14:152-62.

Yla-Outinen L, Joki T, Varjola M, Skottman H, Narkilahti S. Three-dimensional growth matrix for human embryonic stem cell-derived neuronal cells. J Tissue Eng Regen Med 2014;8:186-94.

Yokoi H, Kinoshita T, Zhang S. Dynamic reassembly of peptide RADA16 nanofiber scaffold. Proceedings of the National Academy of Sciences 2005;102:8414-9.

Yoshimi R, Yamada Y, Ito K, Nakamura S, Abe A, Nagasaka T, *et al*. Self-Assembling Peptide Nanofiber Scaffolds, Platelet-Rich Plasma, and Mesenchymal Stem Cells for Injectable Bone Regeneration With Tissue Engineering. J. Craniofac. Surg. 2009;20:1523-30.

Zangi R, Hagen M, Berne BJ. Effect of ions on the hydrophobic interaction between two plates. Journal of the American Chemical Society 2007;129:4678-86.

Zhang J, Hao R, Huang L, Yao J, Chen X, Shao Z. Self-assembly of a peptide amphiphile based on hydrolysed Bombyx mori silk fibroin. Chemical Communications 2011;47:10296-8.

Zhang JM, Teng HX, Zhou XS, Shen DY. Frozen bound water melting induced cooperative hydration of poly(vinyl methyl ether) in aqueous solution. Polymer Bulletin 2002;48:277-82.

Zhang S, Holmes T, DiPersio M, Hynes RO, Su X, A. R. Self-complementary oligopeptide matrices support mammalian cell attachment. Biomaterials 1995;16:1385-93.

Zhang S. Fabrication of novel biomaterials through molecular self-assembly. Nat. Biotech. 2003;21:1171-8.

Zhang SG, Lockshin C, Cook R, Rich A. Unusually stable beta-sheet formation in an ionic self-complementary oligopeptide. Biopolymers 1994;34:663-72.

Zhang SG, Lockshin C, Herbert A, Winter E, Rich A. Zuotin, a putative Z-binding-protein in saccaromycescervisiae. Embo Journal 1992;11:3787-96.

Zhao W, Jin X, Cong Y, Liu Y, Fu J. Degradable natural polymer hydrogels for articular cartilage tissue engineering. Journal of Chemical Technology and Biotechnology 2013;88:327-39.

Zhao X, Nagai Y, Reeves PJ, Kiley P, Khorana HG, Zhang S. Designer short peptide surfactants stabilize G protein-coupled receptor bovine rhodopsin. Proceedings of the National Academy of Sciences of the United States of America 2006;103:17707-12.

Zhao X, Pan F, Xu H, Yaseen M, Shan H, Hauser CAE, *et al*. Molecular self-assembly and applications of designer peptide amphiphiles. Chemical Society Reviews 2010;39:3480-98.

Zhao Y, Tanaka M, Kinoshita T, Higuchi M, Tan T. Nanofibrous scaffold from self-assembly of beta-sheet peptides containing phenylalanine for controlled release. Journal of Controlled Release 2010;142:354-60.

Zhu JM. Bioactive modification of poly(ethylene glycol) hydrogels for tissue engineering. Biomaterials 2010;31:4639-56.

Ziats NP, Pankowsky DA, Tierney BP, Ratnoff OD, Anderson JM. Adsorption of hageman-factor (Factor XII) and other human plasma proteins to biomedical polymers. Journal of Laboratory and Clinical Medicine 1990;116:687-96.

Ziccardi RJ, Cooper NR. Development of an immunochemical test to assess C1 inactivator function in human-serum and its use for the diagnosis of hereditary angioedema. Clinical Immunology and Immunopathology 1980;15:465-71.

Zimm BH, Bragg JK. Theory of the phase transition between helix and random coil in polypeptide chains. Journal of Chemical Physics 1959;31:526-35.

Zisch AH, Lutolf MP, Hubbell JA. Biopolymeric delivery matrices for angiogenic growth factors. Cardiovascular pathology: the official journal of the Society for Cardiovascular Pathology 2003;12:295-310.

Zou Z, Zheng Q, Wu Y, Guo X, Yang S, Li J, *et al*. Biocompatibility and bioactivity of designer self-assembling nanofiber scaffold containing FGL motif for rat dorsal root ganglion neurons. J Biomed Mater Res Part A 2010;95A:1125-31.

Zwischenberger JB, Brunston RL, Swann JR, Conti VR. Comparison of two topical collagen-based hemostatic sponges during cardiothoracic procedures. Journal of Investigative Surgery 1999;12:101-6.

Appendix A

Peptide Information

All peptides were synthesized, characterized and purified successfully by SynBioSci (Livermore, CA). The accuracy of the observed mass was reported as +0.1%, and the purity was analyzed by HPLC and has a +2% deviation for peptides < or 95%.

Table1: HPLC purity, theoretical and obtained molecular mass of peptides

Peptide	Theoretical Mass (g/mol)	Mass Found (g/mol)	Purity
Ac-RADARADARADARADA-NH$_2$	1712.8	1713.2	> 95%
Ac-RADARADARADARADAKKKKK-NH$_2$	2354.7	2354.7	> 95%
Ac-RADARADARADARADASSSSS-NH$_2$	2148.2	2184.4	> 82.2%

Table 2: Physicochemical properties of the custom peptides used in the dissertation

Peptide	Calculated pI$^\$$	Average Hydrophilicity$^\$$	Net Charge (pH = 7.0)$^\$$
(RADA)$_4$	7.1	1.3	0
(RADA)$_4$K$_5$	11.0	1.7	5
(RADA)$_4$S$_5$	7.1	1.0	0
*Obtained from the supplier (SynBioSci) $^\$$Calculated from www.innovagen.com			
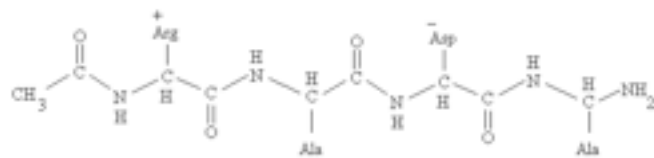
Figure 1: Schematic of (RADA)₄ peptide in aqueous solution
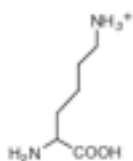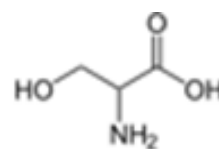
Lysine (Lys, K)   Serine (Ser, S)

Figure 2: Schematic of Lysine and Serine residue structures

Analytical HPLC of the collected fractions showed a single peak after purification of all the peptides (Figures 3-5)
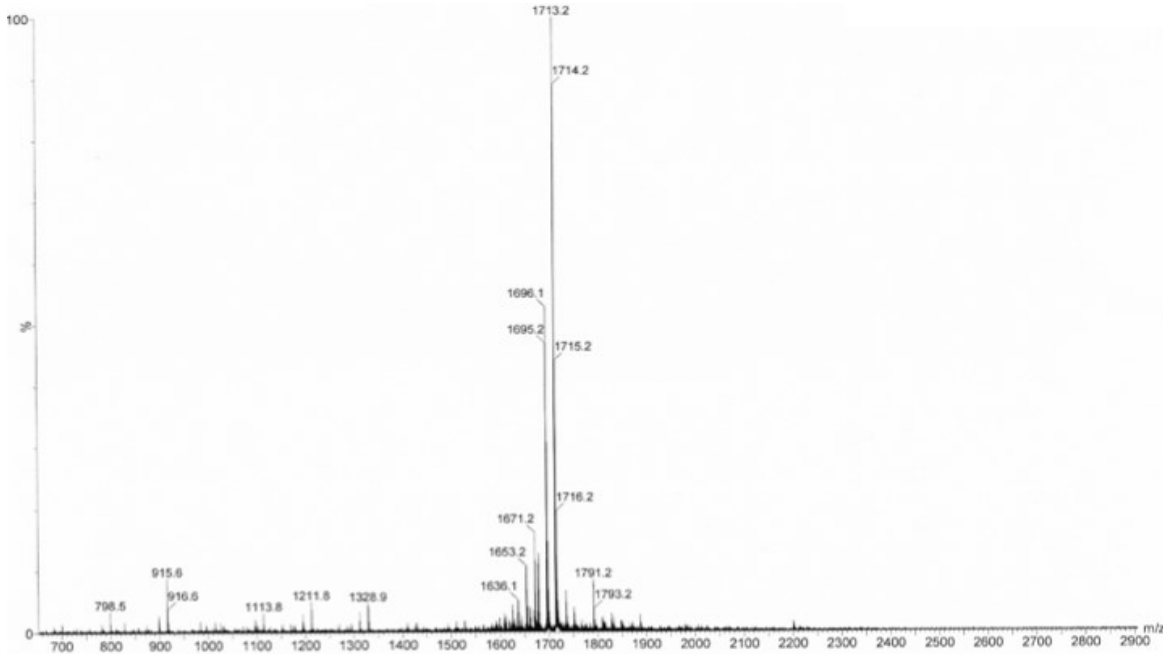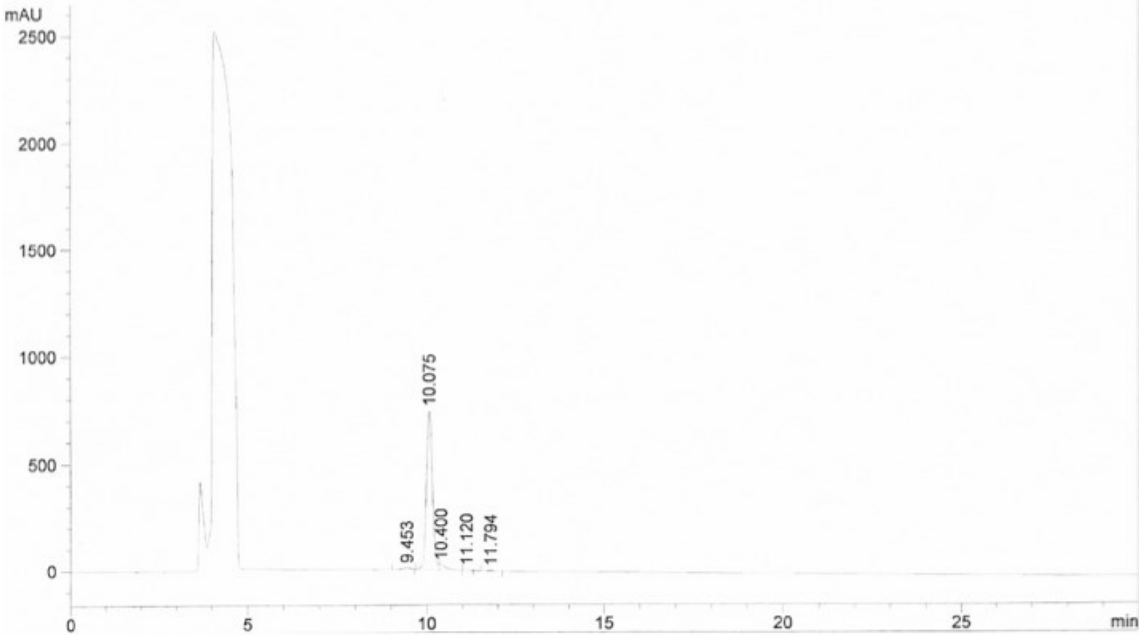
Figure 3: Representative (A) analytical HPLC trace, and (B) MALDI-TOF-MS of (RADA)₄ peptide in aqueous solution
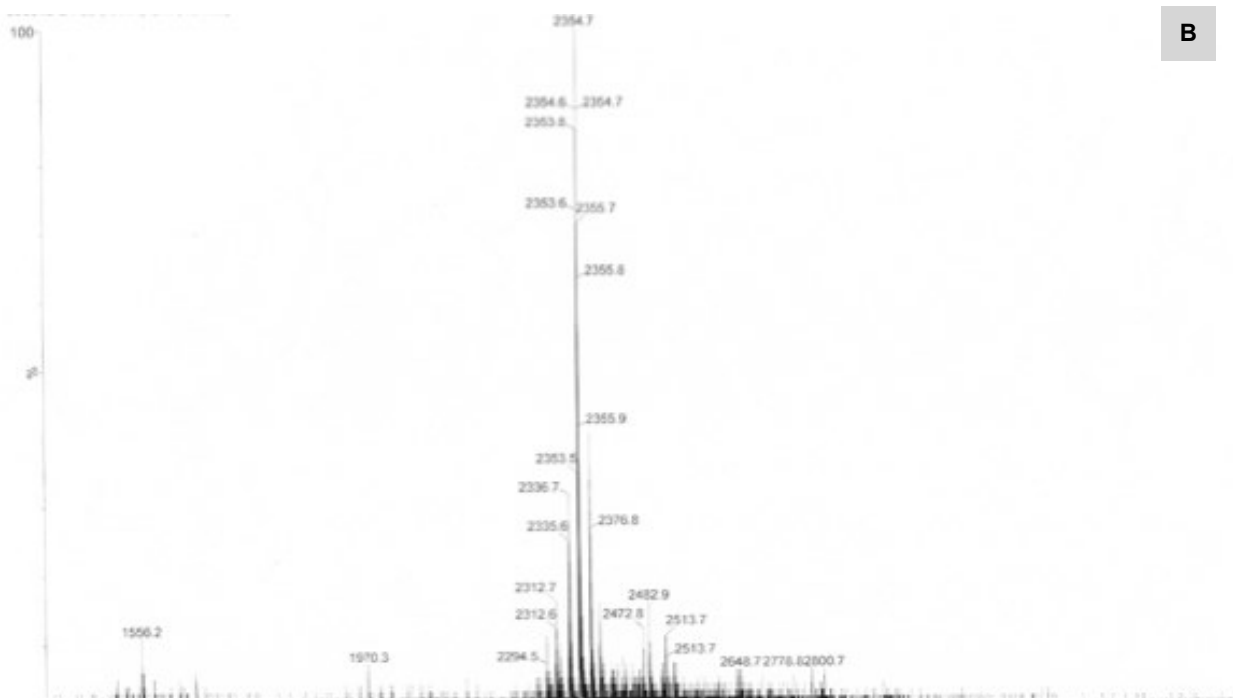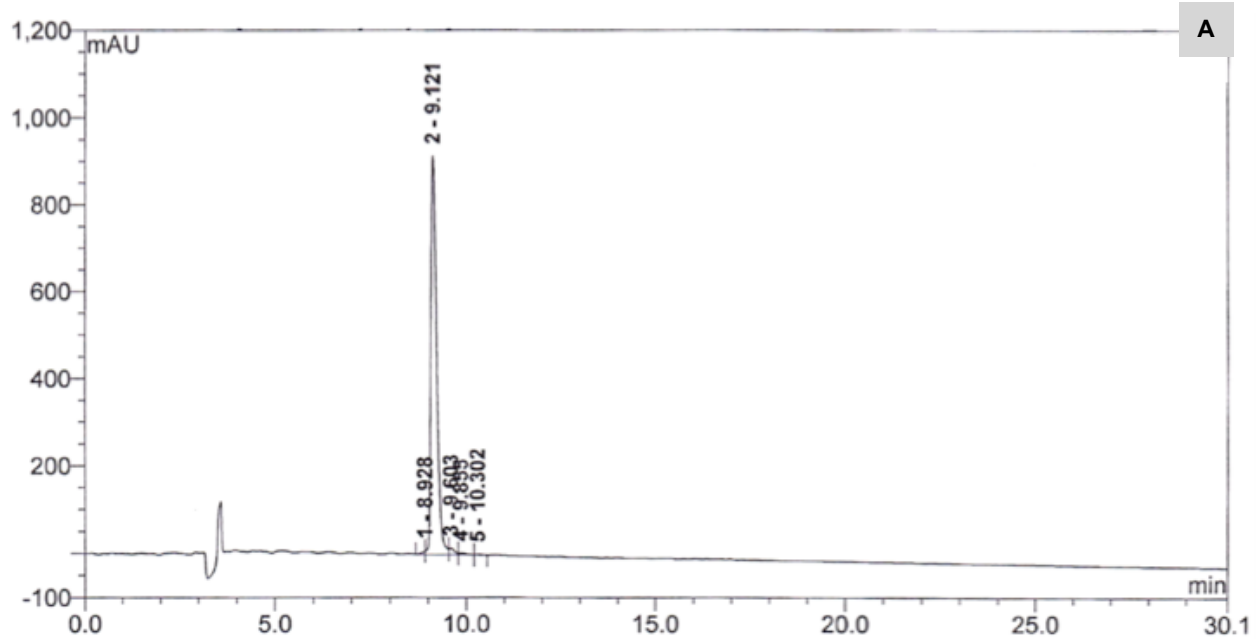
Figure 4: Representative (A) analytical HPLC trace, and (B) MALDI-TOF-MS of (RADA)$_4$K$_5$ peptide in aqueous solution
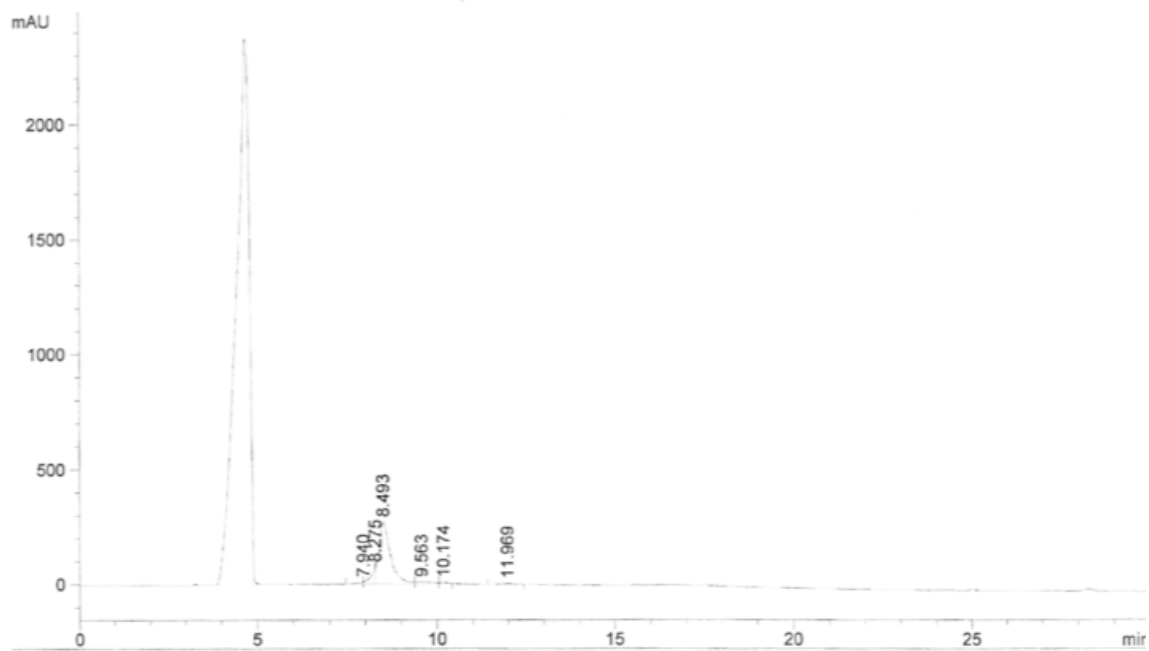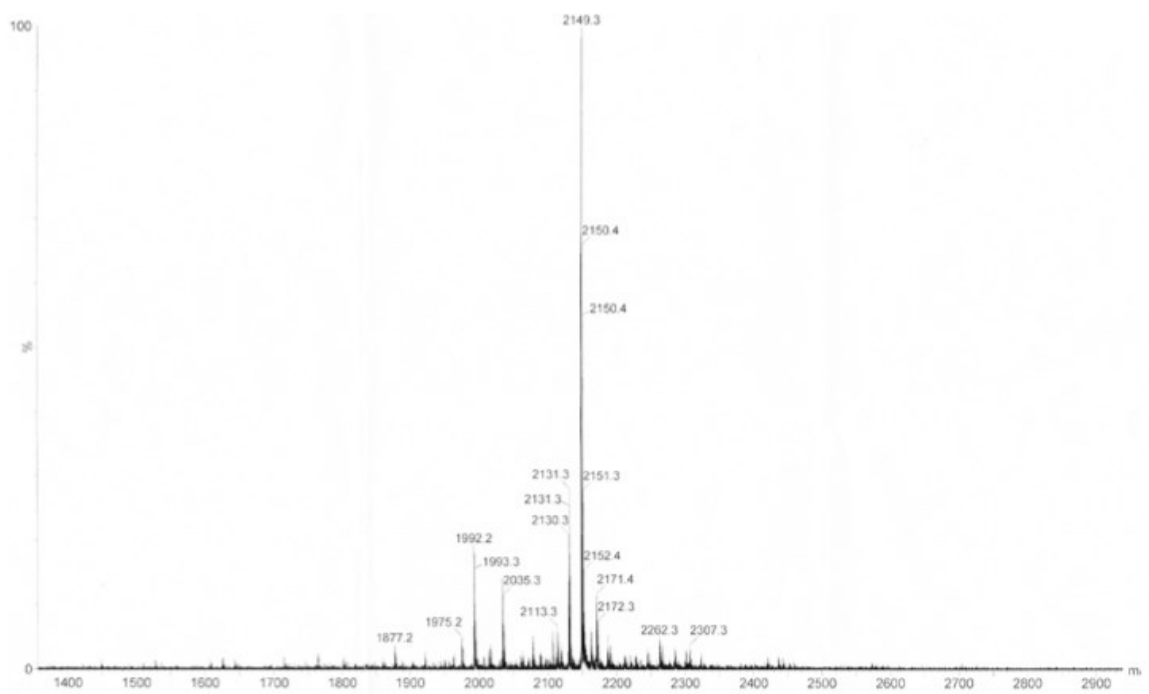
Figure 5: Representative (A) analytical HPLC trace, and (B) MALDI-TOF-MS of (RADA)$_4$S$_5$ peptide in aqueous solution

Appendix B

Circular Dichroism Spectroscopy Protocol

General Operations and Instrument Start-up

1. Warming up of the CD/ORD instrument is necessary prior to use. For measurement in the low wavelength region of ~175-300 nm, purging the optical system with the proper flow rate of 28 L/min nitrogen gas is necessary. The required warm-up time is at least 30 min.

2. The CD-value stability can be checked with the sample while warming up the instrument. The procedure is well described in the instrument specific manual by Jasco Corporation. Briefly, pour an aqueous solution of 0.06% (w/v) ammonium d-10 camphorsulfonate into a 1 cm cell and set the cell in the instrument to make measurements with a wavelength of 291.0 nm for approximately 2 hr in the T-scan mode. If the stabilized CD value (value after base correction) remains within +190.4 mdeg ($\pm$1%), it is normal.

3. Switch on the spectropolarimeter. Switching on the instrument does not turn on the light source. The light source is lit when the measurement program is started. Switch on the attached computer.

4. Open the software named, "Spectra Manager". Select "Spectrum Measurement" program. The program initializes the spectropolarimeter and switches on the light source. Hence, starting up the program may take 1-2 min. The lamp "LED" of the amplifier panel would be turned on green.

Obtaining Circular Dichroism Spectra

1. In the "Spectrum Measurement" program go to "Measurement" → "Parameter" and check if all the parameters have been set right. The parameters and their underlying basis of selection for protein/nanofibers in solution are as given below:

   a. Sensitivity = Standard (100 mdeg)

   b. Starting wavelength = 300 nm

   c. End wavelength = 170-190 nm (depending on the protocol)

   d. Data pitch = 0.5 nm

   e. Scan mode = Continuous

   A continuous scan mode is selected as this response gives priority to the scanning speed. Additionally, measurement time is independent of the step resolution. Henceforth, this mode is best suited for attaining normal data with a better S/N in a short time. This mode is suitable for high-speed scans. Nevertheless, since relatively longer cycle components are mixed in noises on CD, it is advisable to average with accumulation. However, increasing the accumulation increases measurement time significantly, the total measurement time of less than 30 min. is considered to be a tentative criterion to set the number of accumulation, as if the measurement time exceeds 1 hr, the spectrum may be affected by the base line drift of the instrument.

   f. Scan speed = 5 nm/min

   Since CD is based on photo-electric method, a relatively higher scan speed is selected to avoid drift induced noise in the measurement.

   g. Response = 16 sec

   h. Bandwidth = 1.0 nm

   i. Accumulations = 1-10 (protocol specific)

298

Since spectrum S/N is proportional to the square root of the product of response R and the number N of the accumulation, a higher S/N can either be achieved by increasing response time and or increasing number of accumulation.

2. Click "Background Subtraction" from the "Measurement" menu and select a previously saved .jws file format of a background spectrum. The background spectra were collected either using Milli-Q diH$_2$O or buffer in a demountable quartz cuvette with a 0.10 mm of path length.

3. Click "Start" from "Measurement" menu to begin data acquisition. For the given wavelength range the each spectrum takes about 2-3 min.

4. Upon the complete data acquisition of the selected rage of wavelength, the "Spectra Analysis" program opens automatically.

5. The spectrum can be saved by clicking "Save As…" function from the "File" menu. The spectra should be saved in .jws and .txt format. The later format is used for data analysis in Microsoft Excel and CD analysis software.

6. The data can be improved by the smoothing method (data cut function) which is very effective in eliminating remaining noises in view of the measurement time. Precisely, smoothing can be achieved by Processing menu → Correction menu → Data Cut and adjusting the data pitch from 0.1 nm to 0.5 nm or 1.0 nm. Additional smoothing can be performed using the Savitzky-Golay algorithm under curve smoothing (Processing menu → Correction menu → Smoothing).

Circular Dichroism Instrument Turn-off

1. Upon saving all the needed data files, all the programs should be closed.

2. Turn off the spectropolarimeter by using the button located in the front of the machine. The instrument can also be switched off in the "Spectra Manager", by clicking "Instruments" → "Stop".

3. Turn off the nitrogen gas after at least 5-10 min. of switching off the instrument.

Circular Dichroism Spectra Data Analysis

1. The data is collected in machine unites (mdeg) which was converted to Molar Ellipticity (deg.cm^2/dmol) using Microsoft Excel, as outlined in Materials and Methods.

2. Further quantitative and qualitative data analysis was performed by using CDSSTER, accessed from DICROWEB (located at http://www.cryst.bbk.ac.uk/cdweb), and the following parameters were entered:

   a. Registration Information = As given upon setting up the account

   b. Input File Details = Enter the protein/system name and the file location

   About the Data File:

   c. File Format = "Jasco 1.30"

   d. Input Units = "Machine Units"

   Upon selecting this option additional experimental information should be filled in, such as Mean Residue Weight (MRW) of the protein (amu/ Daltons/ number of residues), Path length (cm) and protein concentration (mg/ml)

   e. Initial and Final Wavelengths = Initial is the first wavelength in the data file (~ 300 nm) and final is the last wavelength in the file (~ 170 nm).

   f. Wavelength Step = 0.5 nm

   g. Lowest nm data point (nm) to use in the analysis should be defined.

   Choice of Methods:

   h. Analysis Program = CDSSTR

   The program has a run time from 5-15 min and produces a graphical output.

   i. Reference Set = The program offers a set of 7 reference data sets to choose, from which a set of basis spectra would be selected for analysis. The reference data set that represents the characteristics of the system to be analyzed should be selected for obtaining accurate results.

Advanced options:

j. Optional Scaling Factor = 1.0

Output Options:

k. Output Units = Molar Ellipticity

3. The output is in tabular and graphical format, which can be saved to be accessed at a later time if needed.

Appendix C

Differential Scanning Calorimetry Protocol

General Operations and Sample Set-up

1. Record the mass of hermetic pan and the lid by placing them open-side-up on a microbalance. Weight the sample separately by using tweezers to place the sample in the pans. Generally, the appropriate mass range for samples in DSC is considered from 1-10 mg. For the experiments outlined in this thesis a mass of approximately 5 mg was considered optimum. An accurate measure of the sample mass is imperative to the DSC analysis as it is entered into the machine to give out the data independent of sample size.

2. The pan containing the sample then should be sealed immediately (to avoid evaporation) with the sample press. It was revealed in the experiments conducted for this thesis that a double sealing of the pans (both sides) is imperative for preventing sample loss.

3. The sample pan should be placed in the auto sampler tray and the position number should be recorded. A reference pan, with a known mass should be sealed and kept in the indicated spot.

4. The DSC/TGA Q 2000 Thermal Analyzer is equipped with a mass flow controller to control the flow rate of the gas. Henceforth, the flow rate is controlled through settings chosen using the instrument control software. Specifically, the purge gas source is regulated between 100-140 kPa and the recommended flow rate is 50 mL/min.

5. Instrument calibration is required when using a new cell or changing the purge gas or changing the cooling device. Calibration is carried out in the instrument's calibration mode, which is accessed through the controller. DSC is calibrated following step-to-step instructions outlined in the instrument control software.

Obtaining Differential Scanning Calorimetry Thermogram

7. After checking the connection between the DSC and the controller, switch on the instrument from the controller. The following DSC parameters can be changed through the controller or the attached computer.

8. The left tab on the instrument control software defines experimental parameters. The parameters for hydrogels are as given below:

Summary Tab:

a. Mode = standard

b. Test option = Custom

The custom run should be defined such that the starting temperature is -40°C and end temperature is 60°C. Sample loading temperature should be kept at 40 °C.

c. Input sample name, pan mass, sample mass, reference mass, auto-sampler locations and run comments. Data file name should also be recorded.

Procedure Tab:

d. Heating rate: 5°C/min

A relatively low heating rate is desired as it would ensure the thermal equilibrium of the samples. However, to prevent sample degradation a standard rate of 5°C/min is selected.

Notes Tab:

    e.   Define operator

    f.   Pan type = Aluminum Hermetic

    g.   Nitrogen flow rate should be defined.

9.   Click "Append" to add another cycle of the sample.

10.   After all the cycles are appended, click "Run" to start the experiment.

11.   A sample thermogram (Heat flow *vs*. Temperature) would appear on the bottom right hand side with the progression of the cycle.

12.   The resulting data would be a thermogram of temperature *vs*. Time.

Differential Scanning Calorimetry Data Analysis

1.   The data can be analyzed using the DSC/TGA inbuilt analysis Universal Analysis software 2000. The data file information would require reconfirmation of the already defined experimental conditions. Additionally, the exothermic position should be defined.

2.   Data analysis was performed by defining exothermic peaks using "Integrated Peak Linear Methodology".

3.   The melting enthalpy of the sample was computed by calculating the resulting area under the thermograms and calculating the frozen and non-frozen water contents, as described in the Materials and Methods section.

Appendix D

Critical Point Drying Protocol (BAL-TEC CPD 030)

<u>General Operations and Instrument Start-up</u>

1. Open the CO_2 tank by turning the valve at least 1.5 turns (anticlockwise).

2. Turn on machine (green switch on right of the machine)

3. Pre-cool chamber by pressing "cooling" – it will lower temp to 20° or 5° below room temp.

4. Open lid of chamber and flush line with CO_2 by pressing 'Medium in'. Press 'Medium in' to stop the procedure.

5. Insert specimen (and stirrer if using metal basket) in chamber and replace lid (do not add extra ethanol to chamber and don't tighten lid excessively)

6. Close Metering valve. *Check it as it might be locked in the open position.

7. Press 'Medium in' immediately to allow CO_2 to enter chamber.

8. Press 'Medium in' again after CO_2 level rises above the front window (can look from top to see CO2 level). Let stew for 5 minutes (turn on the stirrer). Temperature should be about 10°C at this point.

9. Heat to 20° C and then cool to 15°C.

10. Let CO_2 out by pressing 'Medium Out'. Don't let CO_2 level drop below specimens (Normally that level is just above the writing on the glass window). Press 'Medium Out' again to stop.

11. Repeat filling and emptying chamber with CO_2 liquid until CO_2 solid sprayed onto paper towel evaporates with out any wet residue (ethanol). This will take at least 4-5 flushes. Heat it to 20°C and then cool it back to 15°C then flush.

12. After flushes are complete, fill the chamber with CO_2. Chamber must be filled <u>just above top of front window</u> as the level will drop with heating.

13. Make sure all valves are closed ($><$ lights should be off) and that Metering Valve is closed to the right (don't tighten too much - pin closure may ware).

14. Heat chamber by first pressing 'cooling' to stop cooling and second pressing 'heating' to start heating. Heating will push the CO_2 through its critical point of 73.8 bar and 31°C. Note: The CO_2 levels will drop as the pressure increase. Raise the temp and pressure above critical values – approximately 80-85 bar and 40°C (max temp of 40°C is maintained automatically).

15. Let sit at critical values for 5 minutes.

16. To start venting CO_2 from chamber, first make sure Metering valve is closed and press 'Gas Out'.

17. Slowly open the Metering valve and watch the gas leave the chamber by placing the exhaust tube in a cup full of water. Do not leave the machine while the pressure is decreasing. The manual say it takes 10 minutes, but it could be longer than a n hour. The slower you exhaust the chamber, the better.

18. Once the pressure is fully down, (P=0), turn off heating by pressing 'heating'. Leave the 'Gas Out' valve open and Metering valve open all the way to make sure the chamber is completely vented. (Listen for bubbles of vented gas in the water.)

19. Close CO_2 tank valve.

20. Open chamber and remove specimen. If chamber is pressurized at all, it will be difficult to empty the chamber. Do not use force.

21. With chamber lid open, press 'Medium in' to flush remaining CO_2 from the line.

22. Close valves.

23. Replace lid.

24. Turn off machine.